SAN DIEGO BAY EELGRASS BLUE CARBON STUDY

2021-2023

Prepared for
San Diego Unified Port District

September 2023

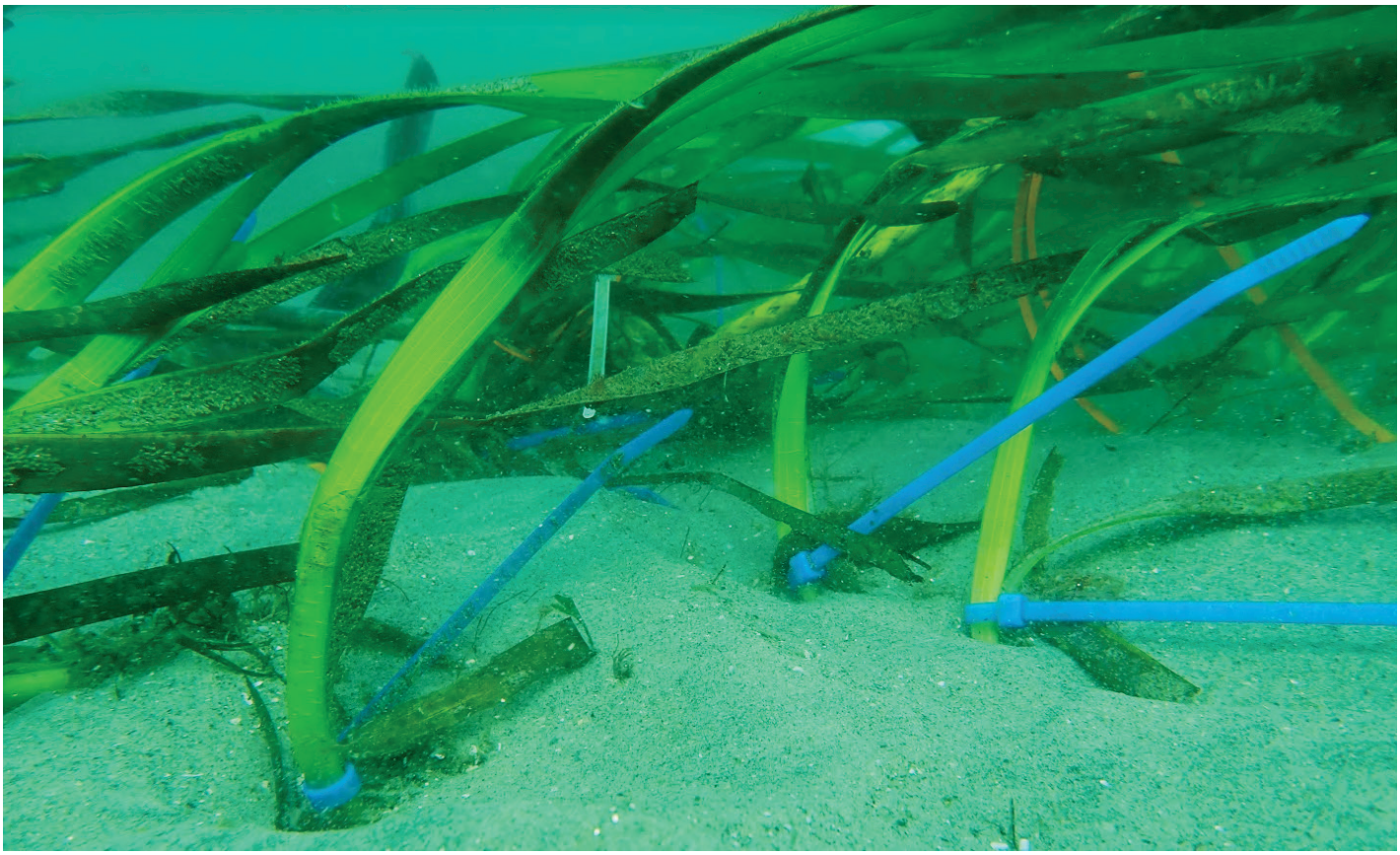

SAN DIEGO BAY EELGRASS BLUE CARBON STUDY

2021-2023

Prepared for
San Diego Unified Port District
Prepared by Environmental Science Associates, Merkel & Associates, and David Tomasko, Ph.D. (Sarasota Bay Estuary Program)

September 2023

Funding provided by the Maritime Administration (MARAD)

Services provided pursuant to this Agreement are intended solely for the use and benefit of the San Diego Unified Port District.

No other person or entity shall be entitled to rely on the services, opinions, recommendations, plans or specifications provided pursuant to this agreement without the express written consent of ESA, 575 Market Street, San Francisco CA 94105.

2355 Northside Drive, Suite 100
San Diego, CA 92108
619.719.4200
esassoc.com

ESA

Atlanta	Palm Beach County	San Diego
Bend	Pasadena	San Francisco
Irvine	Pensacola	San Jose
Los Angeles	Petaluma	Sarasota
Mobile	Portland	Seattle
Oakland	Rancho Cucamonga	Tampa
Orlando	Sacramento	Thousand Oaks

D201800121.03

TABLE OF CONTENTS

List of Figures

List of Tables

Appendices

This page intentionally left blank

EXECUTIVE SUMMARY

The Port of San Diego has been at the forefront of climate action, adopting a Climate Action Plan as early as 2013. For the Port to meet its goals and comply with state regulations, decarbonizing maritime-related sources is of utmost importance. Statewide initiatives like the California Global Solutions Act of 2016 (S.B. 32) mandate a significant 40% reduction in emissions below 1990 levels by 2030. To further accelerate progress, the recently passed California Carbon Neutrality Act (A.B. 1279) sets a clear and binding goal for carbon neutrality, aiming for attainment by 2045 at the latest, with an interim target of 85% emissions reduction compared to 1990 levels.

Recognizing the urgent need to address climate change and support carbon neutrality, the Port of San Diego has taken proactive steps to explore various strategies for reducing greenhouse gas emissions. As part of their commitment to sustainability, the Port has turned its attention to the unique and ecologically vital ecosystems of eelgrass beds in San Diego Bay. These seagrass habitats have emerged as potential blue carbon reservoirs, efficiently sequestering carbon dioxide from the atmosphere and storing it in their biomass and sediment. Understanding the carbon sequestration potential of these eelgrass habitats is important for the Port's comprehensive approach to carbon mitigation and achieving its ambitious climate goals. By investigating the role of blue carbon in seagrass ecosystems, the Port seeks to unlock new opportunities for carbon offset mechanisms and inform future restoration projects that can further contribute to climate mitigation and environmental preservation.

This second year of studying blue carbon in San Diego Bay's eelgrass beds builds upon the previous year's efforts (see Appendix A) with expanded goals:

1. Assess carbon storage variation associated with local environmental conditions.

    a. Conduct follow-up sampling of eelgrass productivity in areas of high nutrient input and during a wet year, as opposed to the drought conditions prior to and during Year 1.

    b. Look at variation within eelgrass beds compared to outside of eelgrass beds (i.e., at an unvegetated site).

    c. Add additional sites with known establishment dates to expand the Year 1 bed age assessment.

    d. Measure sediment grain size distribution and analyze its relationship to carbon storage.

2. Build out a carbon budget for San Diego Bay’s eelgrass beds to understand the relative magnitude of carbon reservoirs and flows between them.

    a. Develop a San Diego Bay-specific sequestration rate.

    b. Collect and assess water quality data to estimate the amount of carbon stored in the water column.

ES.1 Biomass Sampling

San Diego Bay alone accounts for 17% of all eelgrass habitat in the state (Merkel & Associates 2020) – yet despite the broad spatial coverage, the plants are observed to be generally smaller than in other systems. This has been hypothesized to be due to drought, which likely has led to reductions in nutrient loading from the watershed. Repeated biomass and productivity sampling in Year 2 focused on whether biomass near sources of nutrient input (i.e., drain from a golf course, mouth of a river) would be larger or more productive than eelgrass elsewhere. Findings show higher productivity at these "fertilized" sites versus at the reference site, but an overall standing carbon stock lower than at the reference site, indicating an increase in nutrients does not necessarily result in an increase in carbon sequestration. This could be the subject of further study and monitoring, particularly given the wet winter season 2022-2023.

ES.2 Sediment Coring

Additional sediment coring in Year 2 showed that the unvegetated site, which was intended to provide a reference point for analyzing carbon within eelgrass beds, was actually significantly higher in carbon content than all the vegetated sites. This may be due to site location in a historic/abandoned riverbed and at a lower elevation, making it especially depositional, receiving sediment and biomass from surrounding eelgrass beds.

Strong correlations were observed between mud content (<0.074 mm) and age with carbon storage, indicating their potential as predictive factors for carbon stock development.

ES.3 Sequestration Rates

Radioisotope dating was used to estimate sedimentation and carbon sequestration rates. The analyses returned largely irregular profiles, that may be due to dredging/filling history, hydrodynamic disturbances from waves or ships, or disturbance during coring. Some gross approximations for sediment accretion indicate a sediment carbon burial rate of 111-265 g $C/m^2/yr$, which is higher than rates found in the literature for seagrass beds. They should therefore be used with great caution or resampled with methodological changes.

ES.4 Water Quality Sampling

A pair of multi-parameter water quality sondes were deployed in the bay within close proximity, one inside an eelgrass bed and one outside of an eelgrass bed. While temperature and pH were similar at both instruments, the sensor inside the eelgrass bed showed much less pronounced turbidity spikes, likely attributable to the wave attenuation and sediment retention benefits of eelgrass beds.

Analysis of the dissolved oxygen record indicated greater gross photosynthesis inside eelgrass beds in both autumn and spring deployments compared to outside eelgrass beds, where the only photosynthesis is due to phytoplankton. Dissolved oxygen data were also used to calculate a carbon assimilation rate.

ES.5 Carbon Budget

A thorough assessment of a blue carbon ecosystem's stocks depends on accurate assessments of all the various reservoirs and fluxes of carbon within the system (Figure ES-1). While most blue carbon studies focus on biomass and sediment storage, which make up the bulk of the carbon budget in marshes and mangrove forests, this project additionally quantifies the bicarbonate pathway. This chemical pathway, unique to seagrasses, describes how carbon ordinarily buried in sediments (in other blue carbon habitats) is instead stored in the water column.

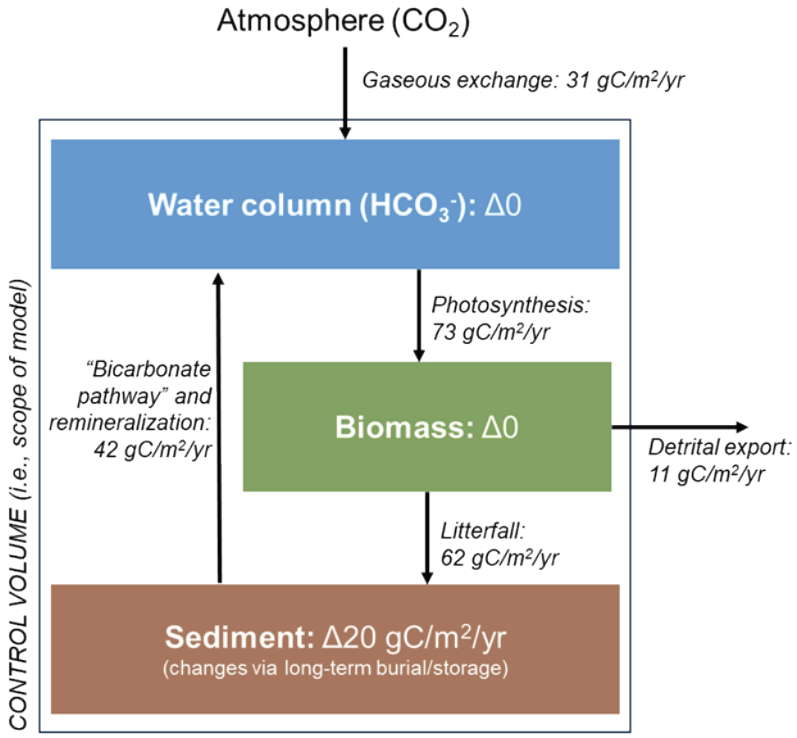

SOURCE: ESA 2023

D201800121.03 San Diego Bay Eelgrass Blue Carbon Study

Figure ES-1
Changing Pools and Fluxes of Carbon in San Diego Bay Seagrass Beds

The carbon budget illustrates the significant role of the bicarbonate pathway in carbon sequestration (Figure ES-1). Through the pathway and through sediment burial, we estimate that San Diego Bay's seagrass habitats are sequestering approximately 1,195 tonnes of CO_2 equivalent annually. This sequestration is comparable to 0.3% of the annual emissions from Port operations, based on the projected 2020 emissions data (Port of San Diego 2013).

ES.6 Conclusions

Overall, this study represents the first known carbon budget constructed for the eelgrass beds of San Diego Bay. It provides a framework for and can be incorporated into future work – a bay-wide blue carbon inventory, for example. The study may also be improved by continued refinements to methods.

This page intentionally left blank

1. INTRODUCTION

Seagrass beds have a remarkable capacity for carbon sequestration, making them significant contributors to "blue carbon." Through photosynthesis, seagrass absorbs carbon dioxide and stores it in leaves, roots, and the surrounding environment. Researchers estimate that the global carbon burial of seagrasses is 48 to 112 teragrams of carbon (Tg C) per year; by comparison, forests' carbon burial rates range from 49 to 79 Tg C per year (Mcleod et al. 2011). Protecting and restoring seagrass beds can help mitigate climate change by reducing greenhouse gas emissions and enhancing carbon sinks.

While carbon markets traditionally focus on land-based projects like afforestation and reforestation, efforts are being made to include blue carbon in carbon offset mechanisms. Some blue carbon methodologies have been approved, and the first U.S. project solely focused on seagrass beds was recently registered in April 2022. However, integration into carbon markets faces challenges such as methodology development, data availability, policy frameworks, and credit costs compared to project expenses. Further research is needed to understand the factors that influence the amount of carbon sequestered within an eelgrass bed in order to quantify potential offsets from a restoration project.

San Diego Bay holds about 17% of California's eelgrass habitat (Merkel & Associates 2020), making it crucial for quantifying seagrass carbon. The Port of San Diego and the Navy have been mapping, monitoring. and managing these habitats, which are a subtype of the seagrasses discussed more generally above, since the early 1990s. Continued management is essential to preserve and increase blue carbon storage in the bay.

By recognizing the climate mitigation benefits of seagrass, the Port and partners can prioritize actions that improve and conserve these habitats. Quantifying blue carbon in San Diego Bay is expected to broaden funding opportunities for estuarine restoration and conservation, particularly as seagrass faces threats from climate change and sea-level rise.

1.1 Project Context

The Port of San Diego was one of the first ports to adopt a Climate Action Plan in 2013, and the decarbonization of maritime-related sources is a critical component to achieve organizational goals and uphold state regulations. The California Global Solutions Act of 2016 (S.B.-32) requires a 40% reduction in State emissions below 1990 levels by 2030. In September 2022, the State passed The California Carbon Neutrality Act, A.B. 1279, that establishes "a clear, legally binding, and achievable goal" that urges carbon neutrality as soon as possible, but no later than 2045, according to the governor's office. A.B. 1279 also sets an 85% emissions reduction target in comparison to 1990 levels. As such, it is important for the Port to seek multiple strategies to decrease GHG emissions through direct source reductions and through carbon sequestration.

In addition to upholding state standards, the Port of San Diego has also developed a Maritime Clean Air Strategy (MCAS) to reduce emissions of criteria pollutants as well as greenhouse gases

(GHGs) from its maritime industry beyond what is mandated by California standards. With a vision of Health Equity for All, the MCAS is a strategic planning document, identifying both short- and long-term goals and objectives to reduce emissions from ocean-going vessels, commercial harbor craft, cargo handling equipment, heavy-duty trucks, and locomotives. The MCAS focuses on the transition to zero emission technologies such as increased use of shore power for ocean-going vessels while at berth and electric trucks that aim to reduce diesel particulate matter (DPM) emissions as well as GHG emissions. The initiatives outlined in the MCAS will reduce health risk impacts on receptors such as nearby residents, children at schools and day care centers, and patients at local hospitals and others.

In advance of the State's goals, the Port seeks to install additional shorepower capacity at its marine terminals, utilize an emission capture and control system to reduce emission from non-shorepower capable vessels, and advance 100% zero emission truck trips and cargo handling equipment by 2030. Additional goals include transitioning Port-owned vehicles and equipment to zero/near zero emission technologies in a manner that meets operational needs. Despite these initiatives, the Port will still require additional emissions reduction strategies to meet State goals and blue carbon may be one such avenue.

1.2 Year 1 Study Overview

In the Year 1 Study (ESA and Merkel & Associates, 2022, Appendix A), the ESA team sampled 12 locations across San Diego Bay (Sites A-J), selecting sites to facilitate comparisons across the following environmental variables:

- Species of eelgrass (*Zostera marina, Zostera pacifica*),
- Ecoregion (Outer Bay, North Bay, North-Central Bay, South-Central Bay, South Bay),
- Depth of eelgrass occurrence (shallow margin, mid-bed, deep fringe), and
- Age of eelgrass beds.

Following the methods established by Howard et al. (2018) and Short and Duarte (2001), each site was analyzed for biomass carbon and sediment carbon, and eelgrass productivity was assessed at two of the sites. The results of the sampling and laboratory analysis showed that, in total, San Diego Bay's eelgrass habitats store around 170,600 tonnes of CO_2 equivalent currently.

Sampling at the 12 locations across the bay provided the following results around the variability of carbon storage:

- The *Z. pacifica* bed generally had lower sediment carbon density compared to *Z. marina* despite *Z. pacifica*'s larger biomass. However, aboveground carbon (i.e., the density multiplied by the biomass) and belowground carbon (i.e., sediment carbon) for the two species were not significantly different from each other ($p > 0.05$).
- Across the bay, the results show a general trend of increasing sediment carbon going southward. In particular, the Outer Bay stored significantly less carbon ($p < 0.05$) than North-Central, South-Central, and South Bay sites, and storage was also significantly different ($p <$

0.05) between the South Bay and the two ecoregions just north of it (North-Central and South-Central).

- The data show that the average carbon content may increase with increasing depth. The middle depth (-5 ft MLLW) showed significantly ($p < 0.05$) more carbon than the shallowest depth (-1 ft MLLW). The deepest cores (-7 ft MLLW) showed a substantial amount of variability, so this depth was not statistically significantly different from the other two depths.
- The older sites had greater amounts of carbon in the sediments than the younger sites. Although there were only four data points, those data suggest a strong linear relationship between eelgrass bed age and carbon content.

The ESA team also estimated eelgrass productivity by measuring eelgrass growth over a period of 12-14 days, similar to the methodology employed in other studies (Kentula and McIntire 1986; Solana-Arellano 2000; Solana-Arellano et al. 2008). The analysis showed that *Z. marina* assimilates 98.0 ± 41.0 mg C/m^2/day and *Z. pacifica* assimilates 237.1 ± 64.4 mg C/m^2/day. Note that assimilation in this context refers to biological sequestration, or what is taken into biomass—it does not guarantee that the carbon will be permanently stored. Comparing the assimilation rate to estimates of carbon sequestration in the literature (Duarte et al. 2005, 2011; McLeod et al. 2011) shows an order of magnitude discrepancy between carbon assimilation rates and carbon sequestration rates. As discussed in Tomasko 2015, this is a fairly common result, and at least a portion of the discrepancy may be due to sequestration into bicarbonate ions in the water column (see Section 3.3).

ESA also developed a habitat evolution model to estimate how eelgrass habitat and blue carbon sequestration could change over time with sea-level rise. The model forecasts that the total extent of habitat will decrease over time, without proactive conservation and restoration efforts. However, this habitat loss does not occur uniformly. Over time, eelgrass encroaches closer to the present-day shoreline, while habitat loss occurs largely in the interior of the bay. Habitat gain is concentrated in the South Bay, while habitat loss is concentrated first in the South-Central Bay but is eventually modeled to occur in all other ecoregions.

The Year 1 study (Appendix A) made the following recommendations for future work, many of which are covered in this Year 2 study:

1. Develop a San Diego Bay–specific sequestration rate to allow for a direct comparison to assimilation rates and to provide more accurate carbon evolution modeling results.
2. Further investigate inorganic carbon pathways and carbon sequestration within the bicarbonate pool to better understand the difference between assimilation and sequestration rates.
3. Collect water quality data to provide additional information on the bicarbonate pathway (through changes in pH) and to be used to estimate productivity through the air-water CO_2 flux to compare against measurements in this study.
4. Refine findings of this study as new sea-level rise projections become available.

5. Assess grain size or other supplementary sediment analyses (e.g., isotope measurements) to further illuminate patterns and causes of carbon storage in the sediment.
6. Sample eelgrass productivity when drought conditions end and eelgrass returns to more "normal" above ground biomass conditions.

1.3 Year 2 Study Overview

ESA, Merkel & Associates, and David Tomasko, Ph.D. prepared this study for the Port to expand the Year 1 efforts to evaluate and inventory carbon sequestration and storage potential of seagrass beds in San Diego Bay. The goal of this work is to:

1. Expand the previous analysis of carbon storage variation associated with differences in local environmental conditions.
    a. Conduct follow-up sampling of eelgrass productivity in areas of high nutrient input and during a wet year, as opposed to the drought conditions prior to and during Year 1.
    b. Look at variation within eelgrass beds compared to outside of eelgrass beds (i.e., unvegetated sites).
    c. Add additional sites with known establishment dates to expand the Year 1 bed age assessment.
    d. Measure sediment grain size distribution and analyze its relationship to carbon storage.
2. Build out a carbon budget for San Diego Bay's eelgrass beds to understand how perturbations to the system (e.g., inputs or removals) may affect the carbon pools.
    a. Develop a San Diego Bay-specific sequestration rate.
    b. Collect and assess water quality data to quantify the amount of carbon stored in the water column.

In Year 1, carbon storage was measured across species of eelgrass, ecoregion, depth of eelgrass occurrence, and age of eelgrass beds. In Year 2, some of these datasets were expanded and a core from an area with no eelgrass was collected to compare to nearby sites with eelgrass.

1.4 Conceptual framework

1.4.1 Carbon Stocks

The term "carbon stock" refers to the quantity of carbon stored in a reservoir, or pool (e.g., soil (sediment), vegetation, water, the atmosphere). Each pool can sequester and release carbon. In eelgrass beds, the main pools of carbon are biomass and sediment carbon (IPCC 2014). The water column also stores carbon in the form of bicarbonate.

Aboveground Biomass

Vegetation sequesters carbon from the atmosphere through photosynthesis and transforms it into biomass. The biomass carbon stock includes the total mass of carbon stored aboveground (e.g., in blades of seagrass, etc.) at a site.

Sediment Carbon Stock and Belowground Biomass

The carbon stored in the sediments comprises another important stock. Due to the small amount of belowground biomass (i.e., rhizome and roots) in seagrass, it is included in the sediment carbon stock. This stock increases over time according to the sediment sequestration rate of the habitat, i.e., the rate at which dead organic matter is incorporated back into the sediment. Sediments in blue carbon habitats are primarily oxygen-poor or anaerobic because they are submerged in water which slows the decomposition of dead organic matter and allows carbon to remain buried in the sediment. Because of the unique anaerobic chemistry of aquatic environment sediments, wetlands and seagrasses store a disproportionately large amount of carbon per area compared to terrestrial habitats, making this stock of particular interest in the context of global climate change.

Bicarbonate in the Water Column

The primary pathway for carbon to enter the ocean is through the exchange of carbon dioxide (CO_2) between the atmosphere and the water surface. As shown in the first equation below, atmospheric CO_2 dissolves in the surface water, leading to the formation of carbonic acid (H_2CO_3). This carbonic acid then dissociates into bicarbonate ions (HCO_3^-) and hydrogen ions (H^+) as shown in the second equation. Bicarbonate ions can then further disassociate into carbonate (CO_3^{-2}) and hydrogen ions (H+), as shown in the third equation.

1. CO_2 (dissolved gas) + H_2O <=> H_2CO_3 (carbonic acid)

2. H_2CO_3 (carbonic acid) <=> H^+ + HCO_3^- (hydrogen ion + bicarbonate)

3. HCO_3^- <=> H^+ + CO_3^{-2} (hydrogen ion + carbonate)

Figure 1-1 shows the relationship between carbon species and pH. Since the pH of the ocean is just over 8, the bicarbonate ion (HCO_3^-) is the most abundant form of dissolved inorganic carbon (DIC) in the ocean.

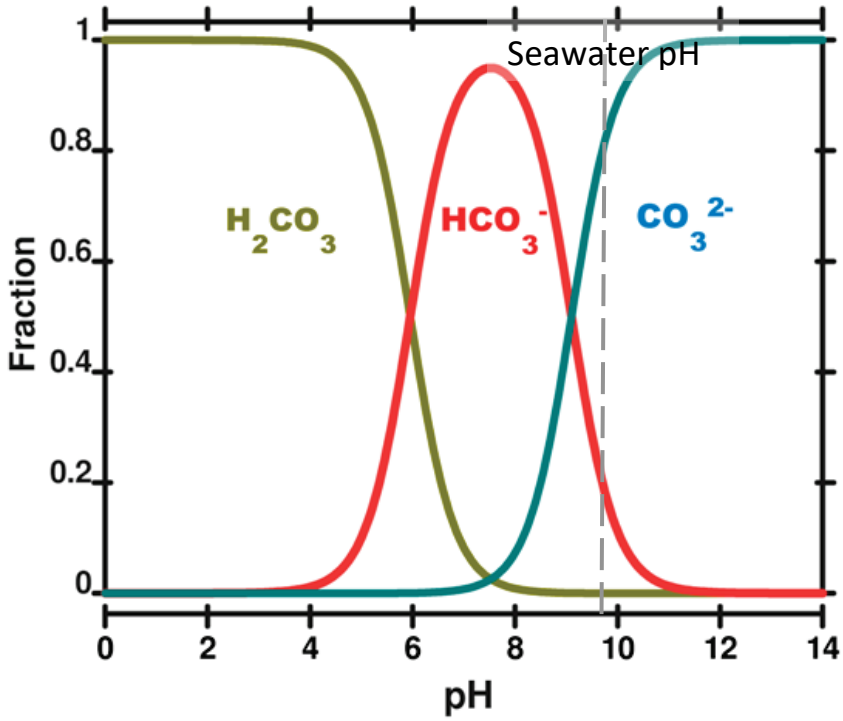

SOURCE: ttps://skepticalscience.com/print.php?n=888

D201800121.03 San Diego Bay Eelgrass Blue Carbon Study

Figure 1-1
Speciation Diagram of the Carbonic Acid System in Seawater as a Function of pH

As CO_2 levels increase in the atmosphere, more CO_2 is dissolved in the ocean. The conversion of carbon dioxide to bicarbonate in the ocean increases the concentration of hydrogen ions which leads to a decrease in seawater pH, causing ocean acidification. But once bicarbonate is present in the ocean, it cannot easily outgas or be released back into the atmosphere as CO_2. While CO_2 can exchange between the atmosphere and the ocean surface through various physical and chemical processes, the conversion of CO_2 into bicarbonate in seawater represents a long-term storage mechanism for carbon. The majority of carbon that enters the ocean as CO_2 remains in the dissolved form of bicarbonate, contributing to the ocean's role as a carbon sink (Rau and Caldeira 1999, Rau et al. 2001, Isobe et al. 2002, Harvey 2008).

Seagrass takes bicarbonate out of the water and converts it to CO_2 for use in photosynthesis, which builds biomass. Work by Yates et al. (2015) has shown that seagrass beds can increase daytime pH values by 0.5 units, indicating the uptake of inorganic carbon during photosynthesis. This means that in addition to providing ecological and blue carbon benefits, seagrass beds can offset the impacts of ocean acidification caused by increased CO_2 in coastal waters (Unsworth et al. 2012).

1.4.2 Carbon Fluxes

Carbon fluxes refer to the movement or transfer of carbon between different carbon pools. The fluxes considered in this study are described below.

Seagrass Assimilation

Seagrass assimilates carbon through photosynthesis, converting CO_2 from the surrounding water into organic carbon compounds, such as sugars and carbohydrates. The equation below explains how seagrass uses sunlight, CO_2, and water (H_2O) to create glucose ($C_6H_{12}O_6$) and oxygen (O_2) as a byproduct.

$$6CO_2 + 6H_2O \xrightarrow{sunlight} C_6H_{12}O_6 + 6O_2$$

Assimilation rates (or productivity rates) measure how much carbon is moving from the water column to the seagrass biomass.

Sediment Sequestration

When seagrass leaves and other parts of the plant die or fall off, they may settle onto the sediment surface where they gradually accumulate over time. Once the organic matter reaches the sediment, a suite of biogeochemical processes contributes to its stabilization and burial. Microbial decomposition by bacteria and other microorganisms breaks down the organic matter, releasing carbon dioxide (which converts to bicarbonate) as a metabolic byproduct. However, as noted in Section 1.4.1, a portion of the carbon persists in the sediment due to factors such as anaerobic conditions (i.e., low oxygen levels) and the organic matter binding to mineral particles. As more organic matter accumulates and sedimentation occurs, the seagrass-derived carbon becomes further buried in the sediment, effectively sequestering it. This process enables the stored carbon to remain in the sediment for long periods, potentially lasting for centuries or even longer.

Bicarbonate Pathway

Sediments in seagrass beds generally have an organic content around 1 percent, whereas mangroves and salt marshes typically have higher organic content ranging from 20 to 80 percent (Burdige and Zimmerman 2002, Duarte et al. 2010, Fourqurean et al. 2012, Chmura et al. 2003). The fate of fixed carbon not exported to the deep ocean or washed ashore can be partially explained through the following equation (Burdige and Zimmerman 2002):

$$CH_2O + O_2 + CaCO_3 \quad \longleftrightarrow \quad Ca^{2+} + 2HCO_3^-$$

This equation explains one way that fixed carbon (CH_2O) in carbonate sediments ($CaCO_3$) can decompose within the oxygenated conditions facilitated by the rhizosphere at seagrass roots. The result of this process is the release of free calcium ions (Ca^{2+}) and the presence of previously fixed carbon in the form of bicarbonate ions (HCO_3^-). Smith (1981) identified this carbon sequestration to the water column in seagrass beds as the bicarbonate pathway. The bicarbonate pathway is believed to be the primary mechanism for carbon sequestration for seagrass beds – see

for example studies conducted in the Bahamas Banks (Burdige and Zimmerman 2002, Burdige et al. 2010) and Tokyo Harbor (Isobe et al. 2012).

1.4.3 Carbon Budget

Based on the principle of conservation of mass, a carbon budget can be used to quantify the fluxes and changes in carbon stocks within a system. A carbon budget allows researchers to quantify components of the system that may be difficult to measure directly and may be applied to understand how perturbations to the system (e.g., inputs or removals) may affect the carbon pools.

Figure 1-2 shows the carbon stocks discussed in Section 1.4.1 (aboveground biomass, sediment stock and belowground biomass, and bicarbonate in the water column) as well as the carbon fluxes (assimilation of carbon by seagrass, sequestration of carbon through burial in sediments, and sequestration of carbon through the bicarbonate pathway).

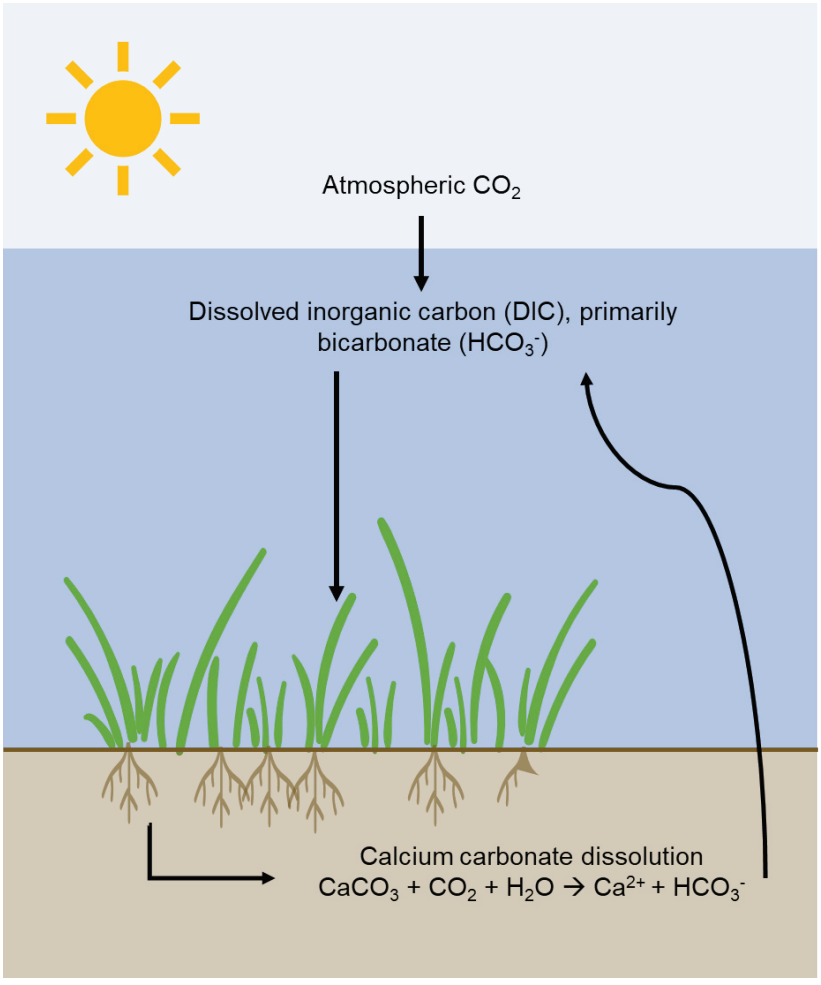

SOURCE: Adapted from Chou et al. 2021

D201800121.03 San Diego Bay Eelgrass Blue Carbon Study

Figure 1-2
Conceptual Model of Carbon Cycling in Seagrass Habitats

2. DATA COLLECTION AND LABORATORY METHODS

2.1 Sampling Scheme

Sites were selected to collect samples for the following analyses:

- Net aboveground productivity
    - Fall 2022 – at a site from Year 1 (Site F) and at a "fertilized" site located at the mouth of the Sweetwater River (Site M).
    - Spring 2023 – at Site F, Site M, and off the Coronado Golf Course drain into Glorietta Bay – Site K).
- Biomass (i.e., count, height and width, and carbon density)
    - Fall 2022 – at a site from Year 1 (Site F) and "fertilized" sites located at the mouth of the Sweetwater River (Site M), and off the Coronado Golf Course drain into Glorietta Bay – Site K).
    - Spring 2023 – at Site F, Site M, and off the Coronado Golf Course drain into Glorietta Bay – Site K).
- Sediment core dating (at two locations from Year 1 and at a site with no eelgrass)
- Grain size (for all coring sites)
- Sediment carbon (at a site with no eelgrass and two sites restored in the 1990s)
- Water quality (pH, dissolved oxygen, turbidity, and temperature)

Figure 2-1 shows the different locations where sampling occurred in order to characterize the carbon storage across the environmental variables. Note that sample locations A-I were sampled in Year 1, and Year 2 samples start with Site K.

SOURCE: ESA, Merkel & Associates

NOTE: Site locations are approximate.

D201800121.03 San Diego Bay Eelgrass Blue Carbon Study

Figure 2-1
Years 1 and 2 Sampling Sites

ESA

Sites were chosen for each parameter based on their characteristics, which are described in Table 2-1. Where possible, samples were taken to overlap with the established eelgrass survey transects to allow for extrapolation to the longer bay-wide eelgrass dataset, which spans spatially over all five ecoregions and temporally from 1987-2020 (Merkel & Associates 2020).

TABLE 2-1
YEAR 2 SAMPLE LOCATION SUMMARY

Location	Cores Collected	Biomass/ Productivity Sampling	Description	Ecoregion	Species
C	2 (1 sediment dating and 1 grain size)		Year 1 site for carbon analysis	North	*Zostera marina*
F	2 (1 sediment dating and 1 grain size)	Yes	Year 1 site for carbon analysis	South	*Zostera marina*
K	None	Yes	Fertilized site – Drain outlet at Glorietta Bay	South-Central	*Zostera marina*
L	4 (3 sediment carbon, 1 grain size)		NEMS 6	South-Central	*Zostera marina*
M	None	Yes	Mouth of Sweetwater River	South	*Zostera marina*
N	4 (3 sediment carbon, 1 grain size)		Loews Coronado	South	*Zostera marina*
O	5 (3 sediment carbon, 1 sediment dating, 1 grain size)		Outside Eelgrass Beds	South	*Zostera marina*

2.2 Biomass

2.2.1 Biomass Carbon

Biomass samples were taken at 3 different depths (-2, -4, and -6 feet MLLW) for three sampling sites (Sites F, K, and M). Sites K and M were identified as sites “fertilized” by greater bird presence and proximity to storm drains that carry pollution and nutrients from the watershed. Site F was sampled as a control, assuming it was not receiving a higher amount of nutrients compared to the other sites. Biomass carbon was measured by determining shoot density and shoot biomass, then measuring for organic carbon content using an elemental analyzer.

Due to the extremely small plants encountered in 2021 and 2022, sampling in spring 2023 was performed to repeat the biomass measurements. However, several adjustments were made to compensate for small plant sizes that neared the minimum laboratory analysis size and to address shoot density variability. Biomass was determined at the shoot level considering all tissue from the meristem at the root-shoot interface to the top of the shoot. While flowering was very sparse in the beds, no flowering stalks were included in the biomass totals. Six replicates of 10 random shoot collections at each site and elevation were used to determine dry weight and carbon content. All data were standardized to biomass per shoot.

These collected shoots were sent to Wallace Laboratories for carbon content analysis. The samples were dried at 70 degrees Celsius (as low as possible to reduce loss of carbon) to measure the plant biomass. The samples were then measured for organic carbon content using an automated elemental analyzer. The resulting values were divided by 10 to determine the average carbon per shoot. These were then multiplied by the mean shoot density per square meter to develop a mean carbon mass per square meter of aboveground plant tissue.

2.2.2 Eelgrass Productivity

Quantifying net aboveground productivity, in conjunction with measuring biomass carbon fractions, can help provide insight into the rate of carbon uptake by the eelgrass plants. By sampling at different depths (i.e., different light availability) or in areas of varied nutrient availability, these variables and their influence on eelgrass productivity can be tested. Productivity was estimated by the procedure established in Tomasko et al. (2001) and others by measuring the distance between a puncture mark made to the blade-sheath junction relative to the upward growth the inner blade over the experimental period.

During fall 2022, this procedure was implemented for 15 individual shoots at the 3 elevations for 3 sites. Using a hypodermic needle, the blades were punched at the blade-sheath junction of the oldest intact blade (Tomasko et. al 2001). At the end of the sampling effort, previously marked shoots were collected, and the newly formed blade material was visually identified by the upward displacement of the needle mark, compared to the "reference" hole from the oldest intact blade. This new material and the old material were then separated, and the area of the new blade material and total blade material was quantified. Narrow-leaved plants have extremely low leaf marking success due to leaf breakage in marked plants. For this reason, productivity investigations targeted larger plants.

Due to the extremely small plants encountered in 2021 and 2022, sampling in spring 2023 was performed to repeat the productivity measurements. The same protocols were applied, except that additional temporary flagging was placed adjacent to marked plants to facilitate relocation for collection.

2.3 Sediment

2.3.1 Sediment Carbon

Triplicate sediment carbon cores were collected at sites L, N, and O (Figure 2-1, Table 2-1) for a total of 9 cores. Cores were taken to 1-meter depth or to refusal (i.e., where the core cannot be pushed any further). Carbon content typically varies most in the upper 20 cm to half-meter (Fourqurean et al. 2012), but sampling deeper cores allowed further exploration of carbon patterns with depth. The cores were subsampled on-site with one sample per 10-cm interval for the top half meter and one for the bottom 50 centimeters. Samples were sent to Weck Laboratories (City of Industry, CA) to analyze dry bulk density and organic carbon content. The samples were held in refrigerators or on ice to minimize decomposition before they were sent to laboratories for analysis.

At the lab, the volume of the samples was measured and the samples were dried at 60 degrees Celsius (as low as possible to reduce loss of carbon) to measure the mass of the dry sediment. This was used to determine the dry bulk density (g/cm^3), defined as the mass of dry sediment divided by the wet sample volume. The samples were then measured for total organic carbon (TOC) content using an automated elemental analyzer.

2.3.2 Grain Size

Core surface samples from all Year 1 sites were sent to a laboratory for sieve analysis to determine sediment texture and grain size. Additional surface samples were collected at selected sites in Year 2 to serve as replicates (for those sites that overlap with Year 1 – C and F) or to expand the dataset further (Sites L, N, O).

To obtain sufficient sample size from the leftover Year 1 samples, the 0-10-cm subsamples were aggregated from the three cores taken from each site. D-2 was chosen to represent Site D (which was sampled at three different depths, i.e., D-1 (shallow), D-2 (mid), D-3 (deep). In Year 2, one larger grab sample was taken to represent the surface sediment at each site. In this way, sediment samples from both years are assumed to be representative across each site, regardless of the individual cores that provide finer-scale data for bulk density and carbon content.

Samples from both years were sent to Wallace Laboratories (El Segundo, CA) for a full grain size distribution assessment using a sieve analysis. Shelly material was removed prior to sieving. Results were analyzed and correlated to the carbon content results for each site.

2.3.3 Radioisotope Dating

One core was collected at each of the three locations specified in Table 2-1 for radioisotope dating. Sediment cores were collected using a vibracore down to 1-meter depth at each location. These cores were subsampled at 1-cm intervals in the top 20 cm, then at 2-cm intervals for the next 20 cm, and finally at 5-cm intervals down to the bottom of the core. These subsamples were then sent to Flett Research, Ltd. (Winnipeg, Canada) for radioisotope dating via Pb-210, Ra-226, and Cs-137 analyses, and to develop age versus depth profiles where applicable. The following description of methodology was provided by Flett Research Ltd.

The Pb-210 method is used to determine the accumulation rate of sediments in lakes, oceans, and other water bodies. In a typical application, the accumulation rate over a period of 100 - 200 years is obtained. From the accumulation rate, the age of sediment from a particular depth in the sediment column can be estimated.

Pb-210 is a naturally occurring radioactive element that is part of the uranium-238 radioactive decay series. The radioactive element uranium has an almost infinite half-life (4.5×10^9 years) and for these purposes can be considered to be present at an unchanging concentration (over time) in the earth's crust. Although the concentration of uranium varies from location to location, it is present in essentially all soils and sediments, at least at some low level. Over time the uranium-238 very slowly decays into uranium-234 (half-life = 248,000 years), which decays into thorium-230 (half-life = 80,000 years), which decays into radium-226 (half-life = 1,620 years). Radium-

226 in the soil exhibits the same level of radioactivity as uranium-238 from which it was originally derived, because of a natural phenomenon called secular equilibrium[1]. The overall result is that radium-226 is found at low and essentially unchanging levels in soils everywhere.

When radioactive radium-226 decays, it produces the radioactive inert gas radon-222 (half-life = ~ 3.8 days). If radon is produced in soils close to the air-soil interface, some of the radon gas can escape to the atmosphere before it decays into the next radioactive element (a nonvolatile metal). This radon emanation is a normal occurrence and thereby causes the terrestrial atmosphere to contain a low (~1 disintegration per minute per litre or DPM/L) but fairly constant level of radioactive gas. After several days' residence time in the atmosphere, the Rn-222 naturally decays to polonium-218, a metallic radionuclide which, over a period of hours/days, falls to the earth with dust and rain. A number of subsequent radioactive decays occur over a period of minutes and Pb-210 (half-life = 22.3 yr) is produced. The Pb-210 which falls into a lake or ocean tends to end up in the sediments over the next few months and becomes permanently fixed on the sediment particles. Within 2 years, polonium-210 (Po-210), the granddaughter of Pb-210, is in secular equilibrium (i.e., the same activity) with the Pb-210. It is actually the alpha emitting Po-210 that is measured because it provides more accurate estimates of the Pb-210 than do direct measurements of Pb-210.

The measured Pb-210 activity (total Pb-210) is the sum of the atmospheric sourced Pb-210 (unsupported Pb-210) AND the Pb-210 originating from Ra-226 originally present in the sediment (supported Pb-210). The supported Pb-210 is usually a minor component of the total Pb-210 and has the same activity as the Ra-226 from where it was derived. The Ra-226 is typically measured (via emanation) at several depths in each core and the activity from the total Pb-210 is subtracted to obtain the unsupported Pb-210 activity. It is the unsupported Pb-210 which is required to calculate the age and sediment accumulation rates.

When applying the Pb-210 technique, it is assumed that sediments at a core site are receiving a constant input of Pb-210 from the atmosphere. Pb-210 that was incorporated into the sediments 22.3 years ago will be only one half as radioactive as when initially deposited. This property of radioactive decay can be used to calculate the age of sediments at other depths in the sediment column and/or the rate of sediment accumulation.

Cs-137 is an artificial radioactive isotope of cesium that was introduced into the environment primarily as a result of nuclear weapons testing and nuclear accidents, such as the Chernobyl disaster. As a result of atmospheric nuclear weapons testing, the annual deposition of Cs-137 peaked in 1963 in the Northern Hemisphere. Although the annual deposition of Cs-137 dropped dramatically in the following years (post-1963), the cumulative deposition of Cs-137 slowly increased and reached the maximum value in 1966, and thereafter the inventory of Cs-137 gradually decreased due to radioactive decay. Cs-137 activity is measured by gamma spectrometry, and it is used as an independent tracer to validate the Pb-210 dating results.

[1] Secular equilibrium refers to a state in which the rate of production of a particular radioactive isotope is equal to its rate of decay. In other words, the amount of the parent isotope being produced (through a decay chain) is balanced by the rate at which it decays into its daughter isotopes.

2.4 Water Quality

Continuous water quality data (i.e., pH, dissolved oxygen (DO), turbidity, and temperature) were collected from October 2022 – January 2023 and from March – May 2023 at two locations: one inside an eelgrass bed and one outside an eelgrass bed (Figure 2-2). Data were collected on an hourly basis using AquaTroll multiparameter sondes set up in South San Diego Bay just offshore of the Chula Vista Wildlife Reserve. Sondes were calibrated prior to deployment and drift checks were performed for QA/QC within 24 hours of instrument retrieval from the site. Note that during the initial deployment from October 2022 – January 2023, one of the pH sensors unexpectedly malfunctioned, so pH data is not reported for this time frame.

Data were used to analyze the potential effects on water quality caused by the eelgrass bed. Continuous DO measurements were used to estimate the amount of primary productivity from sources other than eelgrass such as phytoplankton. These estimates of productivity were compared to the estimate developed from productivity sampling, which are based on eelgrass alone.

SOURCE: ESA 2023

NOTES: EG-IN is within an eelgrass bed, and EG-OUT is outside of an eelgrass bed

D201800121.03 San Diego Bay Eelgrass Blue Carbon Study

Figure 2-2
Target Locations for Sonde Deployment

This page intentionally left blank

3. RESULTS

3.1 Biomass Carbon Pool

While the Year 1 study compared productivity and biomass across the Bay, the Year 2 study focuses on the hypothesis that eelgrass may be larger in areas closer to sources of nutrient input into the Bay. As discussed in the Year 1 study (Appendix A), while the coverage of eelgrass is quite extensive spatially, the individual plants are small.

3.1.1 Biomass Carbon

Canopy Height and Biomass

During the Year 1 study and through long-term observations leading up to the present investigations, it has been noted that the eelgrass canopy height and leaf width have been shrinking over the past several years in San Diego Bay and other low influx bays of southern California. Unfortunately, these metrics have not been regularly tracked and thus anecdotal observations and non-targeted incidental monitoring provide only limited insight into the extent of eelgrass bed change. During the 1990s through at least the early 2010s, the eelgrass canopy throughout most of the subtidal depths of the South and South-Central Bay was typically about 500 – 700 mm in height (K. Merkel, pers. obs.). It is hypothesized that the shrinking canopy height and leaf width is associated with the long-term drought and a reduced nutrient supply being discharged to the bay.

However, the sampling results show that the reference site (Site F, 480 ± 121 mm) was substantially taller than either of the enriched sites, Sweetwater River (Site M, 248 ± 72 mm) or Glorietta Bay (Site K, 276 ± 117 mm) (Figure 3-1), indicating greater bird presence and proximity to storm drains may not be providing missing nutrients. Further, none of the eelgrass was very tall, with the overall average canopy height being only 335 ± 148 mm. This is due to an overall short stature across all beds, despite wide variability in height across sites (Figure 3-1; error bars in figure below and across report show +/- one standard deviation).

The recent 2022-2023 winter that resulted in 143% of the average annual precipitation should begin increasing nutrient loads in the bay and would be expected to stimulate eelgrass growth. In Year 1, Site F had an average canopy height of 310 mm, so eelgrass was substantially taller in Year 2. However, the more open bay reference site (Site F) is approximately twice the size in both average height and biomass (Figure 3-2) as the enriched sites.

Interestingly, the typical pattern of deeper eelgrass tending to be taller was only observed at Glorietta Bay. Average shoot biomass follows the pattern of the average canopy height with the reference site (Site F) typically having greater dry weight biomass than either of the enriched sites (Figure 3-2).

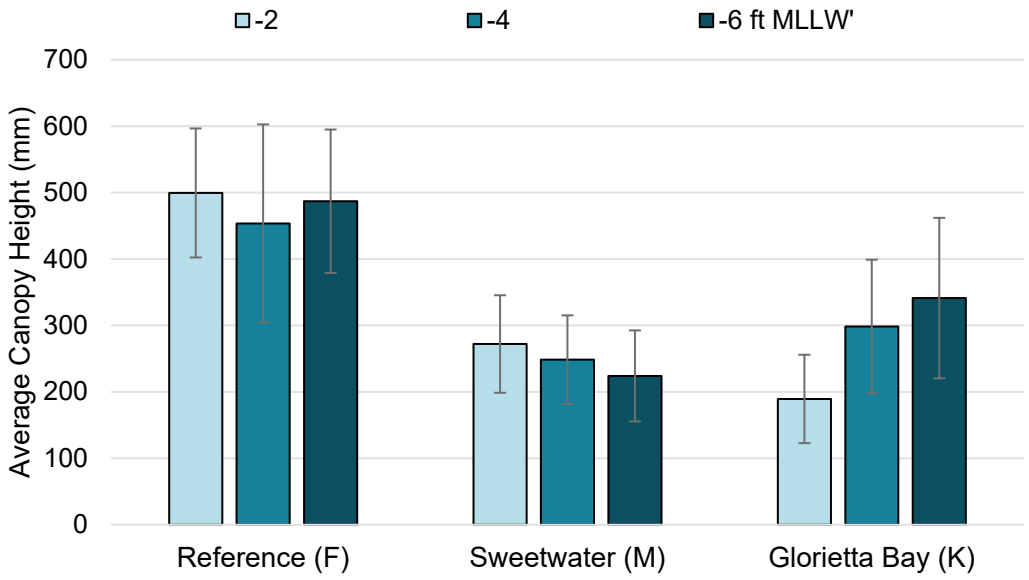

SOURCE: Merkel and Associates 2023

D201800121.03 San Diego Bay Eelgrass Blue Carbon Study

Figure 3-1
Eelgrass Canopy Height - April 2023

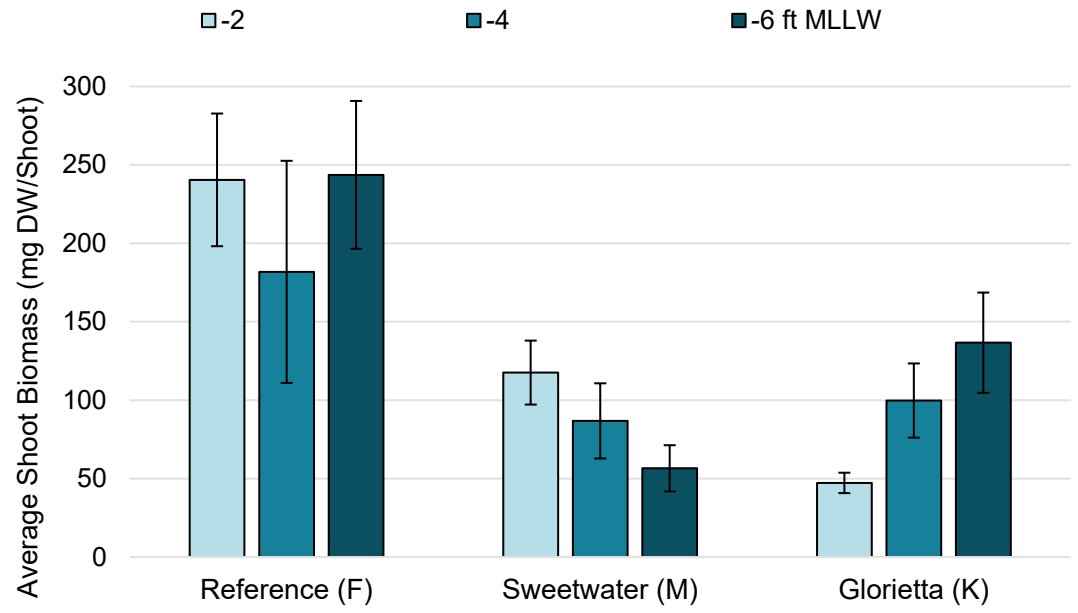

SOURCE: Merkel and Associates 2023

D201800121.03 San Diego Bay Eelgrass Blue Carbon Study

Figure 3-2
Eelgrass Biomass - April 2023

Carbon Content

Biomass carbon content, or carbon density, was analyzed both during Year 1 and Year 2 at the -2-foot elevation of Site F. The Year 1 carbon content at Site F was 27.7 ± 0.02% dry weight compared to 30.26 ± 0.01% dry weight during Year 2. The carbon content varies across sites and depths (Figure 3-3), with an average of 32.07 ± 1.30% dry weight across all sites and elevations.

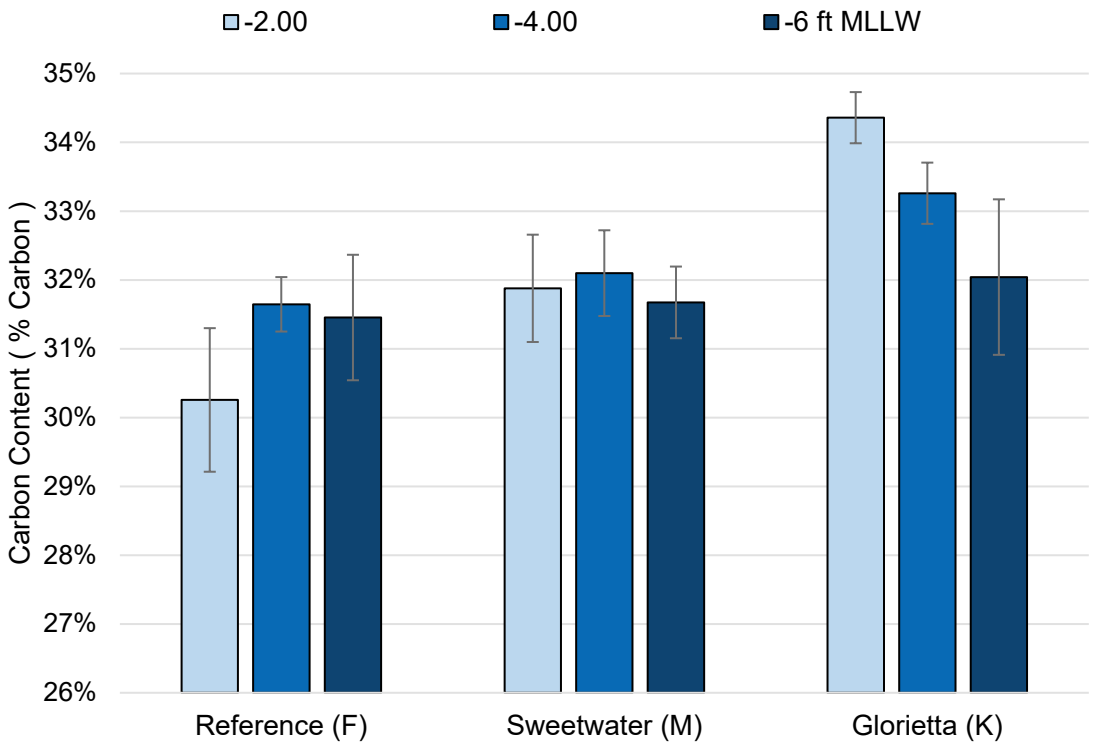

SOURCE: Merkel and Associates 2023

D201800121.03 San Diego Bay Eelgrass Blue Carbon Study

Figure 3-3
Aboveground Biomass Carbon Content - April 2023

Carbon Stock

Aboveground biomass (Figure 3-5) was determined by multiplying shoot density (Figure 3-4) by average shoot biomass and the percent carbon content for each site and elevation. The analysis identified substantive differences in aboveground carbon stock across sites. The reference site (Site F) had a significantly higher above ground carbon density than Glorietta Bay (Site K) and nearly significantly higher content than Sweetwater (Site M), ($p=0.02$ and $p=0.06$, respectively). Aboveground carbon was not significantly different between Sweetwater (Site M) and Glorietta Bay (Site K) ($p=0.42$). As a result of inconsistent trends in carbon stock across depths, no significant differences were noted between depths as explored by serial t-tests.

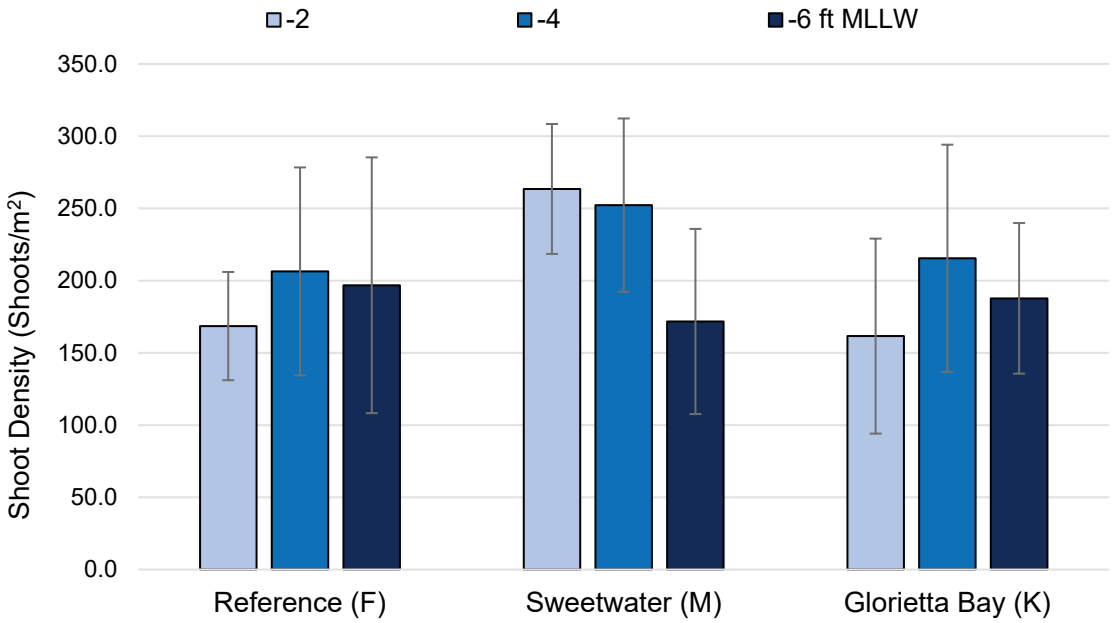

SOURCE: Merkel and Associates 2023

D201800121.03 San Diego Bay Eelgrass Blue Carbon Study

Figure 3-4
Shoot Density - April 2023

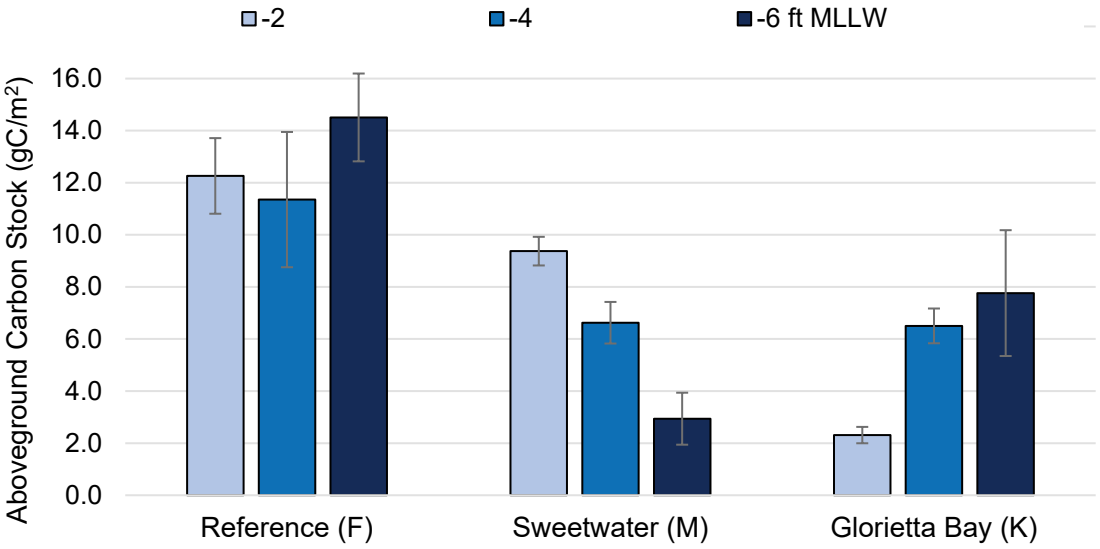

SOURCE: Merkel and Associates 2023

D201800121.03 San Diego Bay Eelgrass Blue Carbon Study

Figure 3-5
Aboveground Carbon Stock - April 2023

Overall, the pattern of aboveground carbon stock followed that of canopy height and biomass. However, while the reference site (Site F) canopy was taller and the biomass proportionally greater than at both the Sweetwater River (Site M) and Glorietta Bay (Site K) sites, slightly higher carbon content within the Glorietta Bay and slightly higher shoot densities at Sweetwater River resulted in a modest degree of mitigation of aboveground carbon stock (Figure 3-5).

The standing stock of carbon within the eelgrass canopy averaged 8.25 ± 0.04 g C /m^2 in April 2023. Standing stock turns over regularly with leaves growing out and being removed by consumption, breakage and shed, or attached senescence and local decay. Some portion of the canopy grown ultimately makes its way to sediment integration, either locally or along the shorelines and in marshes. However, much of the carbon in the canopy is only very temporarily sequestered. As a result, the canopy provides a dynamic carbon pool subject to flux in bed conditions. For this reason, evaluating the stored carbon in the canopy biomass must be based on canopy condition through time rather than seasonal highs and lows of biomass associated with seasonal cycles (Oreska et al. 2017). The present standing stock estimates were completed in April, a month into the recognized eelgrass high growth season in the San Diego region, and thus does not constitute either the peak canopy condition of mid-summer or the low of winter. It is believed that the conditions reflected in the eelgrass canopy standing stock represent a good estimator of the average condition of the canopy throughout the year.

3.1.2 Eelgrass Productivity: Variations Across Sites

As noted in the methods section, due to the small size of plants limiting the capacity to mark shoots without resulting in damage so severe as to cause breakage, larger plants were preferentially sought out for the productivity analysis. It is not known if the plant size selection for practical sampling purposes skews the results. However, for canopy height, biomass, and density metrics associated with standing stock, the larger shoots that were preferentially targeted for effective productivity measurement were not used.

In total, 135 shoots were marked (15 each at 3 sites and 3 elevations). Of these, 85 were ultimately processed to assess productivity. A few marked plants were not relocated for collection, and many were determined to be damaged to the extent that growth could not be adequately assessed. The number of sample shoots that were ultimately recovered and analyzed ranged from 7 to 10 per individual depth station per site with 26-30 samples analyzed per site. This provides a good overall estimator for productivity of the bed and an acceptable estimate of productivity within individual depth strata.

The dry weight productivity, measured carbon content, and mean shoot and areal productivity rates are provided in Table 3-1. The productivity was examined both at the shoot level and at a spatial level considering eelgrass shoot density per square meter. When examining the overall mean of all samples, shoot productivity was determined to be 3.0 ± 0.6 mg C/shoot/day (n=85). It was also possible to explore year-to-year differences on a limited scale by comparing productivity at the Sweetwater site which was sampled in May 2022 during the Year 1 study and April 2023 during this Year 2 investigation. The productivity at the same sampling site and elevation (-2 feet) in 2023 was down approximately 55% from 2022, falling from 1.98 ± 0.83 mg/shoot/day to 0.90

± 0.09 mg/shoot/day. Between 2022 and 2023, the areal productivity also fell by 33% from an overall mean of 327.89 ± 137.10 mg/m^2/day to 219.31 ± 22.29 mg/m^2/day. This productivity difference points to high interannual variability and, potentially, differences in growth rates at the beginning of the growing season (May vs. April). It may be prudent to examine the productivity of beds through the year to develop seasonal curves providing a better estimator of productivity integrated over time. Estimates presented in this study should be considered a rough estimate, as they capture just a single moment in time.

The average turnover rate, which is calculated as the daily leaf biomass production divided by the total shoot biomass and is reported as a percentage of the leaf turned over per day, was 0.9 percent. This means that each shoot is estimated to turn over approximately 3.3 times per year, based on the spring sampling period's rate. In mid-growing season, turnover rate is expected to be higher, while during the low growth winter period, the rate would be expected to be much lower.

TABLE 3-1
EELGRASS PRODUCTIVITY FOR SPRING 2023 SAMPLING PERIOD

Site and Depth Strata	Newly Formed Leaf Material (mg dw /shoot/day)	Newly Formed Leaf Material (mg dw /shoot)	Total Shoot Material (mg dw /shoot)	Turnover Rate (% / day)	Leaf Carbon Content (%)	Shoot Carbon Production (mg C / shoot / day)	Areal Carbon Production (mg C /m^2 / day)	Estimated Annual Areal Carbon Production (g C/m^2/yr)
Site F	0.86	12.1	89.2	1.0%	31.1%	0.27±0.05	54.92±13.23	20.0
-2	0.82	11.6	72.4	1.2%	30.3%	0.25±0.03	42.88±5.02	15.7
-4	0.96	13.5	87.3	1.1%	31.6%	0.30±0.04	67.33±8.80	24.6
-6	0.81	11.3	107.8	0.8%	31.5%	0.25±0.05	54.54±11.37	19.9
Site M	0.93	12.1	116.9	0.8%	31.9%	0.30±0.05	64.94±10.69	23.7
-2	0.90	11.7	103.4	0.9%	31.9%	0.29±0.03	69.96±7.11	25.5
-4	0.86	11.0	116.2	0.7%	32.1%	0.27±0.04	68.70±9.70	25.1
-6	1.03	13.4	126.9	0.8%	31.7%	0.33±0.06	58.05±10.67	21.2
Site K	1	12.0	131.1	0.8%	33.3%	0.33±0.06	67.35±13.46	24.6
-2	1.06	12.7	106.4	1.1%	34.4%	0.36±0.05	65.69±8.94	24.0
-4	1.06	12.7	139.0	0.8%	33.3%	0.35±0.06	77.82±12.24	28.4
-6	0.87	10.4	149.9	0.6%	32.0%	0.28±0.05	57.57±11.28	21.0
Overall	0.93	12.1	112.0	0.9%	32.1%	0.30±0.06	62.23±13.61	22.7

Fertilized and Unfertilized Sites

Sites selected based on expectations of greater nutrient loading (Site M near the mouth of the Sweetwater River, and Site K near a golf course storm drain in Glorietta Bay) had slightly higher productivity rates than the reference site, Site F, which is a more open bay environment but still near the seasonal drainage of Telegraph Creek (Figure 3-6). Differences in productivity by site were found to be significant ($p<0.01$) using a single factor ANOVA.

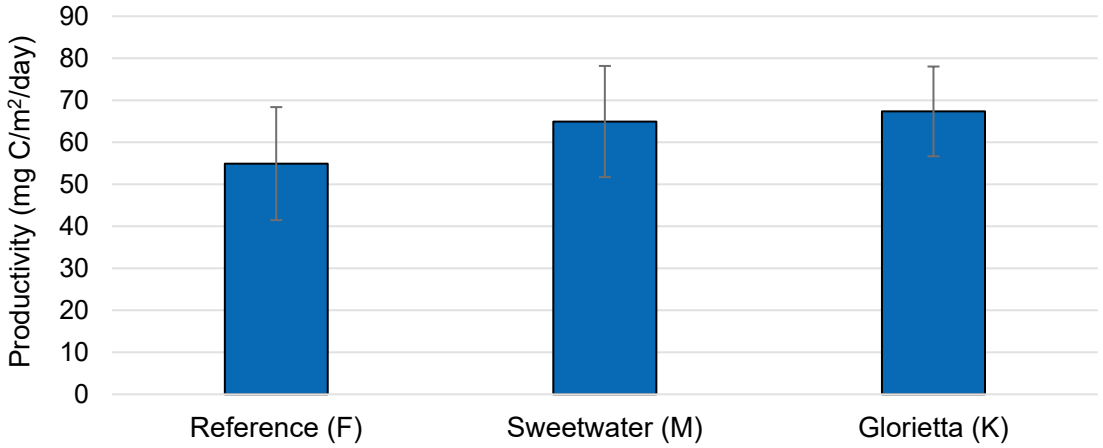

SOURCE: Merkel and Associates 2023

D201800121.03 San Diego Bay Eelgrass Blue Carbon Study

Figure 3-6
Productivity Rate Across All Sites - April 2023

Depth

Conceptually, seagrass at greater depth receives less sunlight, leading to lower productivity, while shallower elevations may experience increased wave energy and occasional drying out. Figure 3-7 shows the productivity is highest at the middle elevation (-4 ft MLLW) sampled within Year 2 seagrass beds, which fits the expected relationship. Differences in productivity by elevation were found to be significant ($p<0.01$) using a single factor ANOVA. Eelgrass exists at a range of depths, so this pattern suggests that San Diego Bay's eelgrass, given current conditions, may be more productive at shallow mid-bed elevations. However, with the progression of sea-level rise, the proportional distribution of bed area is expected to shift with a diminishing extent of the bed occurring in these mid-shallow depths and more of the beds occurring at deeper elevations. This may result in a substantial decrease in overall eelgrass productivity, even if eelgrass persists.

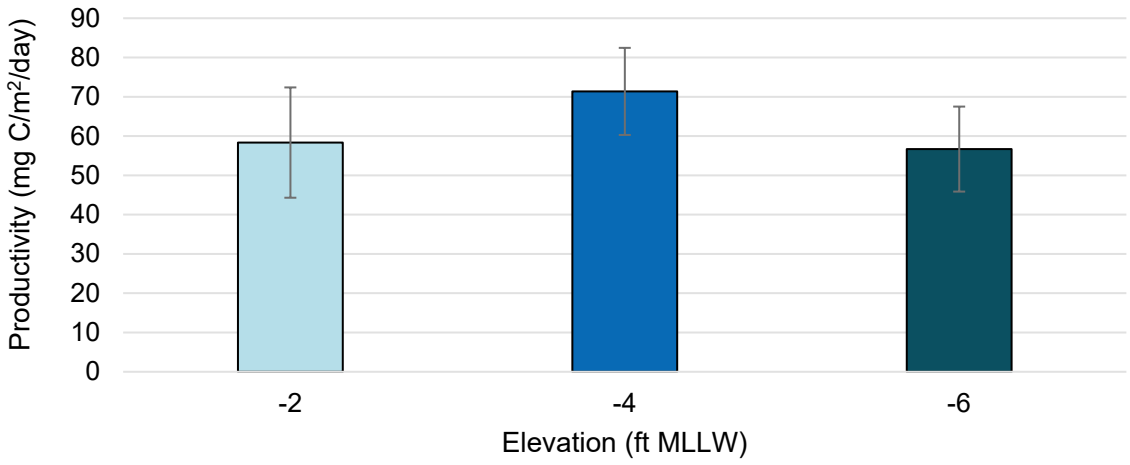

SOURCE: Merkel and Associates 2023

D201800121.03 San Diego Bay Eelgrass Blue Carbon Study

Figure 3-7
Productivity Rate Across Depths - April 2023

3.2 Sediment Carbon Pool

The sediment carbon content was determined based on bulk density and organic matter (OM) content found in each of the samples within a core. Several terms are commonly used in the study and quantification of blue carbon, including the following:

- **Bulk density:** This describes the mass of sediment per unit volume (i.e., grams of sediment per cm^3 [g/cm^3]). This is used in conjunction with the measured organic carbon percentage to determine the carbon density.
- **Organic carbon percentage:** This describes the mass of carbon per the mass of sediment in a sample (i.e., grams of carbon per grams of sediment [g C/g sediment] as a percentage).
- **Sediment carbon density:** This describes the amount of carbon per volume of sediment (i.e., grams of carbon per cm^3 [g C/cm^3]). It is calculated by multiplying bulk density (g/cm^3) and the organic carbon percentage (g C/g sediment).
- **Total carbon per sample:** This term describes the mass of carbon (in grams) contained in the sampling interval or entire core. It is expressed on a per-surface area basis (i.e., g C/cm^2) to allow for spatial extrapolation. It is calculated by multiplying the sediment carbon density (g C/cm^3) by the sample thickness (cm). Note the distinction between carbon density and total carbon per sample: *carbon density* is a per volume metric (i.e., is not dependent on sample thickness/size), while *total carbon per sample* is affected by the size of the sample. For example, a 0.1-meter sample may have more carbon mass than a 0.5-meter sample because the sediment carbon density is greater in the shorter sample.

3.2.1 Belowground Carbon Content

Table 3-2 provides the elevations at which the sediment cores were taken, the core lengths, the average bulk density, average organic carbon percentage, average sediment carbon density, and total carbon within each core. For depth profile plots of the complete dataset, see Appendix B.

Bulk densities for sediments in *Z. marina* beds vary between 0.71 and 1.4 g/cm^3 in the literature (Dahl et al. 2016; Kauffman et al. 2020) and between 0.89 and 1.63 g/cm^3 in San Diego Bay, based on the Year 1 and 2 study results. Sites L and N had average bulk densities greater than the range of bulk densities found in Year 1 (1.57 g/cm^3 and 1.51 g/cm^3, respectively compared to the Year 1 range of 0.89 to 1.47 g/cm^3) and the literature values.

Dahl et al. (2016) reported average sediment carbon contents between 0.05 and 0.35 g/cm^2 for *Z. marina* eelgrass beds in Europe, compared to the lab results from Years 1 and 2 that showed a range from 0.02 to 1.08 g/cm^2 in San Diego Bay (note that samples with undetectable carbon were assumed to have none). Site O, which was not in a *Z. marina* bed, had a higher average sediment carbon (1.5 g/cm^2) than all other sites. This may be due to the location of the site in a channel where organic material may settle out at the bottom of the bay.

TABLE 3-2
MEASURED SEDIMENT DATA

Site	Core	Sample Elevation (m NAVD)	Core Length (m)	Average Elevation (m NAVD)	Bulk Density (g/cm^3)	Organic Carbon Percentage	Sediment Carbon Density (gC/cm^3)	Total Carbon in 1-m Core (MgC/ hectare)
A	1	-2.1	1	-2.1	1.06	0.07%	0.0007	7.3
	2	-2.1	1		1.04	0.06%	0.0006	6.2
	3	-2.2	1.5		1.02	0.05%	0.0005	5.7
B	1	-1.3	1	-1.3	1.08	0.09%	0.0010	9.6
	2	-1.3	1		1.28	0.12%	0.0015	15.1
	3	-1.2	1		1.12	0.09%	0.0011	10.6
C	1	-2.0	1	-2.0	1.10	0.67%	0.0071	71.1
	2	-2.0	1		1.23	0.23%	0.0027	27.4
	3	-2.0	1		0.97	0.55%	0.0048	48.5
D-1	1	-0.3	1	-0.4	0.89	0.17%	0.0016	15.9
	2	-0.4	1		1.18	0.18%	0.0021	21.0
	3	-0.3	1		1.22	0.09%	0.0011	10.7
D-2	1	-1.5	1	-1.6	1.44	0.27%	0.0041	40.8
	2	-1.6	1		1.47	0.26%	0.0038	38.4
	3	-1.6	1		1.34	0.21%	0.0028	27.6
D-3	1	-2.2	1	-2.2	1.28	0.13%	0.0017	8.5
	2	-2.2	1		1.44	0.58%	0.0088	87.9
	3	-2.2	2		1.18	0.13%	0.0018	32.7
E	1	-1.5	1	-1.5	1.22	0.40%	0.0043	42.9
	2	-1.5	1		1.31	0.44%	0.0050	50.1
	3	-1.5	2		1.23	0.22%	0.0024	40.9

TABLE 3-2 (CONTINUED)
MEASURED SEDIMENT DATA

Site	Core	Sample Elevation (m NAVD)	Core Length (m)	Average Elevation (m NAVD)	Bulk Density (g/cm^3)	Organic Carbon Percentage	Sediment Carbon Density (gC/cm^3)	Total Carbon in 1-m Core (MgC/ hectare)
F	1	-1.1	1	-1.4	1.11	0.78%	0.0087	86.9
	2	-1.1	1		1.18	0.85%	0.0099	99.3
	4	-2.0	2.5		1.20	0.68%	0.0076	107.9
G	1	-1.1	1	-1.2	1.32	0.01%	0.0002	1.9
	2	-1.1	1		0.99	0.02%	0.0002	2.2
	3	-1.3	1		1.05	0.02%	0.0002	2.4
H	1	-1.9	1	-1.8	1.31	0.19%	0.0020	20.4
	2	-1.8	1		1.16	0.11%	0.0011	11.1
	3	-1.6	1		1.09	0.13%	0.0015	15.2
I	1	-2.7	1	-2.6	1.36	0.20%	0.0025	24.7
	2	-2.6	1		1.24	0.31%	0.0038	37.7
	3	-2.5	1		1.42	0.14%	0.0018	17.9
J	1	-0.9	1	-0.9	1.07	0.76%	0.0080	79.5
	2	-1.0	1		1.13	0.79%	0.0087	87.2
	3	-1.0	1		1.23	0.77%	0.0094	94.5
L	L01	-1.5	1.0	-1.5	1.50	0.11%	0.0017	16.5
	L02	-1.5	1.0		1.57	0.06%	0.0010	10.4
	L03	-1.5	1.0		1.63	0.08%	0.0013	12.7
N	N01	-3.7	1.0	-3.7	1.51	0.22%	0.0032	31.9
	N02	-3.7	1.0		1.52	0.20%	0.0029	28.9
	N03	-3.7	1.0		1.49	0.25%	0.0036	36.0
O	O01	-5.2	1.0	-5.1	1.10	1.32%	0.0145	144.9
	O02	-5.0	1.0		1.07	1.22%	0.0130	130.3
	O03	-5.0	1.0		1.22	1.27%	0.0156	155.8

NOTES:

Values for sites A-J for bulk density, organic carbon percentage, and sediment carbon density differ slightly from the values presented in the Year 1 study. Previously, the average values for each core were calculated by averaging all of the subsample values equally. The values above were calculated using a weighted average based on the length of the sample (i.e., samples with a length of 50 cm, contributed more to the core's average bulk density than samples with a length of 10 cm). This does not change the resulting total carbon which is based on the sum of the carbon densities of each sample (rather than the average) multiplied by the sample length.

3.2.2 Variation Across Sites

In the Year 1 study, the variation in blue carbon was compared between species (*Z. marina* and *Z. pacifica*), between ecoregions, among bed depths, and by bed age. This Year 2 study provides additional data on bed age and considers blue carbon variation between vegetated and unvegetated sites and grain size and summarizes average sediment carbon by site for the top one meter of sediment.

The average carbon in the top one meter ranged from 2 to 98 Mg C/ha across all sites in seagrass beds. This is comparable to the large range found in literature. For example, Dahl et al. (2016)

measured belowground carbon in *Z. marina* beds in Europe and found total carbon from 5 to 35 Mg C/ha, while Kauffman et al. (2020) found 216.3 Mg C/ha of belowground carbon in *Z. marina beds* in the Pacific Northwest. Table 3-3 and Figure 3-8 show the average sediment carbon in the top 1-meter of sediment across the bay.

TABLE 3-3
EELGRASS SEDIMENT CARBON BY SITE

Site	Carbon to 1-m depth (Mg C/ha)
A	6.4 ± 0.8
B	11.8 ± 3.0
C	49.0 ± 21.9
D*	35.6 ± 7.0
E	44.6 ± 4.8
F	98.0 ± 10.5
G	2.2 ± 0.3
H	15.5 ± 4.6
I	26.8 ± 10.1
J	87.1 ± 7.5
L	13.2 ± 3.1
N	32.3 ± 3.5
O	143.7 ± 12.8

NOTES:
* This is Site D-2 from Year 1.

An ANOVA test was performed on the top-meter carbon across all sites, and the results revealed significant differences at the $\alpha=0.01$ level (i.e., $p<0.01$). The ANOVA test analyzes the variance between the means of the sites and within each site, and a significant finding indicates that the variations in the data are not due to random chance but rather are likely attributable to genuine disparities among the sites. However, the ANOVA test does not identify which specific sites are statistically significant from each other. To identify which specific sites show statistically significant differences, additional post hoc tests are required. The Tukey test was used to compare all possible pairs of site means and to determine if two sites are significantly different from each other at the chosen significance level ($p < 0.05$). Results are reported in the following sections.

SOURCE: ESA, Merkel & Associates

NOTE: Site locations are approximate.

D201800121.03 San Diego Bay Eelgrass Blue Carbon Study

Figure 3-8
Total Carbon in 1-m Core (MgC/hectare)

ESA

Vegetated and Unvegetated Sites

Site O was sampled to assess how much carbon (if any) is found in unvegetated areas of the bay. Since eelgrass beds use photosynthesis to convert carbon in the water to biomass which is then incorporated into the sediments, sites in eelgrass beds typically have higher carbon than sites that are unvegetated (Dahl et al. 2016). However, Site O (unvegetated) had a significantly ($p < 0.05$) higher carbon content than all other sites, which were in eelgrass beds. It is worth noting that seagrass occurs in San Diego Bay in almost all of the locations where the bathymetry allows (i.e., where elevations are not too deep). As a result, Site O was located in a natural channel (the former Otay River bed) and is much deeper than surrounding areas (-5 m NAVD). It seems likely that Site O may have had a higher carbon content due to its location within a lower elevation, trenched area, where nearby plant matter and sediments may fall and collect over time. Since there are limited areas in the South Bay that are unvegetated (and not within a dredged channel), it will likely be difficult to compare vegetated and unvegetated sites with other similar features.

Bed Age

Expanding on the Year 1 study, eelgrass beds of different ages were compared to evaluate variations in the amount of carbon stored in younger and older systems. Site L is a mitigation site from a U.S. Navy project that was planted in 1998. Site N is a restoration site at Loews Coronado that was planted in 1991. Note that Site F is of unknown age – it was documented in 1974 but may have been established many years before.

As shown in Figure 3-9, the Sites L and N generally follow the same pattern that was observed in Year 1, where older sites have greater amounts of accumulated carbon in the sediment compared to the younger, restored sites.

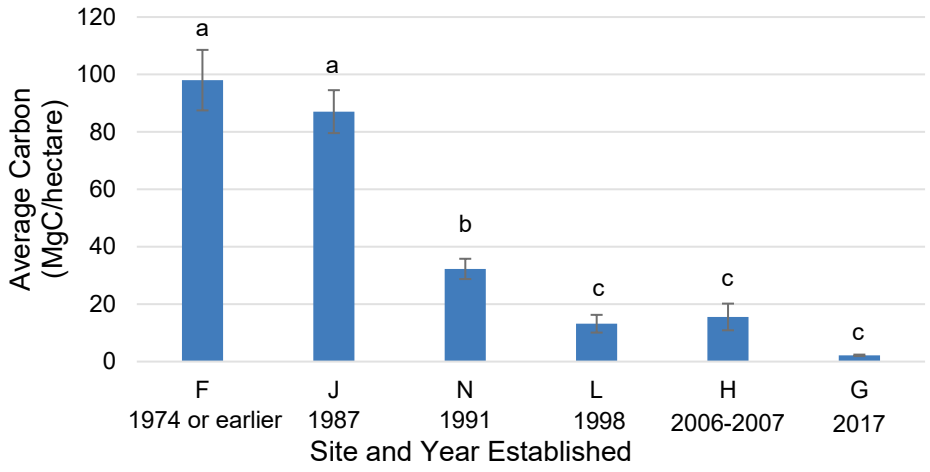

SOURCE: ESA 2023

D201800121.03 San Diego Bay Eelgrass Blue Carbon Study

NOTE: The letters above each bar represent statistical significance from bars with other letters. For example, the "a" above Site F indicates that this site was statistically different from Sites N, L, H, and G (which do not have "a" above the bar), but not statistically different from Site J (which does have an "a" above the bar).

Figure 3-9
Sediment Carbon by Bed Age

When the Tukey test was used to analyze the dated sites (rather than all cores), the results showed that Sites F and J had significantly greater carbon ($p < 0.05$) than the rest of the sites and Site N has significantly greater carbon ($p < 0.05$) than Sites L, H, and G.

Site L shows less carbon than the younger Site H. However, Site L (located in the South-Central region) is the only site in this bed age analysis that is outside of the South Bay. In the Year 1 analysis, South Bay sediments were found to store a greater amount of carbon than the South Central Bay. This indicates that some characteristics of the different ecoregions may help account for why Site L does not fit into the pattern shown by the other sites, which are all in the South Bay.

The material placed at Site J during the restoration project was a mix of marsh mud and upland material that was blended with deeper marine sediments. Broadly, marsh mud is much higher in organic content than marine sediments or the shipyards from which dredge material was taken to create the other restoration sites. We hypothesize that this may account for why Site J is significantly higher than many of the others.

Figure 3-10 shows the average carbon plotted by age of the eelgrass bed. This plot excludes Site F since it could be older than 1974. The linear regression also excludes point J since it has such a high value compared to the other sites which may be due to the different fill material, as explained above. This regression model should be applied with caution since it is based on just four sites.

The slope of the linear regression line could be used as an approximation for the rate of carbon sequestration in restored beds (93.7 $gC/m^2/yr$). This is higher than the rate calculated from sediment coring but within the range of values found in the literature.

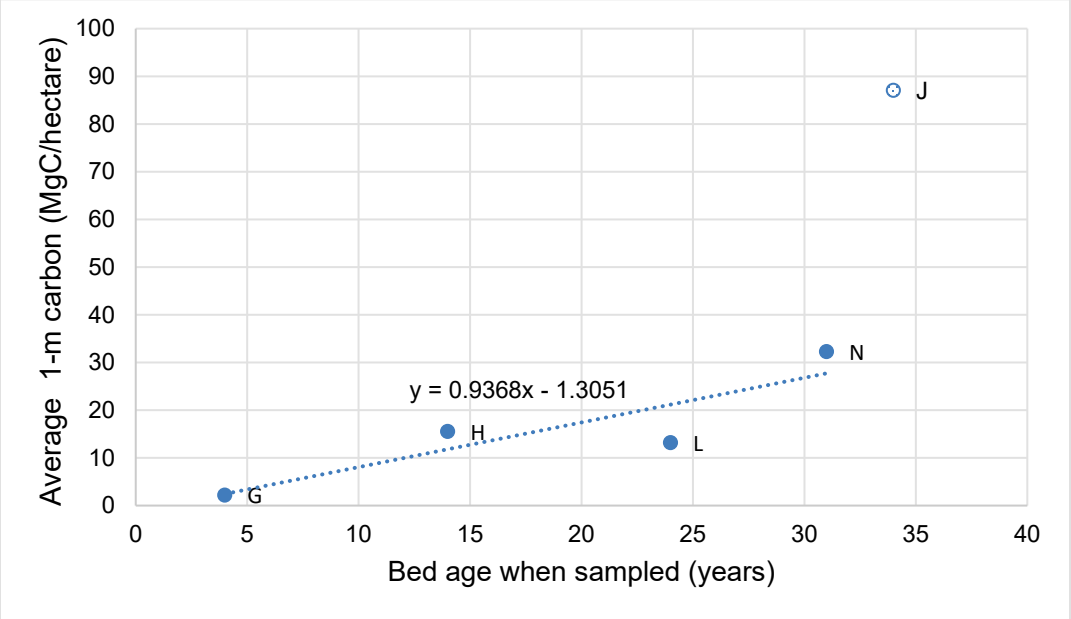

SOURCE: ESA 2023

D201800121.03 San Diego Bay Eelgrass Blue Carbon Study

Figure 3-10
Sediment Carbon as a Function of Bed Age

Grain Size

Finer sediments (grain size <0.074 mm) have been found to correlate to higher amounts of organic carbon, whether due to a higher surface area-to-volume ratio, reduced oxygen availability (which would slow decomposition), or other factors (Dahl et al. 2016, Röhr et al. 2016, Serrano et al. 2016). Following an initial qualitative assessment in Year 1, samples from all Year 1 and 2 sites were sent for laboratory grain size distribution analysis. Sediment sizes across all Year 1 and 2 samples are shown in Figure 3-11.

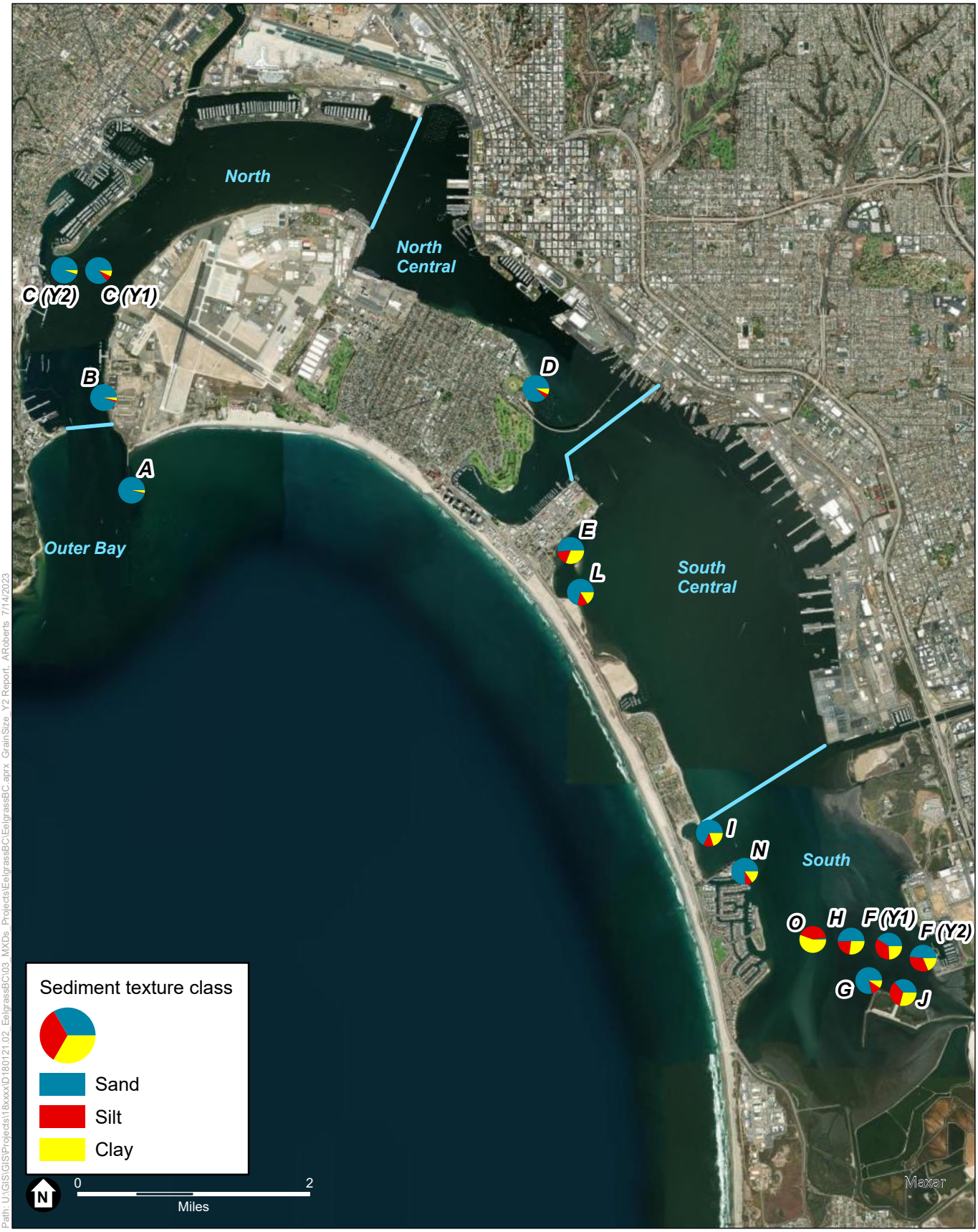

Path: U:\GIS\GIS\Projects\18xxxx\D180121.02_EelgrassBC\03_MXDs_Projects\EelgrassBC\EelgrassBC_aprx_GrainSize_Y2 Report_ARoberts_7/14/2023

SOURCE: ESA, Merkel & Associates

NOTE: Site locations are approximate.

D201800121.03 San Diego Bay Eelgrass Blue Carbon Study

Figure 3-11
Grain Sizing for All Sites

ESA

Soil textures (e.g., loamy sand, silty clay) can be identified based on the proportions of sand, silt, and clay particles in a soil/sediment sample, as shown in Figure 3-12. Results from the lab identified which class each sample was in. Figure 3-13 shows how the organic carbon fraction and bulk density vary across sediment texture classes, from sand to the finer silty clay. Broadly, the classes with a lower percent of sand (silty clay, clay loam, and loam) have higher organic carbon fractions than the sandier classes (sand, sandy loam, loamy sand, sandy clay loam).

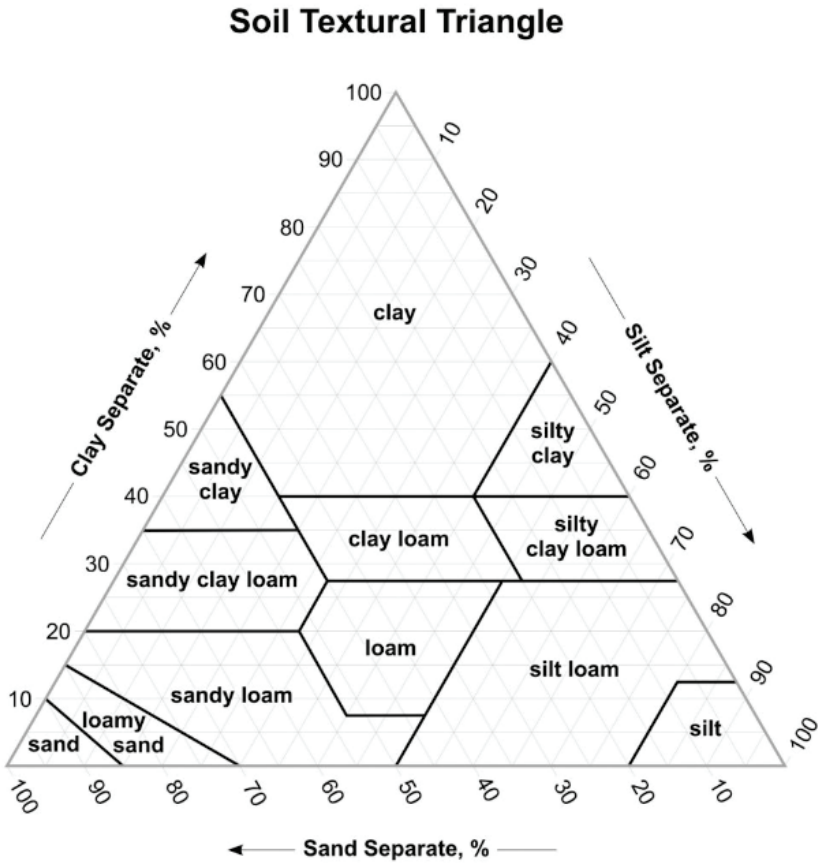

SOURCE: https://kstatelibraries.pressbooks.pub/soilslabmanual/chapter/soil-texture-and-structure/

D201800121.03 San Diego Bay Eelgrass Blue Carbon Study

Figure 3-12
Sediment Texture Triangle

For bulk density, while texture classes are generally clustered over a small range of values (0.4 to 1.8 g/cm^3), there is not a distinct pattern from coarse to fine. Typically, finer-textured soils have lower bulk density than coarser-textured soils, but it is possible that in-situ compaction and the marine environment are exerting other influences on the sediment's physical characteristics.

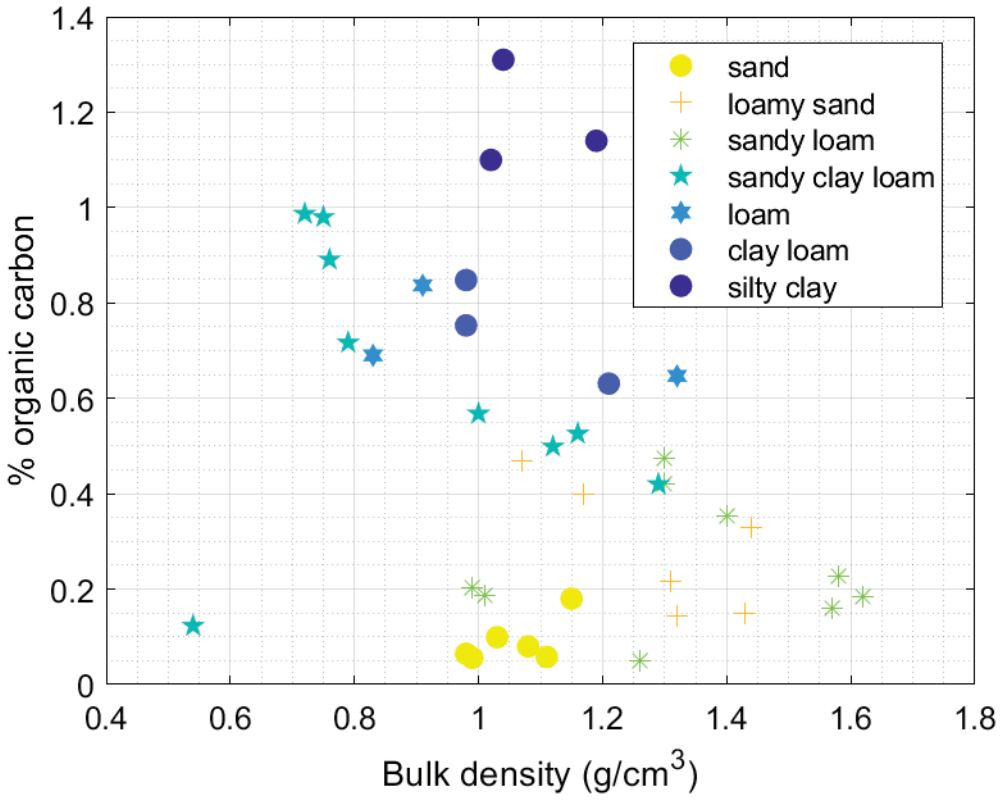

SOURCE: ESA 2023

D201800121.03 San Diego Bay Eelgrass Blue Carbon Study

Figure 3-13
Organic Carbon and Bulk Density for Surface Sediments Grouped by Sediment Texture

Serrano et al. (2016) found that mud content (grain size <0.063 mm) predicted 34 to 91 percent of variability in organic carbon content in small and fast-growing species of seagrass, including the *Zostera* genus, and 78 percent of the variability in bare sediments adjacent to seagrass beds for seagrass beds in Australia and Spain. Röhr et al. (2016) found that sediment silt (grain size 0.002-0.063 mm) fraction explained greater than 46 percent of the variation in carbon stocks in seagrass beds in Finland and Denmark.

Figure 3-14 shows a plot of carbon versus percent mud (<0.074 mm). The linear trendline suggests carbon content can be predicted fairly well by grain size ($R^2 = 0.79$). However, there is more scatter in the data for lower percentages of mud (<25%), which is also where most of the sites fall. In other words, Sites F, J, and O may exert outsize influence on the regression model since they show substantially more mud than the other sites. Future work could sample more coarser-grained sites to further evaluate this relationship.

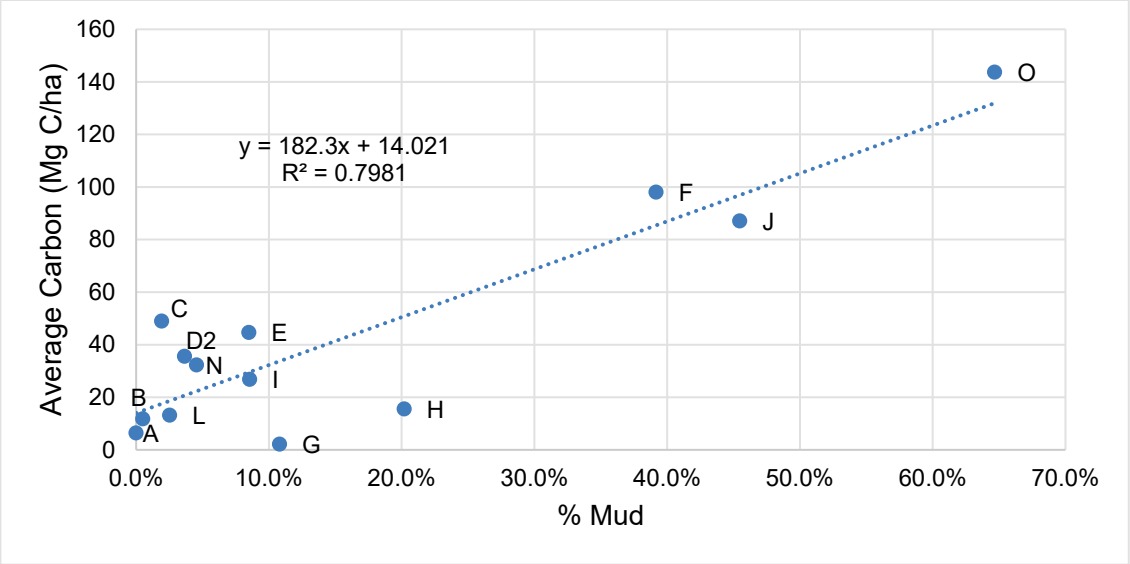

SOURCE: ESA 2023

D201800121.03 San Diego Bay Eelgrass Blue Carbon Study

NOTE: "n" refers to the number of sites with that sediment texture. Number of cores with that texture = 3n.

Figure 3-14
Carbon by Fine Particle Fraction

3.3 Water Column Carbon Pool

The water quality data provide insight into patterns of dissolved oxygen, temperature, pH, and turbidity inside and outside of an eelgrass bed. Appendix C provides results for temperature, pH, and turbidity for the spring deployment of both sondes, as well as dissolved oxygen results for both deployments.

Temperatures and pH values were similar at both gauges (Figures C-1 and C-2). The pH was generally between 8.0 and 8.5, confirming that the dominant form of inorganic carbon in the water is bicarbonate (typical ocean pH is 8.1). Diurnal patterns of pH values also show that autotrophs (e.g., seagrass, macroalgae, phytoplankton, etc.) are affecting the local carbonate buffer system.

Turbidity spikes (Figure C-3) were less pronounced within the eelgrass bed compared to outside of it. This is not surprising considering eelgrass attenuates waves and stabilize sediments through its root system. As a result, the presence of eelgrass helps to mitigate turbidity fluctuations in the water.

The dissolved oxygen (DO) data were used to develop carbon assimilation rates which were compared to those calculated from productivity assessments performed in both Year 1 and 2 of this study.

3.3.1 Dissolved Oxygen Patterns

As discussed in Section 1.4.2, the following equation illustrates the direct relationship between carbon assimilation and oxygen evolution during photosynthesis. Aerobic respiration is simply the equation in reverse.

$$6CO_2 + 6H_2O \xrightarrow{sunlight} C_6H_{12}O_6 + 6O_2$$

This equation allows for the comparison between carbon uptake and oxygen production[2]. In a well-mixed system, like the open waters of San Diego Bay, the levels of DO in the water can indicate if the rate of respiration is higher than photosynthesis or vice versa. When the DO levels are below 100%, it means that respiration is happening faster than photosynthesis. Conversely, when DO levels are above 100%, it indicates that photosynthesis is occurring faster than both respiration and the processes of oxygen diffusion and mixing induced by wind.

DO measurements were plotted against the hours of the day as a tool to determine the overall pattern of DO as a function of time of day as shown in Figure 3-15 (additional plots are included in Appendix C). Using this data, a polynomial equation was developed for each site to predict DO levels at specific times of the day. Note that the regression equation normalizes the hours of the day to a maximum of 1 (i.e., 12pm is 0.50, 6pm is 0.75, etc.).

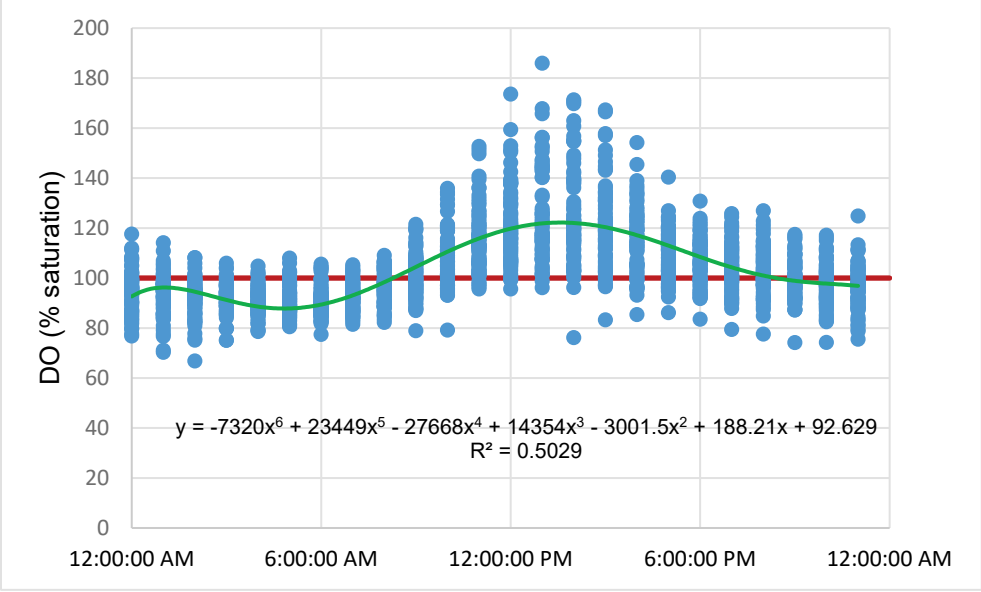

SOURCE: ESA 2023

NOTE: Red line represents 100% saturation. Green line represents polynomial regression corresponding to equation shown

D201800121.03 San Diego Bay Eelgrass Blue Carbon Study

Figure 3-15
Dissolved Oxygen Inside a Seagrass Bed
(Oct 2022-Jan 2023)

[2] Note that the internal oxygen requirements of belowground biomass can alter the relationship between oxygen and inorganic carbon slightly.

The data displayed in Figure 3-15 show a pattern of DO levels in excess of 100% saturation from approximately 9 AM until as late as 9 PM. However, there is a lag period involved with the influence of both respiration and photosynthesis on DO, and levels above 100% saturation can still represent hours with respiration rates higher than photosynthesis, especially just after times of the day with high rates of photosynthesis, which peaks during and after noon, when the sun is highest in the sky and sunlight is strongest. Similarly, DO levels lower than 100% saturation do not necessarily mean that respiration is higher than photosynthesis, especially after long periods of darkness, when the seagrass beds are respiring (in the absence of sunlight).

Instead, the determination of whether or not respiration was in excess of photosynthesis (or vice versa) is based on examining the pattern of changes in DO from hour to hour, while understanding that substantial variation would be expected when comparing sunny days (with higher levels of DO production) vs. cloudy days (with lower levels of DO production expected).

On average, respiration rates exceeded photosynthesis for approximately 15 hours per day during the October to January deployment, and for 14 hours per day during the March to May deployment. The remaining 9 and 10 hours, respectively, represent the number of hours per day (on average) when photosynthetic rates exceeded respiration.

3.3.2 Carbon Assimilation Rate Calculation

Odum (1956) developed an approach to use DO data (in units of mg/L) to calculate carbon assimilation (i.e., primary production) based on the following equation:

$$Q = P - R + D + A$$

Q = Rate of change of oxygen per unit area,

P = Rate of gross primary production per unit area,

R = Rate of respiration per unit area,

D = Rate of oxygen uptake by diffusion per unit area, and

A = Rate of drainage accrual (or the amount of oxygen entering through groundwater input)

For this study, the diffusion term can be neglected because in estuarine locations with sufficient fetch and daily wind-driven and tidally influenced mixing diffusion is small compared to photosynthesis and respiration. Additionally, drainage accrual can be neglected since the water balance in this habitat is not strongly influenced by groundwater input as it is in streams and/or spring-fed lakes. As a result, the equation can be simplified to:

$$Q = P - R$$

Respiration rates are based on the average change in DO levels during periods when DO values are decreasing, which occurred between 14 and 15 hours out of 24, on average. Net primary production can be calculated using the change in DO and the respiration rate, based on the equation above. However, respiration continues to occur during daylight hours, as it is the main pathway through which energy-containing compounds are used in both above and below ground

biomass. As a result, gross primary production or photosynthesis is the net primary production plus respiration during daylight. For both locations, the average rate of decline in DO values (mg/L) was estimated from the 15 hours (October 2022 to January 2023) and 14 hours (March to May 2023) with declining average DO values. For the remaining 9 hours (October 2022 to January 2023) and 10 hours (March to May 2023) per day, the average respiration rate was added to the average net photosynthesis rate to come up with estimates of gross photosynthesis. The result represents the amount of inorganic carbon assimilated at each of the two locations on each of the two occasions (Table 3-4).

TABLE 3-4
DAILY RESPIRATION, PRODUCTION, AND GROSS PHOTOSYNTHESIS RATES

	Oct 2022 to Jan 2023		Mar 2023 to May 2023	
	Inside Bed	**Outside Bed**	**Inside Bed**	**Outside Bed**
Daily respiration (R) (mg O_2/L/day)	2.25	1.95	3.22	1.54
Daily net production (P = Q+R) (mg O_2/L/day)	1.35	1.11	2.28	1.06
Daily gross photosynthesis (gross production = P + R) R) (mg O_2/L/day)	3.60	3.06	5.50	2.60

During both deployments, gross photosynthesis was higher inside seagrass meadows than outside of them. While some photosynthesis is expected to occur in the water column due to phytoplankton, these findings indicate that seagrass contributes to additional carbon uptake.

As expected, the warmer months of March to May were characterized by larger DO fluxes than during the fall and winter months of October to January. In temperate regions such as San Diego Bay, seagrass productivity is lower during the winter months (gross photosynthesis: 3.60 mg O_2/L/d) than in the spring (5.50 mg O_2/L/d).

The volume-based estimates shown in Table 3-4 were converted to area-based estimates by assuming an average depth at all locations of 2 meters, across all tides. A 1-square meter section of bay bottom at that depth contains 2,000 liters of water. Finally, conversion factors of 1.3 and 1.25 were used to convert rates of oxygen evolution to rates of inorganic carbon assimilation for gross photosynthesis and respiration, respectively (Odum 1953). The results are shown in Table 3-5. Rates associated with the seagrass beds were calculated based on the difference in area-normalized rates between areas outside and inside of seagrass beds.

TABLE 3-5
DAILY RESPIRATION, PRODUCTION, AND GROSS PHOTOSYNTHESIS RATES

	Oct 2022 to Jan 2023		Mar 2023 to May 2023	
	Inside Bed	Outside Bed	Inside Bed	Outside Bed
Daily net production (g C/m^2/day)	3.74	3.08	6.24	2.90
Daily production from seagrass (g C/m^2/day)	0.66		3.34	
Yearly production from seagrass (g C/m^2/year)	241		1,219	
Average yearly production from seagrass (g C/m^2/year)	730			

As expected, the rate of carbon uptake from the seagrass beds was much higher during the period of March to May than October to January. This likely reflects a combination of warmer water, longer periods of sunlight per day, and greater strength of sunlight, all of which allow for higher rates of seagrass growth. The average of the two deployments' rates, which cover both an off-season and a growing season period, is 730 g C/m^2/yr. This is a rough estimate of the amount of carbon assimilated per square meter of seagrass bed in addition to the amount from the water column alone.

Consistent with the Year 1 findings, these results also support the conclusion that there is an order of magnitude discrepancy between carbon assimilation rates and carbon sequestration rates. As outlined in Tomasko (2015) there is often much more inorganic carbon assimilated by seagrass beds than is found buried in the sediments below those same beds.

These findings do not diminish the value of seagrass beds as a "blue carbon" feature, but instead point out that the amount of inorganic carbon taken out of the water column by seagrass beds during photosynthesis must have destinations other than being buried in the sediments alone, such as through the bicarbonate pathway, carbonate shell, and export from the beds (typically to shoreline wrack deposits) where it may be buried, or decomposed and released.

3.4 Sedimentation and Sequestration Rates

A Pb-210 profile of a minimally disturbed sediment core should show an approximately exponential decrease in total Pb-210 activity with depth.

In this analysis, Ra-226 analyses were used to determine supported Pb-210 activities and Cs-137 analyses were used to validate the Pb-210 chronology for each core. Cs-137 profiles will not show the same pattern as Pb-210 but rather should correspond to nuclear bomb tests in the 1960s. The write-up and figures in this section are based upon analysis and interpretation of data produced by Flett Research Ltd (Appendix D).

3.4.1 Site C – North Bay

The core collected at Site C in the North Bay was largely composed of shelly material (see Section 3.2.2). Shells do not typically have detectable Pb-210 so they were removed during the laboratory analysis. The remaining sediments produced a detectable but irregular Pb-210 profile in the top 55 cm (extrapolated depth)[3] (first plot in Figure 3-16). The irregular Pb-210 profile suggests non-constant sediment accumulation overall, which meant that models could not be applied to estimate sedimentation rate. There was no Cs-137 detected (third plot in Figure 3-16). However, the detection of unsupported (atmospheric-sourced) Pb-210 in the upper 21.5 cm (extrapolated depth) suggests that those sediments are younger than 44.6 years (Figure 3-17).

[3] Not every sample was tested, so depths are extrapolated between tested samples. For example, the 45-50 and 60-65 cm depth samples were tested, so the extrapolated depth is 55 cm.

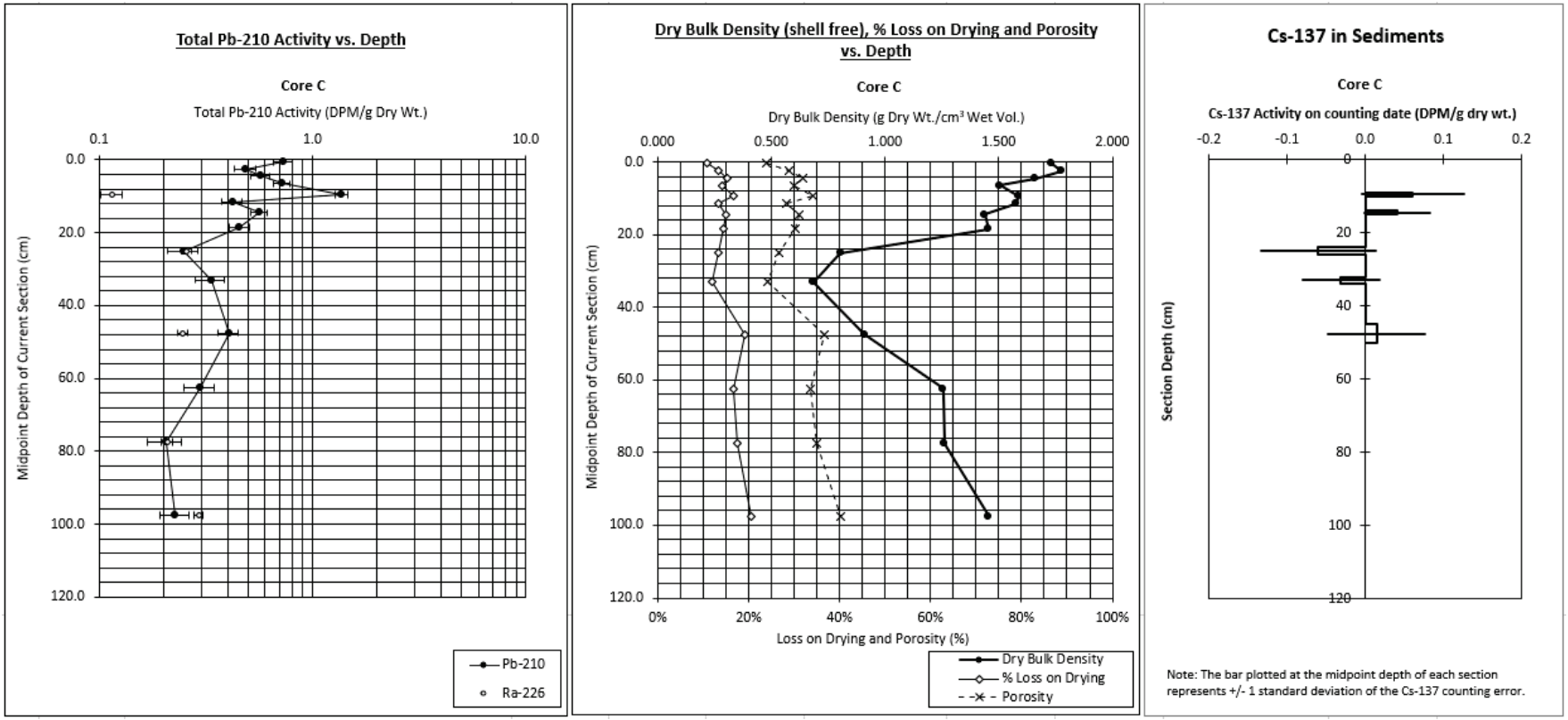

SOURCE: Flett Research Ltd. 2023

D201800121.03 San Diego Bay Eelgrass Blue Carbon Study

NOTES: DPM = disintegrations per minute, which is a measure of the activity of the source of radioactivity. The CS-137 Activity plot shows both positive and negative readings less than 0.1 DPM/g dry wt., indicating no detection of CS-137. See plot for Site O for comparison.

Figure 3-16
Total Pb-210 Activity, Bulk Density, and C2-137 Vs. Depth for the Site C Core

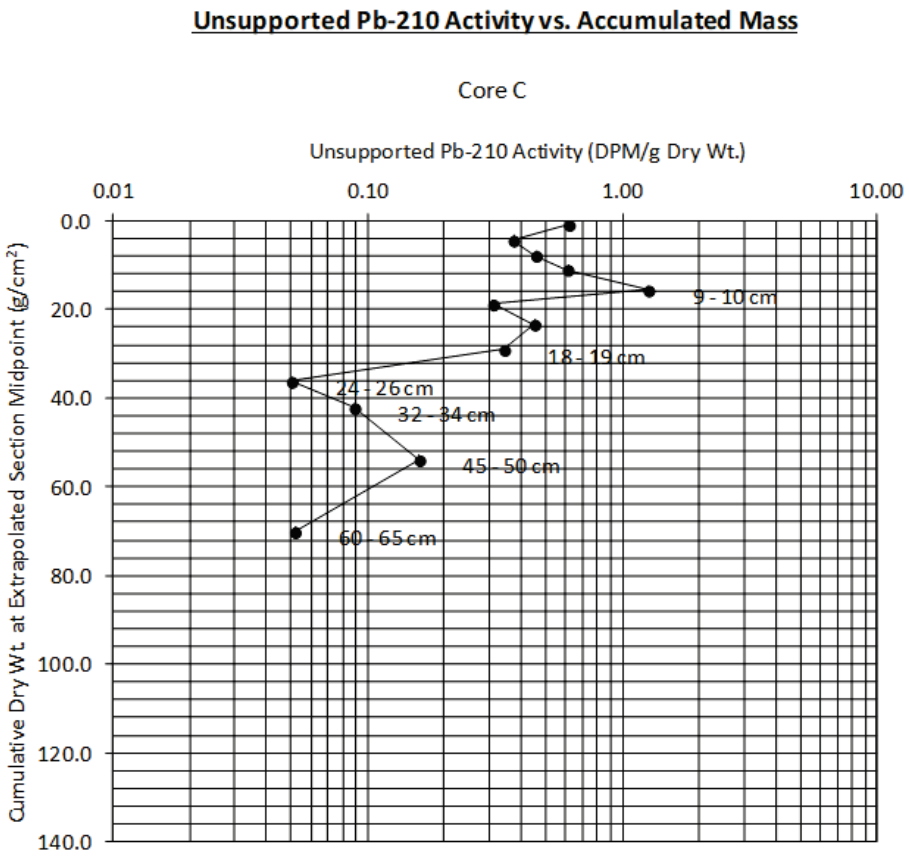

SOURCE: Flett Research Ltd. 2023

D201800121.03 San Diego Bay Eelgrass Blue Carbon Study

NOTE: "Unsupported Pb-210 activity" refers to the atmospheric sourced Pb-210. See Section 2.3.3.

Figure 3-17
Unsupported Pb-210 Activity for the Site C Core

A Constant Rate of Supply (CRS) model[4] was fitted to the radioisotope data for Site C[5]. The CRS model assumes constant input of Pb-210 and a core that is long enough to include all of the measurable atmospheric source Pb-210. Although it appears that the Pb-210 background level may have been achieved at extrapolated depth 70 - 87.5 cm, there is little confidence that a true Pb-210 inventory can be calculated because of the irregular Pb-210 profile.

If one assumes that the Pb-210 activity at the bottom of the core is at the background Pb-210 level, the model can be applied. However, at 24 - 26 cm, the unsupported Pb-210 activity is zero. In order to apply the CRS model, an artificial unsupported Pb-210 activity of 0.05 DPM/g was assigned to this sample.

The estimated age at the bottom of each section is shown in Figure 3-18. The average sediment accumulation rate, from core surface to the extrapolated bottom depth of any section, can be

[4] The CRS model assumes that there is a constant fallout of Pb-210 from the atmosphere, resulting in a constant rate of supply of Pb-210 to the sediments.

[5] A linear regression model was also considered, but because the irregular Pb-210 profile indicated non-constant sediment accumulation, the regression model could not be applied.

calculated by dividing the cumulative dry mass at the bottom of the extrapolated section by the calculated age at that depth. Plots of age vs. depth, sediment accumulation rate vs. depth and sediment accumulation rate vs. age are shown in Figure 3-18.

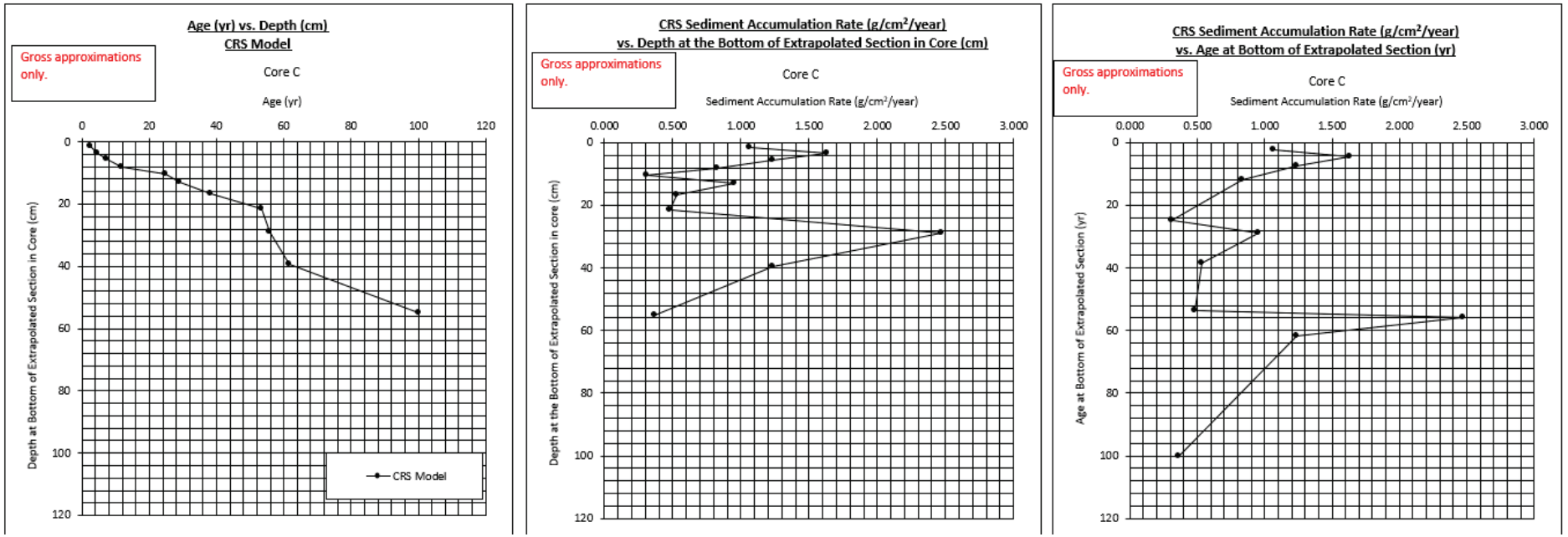

SOURCE: Flett Research Ltd. 2023

D201800121.03 San Diego Bay Eelgrass Blue Carbon Study

Figure 3-18
Age Vs. Depth, Sediment Accumulation Rate Vs. Depth and Sediment Accumulation Rate Vs. Age for Site C

It is unclear whether or not dredging and/or disposal events have occurred at this coring site. The low unsupported Pb-210 activity and Cs-137 activity may be due to hydrodynamic activity which strips the sediment of organic matter for which Pb-210 and Cs-137 have an affinity. Detectable atmospheric sourced Pb-210 was found in the upper 21.5 cm (extrapolated depth) of this core and indicates that these sediments are likely modern (i.e., < 50 yrs old).

It appears that sandy sediments have diluted the atmospheric sourced Pb-210 in core interval of 21.5 - 39.5 cm (extrapolated depth). The CRS model predicts that these sediments were rapidly deposited. This rapid deposit of sandy sediments, which contain little atmospheric sourced Pb-210, would result in the Pb-210 profile observed in Figure 3-17 over the 21.5 - 39.5 cm (extrapolated depth) core interval.

The average sediment accumulation rate (in mm/yr), from core surface to 55 cm (extrapolated depth), can be calculated by dividing the depth at the bottom of the extrapolated section by the calculated age at that depth (55 (cm) / 100.2 (yr) = 0.55 (cm/yr)). It is cautioned that the uncertainty of predicted ages in this core is high and the ages are gross approximations only, due to the relatively low activities and irregular shape of Pb-210 profile.

3.4.2 Site F – South Bay

The core collected at Site F in the South Bay shows a nearly vertical Pb-210 profile (first plot in Figure 3-19). The detected Pb-210 activities are also low (between 0.71-1.11 DPM/g), with similar Ra-226 measurements indicating that atmospheric-sourced Pb-210 was barely detectable in this core (Figure 3-20). Cs-137 was not detected (third plot in Figure 3-19). These results may be due to natural hydrodynamics or port-related activities that disturbed the sediment (e.g., dredging or dredge spoil disposal)..

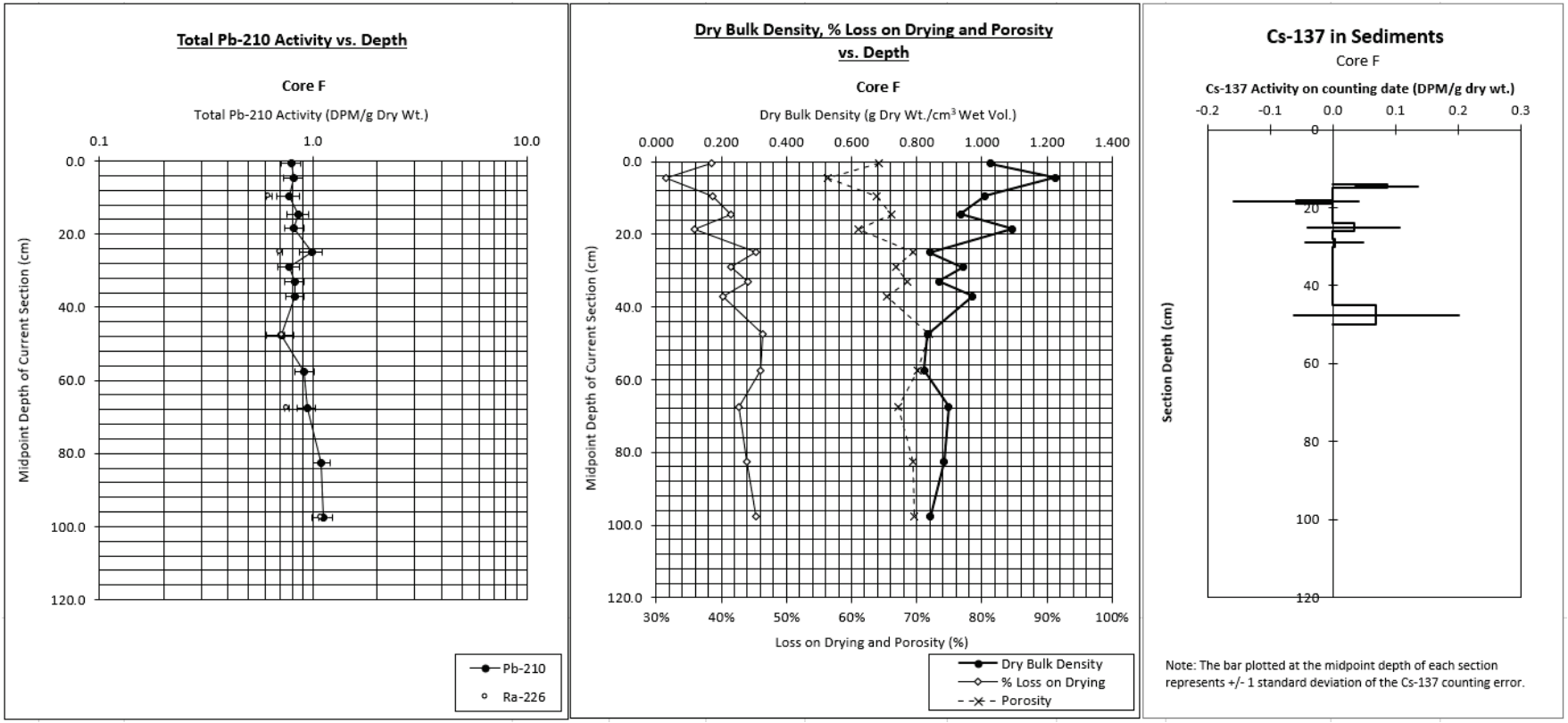

SOURCE: Flett Research Ltd. 2023

D201800121.03 San Diego Bay Eelgrass Blue Carbon Study

NOTES: DPM = disintegrations per minute, which is a measure of the activity of the source of radioactivity.
The CS-137 Activity plot shows both positive and negative readings less than 0.1 DPM/g dry wt., indicating no detection of CS-137. See plot for Site O for comparison.

Figure 3-19
Total Pb-210 Activity, Bulk Density, and C2-137 Vs. Depth for the Site F Core

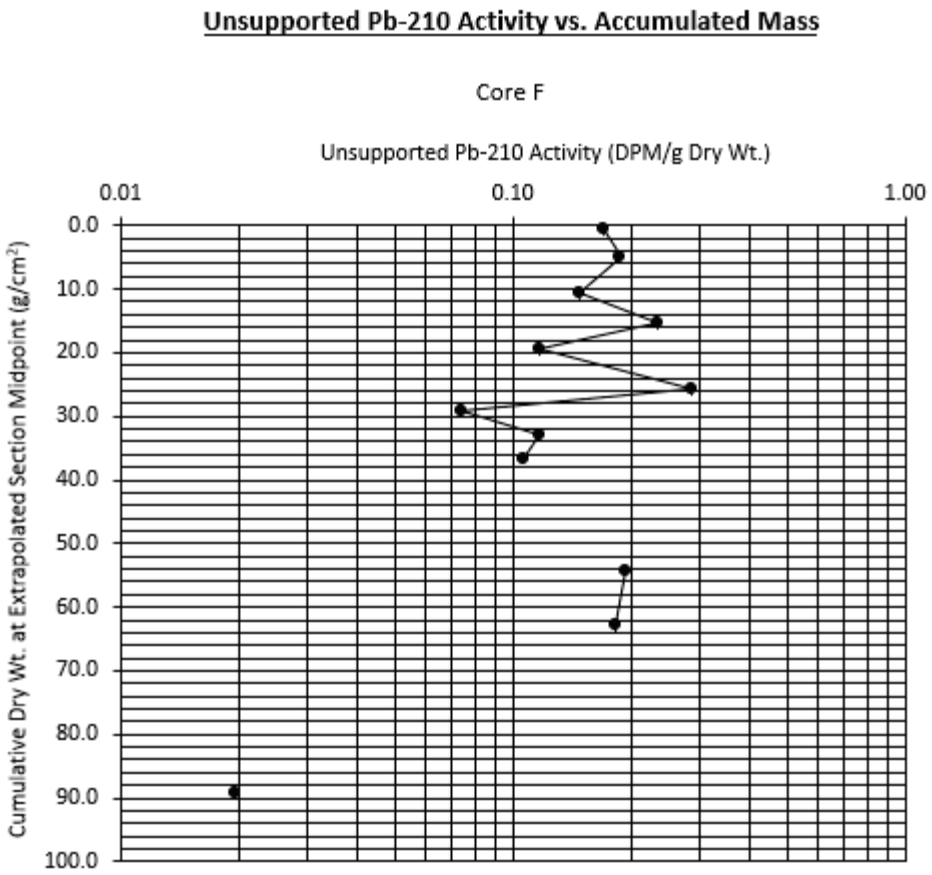

SOURCE: Flett Research Ltd. 2023

D201800121.03 San Diego Bay Eelgrass Blue Carbon Study

Figure 3-20
Unsupported Pb-210 Activity Vs. Depth for the Site F Core

3.4.3 Site O – Unvegetated

The core collected outside an eelgrass bed (Site O) in the historic channel of the Otay River likewise displays a profile that is quite low (between 0.91-1.46 DPM/g) in Pb-210 activity and nearly vertical (first plot in Figure 3-21). However, this core's Ra-226 measurements do indicate the presence of atmospheric (unsupported) Pb-210 activity (Figure 3-22). Additionally, low levels of Cs-137 were detected in samples between 21.5-45 cm (extrapolated depth) in the core (third plot in Figure 3-21). Because Cs-137 spikes are related to nuclear weapons testing, it can be inferred that sediments in this portion of the core were deposited post-1963.

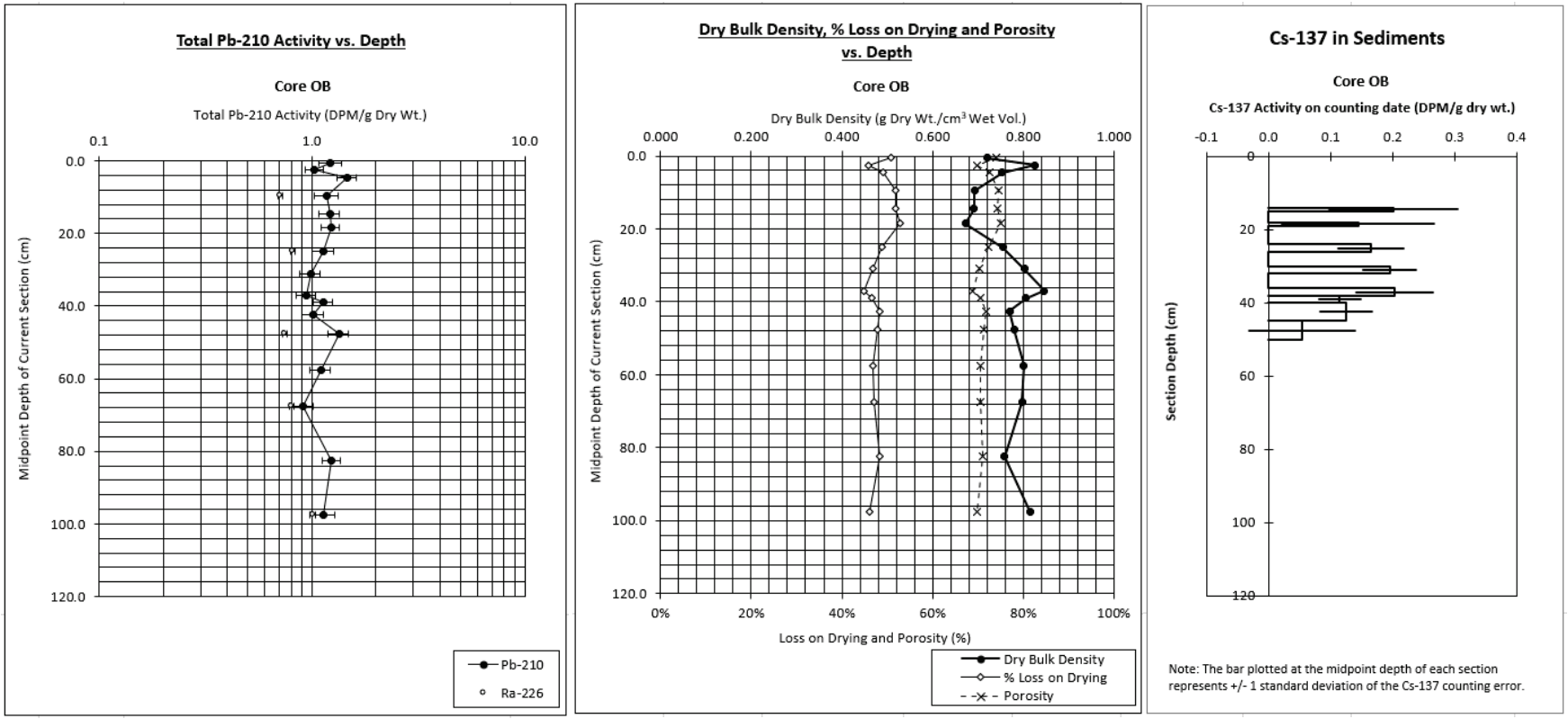

SOURCE: Flett Research Ltd. 2023

D201800121.03 San Diego Bay Eelgrass Blue Carbon Study

NOTES: DPM = disintegrations per minute, which is a measure of the activity of the source of radioactivity. The CS-137 Activity plot shows both positive and negative readings less than 0.1 DPM/g dry wt., indicating no detection of CS-137. See plot for Site O for comparison.

Figure 3-21
Total Pb-210 Activity, Bulk Density, and Cs-137 Vs. Depth for the Site O Core

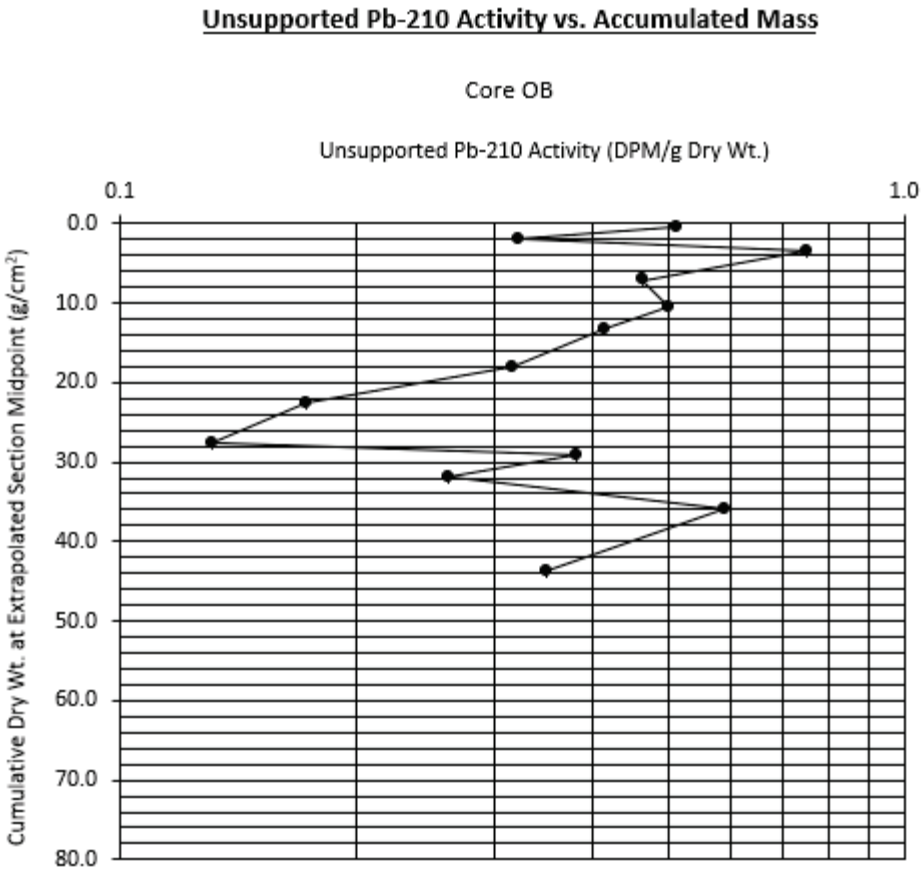

SOURCE: Flett Research Ltd. 2023

D201800121.03 San Diego Bay Eelgrass Blue Carbon Study

Figure 3-22
Unsupported Pb-210 Activity Vs. Accumulated Mass for the Site O Core

Two models—a linear regression and a CRS model—were fitted to the radioisotope data for Site O. Although some variation in the sediment accumulation rate is apparent, it appears that the average sediment accumulation rate in this core interval will be reasonably estimated. This estimate of sediment accumulation rate is used to verify the CRS model for the same core interval. The linear regression model predicts an average accumulation rate of 0.86 g/cm^2/yr, but the CRS model predicted a lower average rate of 0.51 g/cm^2/yr (range: 0.23-1.92 g/cm^2/yr) in the core interval of 3.5 – 28 cm (extrapolated depth) (Figure 3-23).

The average sediment accumulation rate (in mm/yr), from core surface to 52.5 cm (extrapolated depth), can be calculated by dividing the depth at the bottom of the extrapolated section by the calculated age at that depth (52.5 (cm) / 60.4 (yr) = 0.87 (cm/yr)). The range of values in the CRS model, as well as the discrepancy between the rates predicted by the two models, suggests high uncertainty and it is likely that some model assumptions were not met (i.e., there has been dredging, filling, or other significant sediment disturbances). These rates should therefore be used with caution.

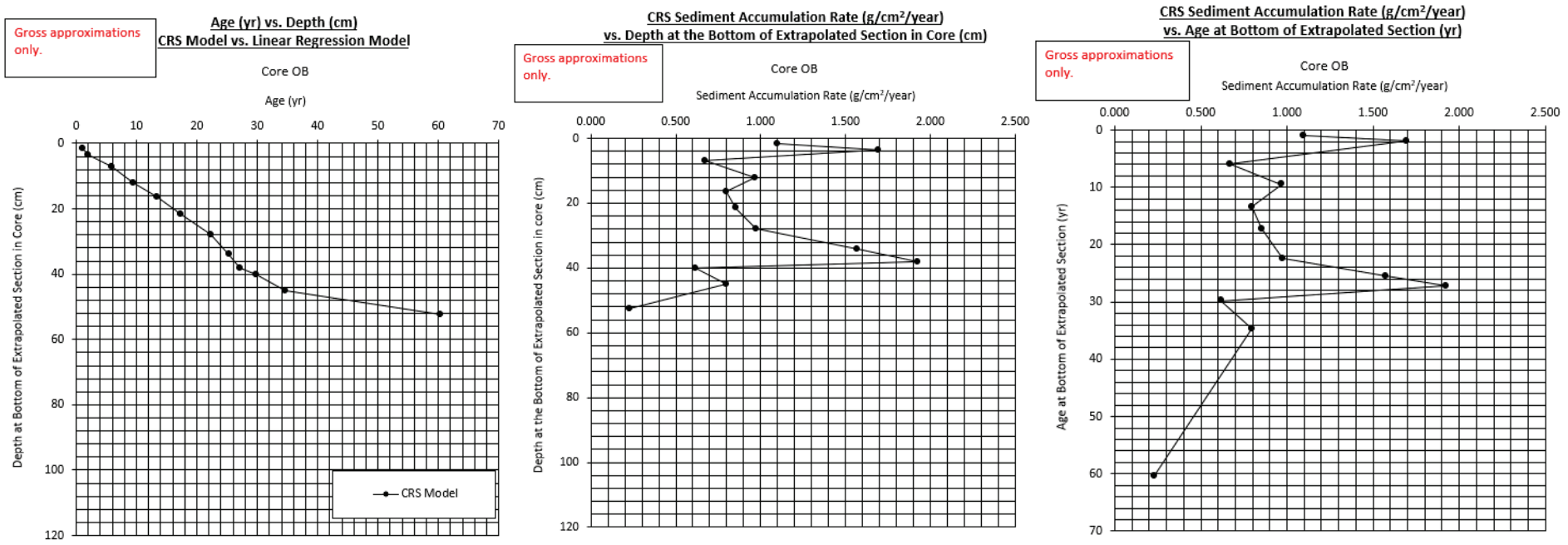

SOURCE: Flett Research Ltd. 2023

D201800121.03 San Diego Bay Eelgrass Blue Carbon Study

Figure 3-23
Age Vs. Depth, Sediment Accumulation Rate Vs. Depth and Sediment Accumulation Rate Vs. Age for Site C

3.4.4 Summary

In summary, none of the three cores analyzed in this study had radioisotope profiles that could be reliably dated. However, some gross estimates could be made from the Sites C and O cores. Combined with the sediment carbon measurements discussed in Section 3.2, rough carbon accumulation rates can be estimated (Table 3-6).

TABLE 3-6
CARBON SEQUESTRATION RATE

Site	Sediment Accretion Rate (cm/yr)	Carbon Density in top 10cm (g C/cm^3)	Carbon Sequestration Rate (g C/cm^2/yr)	Carbon Sequestration Rate (g C/m^2/yr)
C	0.55	0.0482	0.0265	265
F	N/A	0.0073	N/A	N/A
O	0.87	0.0128	0.0111	111

Carbon sequestration rates for seagrass vary widely in the literature, as shown in Table 3-7. Duarte et al. (2005) estimated a global carbon sequestration rate of 83 g C/m^2/yr, while McLeod et al. (2011) estimated 138 g C/m^2/yr. Duarte et al. (2011) measured a sequestration rate of 52.4 g C/m^2/yr for *Z. marina*. The carbon sequestration rate for Site O estimated in Table 3-6 is reasonable but high compared to the literature, while the rate for Site C seems unreasonably high. It would be worth revisiting this analysis in future work, perhaps with methodological changes to the core collection and processing steps.

TABLE 3-7
EELGRASS SEQUESTRATION RATES IN THE LITERATURE

Source	Sequestration Rate (g C/m^2/yr)	Notes
Duarte et al. (2005)	83	global
Greinier et al. (2013)	38	Virginia
Chiu et al. (2013)	20	Korea
McLeod et al. (2011)	138	global
Duarte et al. (2011)	52.4	NW Mediterranean; *Z. marina*
Samper-Villarreal et al. (2018)	50.5	NE Australia

This page intentionally left blank

4. CARBON BUDGET

The data collected in Years 1 and 2 can be used to quantify the conceptual model presented in Section 1.4.3 that shows how carbon flows in a seagrass habitat. The pools and fluxes can be represented as boxes and arrows in what is known as a "box model" (Figure 4-1). Putting together a box model can be an important step in developing greenhouse gas inventories and process-based models (which can be used to model changes to the carbon stocks due to perturbations in the system like sea-level rise or the effect of restoration, etc.).

In Figure 4-1, a "control volume" is drawn around the pools and fluxes of interest. In box modeling, this conceptual volume determines the scope of analysis and defines the (nonphysical) boundary within which all matter must be accounted for. In other words, for the control volume or for any of the boxes within it, we can write the following general "mass balance" equation:

$$\Delta\ Storage = \sum Inputs - \sum Outputs$$

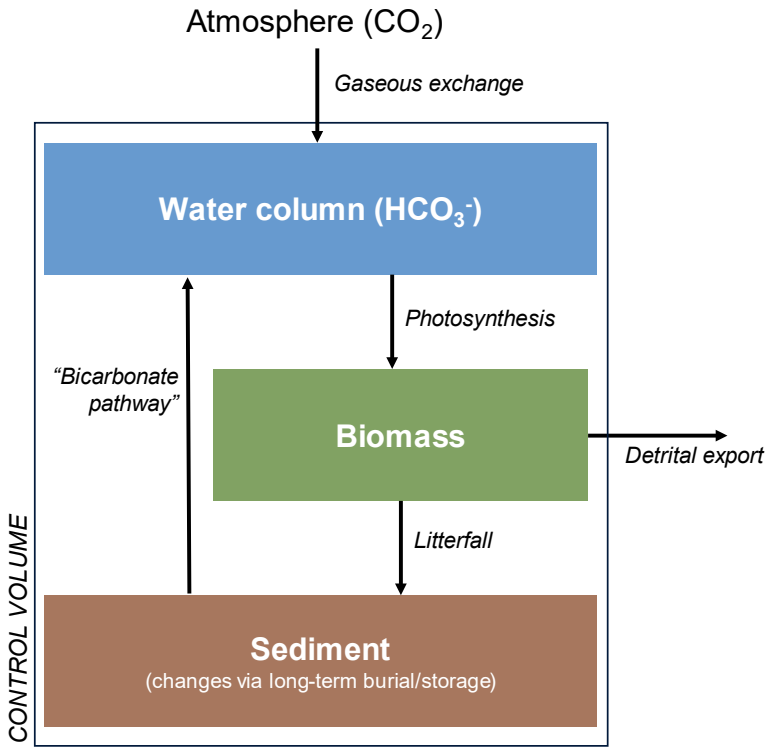

SOURCE: ESA 2023

D201800121.03 San Diego Bay Eelgrass Blue Carbon Study

Figure 4-1
Conceptual Carbon Budget Diagram

Note that the delineation of a control volume specifies what elements are and are not included in the model. This budget does not attempt to capture all of the carbon cycling that occurs in seagrass habitats but rather only that portion that is directly attributable to seagrasses. For instance, outside of the South Bay ecoregion, some sediments contain considerable shell hash,

which contains carbon in the form of calcium carbonate and which participates in its own carbon cycle with the dissolved inorganic carbon in the water column.

4.1 Pools

4.1.1 Water Column Carbon Pool

The water column carbon pool receives carbon in the form of gaseous CO_2 from the atmosphere. It rapidly transforms into the bicarbonate ion (Section 1.4.1), which is also produced when biomass decomposes. Living seagrasses draw on bicarbonate and turn it into CO_2 for photosynthesis. If it assumed that the water column is in equilibrium (i.e., any loss of bicarbonate in the water is quickly replaced by more CO_2 entering the water from the atmosphere), then the *Δ Storage* term can be considered negligible. Therefore, the mass balance equation becomes:

$$0 = Atmospheric\ input + Bicarbonate\ pathway - Photosynthesis$$

4.1.2 Aboveground Carbon Pool

In Year 1, the eelgrass areas from surveys completed by the Naval Facilities Engineering Command Southwest were used to estimate the total aboveground carbon pool, resulting in a total aboveground carbon pool of 388 tonnes CO_2 equivalent for 2020.

While the area of seagrass changes from year to year, it is assumed that this pool generally stays the same over time for the purposes of the box model. This means that year-over-year, the *Δ Storage* term can be considered negligible, simplifying the mass balance equation for this pool to three relevant fluxes:

$$0 = Photosynthesis - Detrital\ export - Litterfall$$

4.1.3 Belowground Carbon Pool

The belowground carbon pool can also be estimated by multiplying the area within an ecoregion by the carbon content. The carbon stored in the top 1-meter of sediment (153,591 tonnes CO_2 equivalent) is several orders of magnitude higher than the carbon stored aboveground.

Since seagrass beds are constantly sequestering carbon in the sediment pool, all terms in the mass balance equation must be considered:

$$\Delta\ Belowground\ carbon\ pool = Litterfall - Bicarbonate\ pathway$$

The carbon sequestration rate for Site C (Section 3.4) from the sediment carbon analysis and radioisotope dating is estimated at 265 gC /m^2/yr. This number is much higher than literature values and suggests the methodology or history of sediment disturbance may have influenced the sediment accretion rate.

Given the small size of the *Z. marina* in San Diego compared to beds around the world, the rate of change of the belowground carbon pool used for this carbon budget exercise is 20 g C/m^2/yr, the low end of the range we found in the literature (Table 3-7).

4.2 Fluxes

4.2.1 Photosynthesis

The water quality data and analysis in Section 3.3 estimated the flux to be 730 g C/m^2/yr. The eelgrass-based productivity analysis showed great interannual (and potentially spatial) variability, with a Year 1 average of 123 g C/m^2/yr and a Year 2 average of 23 g C/m^2/yr. The average between these two years is 73 g C/m^2/yr.

The order of magnitude difference between the eelgrass-based analysis and the water quality-based analysis points to methodological differences and uncertainties. For instance, eelgrass habitats support epiphytes and algae that are also captured in the water-based analysis. There may also be spatial variation – e.g., the sondes were deployed at only one fairly shallow location, while plant-based productivity measurements occurred at more and deeper locations.

This carbon budget analysis will use 73 g C/m^2/yr. This measurement is based on direct measurements of eelgrass and is also more conservative.

4.2.2 Detrital Export

In the context of seagrass ecosystems, detrital export refers to the process of seagrass carbon being transported out of the system. This export represents a significant aspect of the carbon cycle within these coastal habitats. Research efforts have sought to quantify the extent of seagrass detrital export, yielding a wide range of values. However, Heck et al. (2008) found a mean value of around 15% of net primary production of seagrasses is exported. Some of this ends up consumed by heterotrophs (organisms that rely on organic matter for their energy needs) or transported elsewhere where it may be buried in sediments or decomposed.

As long as that decomposition occurs in the ocean, the carbon released as carbon dioxide is converted into the bicarbonate form in the water column and is not outgassed to the atmosphere. However, seagrass may also end up on beaches (Heck et al. 2008) where it can decompose in open air, releasing CO_2 back into the atmosphere. Assuming 15% of the net primary production is exported and ends up on beaches, this flux from the biomass pool out of the control volume represents approximately 11 g C/m^2/yr.

4.2.3 Litterfall

Litterfall refers to the process of seagrass leaves, shoots, and other plant parts falling and accumulating on the seafloor. As part of the natural life cycle of seagrasses, this organic material plays a crucial role in nutrient cycling within the marine environment. Once it settles on the seabed, the litterfall undergoes decomposition, enriching the sediments and providing essential

nutrients for various marine organisms, contributing to the health and productivity of the seagrass ecosystem.

This flux from the biomass pool to the sediment pool can be solved for by substituting the photosynthesis (Section 4.2.1) and detrital export estimates (Section 4.2.2) into the mass balance equation for the biomass pool (Section 4.1.2). If the living plants are assimilating approximately 73 g C/m^2/yr via photosynthesis and 11 g C/m^2/yr are being exported, it follows that approximately 62 g C/m^2/yr of biomass are falling to the sediment pool.

This may be a slight underestimate of the true amount of organic biomass falling to the sediment surface, however. Seagrass blades are home to epiphytes and macroalgae, whose biomass are not captured by the needle marking technique used in this study's productivity analysis. Additionally, we assume that the litter falling to and being buried in the sediments originates from the eelgrass, which may not be wholly the case.

4.2.4 Bicarbonate Pathway

Although a substantial amount of the shed biomass is assumed to fall to the seafloor, the carbon burial rate from literature is 20 g C/m^2/yr. Solving the mass balance equation for the sediment pool (Section 4.1.3) suggests that the bicarbonate pathway (which occurs in the sediment) and remineralization of non-buried litterfall accounts for roughly 42 g C/m^2/yr entering the water column pool.

4.2.5 Gaseous Exchange

The equation in Section 4.1.1 can be used to solve for the gaseous exchange flux in order to close the carbon budget. This suggests that between sediment storage and the bicarbonate pathway (Figure 4-2), San Diego Bay's seagrasses are sequestering about 31 gC/m^2/yr.

4.3 Carbon Budget

Figure 4-2 summarizes the changes in carbon pools and the fluxes within the seagrass beds within San Diego Bay. Assuming 2,598 acres of seagrass based on the most recent survey (2020), the seagrass beds in San Diego Bay sequester approximately 1195 tonnes of CO_2 equivalent per year through burial and the bicarbonate pathway.

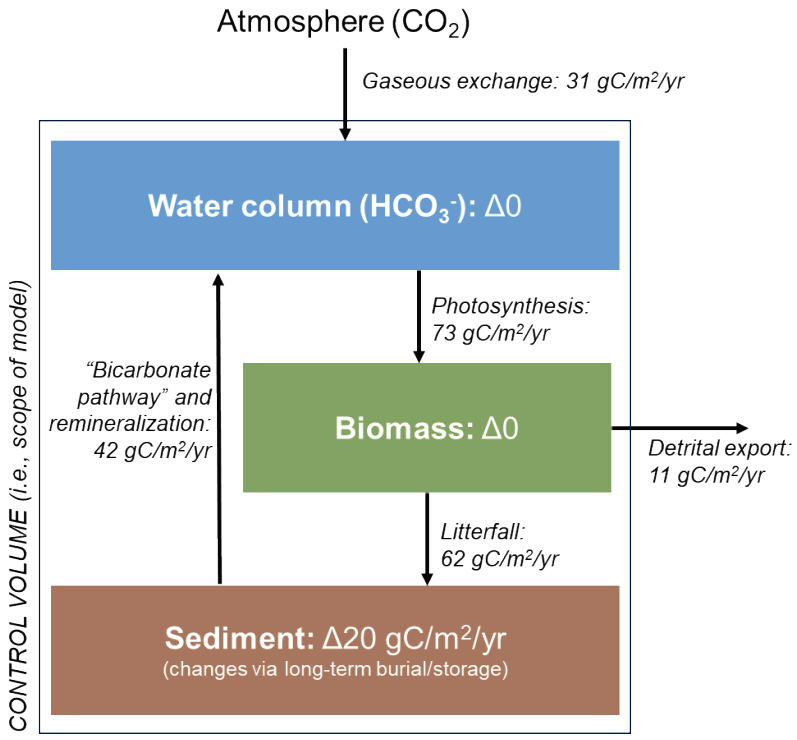

SOURCE: ESA 2023

D201800121.03 San Diego Bay Eelgrass Blue Carbon Study

Figure 4-2
Changing Pools and Fluxes of Carbon in San Diego Bay Seagrass Beds

Wherever possible in Sections 4.1 and 4.2, this study's estimates have been compared to literature values as a check on reasonableness. Additional sampling could improve the model – for example, repeating the radioisotope dating task with improved core extraction methods may lead to more confident estimates of sediment accretion rates, and setting up specialized instrumentation to measure pCO_2 can lead to a direct calculation of the air-sea flux. There are also uncertainties related to the nature of the methods used. For the photosynthetic flux, different methods yielded values from 73 to 730 g C/m^2/yr. The estimate of seagrass sequestration in sediments and through the bicarbonate pathway is related to the estimates of all fluxes, which means that uncertainties in each arrow are passed onto the estimate of sequestration.

In addition, it is important to also note that the present model focuses on carbon in eelgrass plant tissues, sediment, and the water column, but does not take into account secondary carbon stores associated with epiphytic algae. Also omitted are inorganic carbon stores within the carbonate skeletons and shells of organisms within the eelgrass beds, particularly calcareous bryozoans and mollusks. This non-organic carbon may be substantial but not evenly distributed within the bay.

Based on this model, it is recommended that conservation takes precedence over restoration efforts for San Diego Bay eelgrass. This is drawn from the significant disparity between the sediment carbon pool, estimated to be 153,591 tonnes and the carbon burial rate of 20 g C/m2/yr,

equivalent to 210 tonnes of carbon per year across the entire Bay. This perspective underscores the substantial carbon reserves already present in the sediments, making conservation a more viable strategy for maintaining ecosystem carbon balance.

5. CONCLUSION

San Diego Bay's eelgrass habitats play a significant role in carbon storage, currently holding around 153,591 tonnes of CO_2 equivalent in the sediments. Additionally, these habitats are sequestering about 1,195 tonnes of CO_2 equivalent annually. This annual sequestration is comparable to 0.3% of the annual emissions from Port operations, based on the projected 2020 emissions data (Port of San Diego 2013).

Key findings from the study include:

- Biomass sampling and productivity sampling suggest a good deal of interannual variability. For instance, canopy height at the reference site (Site F) slightly increased, while the carbon productivity at the enriched Sweetwater site decreased approximately 55% between the Year 1 and Year 2 sampling periods.
- In Year 1, it was hypothesized that nutrient reduction due to pollution control and drought-reduced water column productivity, had led to diminishing biomass of eelgrass bay-wide. However, higher-nutrient sites (Sites M and K) demonstrated slightly higher productivity rates and shoot density but had lower carbon stock in the biomass when compared to a control site (Site F). This observation warrants further investigation into the causative agents resulting in the present diminutive condition of eelgrass in the bay, for example through manipulative and controlled nutrient augmentation experiments.
- The highest sediment carbon content was surprisingly found at the unvegetated coring site (Site O). We hypothesize this may be due to its location within a lower elevation, trenched area where plant matter and sediments could accumulate over time.
- Strong correlations were observed between mud content (<0.074 mm) and age with carbon storage, indicating their potential as predictive factors for carbon stock development. This supports the Year 1 findings of higher carbon storage in South San Diego Bay where mud is abundant.
- While the radioisotope findings had limitations, they suggest sediment accretion rates at the lower end of the range reported in the literature for seagrass beds (23 g $C/m^2/yr$) compared to 20 to 138 g $C/m^2/yr$ in the literature). Future studies should consider alternate core sampling methods to minimize mixing and refine sequestration rate estimates.
- Dissolved oxygen records within and outside eelgrass beds produced a much higher estimate of carbon assimilation rate compared to eelgrass-based productivity measurements. This indicates methodological and other uncertainties that may be the subject of future research.
- The carbon budget illustrates the important role of the bicarbonate pathway in carbon sequestration. Despite seagrass habitats releasing more produced carbon back into the water column than burying in the sediments, that amount is effectively sequestered as bicarbonate, supplementing sediment burial. Therefore, sequestration into the water column is an important factor to consider when assessing the carbon storage capabilities of eelgrass beds.

Broadly, San Diego Bay is a dynamic system and has a vibrant history of recreational, commercial, industrial, and Naval use that undoubtedly has, and continues to, influence the local carbon cycle. Results from the Year 1 and Year 2 study both provide insight into eelgrass habitats

and the blue carbon benefits they currently provide. Considering the statewide importance of San Diego Bay for eelgrass habitat, responsible management is vital to maintaining blue carbon storage. The Port and Navy have been actively mapping, monitoring, and managing eelgrass since the early 1990s. Moreover, the study's insights can inform future blue carbon projects, which would require understanding of carbon storage and sequestration rates specific to the bay to implement appropriate data collection and monitoring protocols for accurate assessment of these factors. Eelgrass areas in San Diego Bay are already protected by regulations and may not meet additionality requirements for selling blue carbon credits, but this study provides a useful baseline assessment of carbon storage and sequestration in the bay that can be used to explore future blue carbon credit opportunities

This iteration of the San Diego Bay Eelgrass Blue Carbon Study serves as a valuable resource for scientists and policymakers, advancing their understanding of eelgrass habitat's carbon sequestration and capture rates, especially as blue carbon policy and legislative initiatives progress at the state and federal level. The study's initiation at the Port of San Diego also provides information to guide other coastal ports and harbors nationwide exploring blue carbon sequestration opportunities to offset carbon emissions from both water and land operations. Supported by the U.S. Maritime Administration’s (MARAD) Maritime Environmental Technical Assistance (META) program, this research contributes to broader maritime decarbonization efforts for a safer and more efficient U.S. maritime transportation system.

The knowledge gained from this study facilitates the development of comprehensive on-site mitigation plans, empowering ports, natural resource agencies, maritime operations, and other organizations in their pursuit of carbon neutrality. By incorporating on-site mitigation strategies and potentially generating bankable offsets through natural systems like eelgrass habitat restoration, the transportation sector gains greater flexibility within their Scope 1, 2, and 3 emissions inventories (i.e., direct and indirect emissions) to comply with regulations, align with environmental, social, and governance (ESG) initiatives, and ultimately strive for carbon neutrality.

Recommendations for future studies include:

1. Refine sequestration rates by using alternative core sampling methods. It is possible that vibracoring caused mixing of sediment layers, particularly near the tops of the cores, which may have led to enough disturbance to obscure the radioisotope dating profiles.

2. Incorporate refinements in sea-level rise estimates, additional restoration, and changes to water quality as they occur in the future.

3. Examine the impacts of dredging on emissions, particularly in relation to carbon accumulations in sediments. If channel areas are accumulating high amounts of carbon in the sediments as in the case of Site O (non-vegetated site), dredging and placing those materials on land and letting them dry out would result in the release of substantial amounts of carbon. If materials are dredged and deposited offshore, these impacts may be reduced. Future studies could look at cores from dredged channels and see if the carbon sediment is also high in these locations or if regular dredging keeps these channels from accumulating significant amounts of carbon.

4. Use eDNA sampling to understand sources of allochthonous carbon (i.e., carbon that originated from outside seagrass beds) in the system.

5. Develop a bay-wide carbon inventory, incorporating other blue carbon habitats like marshes and mudflats in addition to seagrass habitats.

6. Monitor whether biomass and productivity at higher-nutrient sites increase year-over-year, particularly if Water Year 2023-2024 is also wetter than normal.

7. Measure eelgrass characteristics (e.g., canopy height, turnover rate, productivity, etc.) on a seasonal basis to provide insight into changes over the course of the year.

This page intentionally left blank

6. REFERENCES

Burdige, D.J. and R.C. Zimmerman. 2002. Impacts of seagrass density on carbonate dissolution in Bahamian sediments. *Limnology and Oceanography* 47: 1751-1763.

Burdige, D.J., X. Hu, and R.C. Zimmerman. 2010. The widespread occurrence of coupled carbonate dissolution / reprecipitation in surface sediments on the Bahamas Bank. *American Journal of Science* 310: 492-521.

Chou, W-C., Fan, L-F., Yang, C-C., Chen, Y-H., Hung, C-C., Huang, W-J., Shih, Y-Y., Soong, K., Tseng, H-C., Gong, G-C., Chen, H-Y., and C-K. Su. 2021. "A unique diel pattern in carbonate chemistry in the seagrass meadows of Dongsha Island: the enhancement of metabolic carbonate dissolution in a semienclosed lagoon." *Frontiers in Marine Science*, 8, 717685, doi:10.3389/fmars.2021.727685.

Chmura, G.L., Anisfeld, S.C., Cahoon, D.R., and Lynch, J.C. 2003. "Global carbon sequestration in tidal, saline wetland soils." *Global Biogeochemical Cycles*, 17(4), 1111, doi:10.1029/2002GB001917.

Dahl, M., D. Deyanova, S. Gütschow, M. E. Asplund, L. D. Lyimo, V. Karamfilov, R. Santos, M. Björk, M. Gullström. 2016. "Sediment Properties as Important Predictors of Carbon Storage in *Zostera marina* Meadows: A Comparison of Four European Areas." *PLoS ONE,* 11(12), 1-21. https://doi.org/10.1371/journal.pone.0167493.

Duarte, C.M., Middelburg, J.J. & Caraco, N. 2005. Major role of marine vegetation on the oceanic carbon cycle. *Biogeosciences, 2, 1–8.*

Duarte, C.M., N. Marba, E. Garcia, J.W. Fourqurean, J. Beggins, C. Barron, and E.T. Apostolaki. 2010. Seagrass community metabolism: Assessing the carbon sink capacity of seagrass meadows. *Global Biogeochemical Cycles* 24: 8 pp.

ESA and Merkel & Associates. 2022. San Diego Bay Eelgrass Blue Carbon Study, 2021-2022. Prepared for the San Diego Unified Port District and MARAD. October 2022.

Flett Research Ltd. 2023. Flett Research Radioisotope Services. www.flettresearch.ca/Radioisotope.html

Fourqueran, J.W. and 10 others. 2012. Seagrass ecosystems as a globally significant carbon stock. Nature Geoscience 5:505-509. DOI: 10.1038/ngeo1477.

Greiner, J.T., K.J. McGlathery, J. Gunnell, and B.A. McKee. 2013. Seagrass restoration enhances "blue carbon" sequestration in coastal waters. *PLoS ONE* 8(8): e72469. Doi: 10.1371/journal.pone.0072469

Harvey, L.D.D. 2008. "Mitigating the atmospheric CO2 increase and ocean acidification by adding limestone powder to upwelling regions." *Journal of Geophysical Research*. doi:10.1029/2007JC004373.

IPCC. 2014 “2014: Climate Change 2014: Synthesis Report.” Contribution of Working Groups I, II and III to the Fifth Assessment Report of the Intergovernmental Panel on Climate Change [Core Writing Team, R.K. Pachauri and L.A. Meyer (eds.)]. IPCC, Geneva, Switzerland, 151 pp

Isobe, M. S. Kraines, Y. Suzuki, R. Zimmerman, R. Buddemeier, and D. Wallace. 2002. Feasibility study of an eco-engineering based method to increase atmospheric CO2 fixation into a marine ecosystem. In: Proceedings of the International Workshop for the Seagrass Ecosystem Ecoengineering and Carbon Sequestration Project. Tokyo University, Tokyo, Japan. 10 pp.

Kauffman, J. B., L. Giovanonni, J. Kelly, N. Dunstan, A. Borde, H. Diefenderfer, C. Cornu, C. Janousek, J. Apple, L. Brophy. 2020. “Total ecosystem carbon stocks at the marine-terrestrial interface: Blue carbon of the Pacific Northwest Coast, United States.” *Global Change Biology,* 26(10), 5679-5692. https://doi.org/10.1111/gcb.15248.

Mcleod E., G. L. Chmura, S. Bouillon, R. Salm, M. Björk, C. M. Duarte, C. E. Lovelock, W. H. Schlesinger, B. R. Silliman. 2011. “A blueprint for blue carbon: toward an improved understanding of the role of vegetated coastal habitats in sequestering CO_2.” *Frontiers in Ecology and the Environment*, 9(10), 552-560. https://doi.org/10.1890/110004.

Merkel & Associates. (2020). 2020 San Diego Bay Eelgrass Inventory. Prepared for U.S. Navy Region Southwest Naval Facilities Engineering Command and the Port of San Diego. December 2020.

Moreno-Mateos, D., M. E. Power, F. A. Comin, R. Yockteng. 2012. “Structural and functional loss in restored wetland ecosystems.” *PLOS Biology* 10(1): e1001247. https://doi.org/10.1371/journal.pbio.1001247

Odum, H. (1956). Primary Production in Flowing Waters. Presented as part of a symposium at the American Society of Limnology and Oceanography meeting, East Lansing, Michigan. September 6, 1955. Primary Production in Flowing Waters1 (wiley.com)

Rau, G.H., Caldeira, K. 1999. Enhanced carbonate dissolution: a means of sequestering waste CO2 as ocean bicarbonate. *Energy Conversion Management* 40(17):1803–1813

Rau, G.H., K. Caldeira, K.G. Knauss, B. Downs, and H. Sarv. 2001. Enhanced carbonate dissolution as a means of capturing and sequestering carbon dioxide. First National Conference on Carbon Sequestration Washington, D.C. 7 pp.

Röhr, M.E., C. Boström, P. Canal-Vergés, and M. Holmer. 2016. “Blue carbon stocks in Baltic Sea eelgrass (Zostera marina) meadows.” *Biogeosciences,* 13, 6139-6153. Doi:10.5194/bg-13-6139-2016.

Short, F.T. and C.M. Duarte. 2001. Methods for the measurement of seagrass growth and production. In: Global Seagrass Research Methods. Short, F.T. and R.G. Coles (eds.), Elsevier Science, B.V., Amsterdam. 473 pp.

Smith, S.V. 1981. “Marine Macrophytes as a Global Carbon Sink”. *Science*. 211,838-840. DOI:10.1126/science.211.4484.838

Taskforce on Scaling Voluntary Carbon Markets. 2021. Taskforce on Scaling Voluntary Carbon Markets, Phase I Report. January 2021. https://www.iif.com/Portals/1/Files/TSVCM_Report.pdf.

Tomasko, D.A., Dawes, C.J. and M.O. Hall. 1996. The effects of anthropogenic nutrient enrichment on Turtle Grass (Thalassia testudinum) in Sarasota Bay, Florida. *Estuaries* 19: 448-456.

Tomasko, D.A., Bristol, D.L., Ott, J.A. 2001. Assessment of present and future nitrogen loads, water quality, and seagrass (Thalassia testudinum) depth distribution in Lemon Bay, Florida. *Estuaries*, 24(6A): 926-938.

Tomasko, D.A. (2015). Refining carbon sequestration estimates of seagrass meadows in Tampa Bay. Pp. 259-272, In: Burke, Maya (ed.). 2016. Proceedings, Tampa Bay Area Scientific Information Symposium, BASIS 6: 28-30 September 2015. St. Petersburg, FL. 337 pp.

Unsworth, R.K.F., C.J. Collier, G.M. Henderson, and L.J. McKenzie. 2012. Tropical seagrass meadows modify seawater carbon chemistry: Implications for coral reefs impacted by ocean acidification. *Environmental Research Letters* 7: 9 pp.

Zieman, J.C. and R.G. Wetzel. 1980. Productivity in seagrasses: Methods and rates. Pp. 87-115 In: R.C. Phillips and C.P. McRoy, eds. Handbook of Seagrass Biology: An Ecosystem Perspective. Garland STPM Press, New York.

This page intentionally left blank

Appendix A.
Year 1 Study

FINAL

SAN DIEGO BAY EELGRASS BLUE CARBON STUDY

2021-2022

Prepared for
San Diego Unified Port District

October 2022

FINAL

SAN DIEGO BAY EELGRASS BLUE CARBON STUDY

2021-2022

Prepared for
San Diego Unified Port District

October 2022

Prepared by

ESA Associates
550 West C Street
San Diego, CA 92101

and

Merkel & Associates
5434 Ruffin Road
San Diego, CA 92123

2355 Northside Drive, Suite 100
San Diego, CA 92108
619.719.4200
esassoc.com

Atlanta	Palm Beach County	San Diego
Bend	Pasadena	San Francisco
Irvine	Pensacola	San Jose
Los Angeles	Petaluma	Sarasota
Mobile	Portland	Seattle
Oakland	Rancho Cucamonga	Tampa
Orlando	Sacramento	Thousand Oaks

D201800121.03

TABLE OF CONTENTS

San Diego Bay Eelgrass Blue Carbon Study

List of Figures

Page

List of Tables

GLOSSARY OF TERMS

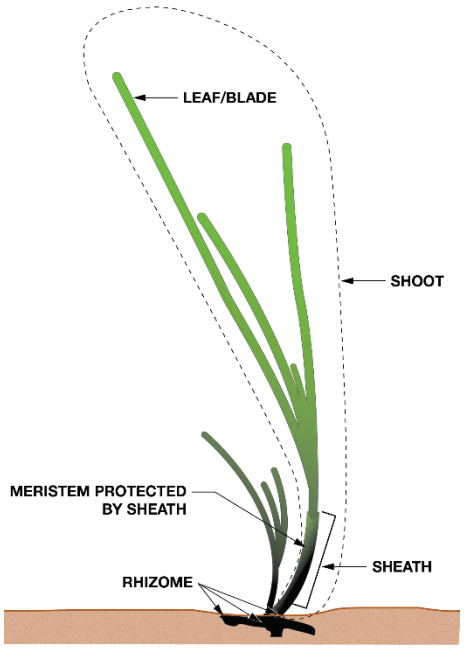

Parts of an Eelgrass Shoot

Allometric equation – A mathematical relationship between an object's dimensions or traits; for this study, an equation relating eelgrass dimensions to biomass.

Assimilation – Carbon assimilation, also called carbon fixation, is the process by which inorganic carbon, usually in the form of carbon dioxide, is converted to organic compounds by living organisms and used to store energy and as a basis for building other important biomolecules. The most prominent example of carbon fixation is photosynthesis.

Blue carbon – Atmospheric carbon dioxide that is captured and stored in coastal and marine ecosystems, including the ocean and coastal seagrass, mangroves, and saltmarsh habitats.

Bulk density – Dry weight of a sediment sample divided by its volume.

Carbon stock/storage – The amount of carbon sequestered from the atmosphere and now stored within a carbon pool, for example, within living plant biomass and soil. This study focuses on the aboveground (i.e., biomass) and the belowground (i.e., roots and sediment) pools.

Eelgrass – A common name for several species of seagrass that grow in the shallow, protected waters of coastal bays and estuaries. Species studied here are the common eelgrass (*Zostera marina*) and the Pacific eelgrass (*Zostera pacifica*).

Mean lower low water (MLLW) – The average of the lower low water elevation each day observed over the 19-year National Tidal Datum epoch[1]

Organic carbon percentage – Calculated by dividing the mass of organic carbon in a sample by the overall mass of the sample.

***p* (p-value)** – A statistical measurement of the probability of obtaining the observed results. A p-value of less than 0.05 is considered statistically significant, with smaller values indicating a stronger significance.

Quadrat – An area of defined size and random placement used to assess characteristics such as plant distribution and density.

Refusal – The point at which a sediment corer cannot be driven further into the earth.

Remineralization – The conversion of organic matter back into inorganic forms. In this study, it is essentially the opposite of carbon sequestration.

Seagrass – A flowering plant which grows in marine environments, of which eelgrasses are a subtype.

Sequestration – The capture of atmospheric carbon dioxide.

Shell hash – Coarse sediment type dominated by broken bits of shells.

Turbidity – A water quality characteristic related to the cloudiness of the water (i.e., due to the amount of suspended matter)

[1] https://tidesandcurrents.noaa.gov/datum_options.html

EXECUTIVE SUMMARY

The Port of San Diego was one of the first ports to adopt a Climate Action Plan in 2013, and the decarbonization of maritime-related sources is a critical component to achieve organization goals and uphold state regulations. The California Global Solutions Act of 2016 (SB-32) requires a 40% reduction in State emissions below 1990 levels by 2030. In September 2022, the State passed The California Carbon Neutrality Act, A.B. 1279, that establishes "a clear, legally binding and achievable goal" that urges carbon neutrality as soon as possible, but no later than 2045, according to the governor's office. A.B. 1279 also sets an 85 percent emissions reduction target for that in comparison to 1990 levels. As such, it is important for the Port to seek multiple strategies to decrease GHG emissions through direct source reductions and through carbon sequestration.

Growing recognition of the ability of wetlands and seagrasses to combat climate change by sequestering and storing atmospheric carbon has led to increased interest in quantifying the greenhouse gas (GHG) benefits of coastal ecosystems. So-called "coastal blue carbon" is of great significance for both carbon sequestration and storage, as wetlands (both freshwater and saline) store 20–30% of global sediment carbon while making up just 5–8% of global land surface (Nahlik and Fennessy 2016). Mechanisms and procedures have also been developed to connect coastal wetland management to the carbon market, where appropriate.[2] For example, this year, The Nature Conservancy launched the first blue carbon credit project in the U.S. with the Virginia Eastern Shore seagrass restoration project.[3]

San Diego Bay is of special interest for quantifying the carbon of seagrass meadows, as it contains about 17% of the eelgrass habitat within California (Merkel & Associates 2020). Due to its statewide importance, the eelgrass in the bay has been mapped, monitored, and managed by the Port of San Diego (Port) and the Navy since the early 1990s. Seagrass meadows not only trap and store carbon generated by the seagrass itself, but up to 50% of the stored carbon in the sediments of seagrass meadows originates from somewhere else (Kennedy et al. 2010).

Quantifying blue carbon in San Diego Bay can be a means of assessing the benefits of seagrass bed restoration on GHG offsets. The addition of climate mitigation benefits is expected to broaden the pool of potential funds for the Port and others to do restoration and conservation, particularly as ecosystems like seagrass meadows are threatened by climate change and sea-level rise. Where carbon financing is not appropriate, recognition of the climate values of seagrasses

2 http://www.v-c-s.org/methodologies/methodology-tidal-wetland-and-seagrass-restoration-v10

3 https://registry.verra.org/app/projectDetail/VCS/2360

could help the Port and its partners prioritize actions that improve and conserve these habitats in the context of climate adaptation.

ESA and Merkel & Associates prepared this study for the Port to evaluate and inventory carbon sequestration and storage potential of seagrass beds in San Diego Bay, including both the common eelgrass (*Zostera marina*) found throughout San Diego Bay and the broad-leaved, slower-growing Pacific eelgrass (*Zostera pacifica*) that grows near the bay's mouth. Given the spatial and biological heterogeneity across San Diego Bay, it was anticipated that carbon storage may differ across eelgrass beds based on a number of factors, including:

- Species of eelgrass (*Z. marina, Z. pacifica*);
- Ecoregion (Outer Bay, North Bay, North-Central Bay, South-Central Bay, South Bay);
- Depth of eelgrass occurrence (shallow margin, mid-bed, deep fringe), and;
- Age of eelgrass beds.

The ESA team sampled 12 locations across San Diego Bay, selecting sites to facilitate comparisons across the environmental variables listed above. Following the methods established by Howard et al. (2018) and Short and Duarte (2001), each site was analyzed for biomass carbon, sediment carbon, and eelgrass productivity. The results of the sampling and laboratory analysis show that, in total, San Diego Bay's eelgrass habitats store around 170,600 tonnes of CO_2 equivalent currently. This is comparable to just under half a years' worth of emissions from Port operations (Port of San Diego 2013). Continuing to manage these habitats will be important to maintaining blue carbon storage in San Diego Bay.

Sampling at the 12 locations across the bay provided the following results around the variability of carbon storage:

- The *Z. pacifica* bed had lower sediment carbon storage compared to *Z. marina* despite *Z. pacifica*'s larger biomass. However, aboveground and belowground carbon for the two species were not significantly different from each other ($p > 0.05$).
- Across the bay, the results show a general trend of increasing sediment carbon going southward. In particular, the Outer Bay stored significantly less carbon ($p < 0.05$) than North Central, South Central, and South Bay sites, and storage was also significantly different ($p < 0.05$) between the South Bay and the two ecoregions just north of it (North Central and South Central).
- The data show that the average carbon content may increase with increasing depth. The middle depth (-5 ft MLLW) showed significantly ($p < 0.05$) more carbon than the shallowest depth (-1 ft MLLW). The deepest cores (-7 ft MLLW) showed a substantial amount of variability, so this site was not statistically significant from the other two depths.
- The older sites had significantly ($p < 0.01$) greater amounts of carbon in the soils than the younger sites. For example, the site that was planted in 1987, had significantly ($p < 0.01$) more carbon than the site that was restored in 2006-2007, which had significantly ($p < 0.05$) more carbon than the site that was restored more recently in 2017. The data depicts a strong linear relationship between eelgrass bed age and carbon content although this is based on n=4.

The ESA team also estimated eelgrass productivity by measuring eelgrass growth over a period of 12 days, similar to the timeframe employed in other studies (Kentula and McIntire 1986; Solana-Arellano 2000; Solana-Arellano et al. 2008). The analysis showed that *Z. marina* assimilates 98.0 ± 41.0 mg C/m^2/day and *Z. pacifica* assimilates 237.1 ± 64.4 mg C/m^2/day. Note that assimilation in this context refers to biological sequestration, or what is taken into biomass—it does not guarantee that the carbon will be buried into the sediments. Comparing the assimilation rate to estimates of carbon sequestration in the literature (Duarte et al. 2005, 2011; McLeod et al. 2011) shows an order of magnitude discrepancy between carbon assimilation rates and carbon sequestration rates. As discussed in Tomasko 2015, this is a fairly common result, and at least a portion of the discrepancy may be due to sequestration into bicarbonate ions in the water column, which is something that will be analyzed in Year 2 of this study.

ESA also developed a habitat evolution model to estimate how eelgrass habitat and blue carbon sequestration could change over time with sea-level rise. The model assumes that eelgrass colonization continues to be correlated with depth as sea levels change. The model forecasts that the total extent of habitat will decrease over time. However, this habitat loss does not occur uniformly. Over time, eelgrass encroaches closer to the present-day shoreline, while habitat loss occurs largely in the interior of the bay. Habitat gain is concentrated in the South Bay, while habitat loss is concentrated first in the South Central Bay but is eventually modeled to occur in all other ecoregions.

Expansion of seagrasses into newly inundated areas throughout the bay where other important blue carbon habitats may be lost is crucial to slowing the loss of eelgrass habitat with sea-level rise and maintaining the bay's overall carbon sequestration potential. If this seagrass expansion with sea-level rise does not occur, then it is likely that carbon sequestration would decrease. Additionally, if sea-level rise stresses the ecosystem, loss of eelgrass could become part of a positive feedback loop leading to further losses, as seagrass meadows filter particulates out of the water column, and thus improve water clarity, which is needed for eelgrass to thrive.

While the existing eelgrass in San Diego Bay is already protected by regulations, and therefore would not meet the additionality requirements to sell blue carbon credits, this study provides new research to inform future blue carbon projects. To bring a blue carbon project to market, local data is needed to accurately predict how much carbon will be sequestered by the project. This study provides needed information on how carbon content varies by eelgrass species, location, depth, and age of the bed. In particular, the trend showing that older restored eelgrass beds have higher amounts of carbon in the sediments compared to newer restored beds could provide justification for restoring eelgrass beds to sequester blue carbon with the understanding that carbon would build up in the sediments over time.

The following recommendations are made for future studies:

1. Developing a San Diego Bay–specific sequestration rate would allow for a direct comparison to assimilation rates and would provide more accurate carbon evolution modeling results.

2. Further investigations into inorganic carbon pathways and carbon sequestration within the bicarbonate pool should be undertaken to better understand the difference between assimilation and sequestration rates.
3. Water quality data could provide additional information on the bicarbonate pathway (through changes in pH) and could be used to estimate productivity through the air-water CO_2 flux to compare against measurements in this study.
4. Refinements in sea-level rise estimates could affect the findings of this study and should be considered as new studies become available.
5. Grain size or other supplementary sediment analyses (e.g., isotope measurements) could help further illuminate patterns and causes of carbon storage in the sediment.
6. Follow-up sampling of eelgrass productivity could be conducted when drought conditions end and eelgrass returns to more "normal" above ground biomass conditions.

SECTION 1
Introduction

Growing recognition of the ability of wetlands and seagrasses to combat climate change by sequestering and storing atmospheric carbon has led to increased interest in quantifying the greenhouse gas (GHG) benefits of coastal ecosystems. To date, much of the science and practice of biological carbon sequestration and the development of associated carbon offset projects has focused on forestry, where the science and tools necessary to calculate GHG benefits are fairly well developed. However, more recently, organizations and agencies from the local to the international scale have begun to quantify the carbon storage and sequestration capacities of wetlands and aquatic habitats, especially salt marshes, mangroves, and seagrass beds (see, for example, National Wetlands Newsletter 36:1). So-called "coastal blue carbon" is of great significance for both carbon sequestration and storage, as wetlands (both freshwater and saline) store 20–30% of global sediment carbon while making up just 5–8% of global land surface (Nahlik and Fennessy 2016).

Mechanisms and procedures have also been developed to connect coastal wetland management to the carbon market, where appropriate.[4] A growing number of case studies are amassing to inform management agencies and policy developers on coastal wetland management and carbon finance markets (Sheehan et al. 2019; Crooks et al. 2014). This year, The Nature Conservancy launched the first blue carbon credit project in the U.S. with the Virginia Eastern Shore seagrass restoration project.[5]

San Diego Bay is of special interest for quantifying the carbon of seagrass meadows, as it contains about 17% of the eelgrass habitat within California (Merkel & Associates 2020). Due to its statewide importance, the eelgrass in the bay has been mapped, monitored, and managed by the Port of San Diego (Port) and the Navy since the early 1990s. Seagrass meadows not only trap and store carbon generated by the seagrass itself, but up to 50% of the stored carbon in the sediments of seagrass meadows originates from somewhere else (Kennedy et al. 2010). Researchers estimate that the global carbon burial of seagrasses is 48 to 112 teragrams of carbon (Tg C) per year; by comparison, forests' carbon burial rates range from 49 to 79 Tg C per year (Mcleod et al. 2011).

Quantifying blue carbon can be a means of assessing the benefits of seagrass bed restoration on GHG offsets. The addition of climate mitigation benefits is expected to broaden the pool of potential funds for the Port and others to do estuarine restoration and conservation, particularly as ecosystems like seagrass meadows are threatened by climate change and sea-level rise. Where

4 http://www.v-c-s.org/methodologies/methodology-tidal-wetland-and-seagrass-restoration-v10

5 https://registry.verra.org/app/projectDetail/VCS/2360

carbon financing is not appropriate, recognition of the climate values of seagrass could help the Port and its partners prioritize actions that improve and conserve these habitats in the context of climate adaptation.

1.1 Project Context

The Port of San Diego was one of the first ports to adopt a Climate Action Plan in 2013, and the decarbonization of maritime-related sources is a critical component to achieve organization goals and uphold state regulations. The California Global Solutions Act of 2016 (SB-32) requires a 40% reduction in State emissions below 1990 levels by 2030. In September 2022, the State passed The California Carbon Neutrality Act, A.B. 1279, that establishes "a clear, legally binding and achievable goal" that urges carbon neutrality as soon as possible, but no later than 2045, according to the governor's office. A.B. 1279 also sets an 85 percent emissions reduction target for that in comparison to 1990 levels. As such, it is important for the Port to seek multiple strategies to decrease GHG emissions through direct source reductions and through carbon sequestration.

In addition to upholding state standards, the Port of San Diego has also developed a Maritime Clean Air Strategy (MCAS) to reduce emissions of criteria pollutants as well as greenhouse gases (GHGs) from its maritime industry beyond what is mandated by California standards. With a vision of Health Equity for All, the MCAS is a strategic planning document, identifying both short- and long-term goals and objectives to reduce emissions from ocean-going vessels, commercial harbor craft, cargo handling equipment, heavy-duty trucks, and locomotives. The MCAS focuses on the transition to zero emission technologies such as increased use of shore power for ocean-going vessels while at berth and electric trucks that aim to reduce diesel particulate matter (DPM) emissions as well as GHG emissions. The initiatives outlined in the MCAS will reduce health risk impacts on receptors such as nearby residents, children at schools and day care centers, and patients at local hospitals and others.

In advance of the State's goals, the Port seeks to install additional shorepower capacity at its marine terminals as well as utilize an emission capture and control system to reduce emission from non-shorepower capable vessels; and advance 100% zero emission truck trips and cargo handling equipment by 2030. Additional goals include transitioning Port-owned vehicles and equipment to zero/near zero emission technologies in a manner that meets operational needs.

1.2 Project Overview

ESA and Merkel & Associates prepared this study for the Port to evaluate and inventory carbon sequestration and storage potential of seagrass beds in San Diego Bay, including both common eelgrass (*Zostera marina*) and the broad-leaved, slower-growing Pacific eelgrass (*Zostera pacifica*) that grows near the mouth of San Diego Bay. The goal of this work is to:

1. Establish typical baseline carbon stocks that currently exist in eelgrass beds throughout San Diego Bay.

2. Characterize variation in carbon pools associated with variation in local environmental conditions.
3. Assess and better understand the carbon sequestration capacity of both newly established (as a result of restoration projects or other human intervention) and existing eelgrass beds to support future natural resources management efforts.

Given the spatial and biological heterogeneity across San Diego Bay, it was hypothesized that carbon storage may differ across eelgrass beds based on a number of factors, including:

- Species of eelgrass (*Z. marina, Z. pacifica*);
- Ecoregion (Outer Bay, North Bay, North-Central Bay, South-Central Bay, South Bay; see **Figure 1-1** below);
- Depth of eelgrass occurrence (shallow margin, mid-bed, deep fringe), and;
- Age of eelgrass beds.

Seagrass meadows are generally composed of three major carbon pools: aboveground living biomass (i.e., the leaves of seagrass), belowground living biomass (roots and rhizomes), and sediment carbon stock. The baseline sampling plan has been designed to capture the carbon stock in all three pools as they vary across these different environments.

San Diego Bay Eelgrass Blue Carbon Study

Figure 1-1
San Diego Bay Site Map

ESA

1.3 Conceptual Framework

The term "carbon stock" refers to the quantity of carbon stored in a reservoir, or pool (e.g., soil, vegetation, water, the atmosphere). Each pool can sequester and release carbon. In eelgrass beds, the main pools of carbon are biomass and sediment carbon (IPCC 2013).

Vegetation sequesters carbon, in the form of carbon dioxide (CO_2), from the atmosphere through photosynthesis and transforms it into biomass. The biomass carbon stock includes the total mass of carbon stored aboveground (e.g., in leaves of seagrass) and belowground (e.g., in roots and rhizomes) at a site.

Sediments comprise another important carbon pool. This stock increases over time according to the sediment sequestration rate of the habitat, i.e., the rate at which dead organic matter is incorporated back into the sediment. Coastal wetland sediments are primarily anaerobic, or oxygen-poor, because they are submerged in water which slows the decomposition of dead organic matter and allows carbon to remain buried in the sediment. Because of the unique anaerobic chemistry of wetland and other aquatic habitats' sediments, wetlands and seagrasses store a disproportionately large amount of carbon per area compared to terrestrial habitats, making this stock of particular interest in the context of global climate change.

Dead organic matter is important in woody wetlands (e.g., forested wetlands), where it comprises a large fraction of the aboveground carbon stock. Since San Diego Bay does not include forested wetlands, we did not analyze this pool for the project.

1.4 Analysis Accuracy

The Intergovernmental Panel on Climate Change's (IPCC's) tier system reflects the degree of certainty or accuracy of a carbon assessment:

- Tier 1 – These assessments have the least accuracy and certainty and are based on simplified assumptions and published IPCC default values for activity data[6] and emissions factors. Tier 1 assessments may have a large error range of +/- 50% for aboveground pools and +/- 90% for the variable sediment carbon pools.
- Tier 2 – These assessments include some country- or site-specific data and hence have increased accuracy and resolution. For example, a country may know the mean carbon stock for different ecosystem types within that country.
- Tier 3 – These assessments require highly specific data of the carbon stocks in each component ecosystem or land use area, and repeated measurements of key carbon stocks through time to provide estimates of change or flux of carbon into or out of the area. Estimates of carbon flux can be provided through direct field measurements or by modeling.

This assessment will provide Tier 3 data for San Diego Bay, which is the most accurate level of data. Analyzing the carbon stocks at a Tier 3 level will facilitate future use of the data to analyze changes to carbon stocks and GHG fluxes over time with sea-level rise, restoration, or other

[6] Geographical data showing the types of land coverage and use in a given area.

changes to the bay. Additionally, Tier 3 data would be required to validate blue carbon credits if a market project is developed in the future.

SECTION 2
Field Data Collection and Laboratory Methods

The ESA team sampled 12 locations across San Diego Bay, selecting sites to facilitate comparisons across the environmental variables listed in Section 1.2 Project Overview. Each site was analyzed for biomass carbon, sediment carbon, and eelgrass productivity following the methods established by Howard et al. (2018) and Short and Duarte (2001).

Table 2-1 summarizes the sampling locations. Sampling depths were intended to be around -4 ft mean lower low water (MLLW) except for sample D-1, which was shallower, and D-3, which was deeper. However, achieving this exact elevation in the field proved to be more difficult than expected, so depths vary across the sites, as listed in Table 2-1. Additionally, seagrass in the outer bay has been dynamic in recent years and so the location of Site B was shifted slightly north, closer to the entrance of the bay.

TABLE 2-1
SAMPLE LOCATION SUMMARY

Replicates	Location	Ecoregion	Depth	Species	Year established
1-3	A	Outer Bay	-7.4 ft MLLW	*Zostera pacifica*	Since at least 1992
4-6	B	Outer Bay	-4.6 ft MLLW	*Zostera marina*	Since at least late 1970s
7-9	C	North	-7.0 ft MLLW	*Zostera marina*	Since at least late 1970s
10-12	D-1	North Central	-1.6 ft MLLW	*Zostera marina*	Since at least 1992
13-15	D-2	North Central	-5.5 ft MLLW	*Zostera marina*	Since at least 1992
16-18	D-3	North Central	-7.7 ft MLLW	*Zostera marina*	Since at least 1992
19-21	E	South Central	-5.2 ft MLLW	*Zostera marina*	Since at least early 1980s
22-24	F	South	-1.9 ft MLLW	*Zostera marina*	1974 or earlier (native)
25-27	G	South	-4.3 ft MLLW	*Zostera marina*	2017 (BAE Pier 1)
28-30	H	South	-6.3 ft MLLW	*Zostera marina*	2006-2007 (South Bay Borrow Pit)
31-33	I	South	-8.9 ft MLLW	*Zostera marina*	Unknown
34-36	J	South	-3.4 ft MLLW	*Zostera marina*	1987 (Chula Vista Wildlife Reserve)

NOTES:

Elevations were collected in ft NAVD88 in the field. A conversion of NAVD – 0.43 ft = MLLW was used throughout the bay (NOAA Tides and Currents for San Diego Bay, Stn. 940170).

To collect biomass carbon data, triplicate quadrats were set at each site. Within each 25 cm by 25 cm quadrat, the average eelgrass height and the number of shoots were measured. At both a quadrat in a *Z. marina* bed and one in a *Z. pacifica* bed, 50 individual shoots over the range of

observable heights and widths were cut and sent to Wallace Laboratories (El Segundo, CA) for analysis of carbon content.

Triplicate sediment cores were collected at each site to understand belowground carbon storage. Cores were taken to 1-meter depth or to refusal (i.e., where the core cannot be pushed further), and one core per ecoregion (Figure 1-1) was taken to 3-meter depth or to refusal. These cores were subsampled on-site into 10-cm intervals for the top half meter and into 50-cm intervals thereafter. These samples were sent to Weck Laboratories, Inc. (City of Industry, CA) for analysis of dry bulk density and carbon content.

Eelgrass productivity was determined by measuring eelgrass growth over a period of 12 days, similar to the timeframe employed in other studies (Kentula and McIntire 1986; Solana-Arellano 2000; Solana-Arellano et al. 2008). Following established methods of directly marking shoots to obtain a growth rate over time, individual eelgrass shoots were marked just above the meristem at the blade-sheath junction with a hypodermic needle (Tomasko et al. 2001; Ibarra-Obando and Boudouresque 1994; Short and Duarte 2001). Multiple shoots were marked in 20 clusters of approximately five shoots per cluster in order to ensure that 20 shoots could be easily relocated and collected from two sampled locations: one *Z. marina* bed (at the mouth of the Sweetwater River in the south ecoregion[7]) and one *Z. pacifica* bed (Site A, Outer Bay). These blades were marked with zip ties to facilitate recovery at the end of the 12 days, when shoots were collected and taken to the laboratory to measure the upward displacement of the scar on the "new" blade compared to the needle mark remaining on the older, outside blade where the puncture was first made.

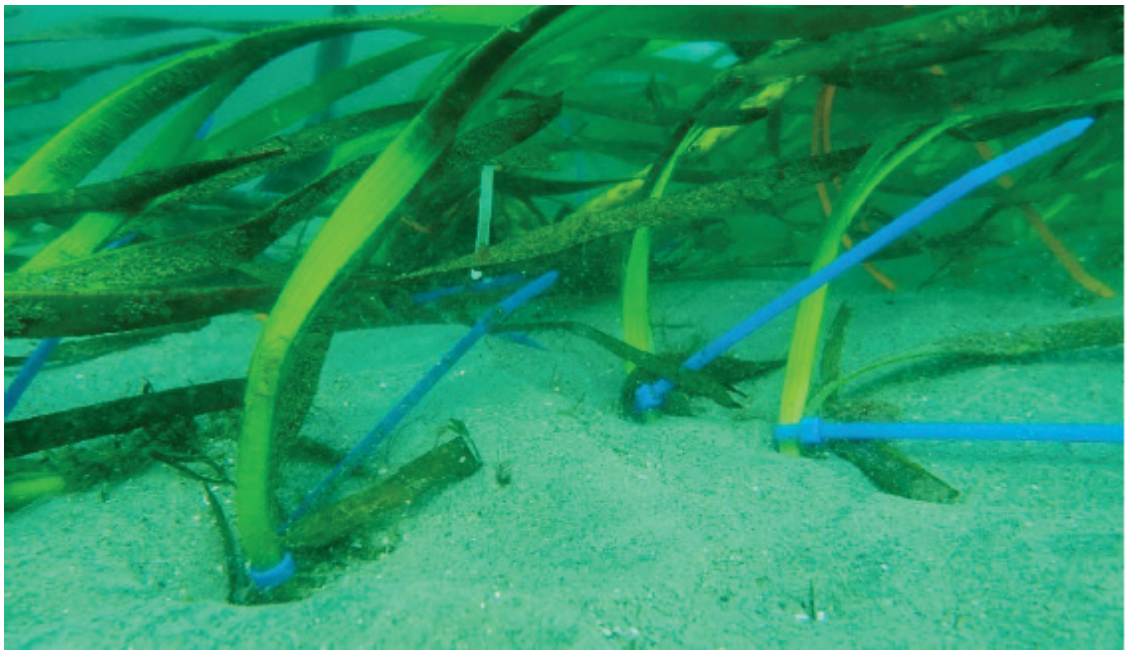

Figure 2-1. Zip Ties Identifying Marked Shoots of *Z. Pacifica*

7 The productivity sampling was originally conducted in the fall of 2021 at Site B, but due to the small eelgrass blades, the marked shoots could not be found or recovered. The sampling was repeated in the spring of 2022 near the Sweetwater River where eelgrass grows taller.

SECTION 3
Aboveground Carbon Data Analysis

3.1 Biomass Data

Table 3-1 summarizes the number of shoots, density, dimensions, and weight at each site in the study. Weight was measured in the lab only for sites A and F and with values for the other sites derived from allometric equations, as discussed in Section 3.3 below.

Measurements at Site A for *Z. pacifica* show that this species is much larger than *Z. marina* (Sites B–J) with a mean and standard deviation leaf area of 75 ± 40 cm^2 compared to 9 ± 6 cm^2. The weight of *Z. pacifica* (1.99 ± 1.26 g) was correspondingly greater than that of *Z. marina* (0.06 ± 0.09 g). However, there was no statistical difference between the eelgrass weight at any of the sites ($p > 0.05$).

Measurements of *Z. pacifica* are rare in the literature, but Duarte (1991) compiled eelgrass architecture data across 27 seagrass species, including *Z. marina*. Based on 16 papers, Duarte found an average leaf surface area and shoot weight for *Z. marina* of 34.65 cm^2 and 0.272 g, respectively. Assuming 4.2 leaves per shoot (Duarte 1991), the San Diego Bay *Z. marina* has an average leaf surface area of 37.8 cm^2 and shoot weight of 0.06 g.

Notably, the leaf area and biomass for eelgrass in this study was substantially lower than both means reported by Duarte (1991), and the historic conditions observed in San Diego Bay eelgrass beds. This may be the result of a long-term shortage in nutrient load to the bay due to persistent drought conditions that have prevailed from 2011-2019 as well as improved watershed controls on runoff. Over this period, a notable expansion of eelgrass to deeper bay depths has been noted (Merkel & Associates 2020). There has also been a notable reduction in overall canopy height and biomass throughout the beds over the past many years (K. Merkel, pers. Obs.). The link between prevailing drought and nutrient and turbidity reduction benefiting eelgrass extent in deeper waters through improved water clarity is discussed in the long-term monitoring program report; however, the ramifications of nutrient load reduction impacting eelgrass vigor is only touched on as this concern is only recently emerging as long-term monitoring is beginning to reveal patterns of increasingly diminutive size of plants comprising the beds within low-influx embayments of Southern California (Merkel, unpublished data).

TABLE 3-1
MEASURED BIOMASS DATA

Site	Quadrat	# of Shoots	Shoot Density (shoot/m^2)	Average Shoot Density (shoot/m^2)	Average Leaf Length (cm)	Average Leaf Area (cm^2)	Average Shoot Weight (g)[1]
A (*Z. pacifica*)	1	12	192	197	69	75	1.99
	2	10	160				
	3	15	240				
	Extra[2]	13	n/a				
B (*Z. marina*)	1	41	656	619	42	14	0.13
	2	40	640				
	3	35	560				
C (*Z. marina*)	1	15	240	245	39	12	0.08
	2	15	240				
	3	16	256				
D-1 (*Z. marina*)	1	34	544	891	25	6	0.03
	2	81	1296				
	3	52	832				
D-2 (*Z. marina*)	1	27	432	629	26	7	0.03
	2	43	688				
	3	48	768				
D-3 (*Z. marina*)	1	49	784	731	27	7	0.03
	2	49	784				
	3	39	624				
E (*Z. marina*)	1	38	608	677	32	9	0.05
	2	36	576				
	3	53	848				
F (*Z. marina*)	1	17	272	384	35	12	0.08[3]
	2	28	448				
	3	27	432				
G (*Z. marina*)	1	17	272	416	29	10	0.07
	2	37	592				
	3	24	384				
H (*Z. marina*)	1	22	352	485	30	8	0.05
	2	27	432				
	3	42	672				
I (*Z. marina*)	1	23	368	480	27	7	0.04
	2	28	448				
	3	39	624				

TABLE 3-1 (CONTINUED)
MEASURED BIOMASS DATA

Site	Quadrat	# of Shoots	Shoot Density (shoot/m^2)	Average Shoot Density (shoot/m^2)	Average Leaf Length (cm)	Average Leaf Area (cm^2)	Average Shoot Weight (g)[1]
J (*Z. marina*)	1	16	256	363	38	12	0.08
	2	22	352				
	3	30	480				

NOTES:

1. Only sites A and F were tested for weight. Values for the other sites are derived from allometric equations, as discussed in Section 3.3.
2. Extra samples were collected to reach the 50 samples that were tested for weight.
3. Twenty-two of the samples in quadrat 3 were not analyzed for weight since 50 samples had already been reached with quadrat 1 and quadrat 2

3.2 Aboveground Carbon Content

The average carbon contents measured for *Z. pacifica* and *Z. marina* were 24.2 ± 0.04 and 29.9 ± 0.02% dry weight, respectively. The difference in carbon content for the two species was found to be statistically significant ($p < 0.001$).

Duarte (1990) reviewed carbon content reported in the literature across 27 seagrass species at 30 locations and found an average carbon concentration of 33.6 ± 0.31% dry weight. Ten studies with 46 measurements looked at *Z. marina*, and no data was provided for *Z. pacifica*. Data for *Z. marina* spanned a large range (29-42%) but averaged closer to 36 percent. More recent studies have found *Z. marina* carbon content ranging from 34.4 to 38.8 percent dry weight in Europe (Dahl et al. 2016), 35 ± 0.32% in Denmark, and 38 ± 0.24% (Röhr et al. 2016). The San Diego Bay *Z. marina* carbon content appears low based on the literature, although it is within the range found by Duarte (1990).

Note that the sample mass collected resulted in fairly low weights sent to the lab (near the minimum mass required). If carbon crediting is pursued in the future, additional samples with a greater combined sample weight should be collected and tested to confirm these results. Further, a broader distribution of sampling should be undertaken.

3.3 Allometric Equations Relating Size and Weight

Allometric equations have been shown to provide a consistent alternative to tedious and destructive sampling methods by providing a relationship between eelgrass dimensions and weight (Duarte 1991; Echavarria-Heras et al. 2011). Previous studies have analyzed the relationships between various size parameters and weight using exponential or linear relationships (Echavarria-Heras et al. 2009, 2013, 2011a, 2011b). Assuming the dry sample weight of a shoot of eelgrass can be allometrically scaled in terms of the area of the leaf gives the following:

$$w = \alpha A^{\beta} \quad \text{Equation 1}$$

where w = weight of the dried sample, A = the area of the leaf of eelgrass, and α and β are parameters. A can be estimated by multiplying the length of the leaf (measured between the ligule and the tip) and the width of the leaf (measured at a point halfway). Since the width of eelgrass leaves is fairly constant, the weight of a sample should also allometrically scale in terms of the length of the leaf,

$$w = \gamma L^{\delta} \text{ Equation 2}$$

Where L = length and γ and δ are different parameters than in Equation 1. Echavarria-Heras et al. 2011a, 2011b, and 2013 verified this model through a consistent fitting of their data. Echavarria-Heras et al. 2011a and 2011b also considered the linear relationship between weight and leaf length,

$$w = \varepsilon L \text{ Equation 3}$$

where ε is a parameter.

Using the eelgrass size and weight data from 50 samples each collected at sites A and F (representing *Z. pacifica* and *Z. marina*, respectively), parameters were fit for Equations 1-3 (**Table 3-2**). The coefficient of determination (R^2), which shows how well the regression model fits the data, and the concordance correlation index ($\hat{\rho}$) (Lin 1989), which measures the correlation between data, were used to test the predictive quality of the models. For both values, a higher number represents a better fit.

TABLE 3-2
VALUES OF THE PARAMETERS, R^2, AND $\hat{\rho}$ RESULTING FROM THE FITTINGS OF THE ALLOMETRIC MODELS

Equation	Model Type	Species	Parameters		R^2	$\hat{\rho}$
Equation 1	$m = \alpha A^{\beta}$		α	β		
		Z. marina	1.4 x 10^{-7}	1.85	0.77	0.81
		Z. pacifica	1.3 x 10^{-4}	1.08	0.89	0.94
Equation 2	$m = \gamma L^{\delta}$		γ	δ		
		Z. marina	1.1 x 10^{-10}	3.42	0.63	0.79
		Z. pacifica	6.3 x 10^{-4}	1.58	0.82	0.90
Equation 3	$m = \varepsilon L$		ε			
		Z. marina	2.57 x 10^{-4}		0.33	0.39
		Z. pacifica	3.06017 x 10^{-3}		0.75	0.82

Equation 1 provided the best fit for both species of eelgrass. The *Z. pacifica* data was fit with α = 0.00013 and β = 1.08 with a determination coefficient of R^2 = 0.89 and $\hat{\rho}$ = 0.94. The *Z. marina* data was fit with α = 0.00000014 and β = 1.85 with R^2 = 0.77 and $\hat{\rho}$ = 0.81. The resulting parameters based on Equation 2 show that the simpler allometric model also holds. However, since both the coefficient of determination and the concordance correlation index showed better fits for the parameters associated with Equation 1 rather than either Equations 2 or 3, the Equation 1 fit was used for the rest of this study.

3.4 Variation Across Sites

The allometric equations derived in the previous section were used to estimate the weight of each shoot based on the measured leaf width and length for the sites where leaf weight was not measured (i.e., Sites B, C, D, E, G, H, I, and J). The total biomass was then calculated by summing it across the quadrat. **Table 3-3** presents the total biomass for each site and the total aboveground carbon (biomass multiplied by carbon content).

Fourqurean et al. (2012) found a global average of 0.755 ± 0.128 Mg C/ha for aboveground carbon for seagrass. The results for this study show aboveground carbon contents an order of magnitude less than Fourqurean et al. for *Z. marina* and comparable for *Z. pacifica* (Table 3-3).

TABLE 3-3
EELGRASS BIOMASS AND CARBON BY SITE

Site	Biomass (g/m^2)	Carbon (Mg C/ha)
A (*Z. pacifica*)	366 ± 171	0.89 ± 0.41
B (*Z. marina*)	80 ± 43	0.24 ± 0.13
C (*Z. marina*)	21 ± 7	0.06 ± 0.02
D-1 (*Z. marina*)	23 ± 7	0.07 ± 0.02
D-2 (*Z. marina*)	18 ± 4	0.05 ± 0.01
D-3 (*Z. marina*)	23 ± 11	0.07 ± 0.03
E (*Z. marina*)	35 ± 16	0.11 ± 0.05
F (*Z. marina*)	22 ± 6	0.07 ± 0.02
G (*Z. marina*)	28 ± 5	0.08 ± 0.02
H (*Z. marina*)	23 ± 7	0.07 ± 0.02
I (*Z. marina*)	18 ± 10	0.05 ± 0.03
J (*Z. marina*)	29 ± 11	0.09 ± 0.03

3.4.1 Species

Figure 3-1 compares aboveground carbon between Sites A and B to illustrate the difference between *Z. pacifica* and *Z. marina*. Likely because of its larger size, *Z. pacifica* had greater biomass (366 ± 171 g/m^2) and carbon content (0.89 ± 0.41 MgC/ha) than *Z. marina* (biomass: 80 ± 43 g/m^2 and carbon content: 0.24 ± 0.13 MgC/ha). However, this difference is not significant ($p > 0.05$).

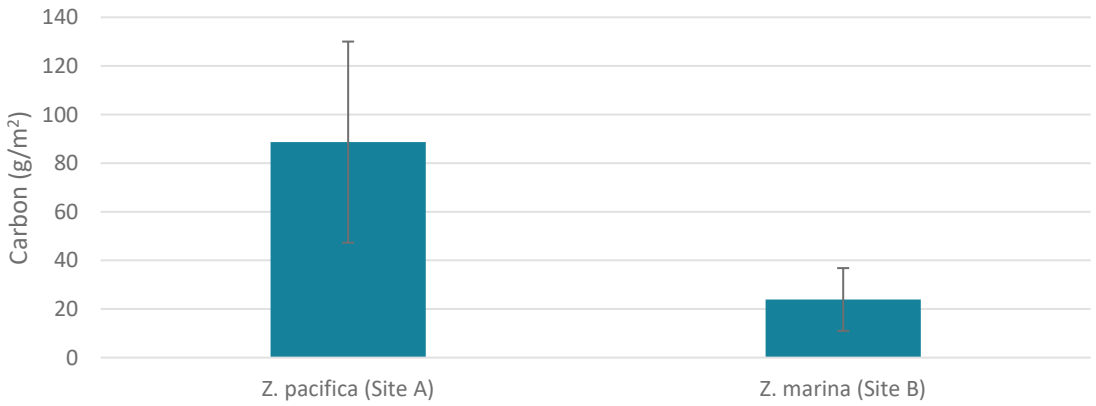

Figure 3-1. Carbon in Biomass by Species[8]

3.4.2 Ecoregion

Figure 3-2 compares aboveground carbon between Sites B, C, D-2, E, and F to illustrate the difference between the ecoregions within the bay. The Outer Bay site showed the greatest biomass and carbon content, although it was not significantly different from the other sites ($p > 0.05$).

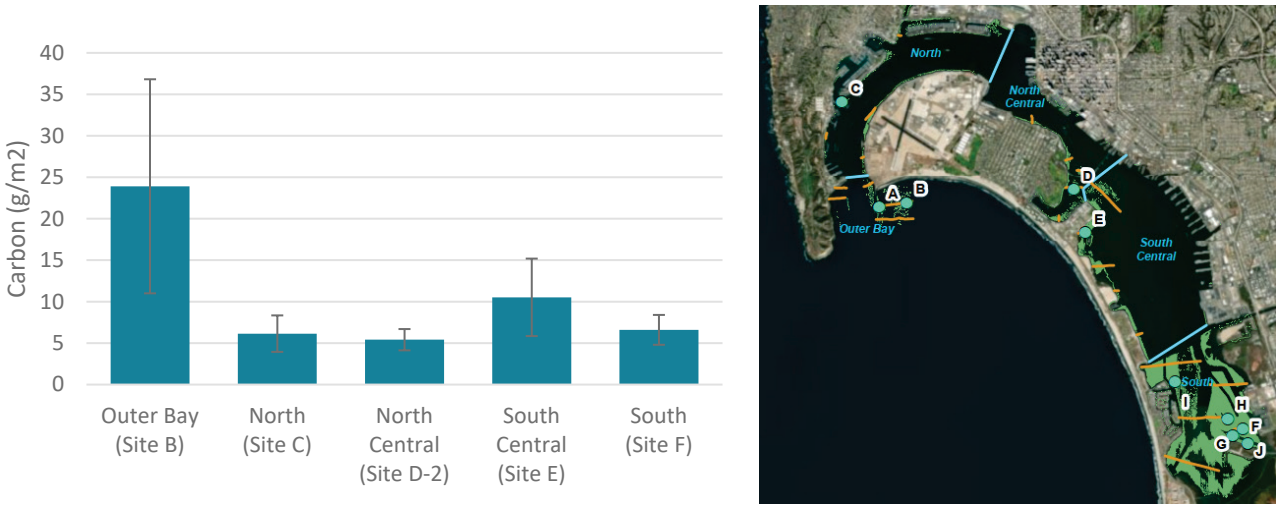

Figure 3-2. Carbon in *Z. marina* Biomass by Ecoregion

Sites I and F, both within the South Bay, provide a comparison between the denser east bay vegetation and the more fragmented west bay vegetation. However, the average biomass within the quadrat was similar between the east (22 ± 6 g/m^2) and the west (18 ± 10 g/m^2) as was the average carbon content (east: 7 ± 2 gC/m^2 and west: 5 ± 3 gC/m^2).

8 For this and the following plots, the bar represents the average value across the triplicate samples and the whisker represents ± one standard deviation.

3.4.3 Bed Depth

Figure 3-3 depicts the aboveground carbon between Sites D-1, D-2, and D-3 to illustrate the difference between bed elevations. While Serrano et al. (2014) found that water depth could be associated with higher primary production and larger biomass carbon stock, the sampling results showed minimal differences between the varying depths.

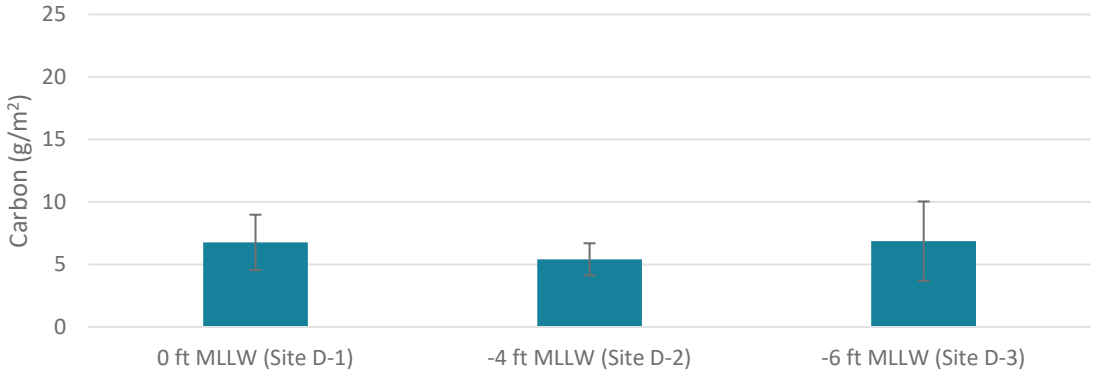

Figure 3-3. Carbon in *Z. marina* Biomass by Elevation

3.4.4 Bed Age

Figure 3-4 depicts the aboveground carbon between Sites F, J, H, and G, to illustrate the difference in bed age. The sampling results for biomass showed minimal differences between the varying bed ages.

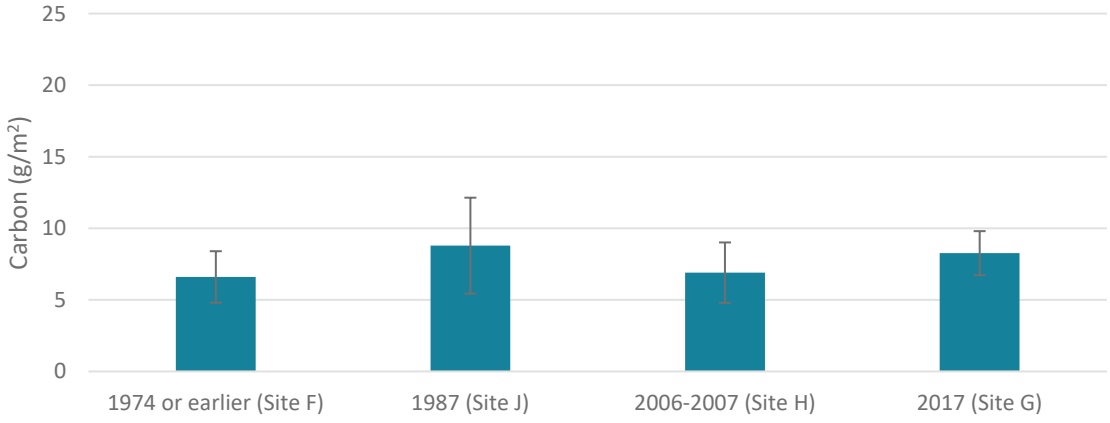

Figure 3-4. Carbon in Biomass by Bed Age

3.5 Productivity

The tables below summarize the growth and biomass accumulation on a daily basis for eelgrass within the study. The mean growth was calculated per shoot for *Z. marina* and *Z. pacifica* based on dry weight mass over the duration of the field study (**Table 3-4**). The measured density of

eelgrass beds was determined to range considerably between the more robust *Z. pacifica* plants (88.00 ± 22.71 shoots/m^2) and smaller *Z. marina* (165.60 ± 47.09 shoots/m^2). Finally, the productivity was determined on a *per square meter* basis by multiplying the average productivity of a shoot by the average number of shoots within a square meter of the eelgrass beds, as shown in **Figure 3-5**. The analysis showed that *Z. marina* has a productivity of 327.89 ± 137.10 mg/day/m^2 while *Z. pacifica* has a productivity of 979.88 ± 265.91 mg/day/m^2.

TABLE 3-4.
EELGRASS PRODUCTIVITY FOR SAN DIEGO BAY EELGRASS (MAY 2022)

Productivity Sample #	*Z. marina* Shoot Growth (mg/day/shoot)	*Z. pacifica* Shoot Growth (mg/day/shoot)
1	2.76	13.95
2	2.69	11.51
3	2.23	9.18
4	1.29	13.98
5	0.93	7.07
Mean Growth (± SD)	**1.98 ± 0.83**	**11.14 ± 3.02**

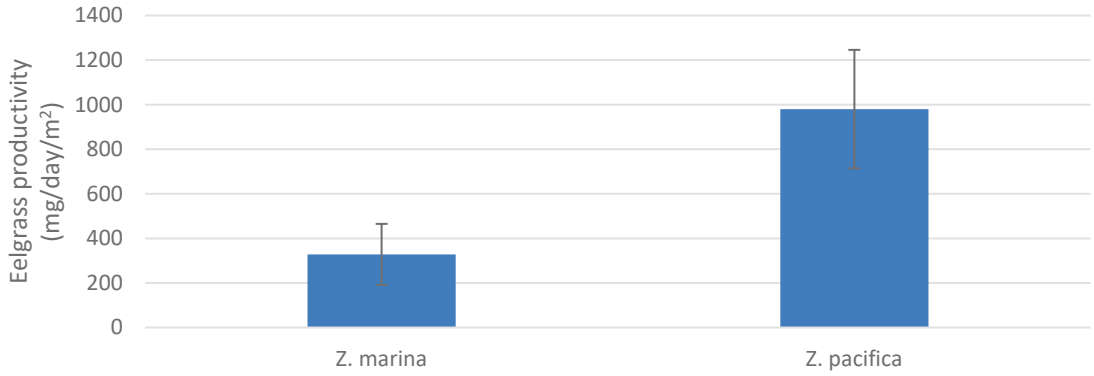

Figure 3-5. Eelgrass Productivity

Multiplying the carbon content results from Section 3.2 with the eelgrass biomass productivity results in the carbon assimilation of the biomass. *Z. marina* assimilates 98.0 ± 41.0 mg C/m^2/day and *Z. pacifica* assimilates 237.1 ± 64.4 mg C/m^2/day. Note that assimilation in this context refers to biological sequestration, or what is taken into biomass—it does not guarantee that the carbon will be buried into the sediments. **Table 3-5** shows the productivity by site.

TABLE 3-5
EELGRASS CARBON ASSIMILATION BY SITE

Site	Average Shoot Density (shoots/m^2)	Average Assimilation (g C/m^2/yr)
A (*Z. pacifica*)	197 ± 40	194 ± 73
B (*Z. marina*)	619 ± 51	609 ± 263
C (*Z. marina*)	245 ± 9	241 ± 103
D-1 (*Z. marina*)	891 ± 379	876 ± 527
D-2 (*Z. marina*)	629 ± 176	619 ± 315
D-3 (*Z. marina*)	731 ± 92	719 ± 318
E (*Z. marina*)	677 ± 149	666 ± 319
F (*Z. marina*)	384 ± 97	378 ± 187
G (*Z. marina*)	416 ± 162	409 ± 236
H (*Z. marina*)	485 ± 167	478 ± 261
I (*Z. marina*)	480 ± 131	472 ± 238
J (*Z. marina*)	363 ± 112	357 ± 188

NOTE: Because the sampled Z. marina productivity rate was much lower than the literature, the sampled Z. pacifica productivity rate and carbon fraction were applied to extrapolate for all sites in Table 3-5.

Carbon sequestration rates for seagrass vary widely in the literature, as shown in **Table 3-6**. Duarte et al. (2005) estimated a global carbon sequestration rate of 83 g C/m^2/yr, while McLeod et al. (2011) estimated 138 g C/m^2/yr. Duarte et al. (2011) measured a sequestration rate of 52.4 g C/m^2/yr for *Z. marina*.

TABLE 3-6
EELGRASS SEQUESTRATION RATES IN THE LITERATURE

Source	Sequestration Rate (g C/m^2/yr)	Notes
Duarte et al. (2005)	83	global
Greinier et al. (2013)	38	Virginia
Chiu et al. (2013)	20	Korea
McLeod et al. (2011)	138	global
Duarte et al. (2011)	52.4	NW Mediterranean; *Z. marina*
Samper-Villarreal et al. (2018)	50.5	NE Australia

Comparing the values in Tables 3-5 and 3-6 show an order of magnitude discrepancy between carbon assimilation rates and carbon sequestration rates. As discussed in Tomasko 2015, at least a portion of the discrepancy may be due to sequestration into bicarbonate ions in the water column, which is something that will be analyzed in Year 2 of this study.

This page intentionally left blank

SECTION 4
Belowground Carbon Data Analysis

The belowground carbon stock was determined based on the dry bulk density and organic carbon content found in each of the samples within a core. Several terms are commonly used in the study and quantification of blue carbon, including the following:

- **Bulk density**: This describes the mass of sediment per unit volume (i.e., grams of sediment per cm^3 [g/cm^3]). This is used in conjunction with the measured organic carbon percentage to determine the carbon density.
- **Organic carbon percentage**: This describes the mass of carbon per the mass of sediment in a sample (i.e., grams of carbon per grams of soil [gC/g soil] as a percentage).
- **Sediment carbon density**: This describes the amount of carbon per volume of sediment (i.e., grams of carbon per cm^3 [gC/cm^3]). It is calculated by multiplying bulk density (g/cm^3) and the organic carbon percentage (g C/g soil).
- **Total carbon per sample**: This term describes the mass of carbon (in grams) contained in the sampling interval or entire core. It is expressed on a per-surface area basis (i.e., gC/cm^2) to allow for spatial extrapolation. It is calculated by multiplying the sediment carbon density (gC/cm^3) by the sample thickness (cm). Note the distinction between carbon density and total carbon per sample: *carbon density* is a per volume metric (i.e., is not dependent on sample thickness/size), while *total carbon per sample* is affected by the size of the sample. For example, a 0.1-meter sample may have more carbon mass than a 0.5-meter sample because the soil carbon density is greater in the shorter sample.

4.1 Belowground Carbon Content

Table 4-1 provides the elevations at which the sediment cores were taken, the core lengths, the average bulk density, average organic carbon percentage, average sediment carbon density, and total carbon within each core. For the complete dataset, see Section 4.3.

All sites were sampled to a depth of 1-meter or to refusal, whichever was reached first. We attempted to sample one core in each ecoregion (i.e., at Sites B, C, D-3, E, and F) to 3-meters' depth, but in all cases the Vibracore met refusal (i.e., the corer could not be pushed any deeper) before reaching that depth. Carbon content typically varies most in the upper 20 cm to half-meter (Fourqurean et al. 2012), but sampling deeper cores allowed further exploration of carbon patterns with depth.

Bulk density for sediments in *Z. marina* beds vary between 0.71 and 1.4 g/cm^3 in the literature (Dahl et al. 2016; Kauffman et al. 2020) and between 0.93 and 1.44 g/cm^3 in San Diego Bay,

based on these study results. Bulk density for sediments in *Z. pacifica* beds averaged 1.04 g/cm^3 at the outer bay sampling site, slightly lower than the measurements for *Z. marina*.

Dahl et al. (2016) reported sediment carbon contents between 0.05 and 0.35 g/cm^2 for *Z. marina* eelgrass beds in Europe, compared to the lab results that showed a range from 0.02 to 1.08 g/cm^2 for *Z. marina* in San Diego Bay. The sediment carbon content for *Z. pacifica* ranged from 0.06 to 0.07 g/cm^2.

In aggregate, the percent organic carbon data does not show a correlation with bulk density. However, stratifying the plot based on sediment texture (based on visual assessment) shows that the sandy sediment classes (mud/sand, sand, and sand/shell) appear to have the lowest carbon fractions. Clayey sediments as a group were also fairly low in carbon fraction. Muddy sediments and samples with shell hash generally show higher carbon content, but also a much larger range.

Figure 4-1 was constructed from the data for one core from each site (excluding the younger sites G and H). Note that the classification in Figure 4-1 and all references to sediment texture throughout the report are based on visual observation and not laboratory sieve analyses.

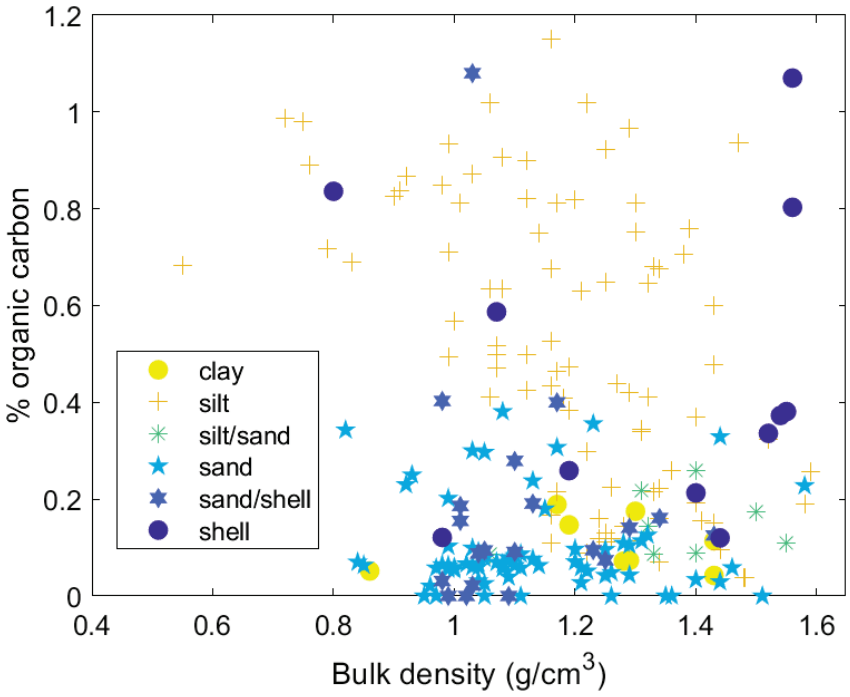

Figure 4-1. Percent Organic Carbon and Bulk Density of Various Sediment Grain Classes

TABLE 4-1
MEASURED SEDIMENT DATA

Site	Core	Sample Elevation (m NAVD)	Core Length (m)	Average Elevation (m NAVD)	Average Elevation (ft MLLW)	Bulk Density (g/cm^3)	Organic Carbon Percentage	Sediment Carbon Density (gC/cm^3)	Total Carbon in 1-m Core (MgC/hectare)
A (***Z.pacifica***)	1	-2.1	1	-2.1	-7	1.05	0.07%	0.0007	7.3
	2	-2.1	1			1.07	0.06%	0.0006	6.2
	3	-2.2	1.5			1.01	0.05%	0.0006	5.7
B (***Z.marina***)	1	-1.3	1	-1.3	-5	1.05	0.09%	0.0009	9.6
	2	-1.3	1			1.23	0.10%	0.0012	15.1
	3	-1.2	1			1.14	0.11%	0.0012	10.6
C (***Z.marina***)	1	-2.0	1	-2.0	-7	1.15	0.40%	0.0044	71.1
	2	-2.0	1			1.26	0.21%	0.0025	27.4
	3	-2.0	1			1.08	0.36%	0.0036	48.5
D-1 (***Z.marina***)	1	-0.3	1	-0.4	-2	0.93	0.23%	0.0022	15.9
	2	-0.4	1			1.09	0.22%	0.0024	21.0
	3	-0.3	1			1.23	0.13%	0.0016	10.7
D-2 (***Z.marina***)	1	-1.5	1	-1.6	-6	1.38	0.21%	0.0030	40.8
	2	-1.6	1			1.44	0.20%	0.0030	38.4
	3	-1.6	1			1.32	0.17%	0.0022	27.6
D-3 (***Z.marina***)	1	-2.2	1	-2.2	-8	1.28	0.13%	0.0017	8.5
	2	-2.2	1			1.36	0.43%	0.0063	87.9
	3	-2.2	2			1.29	0.25%	0.0036	32.7
E (***Z.marina***)	1	-1.5	1	-1.5	-5	1.09	0.53%	0.0053	42.9
	2	-1.5	1			1.13	0.56%	0.0056	50.1
	3	-1.5	2			1.07	0.40%	0.0037	40.9
F (***Z.marina***)	1	-1.1	1	-1.4	-2	1.10	0.76%	0.0084	86.9
	2	-1.1	1			1.25	0.81%	0.0100	99.3
	4	-2.0	2.5			1.20	0.78%	0.0090	107.9
G (***Z.marina***)	1	-1.1	1	-1.2	-4	1.36	0.02%	0.0003	1.9
	2	-1.1	1			1.01	0.04%	0.0004	2.2
	3	-1.3	1			1.02	0.04%	0.0004	2.4
H (***Z.marina***)	1	-1.9	1	-1.8	-6	1.23	0.24%	0.0023	20.4
	2	-1.8	1			1.12	0.14%	0.0014	11.1
	3	-1.6	1			1.24	0.18%	0.0022	15.2
I (***Z.marina***)	1	-2.7	1	-2.6	-9	1.28	0.31%	0.0037	24.7
	2	-2.6	1			1.21	0.40%	0.0048	37.7
	3	-2.5	1			1.36	0.23%	0.0030	17.9
J (***Z.marina***)	1	-0.9	1	-0.9	-3	1.13	0.69%	0.0077	79.5
	2	-1.0	1			1.20	0.73%	0.0085	87.2
	3	-1.0	1			1.19	0.75%	0.0087	94.5

NOTES:

Elevations were collected in ft NAVD88 in the field. A conversion of NAVD – 0.43 ft = MLLW was used throughout the bay (NOAA Tides and Currents for San Diego Bay).

4.2 Variation Across Sites

Table 4-2 summarizes average sediment carbon by site for the top one meter of sediment. This allows for a high-level comparison across the environmental variables of interest. The carbon in the top one meter ranged from 1.9 to 107.9 Mg C/ha. This is comparable to the large range found in the literature. For example, Dahl et al. (2016) measured belowground carbon in *Z. marina* beds in Europe and found total carbon from 5 to 35 Mg C/ha, while Kauffman et al. (2020) found 216.3 Mg C/ha of belowground carbon in *Z. marina beds* in the Pacific Northwest. **Figure 4-2** shows the average sediment carbon for the top 1-meter of sediment across the bay.

TABLE 4-2
EELGRASS SOIL CARBON BY SITE

Site	Carbon to 1-m depth (Mg C/ha)
A	6.4 ± 0.8
B	11.8 ± 3.0
C	48.0 ± 21.9
D-1	15.8 ± 5.2
D-2	35.6 ± 7.0
D-3	43.0 ± 40.7
E	44.6 ± 4.8
F	98.0 ± 10.5
G	2.2 ± 0.3
H	15.5 ± 4.6
I	26.8 ± 10.1
J	87.1 ± 7.5

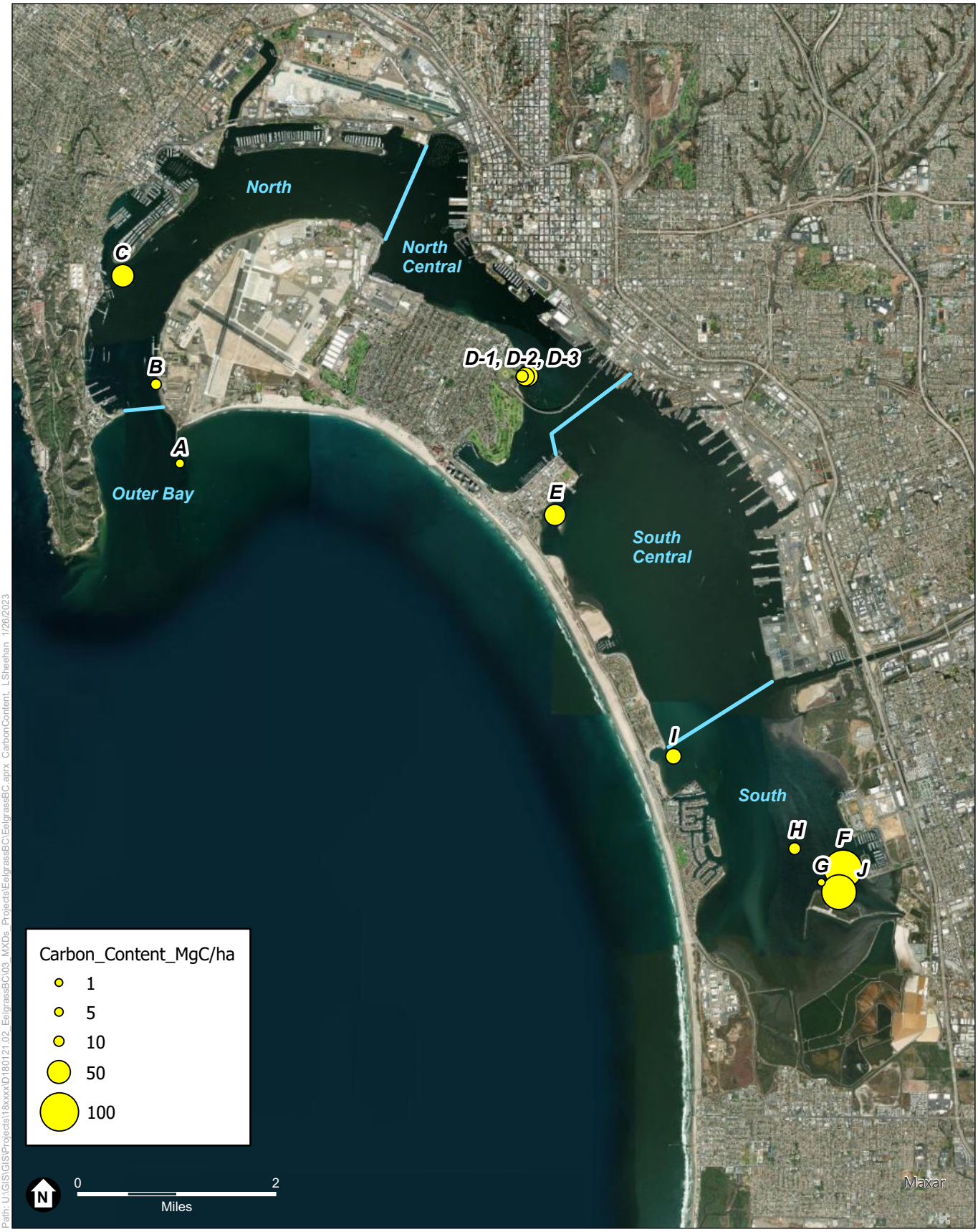

Path: U:\GIS\GIS\Projects\18xxxx\D180121.02_EelgrassBC\03_MXDs_Projects\EelgrassBC\EelgrassBC_aprx_CarbonContent_LSheehan_1/26/2023

SOURCE: ESA, 2021

San Diego Bay Eelgrass Blue Carbon Study

Figure 4-2
Total Carbon in 1-m Core (MgC/hectare)

ESA

4.2.1 Species

Sites A and B represented *Z. pacifica* and *Z. marina* beds, respectively. The *Z. pacifica* bed had lower sediment carbon storage despite the plants' larger biomass compared to *Z. marina* (**Figure 4-3**). This may be due to non-biological factors, including the greater wave energy and detrital transport away from Site A compared to Site B, which may cause less carbon to remain in place. The sandy sediment and high circulation within the open coastal Site A would naturally be less likely to retain and sequester particulate organic matter and thus accumulate organic carbon. However, the two species were not significantly different from each other ($p > 0.05$).

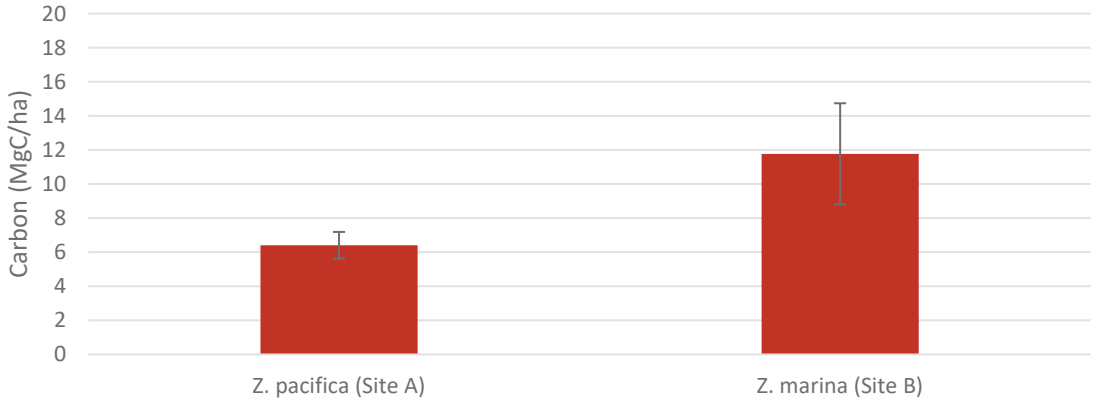

Figure 4-3. Sediment Carbon by Species

4.2.2 Ecoregion

Figure 4-4 compares the total belowground carbon between Sites B, C, D-2, E, and F to illustrate the difference between the ecoregions within the bay. This plot shows a general trend of increasing carbon going southward within the bay. In particular, the Outer Bay stored significantly less carbon ($p < 0.05$) than North Central, South Central, and South Bays, and storage was also significantly different ($p < 0.05$) between the South Bay and the two ecoregions just north of it (North Central and South Central).

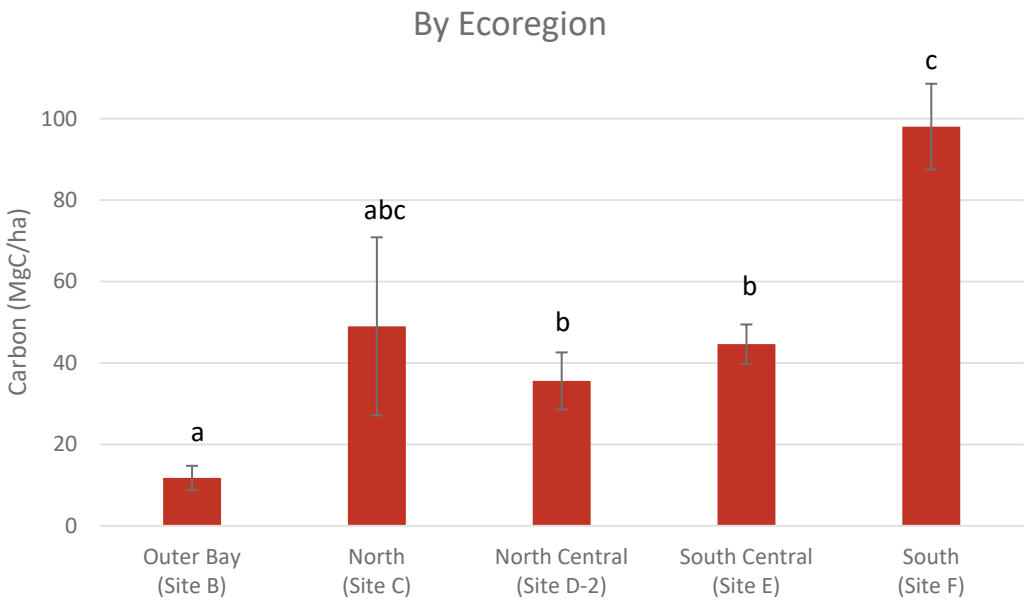

Note: The letters above each bar represent statistical significance from bars with other letters. For example, the "a" above Outer Bay indicates that this site was statistically different from the North Central, South Central, and South sites (which do not have "a" above the bar), but not statistically different from the North site (which does have an "a" above the bar).

Figure 4-4. Sediment Carbon by Ecoregion

4.2.3 Bed Depth

Sites D-1, D-2, and D-3 allow for comparison across depth. The data shows that the average carbon content may increase with increasing depth (**Figure 4-5**). The middle depth (-5 ft MLLW) showed significantly ($p < 0.05$) more carbon than the shallowest depth (-1 ft MLLW). The deepest cores (-7 ft MLLW) showed a substantial amount of variability, so this site was not statistically significant from the other two depths.

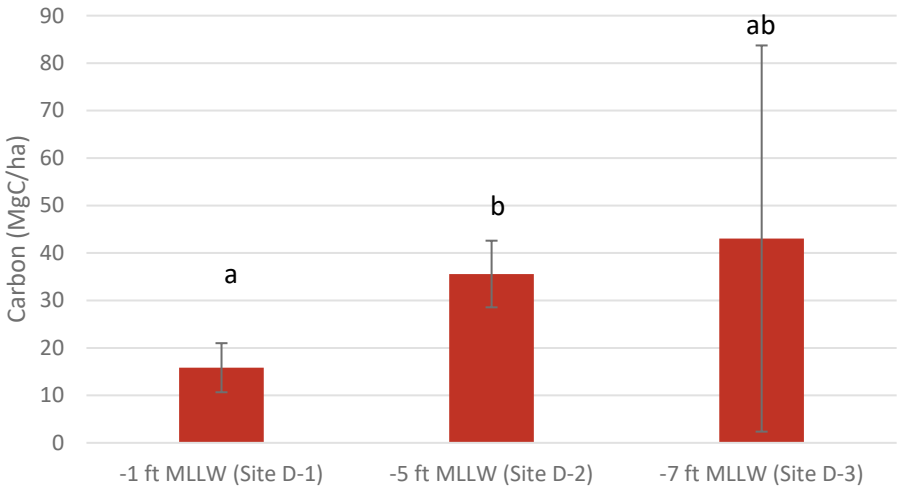

Figure 4-5. Sediment Carbon by Bed Depth

As discussed in Section 2, sampling depths varied more than intended across the other sites. When the carbon content for all sites is analyzed by depth, the pattern is less clear. As shown in **Figure 4-6**, the two highest carbon content sites (Sites F and J) were taken at shallow depths (-1.9 and -3.4 ft MLLW, respectively).

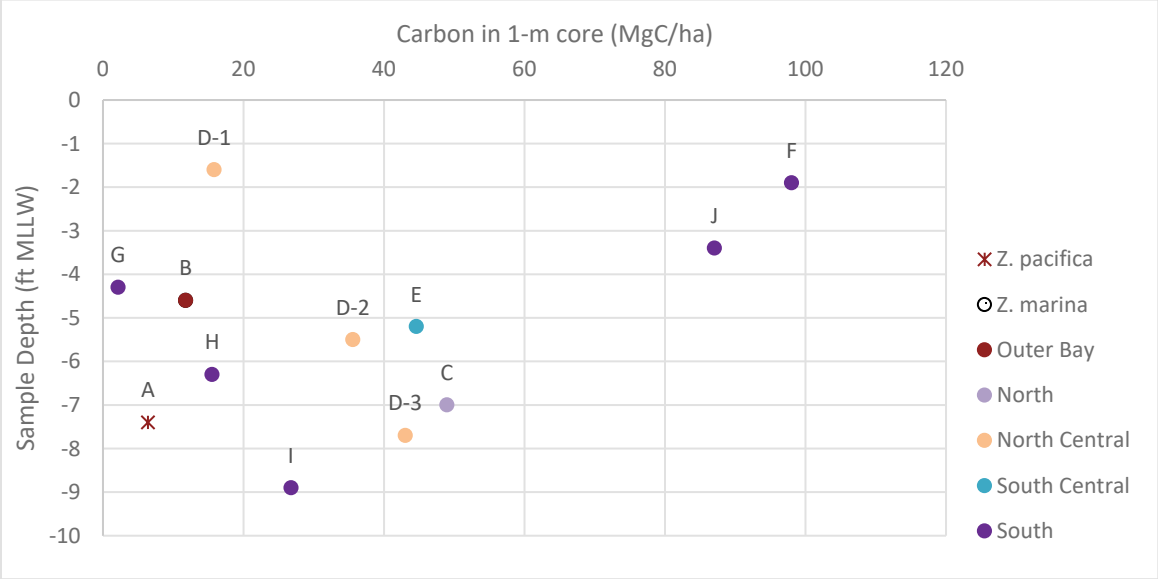

Figure 4-6. Sediment Carbon by Bed Depth for All Sites

4.2.4 Bed Age

Eelgrass beds of different ages were compared to evaluate variations in the amount of carbon stored in younger and older systems. As shown in **Figure 4-7**, the older sites (Sites F and J) had significantly ($p < 0.01$) greater amounts of carbon in the soils than the younger sites (Sites G and H). Additionally, Site J, which was planted in 1987, had significantly ($p < 0.01$) more carbon than Site H, which was restored in 2006-2007, which had significantly ($p < 0.05$) more carbon than Site G was restored more recently in 2017.

Site J was planted in 1987 on the Chula Vista Wildlife Reserve, an island constructed between 1974 and 1979 with fill material from the construction of the Chula Vista Marina Basin. Site H was planted in 2006-2007 on fill placed by scow dump in a sediment borrow site depression during the same period from a prior upland fill. Finally, Site G was planted in 2017 on sediment fill that was hydraulically placed in a decommissioned cooling water channel to develop eelgrass habitat (Merkel, pers. Obs.).

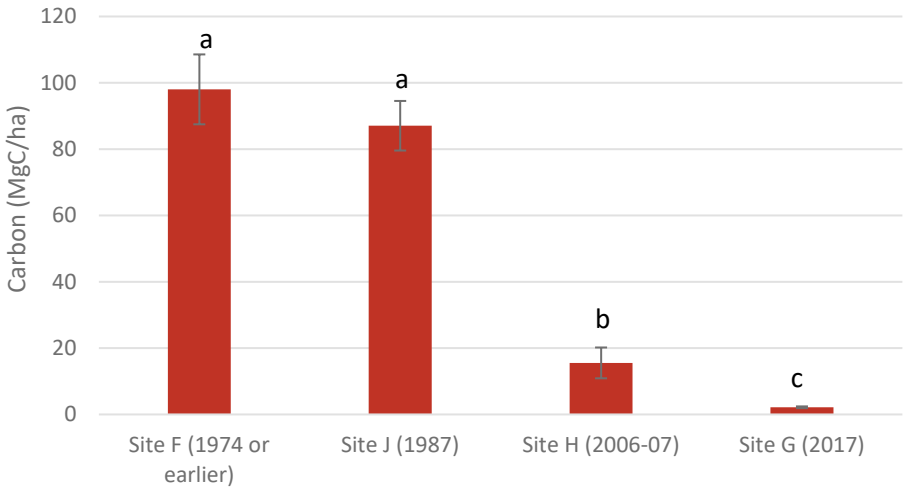

Figure 4-7. Sediment Carbon by Bed Age

As shown in **Figure 4-8**, the data depicts a strong linear relationship between eelgrass bed age and carbon content. Additionally, Sites J, H, and G were all restoration projects involving fill placement to raise bay floor elevations, so carbon accumulation may continue to develop as the sites mature. A meta-analysis of 621 wetland restoration sites around the globe showed that, while hydrologic functions are quick to recover to levels comparable to reference sites, biological and biogeochemical functions (including carbon storage) often lag behind throughout the century-long analysis period (Moreno-Mateos et al. 2012).

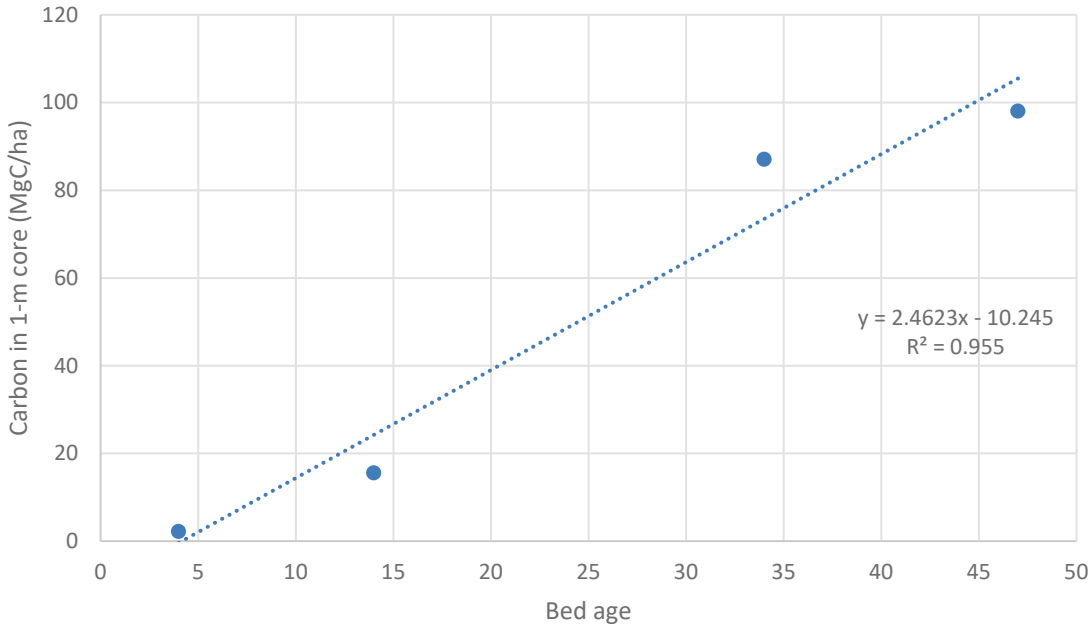

Figure 4-8. Sediment Carbon Related to Bed Age

4.3 Variation Along Depth of Core

Along with examining the spatial variability of carbon content, it is also important to understand how carbon content varies down cores. **Figure 4-9** shows all bulk density profiles, **Figure 4-10** shows all percent organic carbon profiles, and **Figure 4-11** shows all carbon density profiles.

Bulk density profiles do not display any outstanding patterns except a slight shift to more dense sediment compositions further south in the bay. Within each site, the triplicate profiles are generally in good agreement with one another. Bulk density of samples collected below 1-meter depth were not particularly lower than in the rest of the core.

The percent organic carbon profiles display much greater variation both across the bay and within the sets of triplicates. Not including the two youngest sites (Sites G and H), the percent of organic carbon (i.e., g C / g sediments) is highest in the South Central and South Bay ecoregions. Additionally, those profiles show more variation down the core. Samples from below 1-meter depth tended to be lower in carbon than the rest of the core.

It is often expected that carbon content will be greatest at the surface (Kindeberg et al. 2019) where organic matter is input into the sediment column and will then decrease with depth as mixing and remineralization slowly decrease the carbon store. This was observed at several sites in this study (e.g., Sites D-1, G, and H), where the profiles appeared to reach an asymptote, from which we infer that carbon below that depth is buried and unlikely to change.

However, a plurality of depth profiles from this study show greater complexity and follow a more mixed or indistinct pattern. None of the profiles show monotonically increasing carbon percentage with depth, which was observed in a minority of sites (i.e., 7 of 47) in a study aggregating cores from *Z. marina* beds throughout the Northern Hemisphere (Kindeberg et al. 2019).

More mixed profiles, along with the variability between triplicates, such as those observed at Sites F, D-3, and C complicate the process of using discrete cores to extrapolate carbon estimates across areas and into the ground as the pattern is not consistent or predictable with depth. For instance, cores at Site D-3 show sharp jumps in carbon density at 40–100 cm depth (Core 2) and at 10–30 cm depth (Core 3) to values an order of magnitude larger than elsewhere in the core. Given the relatively low carbon content of these sediments, it is possible that the inclusion of a small fragment of plant matter may have caused the jumps observed above. Indeed, Kindeberg (2019) found that these mixed profiles were associated with bioturbation and high mixing.

The cores that were taken beyond 1-meter depth all showed additional carbon is stored below the top 1-meter. The longer cores showed that the top 1-meter contained 56-90% of the carbon within the core.

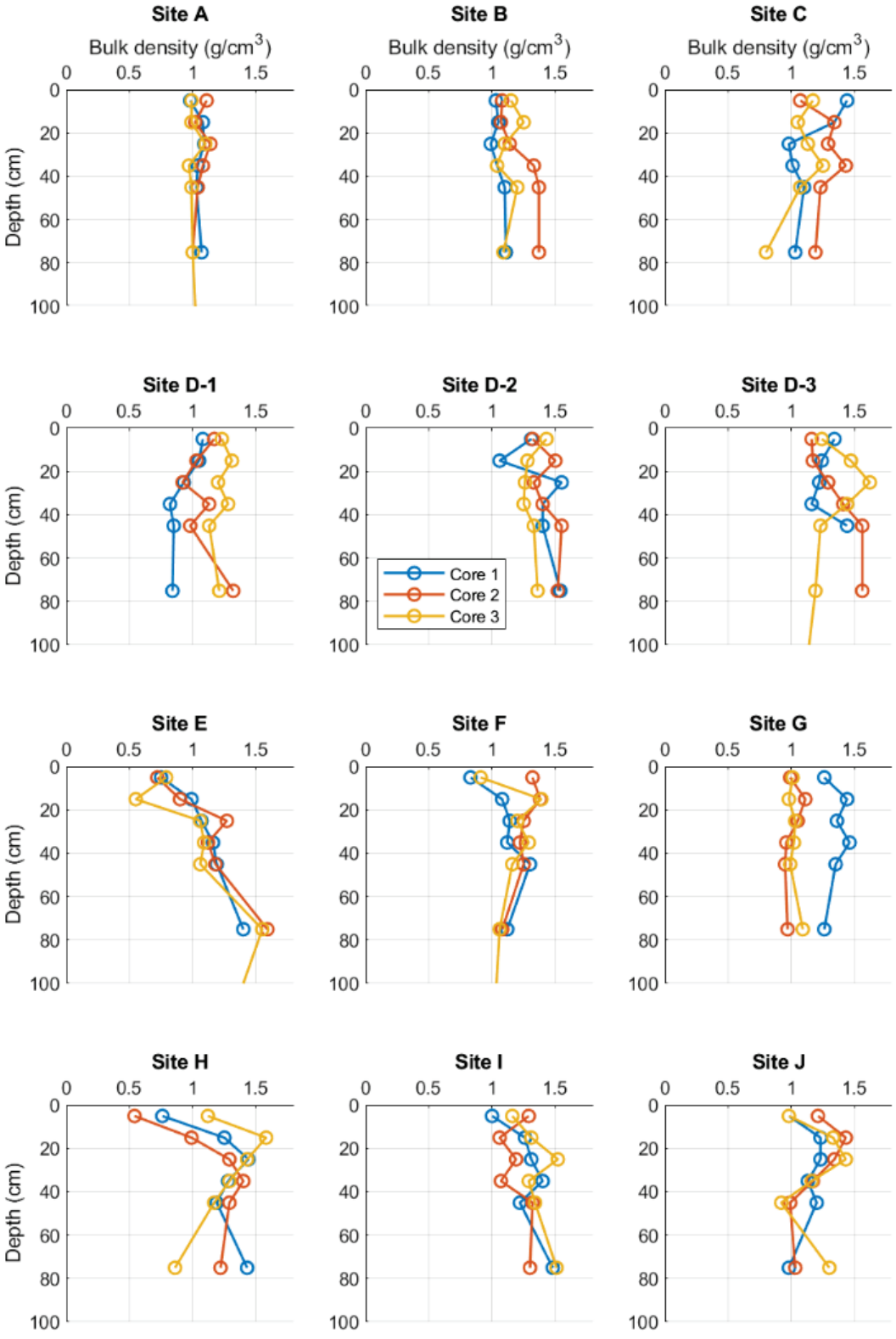

San Diego Bay Eelgrass Blue Carbon Study

Figure 4-9
Bulk Density by Depth

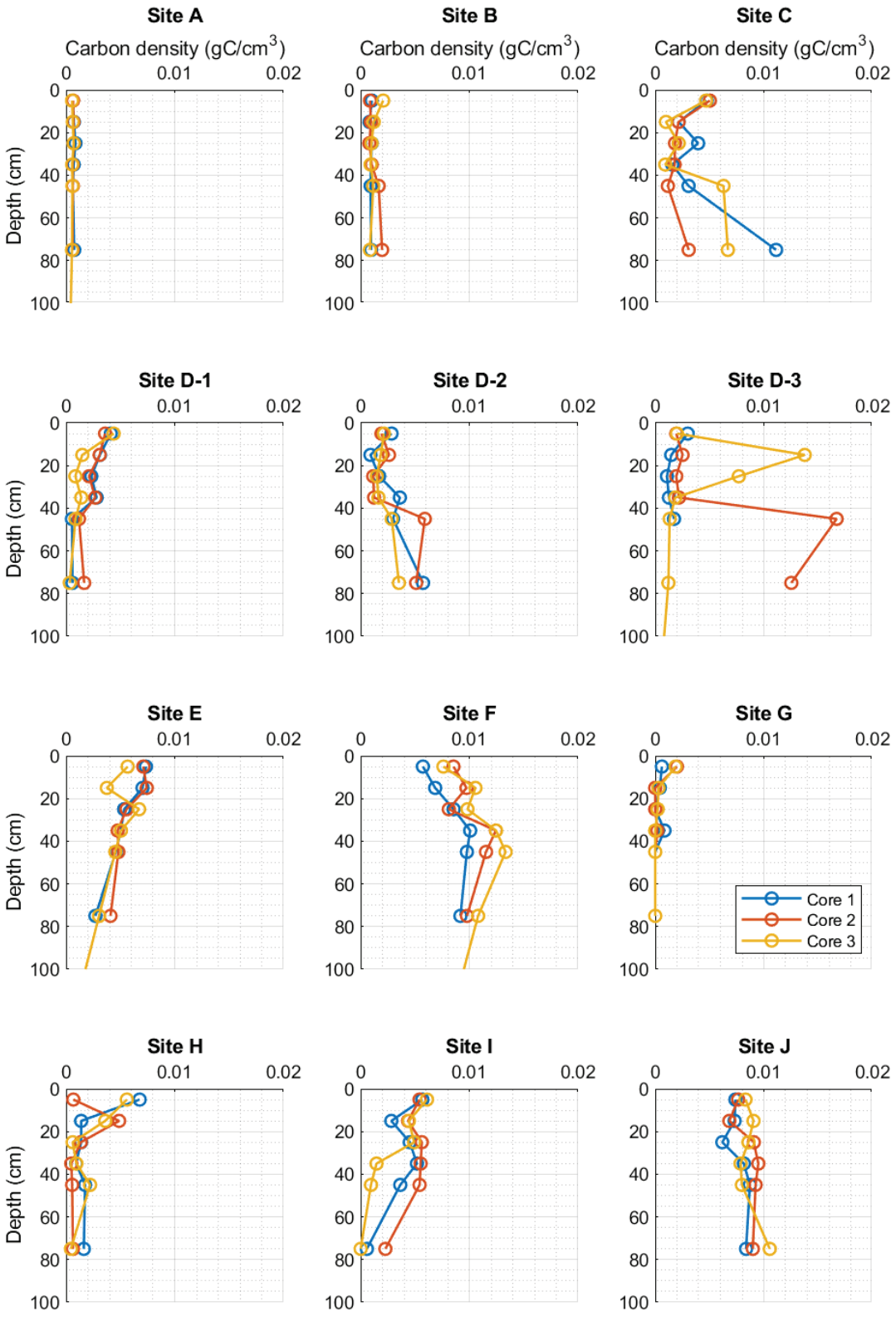

San Diego Bay Eelgrass Blue Carbon Study

Figure 4-10
Percent organic carbon profiles for all sediment cores

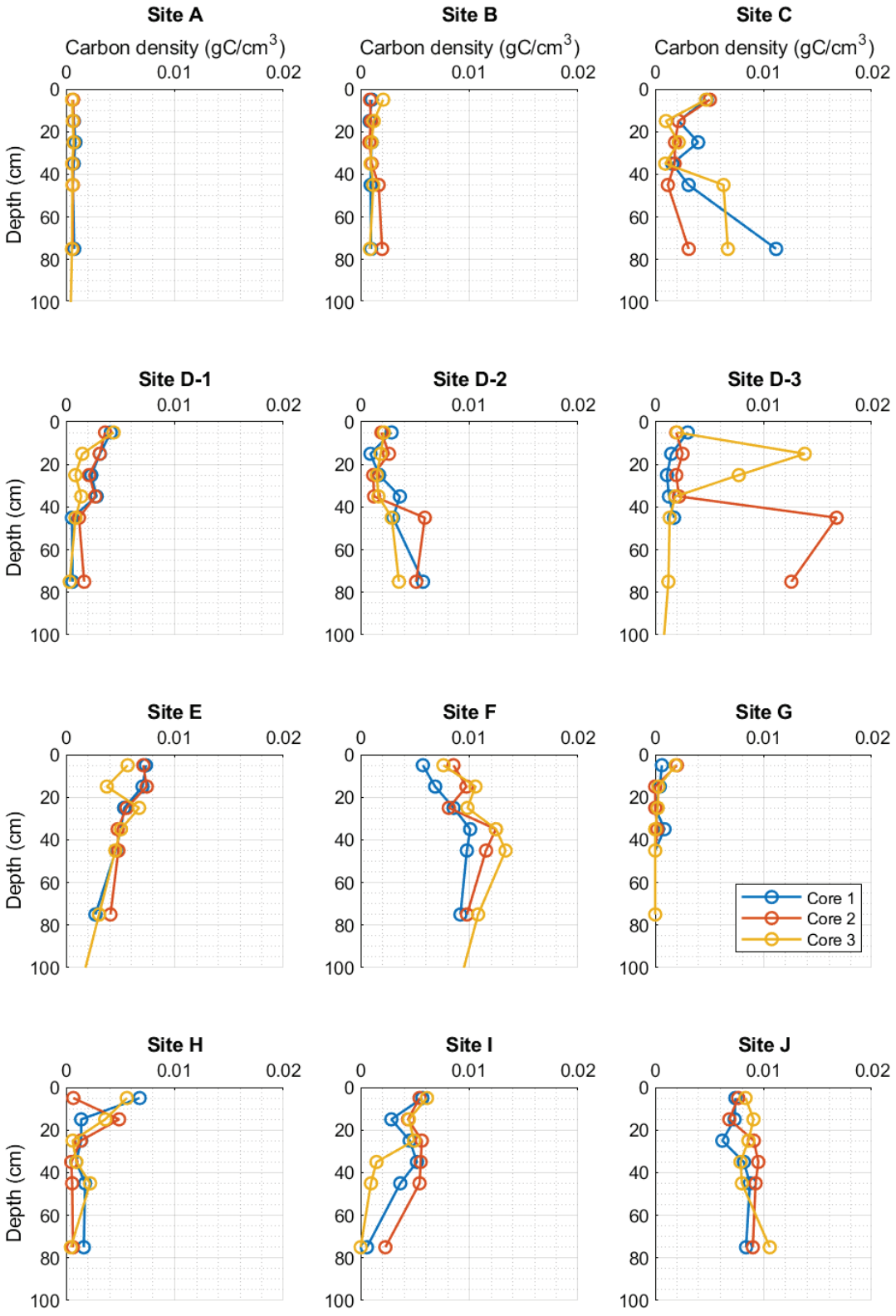

San Diego Bay Eelgrass Blue Carbon Study

Figure 4-11
Carbon density profiles for all sediment cores

Comparing sites in the South Bay (Sites F, I, and J) with the nearby younger restoration Sites H (established 2006–2007) and G (2017) reveals that while carbon content at the younger restoration sites decreases with depth, the profiles are more indistinct in the other sites. The sediment at Sites G and H was more varied, consisting of fines, sands, and shell hash. By comparison, the sediment at Sites F, I, and J was much more uniform and dominated by mud. Some cores had more compacted clay at depth (i.e., in the deepest one or two samples). The variation in sediments of Sites G and H could be a result of fill used in the restoration resulting in higher carbon near the surface from the eelgrass and less carbon below in the fill.

SECTION 5
Total Carbon Quantification

5.1 Aboveground Carbon Pool

Since 2007, Naval Facilities Engineering Command Southwest has undertaken biannual monitoring of permanently established transects at 25 locations throughout the bay. Additionally, bay-wide eelgrass surveys have been jointly performed by the Navy and the Port every three to five years. Total eelgrass acreage in San Diego Bay has varied from 1,091 acres in 1993 to a high of 2,598 acres in 2020. **Figure 5-1** shows the eelgrass extent in San Diego Bay.

The eelgrass areas from these surveys can be used to estimate the total aboveground carbon pool by ecoregion, as shown in **Table 5-1**. We assumed that 80% of the Outer Bay is made up of *Z. pacifica* and 20% is *Z. marina* (correspondence with K. Merkel, January 28, 2022). Due to the high carbon content in *Z. pacifica* (Section 3.4.1), the outer bay shows the highest aboveground carbon in the bay (**Figure 5-2**). In years when the acreage of eelgrass in the Outer Bay is lower, the total estimated aboveground carbon stored in the bay's eelgrasses is also lower. However, it should be noted that while bed area has increased over time, in recent years, the overall biomass of eelgrass is believed to have declined substantially with more diminutive plants comprising most of the *Z. marina* beds in the bay, as discussed in Section 3.1.

TABLE 5-1
HISTORIC ABOVEGROUND CARBON IN SAN DIEGO BAY (TONNES CO_2 EQUIVALENT)

Ecoregion	1993	1999	2004	2008	2011	2014	2017	2020
Outer Bay (*Z. pacifica*)	27	37	435	301	291	238	35	94
Outer Bay (*Z. marina*)	2	3	29	20	20	16	2	6
North	5	8	8	8	12	10	10	15
North Central	5	10	6	7	11	8	9	5
South Central	41	52	43	32	37	26	26	72
South	74	113	133	70	115	145	137	195
Total	**154**	**224**	**654**	**439**	**484**	**444**	**220**	**388**

NOTES:

Results from Sites D-1, D-2, and D-3 were averaged for the North Central ecoregion, while Sites F, G, H, I, and J were averaged from the South ecoregion.

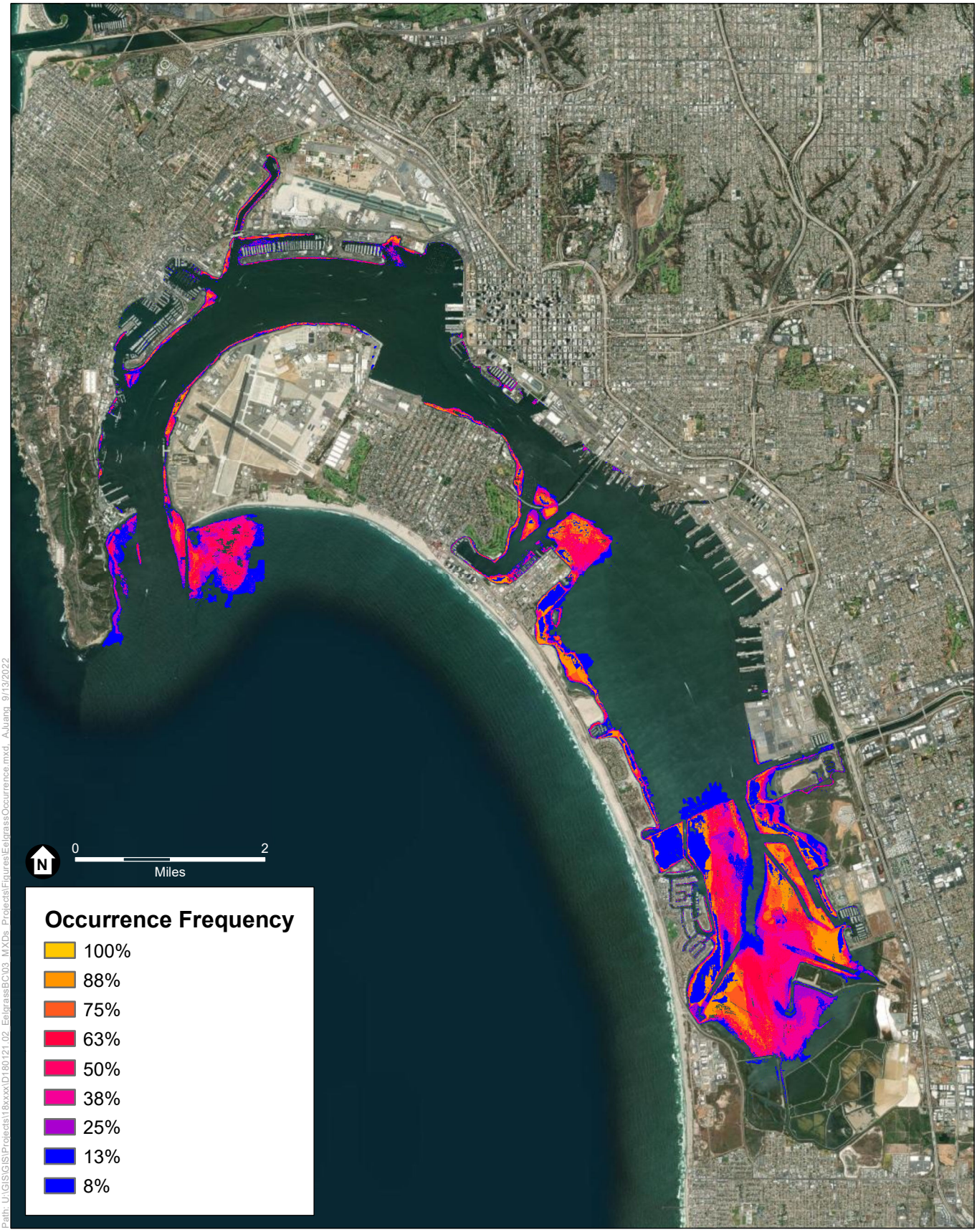

Path: U:\GIS\GIS\Projects\18xxxx\D180121 02_EelgrassBC\03_MXDs_Projects\Figures\EelgrassOccurrence.mxd_AJuang_9/13/2022

SOURCE: Merkel

San Diego Bay Eelgrass Blue Carbon Study

Figure 5-1
Eelgrass Extent and Occurrence (1993-2020)

ESA

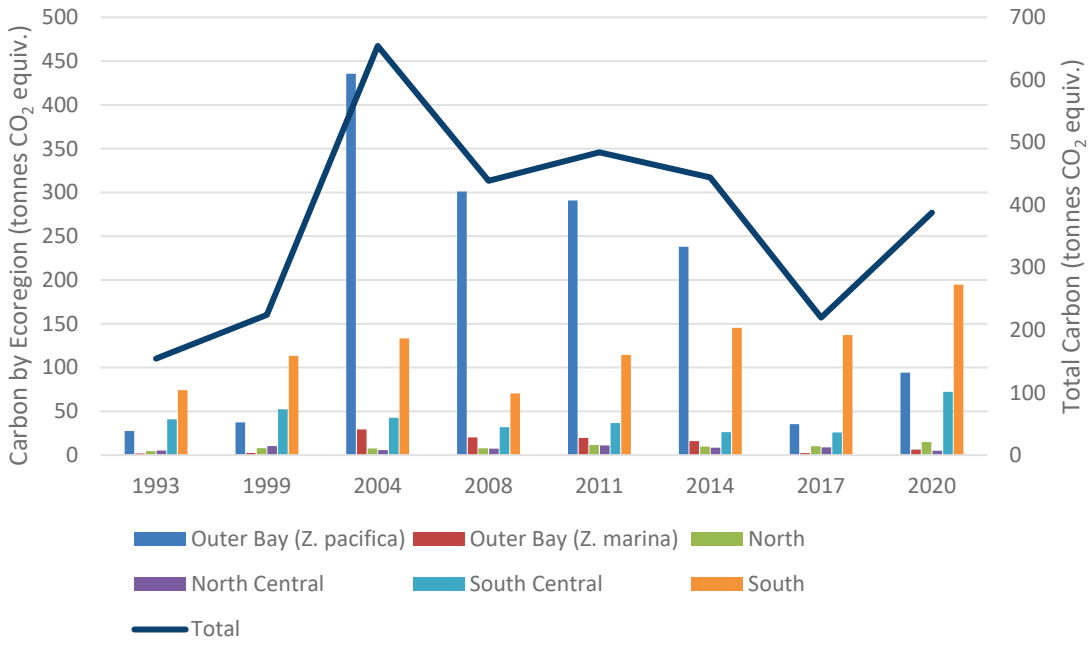

Figure 5-2. Total Aboveground Carbon in San Diego Bay Over Time

5.2 Belowground Carbon Pool

Similarly, the belowground carbon pool can be estimated by multiplying the area within an ecoregion by the carbon content. **Table 5-2** shows the resulting belowground carbon within the bay for 2020. The carbon stored in the top 1-meter of sediment is several orders of magnitude higher than the carbon stored aboveground.

TABLE 5-2
BELOWGROUND CARBON IN SAN DIEGO BAY

Ecoregion	Belowground Carbon (tonnes CO_2 equiv.)
Outer Bay	1,000
North	11,840
North Central	2,530
South Central	30,670
South	124,530
Total	**170,560**

NOTES:

Based on 2020 eelgrass areas

Since the longer cores suggested that the top 1-meter of sediment stores 56-90% of the total carbon, the total belowground carbon pool could be as large as 187,617 – 245,608 tonnes CO_2 equivalent.

5.3 Total Carbon Pool

Combining aboveground and belowground carbon gives the total eelgrass carbon pool in San Diego Bay (**Table 5-3**). The patterns are similar to the belowground carbon since the aboveground carbon is much smaller. The majority of the carbon within the bay is belowground in the South ecoregion (73.0%).

TABLE 5-3
TOTAL EELGRASS CARBON IN SAN DIEGO BAY

Ecoregion	Carbon (tonnes CO_2 equiv.)	Percentage of Total
Outer Bay	1,100	0.7%
North	11,850	6.9%
North Central	2,530	1.5%
South Central	30,740	18.0%
South	124,700	73.0%
Total	**170,900**	**100%**

NOTES:

Results for Z. pacifica and Z. marina were added together for the Outer Bay. Results from Sites D-1, D-2, and D-3 were averaged for the North Central ecoregion, while Sites F, G, H, I, and J were averaged from the South ecoregion.

The total ecosystem carbon in San Diego Bay ranged from 2-98 Mg C/ha, which is within the range that has been found in the literature (Fourqurean et al. 2012; Kauffman et al. 2020; Kim et al. 2022). **Table 5-4** presents carbon content values in the literature compared to what we have found with this study.

TABLE 5-4
CARBON CONTENT VALUES IN THE LITERATURE

Paper	Study Location	Species	Seagrass Bed Total Carbon Content (Mg C/ha)
Fourqurean et al. 2012	Global	Variable	0.001 – 23
Dahl et al. 2016[a]	Europe	*Z. marina*	70 – 190
Rohr et al. 2016	Finland and Denmark	*Z. marina*	0.2 – 43
Kauffman et al. 2020	Pacific Northwest, USA	*Z. marina*	46 – 389
Kim et al. 2022	Korea	*Z. marina*	49 – 125
This study	San Diego, CA, USA	*Z. marina*	2 – 98

NOTES:

a. We multiplied the reported bulk density by the percent carbon and added the aboveground and belowground biomass to develop these values.

5.4 Carbon Assimilation Rates

The eelgrass areas combined with the productivity data results in the assimilation rates within the bay. **Table 5-5** shows the assimilation rates over time. See Section 3.5 and Table 3.5 for assumptions and methods.

TABLE 5-5
EELGRASS ASSIMILATION IN SAN DIEGO BAY (TONNES CO_2 EQUIVALENT/YEAR)

Ecoregion	1993	1999	2004	2008	2011	2014	2017	2020
Outer Bay (Z. pacifica)	60	82	954	659	637	521	77	207
Outer Bay (Z. marina)	47	64	748	517	499	409	61	162
North	179	314	299	306	454	381	397	584
North Central	616	1,201	676	857	1,283	988	1,042	593
South Central	2,589	3,318	2,700	2,021	2,323	1,658	1,643	4,582
South	4,333	6,619	7,778	4,108	6,681	8,484	7,998	11,359
Total	**7,824**	**11,598**	**13,154**	**8,467**	**11,878**	**12,441**	**11,218**	**17,485**

NOTES:

Results from Sites D-1, D-2, and D-3 were averaged for the North Central ecoregion, while Sites F, G, H, I, and J were averaged from the South ecoregion.

5.5 Carbon Over Time with Sea-Level Rise

5.5.1 Sea-Level Rise

In 2019, the Port of San Diego completed its Sea Level Rise Vulnerability and Coastal Resiliency Report pursuant to Assembly Bill 691. As part of this report, the Port chose sea-level rise projections representing the 50th and 95th percentiles from the 2018 Ocean Protection Council (OPC) guidance (**Table 5-6**). We used the Port's medium-term (2050) projection and the two long-term (2100) projections in order to bracket the uncertainty inherent in longer-term projections.

TABLE 5-6
PORT OF SAN DIEGO'S SELECTED SEA-LEVEL RISE PROJECTIONS (IN FEET)

	2030	2050	2100
95th Percentile Projection	0.7	1.4	4.5
50th Percentile Projection	n/a	(0.9)	2.6

Note: values in parentheses represent OPC projections that were not adopted by the Port of San Diego. They are included here for context.

5.5.2 Habitat Evolution Methods

Eelgrass can grow at specific elevation bands dictated in large part by light penetration fixing the lower depth of beds and desiccation stress establishing the upper limits of the beds. In San Diego Bay, eelgrass has colonized most of the available area within this elevation range and fluctuates

in distribution based on variability in the controlling environmental parameters (Merkel & Associates 2000; Merkel and Sutton 2000). ESA developed a habitat evolution model that assumes eelgrass colonization continues to be correlated with depth as sea levels change. Note that this model does not account for the possible influence of other factors, such as rising temperatures, water quality changes, human activity within the bay, etc. that have previously been shown to be important to the distribution of eelgrass within the bay (Merkel & Sutton 2000).

The model is based on the Port's bay-wide eelgrass occurrence frequency dataset, which is based on mapped eelgrass extent throughout San Diego Bay in 1993, 1999, 2004, 2008, 2011, 2014, 2017, and 2020 (Merkel & Associates 2020). Across these surveys, eelgrass was found between -21 and -0.4 ft NAVD88[9], and it was most likely to occur between roughly -6.4 and -0.4 ft NAVD88. *Z. pacifica* at the mouth of the bay accounts for the majority of the deeper eelgrass, while *Z. marina* accounts for the shallower eelgrass. Notably, eelgrass extended much deeper in 2020 than it has during prior survey years (Merkel & Associates 2020).

Approximate elevation ranges were selected to represent the likelihood of eelgrass occurrence. The elevation ranges were then applied to the Coastal National Elevation Database (CoNED) topobathy dataset. For example, any elevation between -4.5 and -6.5 was categorized as 33% likely to occur, while elevations between -3 and -0.5 were categorized as 88% likely to occur.

The results are compared to the actual observed occurrence in **Figure 5-3**. Since it is based solely on elevation and does not consider other biological factors, the model can only approximately predict eelgrass occurrence frequency on either end of the bay (i.e., Outer Bay and South Bay). However, it does an acceptable job of predicting the spatial extent of eelgrass. The variation in eelgrass occurrence does not correspond with elevations exactly, so the model results should be considered an approximate representation of future conditions.

[9] North American Vertical Datum of 1988

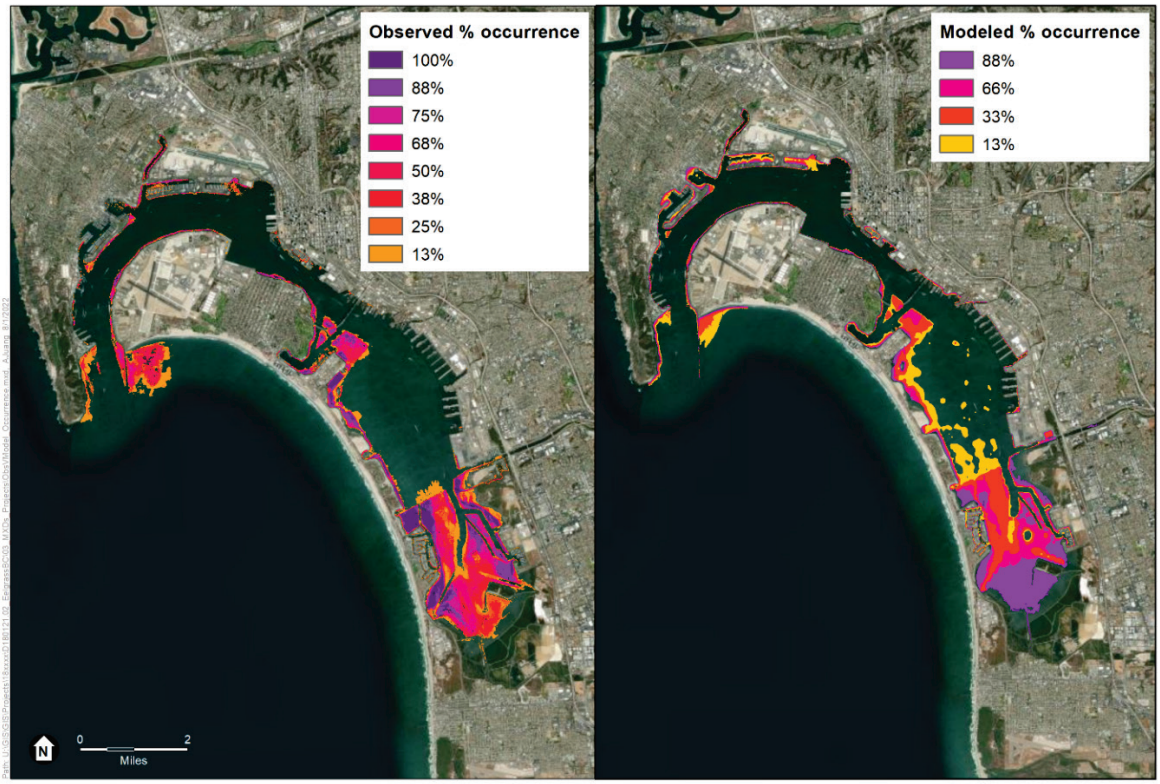

Figure 5-3. Observed vs Modeled Eelgrass Occurrence

The elevation model can be used to project how eelgrass habitat acreages may evolve over time under various sea-level rise scenarios based on habitat elevations. **Table 5-7** shows the results of the model for different amounts of sea-level rise.

TABLE 5-7
PREDICTED EELGRASS HABITAT WITH SEA-LEVEL RISE

	Area (ha) by % occurrence				
	<13%	33%	66%	88%	Weighted Total
Existing	501	326	226	451	686
0.7 ft SLR	474	292	226	464	685
1.4 ft SLR	485	284	214	448	661
2.6 ft SLR	532	278	331	258	572
4.5 ft SLR	497	398	163	119	376

Figure 5-4 shows the seagrass habitat over time for San Diego Bay from 2020 to 2100. The model forecasts that the total extent of habitat will decrease over time. However, this habitat loss does not occur uniformly. Over time, eelgrass encroaches closer to the present-day shoreline, while habitat loss occurs largely in the interior of the bay. Habitat gain is concentrated in the South Bay, while habitat loss is concentrated first in the South Central Bay but is eventually modeled to occur in all other ecoregions. The bathymetry and bay margin conditions has much to

do with whether sea-level rise will result in gains or losses within a particular location, and the heavily urbanized margins of the bay generally leave little room for shoreward migration of eelgrass in all but the South Bay. **These results should be interpreted with some caution**, as the model provides a very simplified presentation of dominant controlling factors. Additionally, accretion is not included in the model and could help seagrasses keep pace with sea-level rise.

5.5.3 Carbon Pool Evolution

Using the sequestration rates from the literature discussed in Section 3.5, we can estimate the amount of carbon sequestered in the future with different amounts of sea-level rise (**Table 5-8**).

TABLE 5-8
CUMULATIVE EELGRASS CARBON SEQUESTRATION (TONNES CO_2 EQUIVALENT)

	By 2030	By 2050	By 2100
Low carbon sequestration (rate from Duarte et al. 2011)			
95th Percentile SLR Projection	10,500	23,300	50,800
50th Percentile SLR Projection			79,600
High carbon sequestration (rate from McLeod et al. 2011)			
95th Percentile SLR Projection	27,800	61,200	133,600
50th Percentile SLR Projection			209,600

While the eelgrass habitats do continue to sequester carbon through the end of the century, these results must still be read in the context of the diminishing habitat areas projected in Table 5-7 (i.e., total seagrass habitat decreasing from 686 acres today to 376 acres with 4.5 ft of sea-level rise).

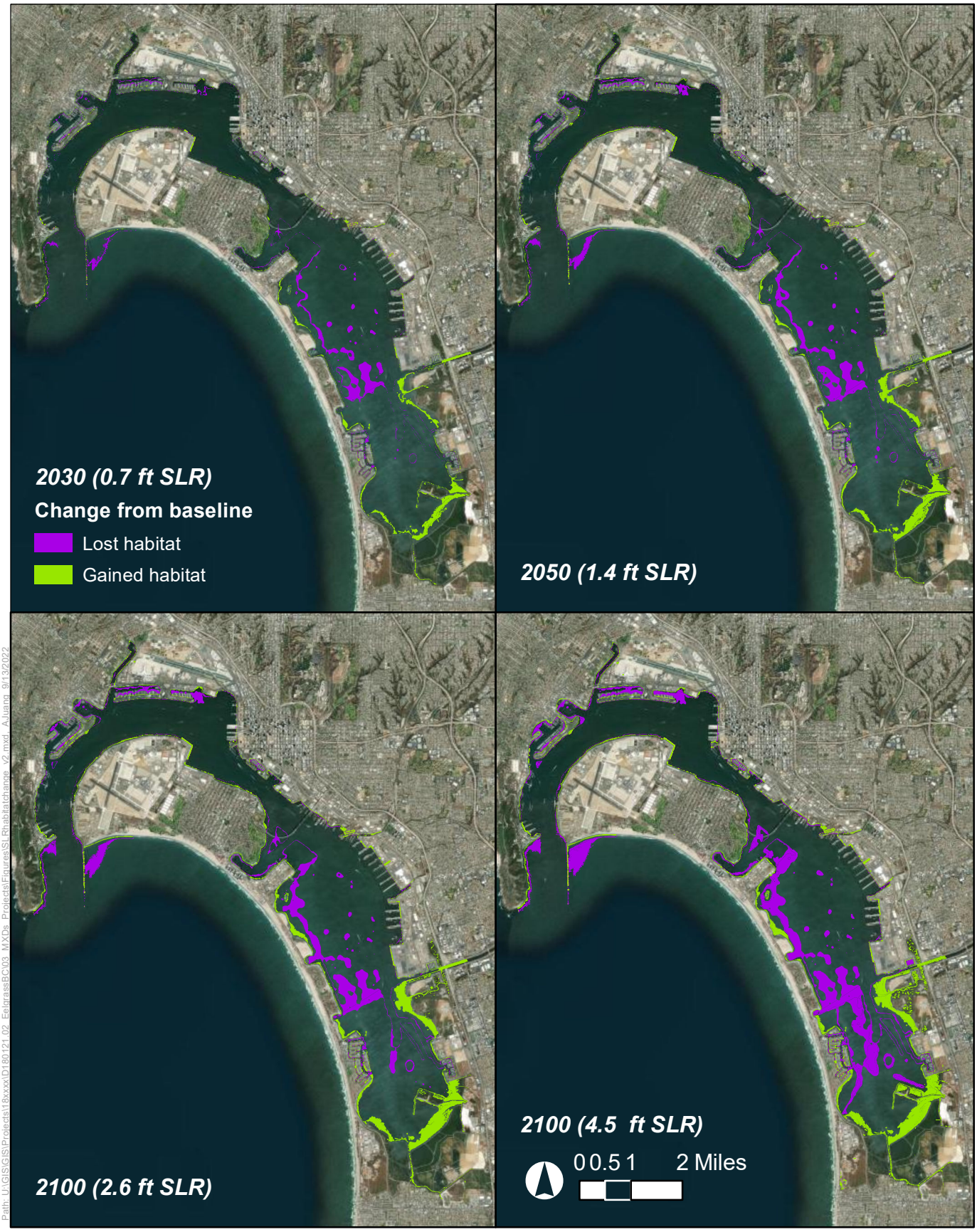

Path: U:\GIS\GIS\Projects\18xxxx\D180121_02_EelgrassBC\03_MXDs_Projects\Figures\SI_Rhabitatchange_v2.mxd A.Juang 9/13/2022

SOURCE: Merkel, USGS

San Diego Bay Eelgrass Blue Carbon Study

Figure 5-4
Habitat Evolution Model Results

ESA

This page intentionally left blank

SECTION 6
Conclusions

San Diego Bay's eelgrass habitats store around 170,600 tonnes of CO_2 equivalent currently (i.e., in total, not on an annual basis). This figure is comparable to about half a years' worth of emissions from Port operations based on the predicted 2020 emissions data (Port of San Diego 2013). The Year 2 follow-up study planned for 2022-2023 will shed light on the habitats' annual sequestration abilities to facilitate a more direct estimate of annual emissions versus annual seagrass carbon sequestration.

The aboveground carbon content of the bay's seagrass beds is lower than values in the literature, potentially due to reduced nutrient load in the bay as discussed in Section 3.1. However, the total ecosystem carbon (i.e., sum of aboveground and belowground carbon) are within the range found in the literature (Fourqurean et al. 2012; Kauffman et al. 2020; Kim et al. 2022). The average ecosystem carbon for the bay is 36.0 ± 45.3 Mg C/ha, and up to 46.3 Mg C/ha if carbon below the top one meter is considered. The bay has been identified as having statewide significance for eelgrass habitat, supporting approximately 17% of California's eelgrass habitat in any given year (Merkel & Associates 2020). As a result, the Port and Navy have mapped, monitored, and managed eelgrass within the bay since the early 1990s. Continuing to manage these habitats will be important to maintaining blue carbon storage in San Diego Bay.

Management of eelgrass habitats is also important because these habitats may evolve over time due to sea-level rise. Based on the habitat evolution model results, San Diego Bay's eelgrass habitats may experience a net loss of area with sea-level rise but are nonetheless expected to remove a total of between 50,800 and 209,600 tonnes of CO_2 from the atmosphere by 2100, comparable to removing all ocean-going vessels for ten months to over 3 years (Port of San Diego 2013, 2016). If higher sea-level rise projections are realized, creating more space for landward habitat migration will be necessary to maintain eelgrass and other coastal blue carbon habitats.

Further improvements in water quality may help drive further expansion of seagrasses into deeper waters and also slow the rate of the migration of this boundary with sea-level rise. However, it is believed the increased water clarity is due to pollution control (i.e., nutrient reduction) and drought-reduced water column productivity, which has led to diminishing biomass of eelgrass bay-wide. It is critical that this benefit-cost relationship be better understood.

Additionally, expansion of seagrasses into newly inundated areas throughout the bay where other important blue carbon habitats may be lost is crucial to slowing the loss of eelgrass habitat and maintaining the bay's overall carbon sequestration potential. If this seagrass expansion with sea-

level rise does not occur, then it is likely that carbon sequestration would decrease. Additionally, if sea-level rise stresses the ecosystem, loss of eelgrass could become part of a positive feedback loop leading to further losses, as seagrass meadows filter particulates out of the water column, and thus improve water clarity.

The Port has recently (December 2021) implemented a native oyster living shoreline restoration project which was designed to protect intertidal habitats from erosion. Monitoring of this pilot project is expected to provide best practices to inform additional living shorelines projects that could help maintain elevations for eelgrass habitat into the future. Similarly, the Navy and Port are working towards seeking opportunities for in-bay beneficial reuse of dredged sediments to raise the bay floor in order to add eelgrass habitat ahead of losses predicted due to sea-level rise.

Mechanisms and procedures have also been developed to connect coastal wetland management to the carbon market, where appropriate.[10] A growing number of case studies can inform management agencies and policy developers on coastal wetland management and carbon finance markets (Sheehan et al. 2019; Crooks et al. 2014). While the existing eelgrass in San Diego Bay is already protected by regulations, and therefore would not meet the additionality requirements to sell blue carbon credits, this study provides new research to inform future blue carbon projects. To bring a blue carbon project to market, local data is needed to accurately predict how much carbon will be sequestered by the project. This study provides needed information on how carbon content varies by eelgrass species, location, depth, and age of the bed. In particular, the trend suggesting that older restored eelgrass beds have higher amounts of carbon in the sediments compared to newer restored beds could provide justification for restoring eelgrass beds to sequester blue carbon with the understanding that carbon would build up in the sediments over time.

This iteration of the Eelgrass Blue Carbon Study, along with a second year of research funded by MARAD's Maritime Environmental and Technical Assistance (META) Program on the bicarbonate pathway, will help scientists and policy makers better understand the carbon sequestration and capture rates of eelgrass habitats. Initiating this study at the Port of San Diego can lend information to other similar coastal ports throughout the nation that are investigating blue carbon sequestration to offset waterside and landside carbon emissions at ports. The MARAD META program helped to fund this study as part of a broader effort to address overall maritime decarbonization in support of a safe and efficient U.S. maritime transportation system. This knowledge will assist ports, natural resource agencies, maritime operations, and other organizations to successfully build comprehensive on-site mitigation plans to support the pursuit of carbon neutrality. The transportation sector can incorporate both on-site mitigation and potentially the creation of bankable offsets via natural systems like eelgrass habitat restoration. This will allow for more optionality within their Scope 1, 2, and 3 emissions inventories to align with regulations, environmental, social, and governance (ESG) initiatives and ultimately the pursuit of carbon neutrality.

[10] http://www.v-c-s.org/methodologies/methodology-tidal-wetland-and-seagrass-restoration-v10

The following recommendations are made for future studies:

1. Developing a San Diego Bay–specific sequestration rate would allow for a direct comparison to assimilation rates and would provide more accurate carbon evolution modeling results.
2. A potential pathway for carbon sequestration mediated by seagrasses in carbonate sediments has been noted within this study. Further investigations into inorganic carbon pathways and carbon sequestration within the bicarbonate pool should be undertaken to test this hypothesis.
3. Water quality data could provide additional information on the bicarbonate pathway (through changes in pH) and could be used to estimate productivity through the air-water CO_2 flux to compare against measurements in this study.
4. Refinements in sea-level rise estimates, additional restoration, and changes to water quality could affect the findings of this study and should be considered.
5. Grain size or other supplementary sediment analyses (e.g., isotope measurements) could help further illuminate patterns and causes of carbon storage in the sediment.
6. Conduct follow-up sampling of eelgrass productivity when drought conditions end, and eelgrass returns to more "normal" aboveground biomass conditions.

This page intentionally left blank

REFERENCES

California Ocean Protection Council. 2018. *State of California Sea-Level Rise Guidance*. 2018 Update.

Chiu, S., Y. Huanga, and H. Lina. 2013. "Carbon budget of leaves of the tropical intertidal seagrass Thalassia hemprichii". *Estuarine, Coastal and Shelf Science* 125: 27-35.

Crooks, S., J. Rybczyk, K. O'Connell, D. L. Devier, K. Poppe, S. Emmett-Mattox. 2014. *Coastal Blue Carbon Opportunity Assessment for the Snohomish Estuary: The Climate Benefits of Estuary Restoration*. Report by Environmental Science Associates, Western Washington University, EarthCorps, and Restore America's Estuaries.

Dahl, M., D. Deyanova, S. Gütschow, M. E. Asplund, L. D. Lyimo, V. Karamfilov, R. Santos, M. Björk, M. Gullström. 2016. "Sediment Properties as Important Predictors of Carbon Storage in *Zostera marina* Meadows: A Comparison of Four European Areas." *PLoS ONE,* 11(12), 1-21. https://doi.org/10.1371/journal.pone.0167493.

Duarte, C. 1990. "Seagrass nutrient content." *Marine Ecology Progress Series,* 67(2), 201-207. http://www.jstor.org/stable/24816762.

Duarte, C. 1991. "Allometric scaling of seagrass form and productivity." *Marine Ecology Progress Series,* 77(2/3), 289-300. http://www.jstor.org/stable/24826581.

Duarte, C., J. Middleburg, N. Caraco. 2005. "Major role of marine vegetation on the oceanic carbon cycle." *Biogeosciences,* 2, 1-8, https://doi.org/10.5194/bg-2-1-2005.

Duarte, C., H. Kennedy, N. Marbà, I. Hendriks. 2011. "Assessing the capacity of seagrass meadows for carbon burial: Current limitations and future strategies." *Ocean & Coastal Management,* https://doi.org/10.1016/j.ocecoaman.2011.09.001.

Echavarria-Heras, H., E. Solana-Arellano, E. Franco-Vizcaíno. 2009. "An allometric method for the projection of eelgrass leaf biomass production rates." *Mathematical Biosciences,* 223(1), 58-65. https://doi.org/10.1016/j.mbs.2009.10.008.

Echavarria-Heras, H., E. Solana-Arellano, C. Leal-Ramírez, E. F. Vizcaino. 2013. "An allometric method for measuring leaf growth in eelgrass, *Zostera marina*, using leaf length data." *Botanica Marina,* 56(3), 275-286. https://doi.org/10.1515/bot-2012-0215.

Echavarria-Heras, H., K.-S. Lee, E. Solana Arellano, E. Franco-Vizcaíno. 2011a. "Formal analysis and evaluation of allometric methods for estimating above-ground biomass of eelgrass." *Annals of Applied Biology,* 159(3), 503-515. https://doi.org/10.1111/j.1744-7348.2011.00511.x.

Echavarria-Heras, H., E. Solana-Arellano, K. S. Lee, S. Hosokawa, E. Franco-Vizcaíno. 2011b. "An Evaluation of Leaf Biomass: Length Ratio as a Tool for Nondestructive Assessment in Eelgrass (*Zostera marina* L.)." *The Scientific World Journal*, 2012, 1-8. https://doi.org/10.1100/2012/543730.

Fourqurean, J. W., C. M. Duarte, H. Kennedy, N. Marbà, M. Holmer, M. A. Mateo, E. T. Apostolaki, G. A. Kendrick, D. Krause-Jensen, K. J. McGlathery, O. Serrano. 2012. "Seagrass ecosystems as a globally significant carbon stock." *Nature Geoscience,* 5, 505-509. https://doi.org/10.1038/ngeo1477.

Greiner, T., K. McGlathery, J. Gunnell, and B. McKee. 2013. "Seagrass restoration enhances 'blue carbon' sequestration in coastal waters". *PLoS ONE* 8(8): e72469. Doi: 10.1371/journal.pone.0072469.

Howard, J., S. Hoyt, K. Isensee, E. Pidgeon, M. Telszewski. 2018. *Coastal Blue Carbon: methods for assessing carbon stocks and emissions factors in mangroves, tidal salt marshes, and seagrass meadows.* Report by Conservation International, IOC-UNESCO, and IUCN.

Ibarra-Obando, S. E., C. F. Boudouresque. 1994. "An improvement of the Zieman leaf marking technique for *Zostera marina* growth and production assessment." *Aquat. Bot.,* 47(3-4) 293-302. https://doi.org/10.1016/0304-3770(94)90059-0.

IPCC (Intergovernmental Panel on Climate Change). 2013. *2013 Supplement to the 2006 IPCC Guidelines for National Greenhouse Gas Inventories: Wetlands.* IPCC, Switzerland.

Kauffman, J. B., L. Giovanonni, J. Kelly, N. Dunstan, A. Borde, H. Diefenderfer, C. Cornu, C. Janousek, J. Apple, L. Brophy. 2020. "Total ecosystem carbon stocks at the marine-terrestrial interface: Blue carbon of the Pacific Northwest Coast, United States." *Global Change Biology,* 26(10), 5679-5692. https://doi.org/10.1111/gcb.15248.

Kennedy, H., J. Beggins, C. M. Duarte, J. W. Fourqurean, M. Holmer, N. Marbà, J. J. Middelburg. 2010. "Seagrass sediments as a global carbon sink: Isotopic constraints." Global Biogeochemical Cycles, 24, GB4026. https://doi.org/10.1029/2010GB003848.

Kentula, M.E. and C.D. McIntire. 1986. "The autoecology and production dynamics of eelgrass (Zostera marina. L.) in Netarts Bay, Oregon." Estuaries, 9, 188-199.

Kindeberg, T., E. Röhr, P.-O. Moksnes, C. Boström, M. Holmer. 2019. "Variation of carbon contents in eelgrass (Zostera marina) sediments implied from depth profiles." Biology *Letters*, 15(6). https://doi.org/10.1098/rsbl.2018.0831.

Lin, L. I. 1989. "A Concordance Correlation Coefficient to Evaluate Reproducibility." *Biometrics,* 45, 255-268. http://dx.doi.org/10.2307/2532051.

Mcleod E., G. L. Chmura, S. Bouillon, R. Salm, M. Björk, C. M. Duarte, C. E. Lovelock, W. H. Schlesinger, B. R. Silliman. 2011. "A blueprint for blue carbon: toward an improved understanding of the role of vegetated coastal habitats in sequestering CO_2." *Frontiers in Ecology and the Environment*, 9(10), 552-560. https://doi.org/10.1890/110004.

Merkel, K.W. and D. Sutton. 2000. Development of a Numeric Model for Explaining Eelgrass Distribution in South San Diego Bay. January 2000.

Merkel & Associates. 2000. Environmental Controls on the Distribution of Eelgrass (*Zostera marina* L.) in South San Diego Bay: An Assessment of the Relative Roles of Light, Temperature, and Turbidity in Dictating the Development and Persistence of Seagrass in a Shallow Back-bay Environment. Prepared for Duke Energy and California Regional Water Quality Control Board, San Diego Region, January 2000.

Merkel & Associates. 2020. 2020 San Diego Bay Eelgrass Inventory. December 2020.

Moreno-Mateos, D., M. E. Power, F. A. Comín, R. Yockteng. 2012. "Structural and Functional Loss in Restored Wetland Ecosystems." *PloS Biology,* 10(1), e1001247. https://doi.org/10.1371/journal.pbio.1001247.

Nahlik, A. M. and M. S. Fennessy. 2016. "Carbon storage in US wetlands." *Nature Communications*, 7, 13835. https://doi.org/10.1038/ncomms13835.

Port of San Diego. 2013. Climate Action Plan. Port-of-San-Diego-Climate-Action-Plan.pdf (windows.net)

Port of San Diego. 2016. Climate Action Plan, Overview of Methods and Results for the Recalibrated 2006 Baseline Greenhouse Gas Inventory and 2016 Greenhouse Gas Inventory Progress Report. Prepared by ICF.

Port of San Diego. 2019. Sea Level Rise Vulnerability Assessment and Coastal Resiliency Report.

Röhr, M. E., C. Boström, P. Canal-Vergés, M. Holmer. 2016. "Blue carbon stocks in Baltic Sea eelgrass (*Zostera marina*) meadows." *Biogeosciences*, 13(22), 6139-6153. https://doi.org/10.5194/bg-13-6139-2016.

Röhr, M. E., Holmer, M., Baum, J. K., Björk, M., Boyer, K., Chin, D., et al. 2018. Blue carbon storage capacity of temperate eelgrass (Zostera marina) meadows. Global Biogeochemical Cycles,32, 1457–1475. https://doi.org/10.1029/2018GB005941

Samper-Villarreal, J., P. Mumby, M. Saunders, L. Barry, A. Zawadzki, H. Heijnis, G. Morelli, C. Lovelock. 2017. "Vertical accretion and carbon burial rates in subtropical seagrass meadows increased following anthropogenic pressure from European colonization". Estuarine, Coastal and Shelf Science 202: 40-53.

Serrano, O., P. S. Lavery, M. Rozaimi, M. Á. Mateo. 2014. "Influence of water depth on the carbon sequestration capacity of seagrasses." *Global Biogeochemical Cycles,* 28(9) 950-961. https://doi.org/10.1002/2014GB004872.

Sheehan, L., E. T. Sherwood, R. P. Moyer, K. R. Radabaugh, S. Simpson. 2019. "Blue Carbon: an Additional Driver for Restoring and Preserving Ecological Services of Coastal Wetlands in Tampa Bay (Florida, USA)." *Wetlands,* 39, 1317-1328. https://doi.org/10.1007/s13157-019-01137-y.

Solana-Arellano, E., H. Echavarria-Heras, O. Flores-Uzeta. 2000. "An upgraded method to relocate marked shoots of the seagrass Zostera marina." *Revista de Biología Tropical*, 48(4), 927-930.

Solana-Arellano, E., H. Echavarria-Heras, E. Franco-Vizcaíno. 2008. "An economical non-destructive method for estimating eelgrass, Zostera marina (Potamogetonaceae) leaf growth rates: formal development and use in northwestern Baja California." *Revista de Biología Tropical* 56(3), 1003-1013.

Short, F.T. and C.M. Duarte. 2001. Methods for the measurement of seagrass growth and production. In Global Seagrass Research Methods. Short, F.T. and R.G. Coles (eds.). 2001. Elsevier Science B.V., Amsterdam. 473 pp.

Tomasko, D. 2015. "Quantification of carbon sequestration rates for seagrass." Project Memo. Prepared by Environmental Science Associates (ESA).

Tomasko, D. A., D. L. Bristol, J. A. Ott. 2001. "Assessment of Present and Future Nitrogen Loads, Water Quality, and Seagrass (*Thalassia testudinum*) Depth Distribution in Lemon Bay, Florida." *Estuaries*, 24(6A), 926-938. https://doi.org/10.2307/1353183.

Appendix B.
Sediment Depth Profiles

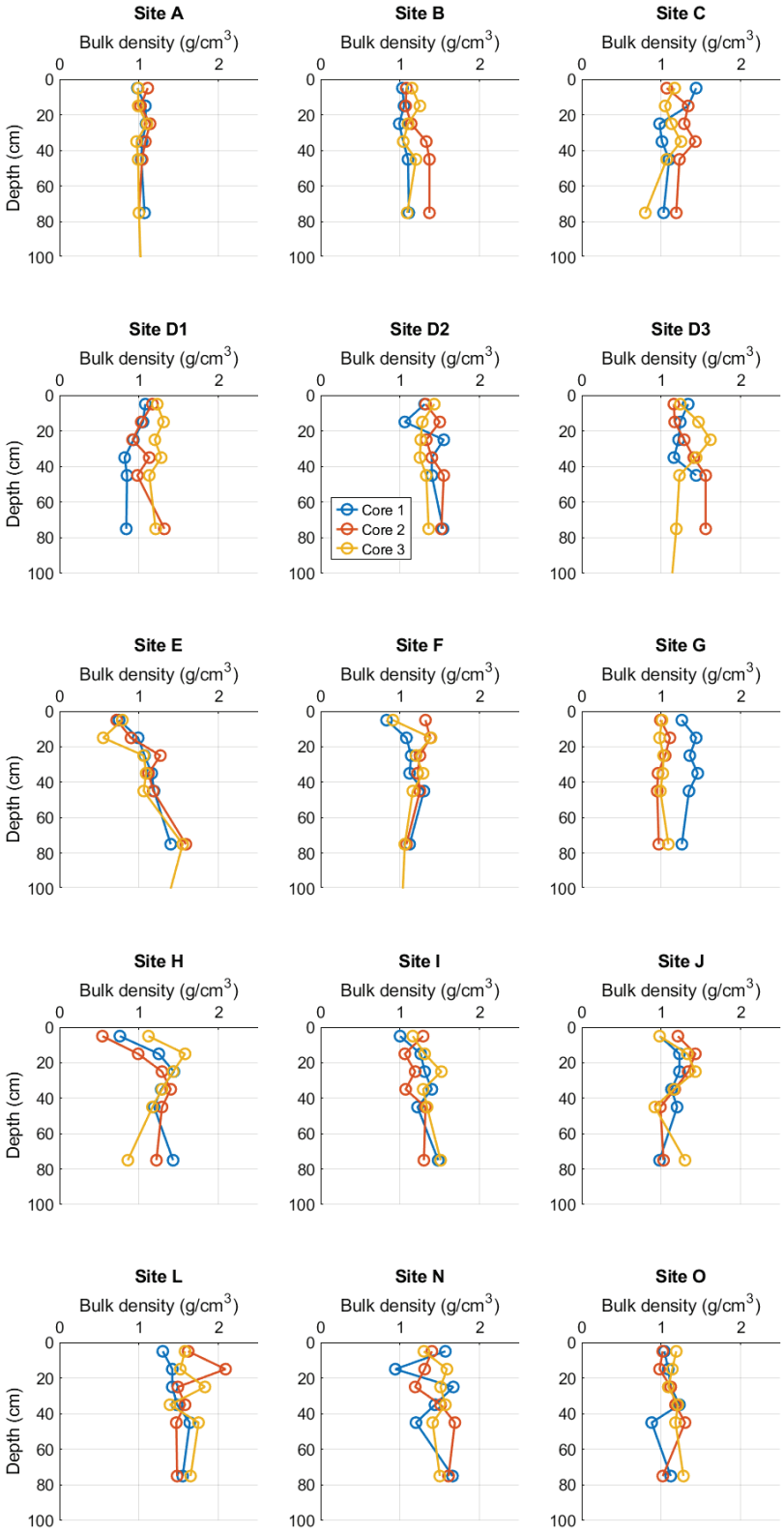

SOURCE: ESA 2023

D201800121.03 San Diego Bay Eelgrass Blue Carbon Study

Figure B-1
Bulk Density profiles

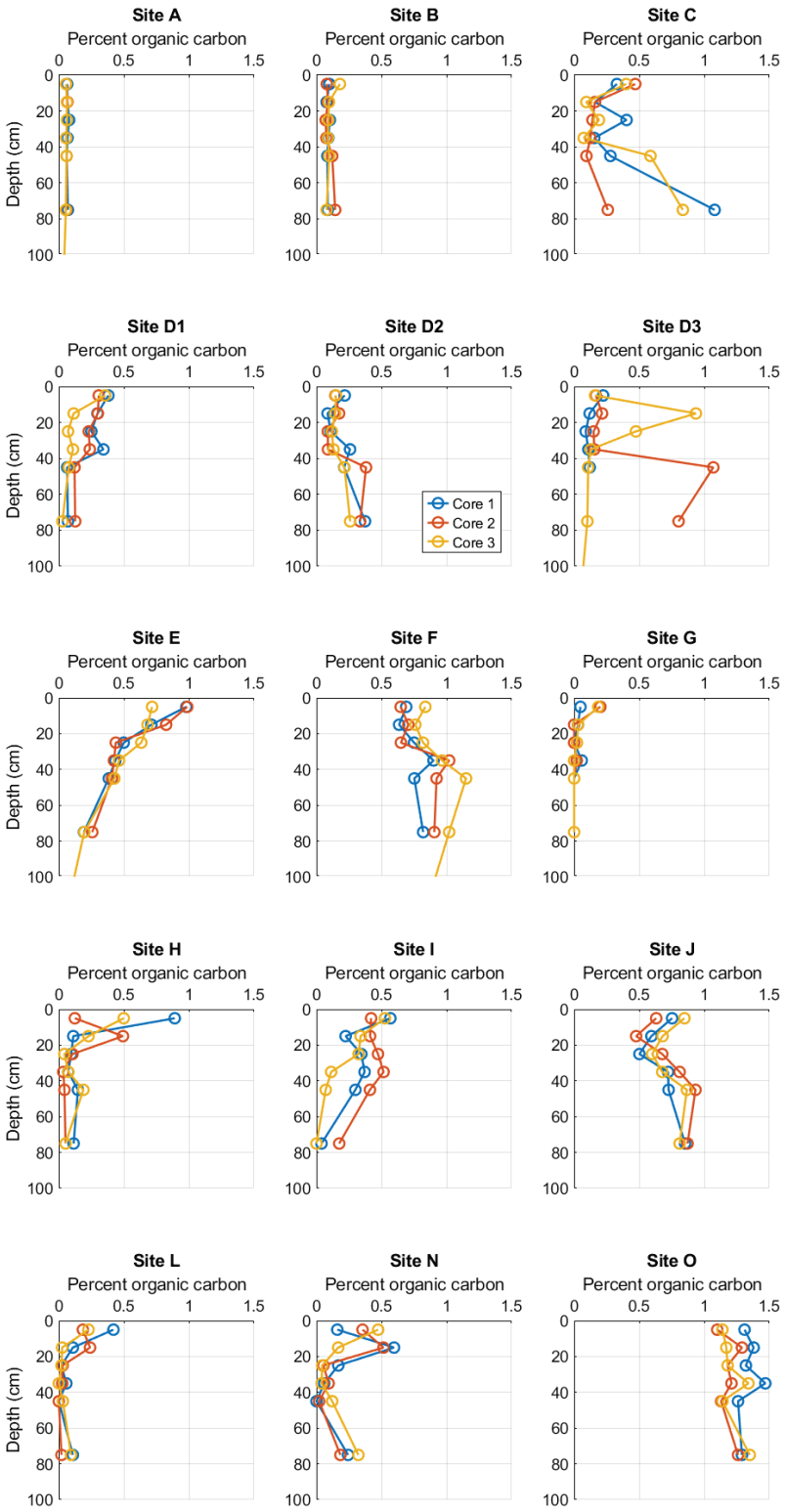

SOURCE: ESA 2023

D201800121.03 San Diego Bay Eelgrass Blue Carbon Study

Figure B-2
Organic Carbon Fraction Profiles

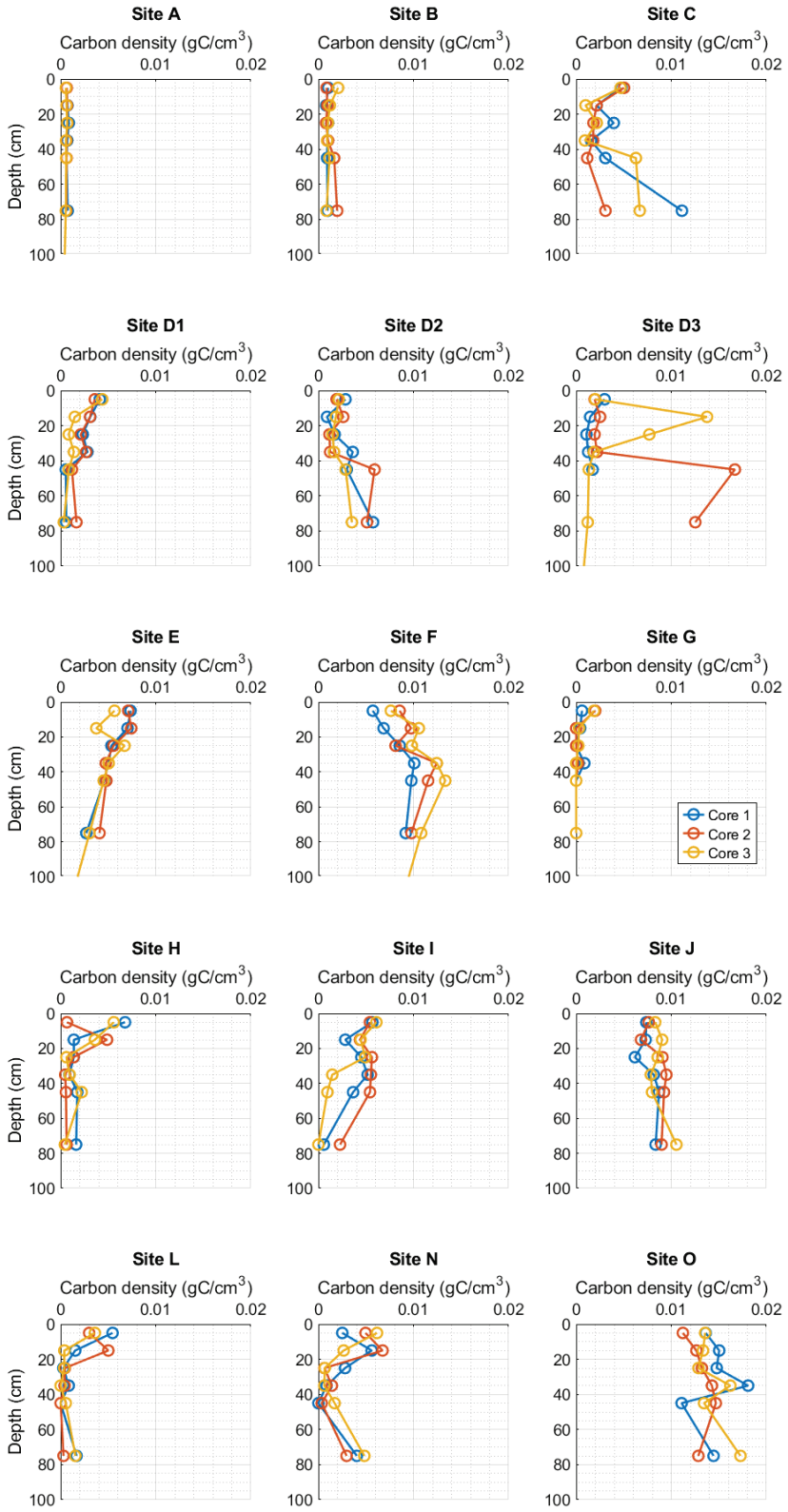

SOURCE: D201800121.03 San Diego Bay Eelgrass Blue Carbon Study

Figure B-3
Carbon Density Profiles

Appendix C.
Water Quality Plots

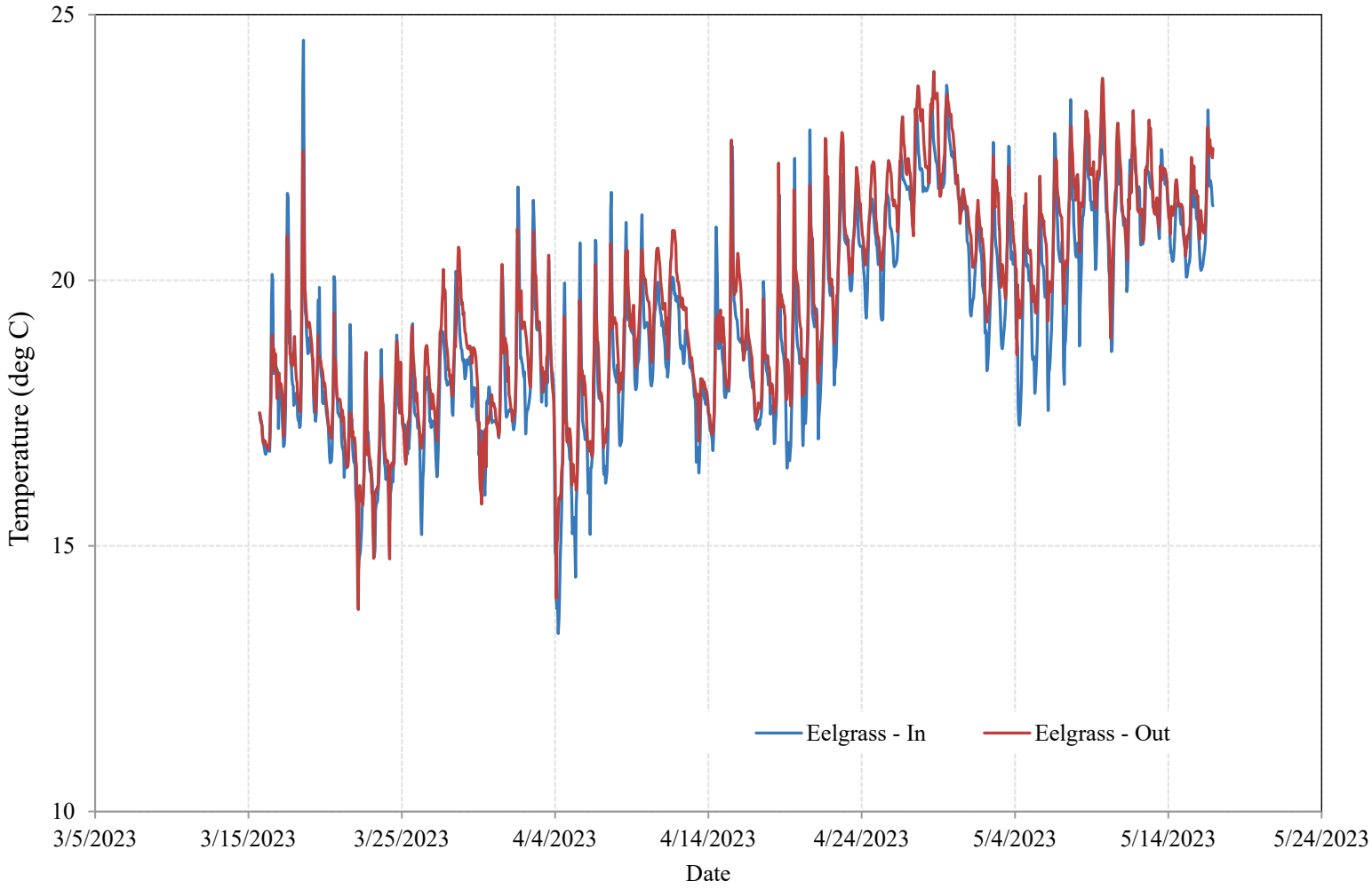

D201800121.03 San Diego Eelgrass Blue Carbon Study

Figure C-1

Temperature (Mar 2023 – May 2023)

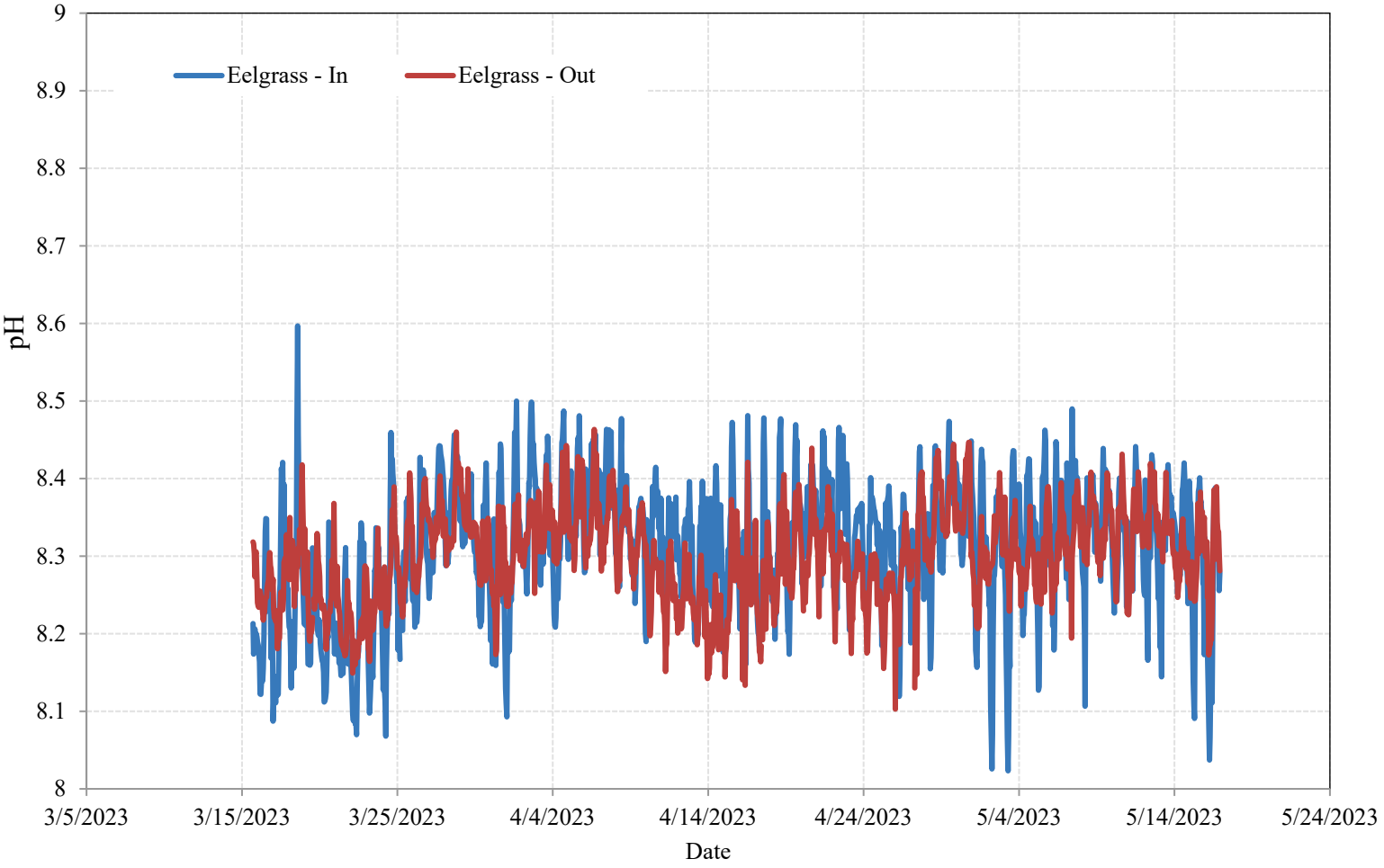

D201800121.03 San Diego Eelgrass Blue Carbon Study

Figure C-2

pH (Mar 2023 – May 2023)

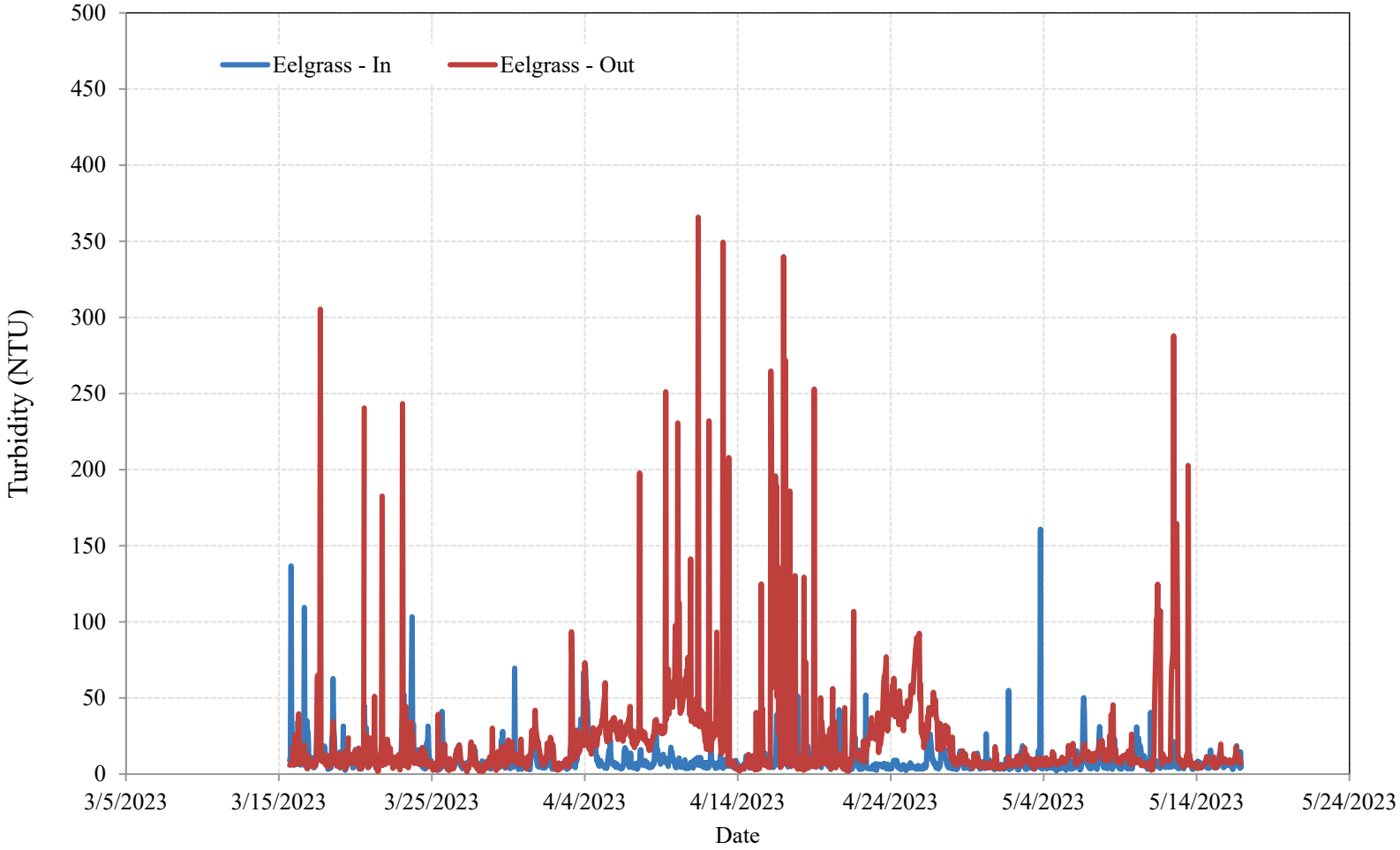

D201800121.03 San Diego Eelgrass Blue Carbon Study

Figure C-3

Turbidity (Mar 2023 – May 2023)

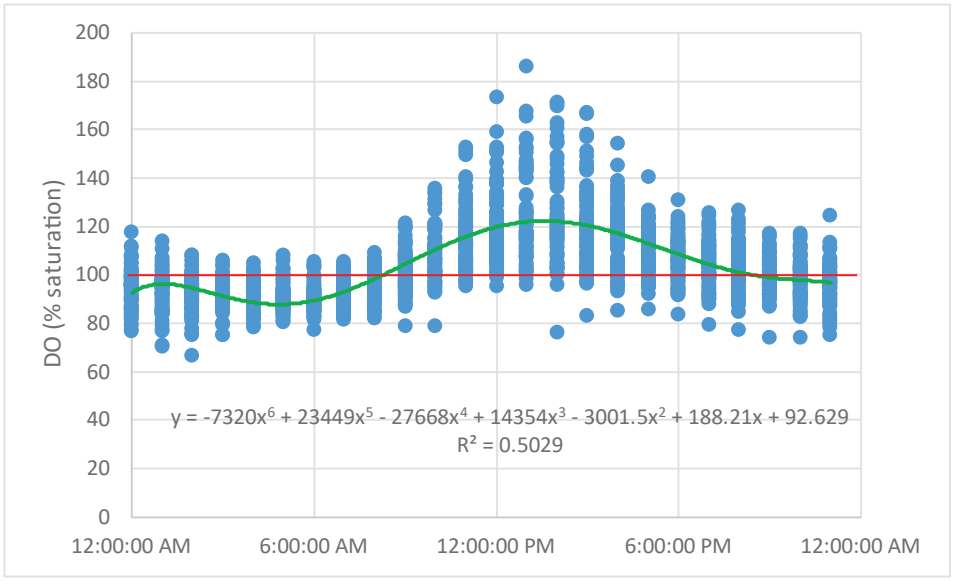

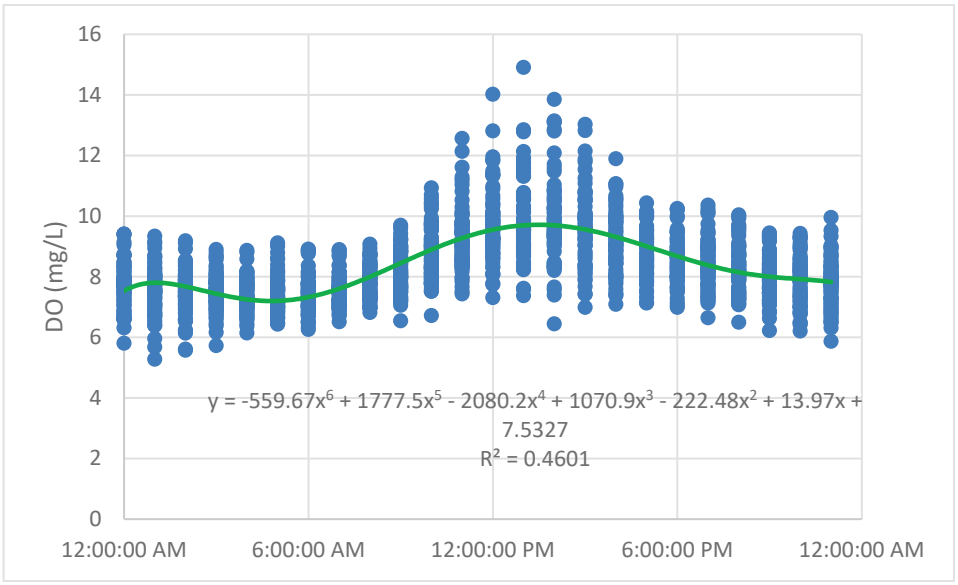

NOTES: Red line represents 100% saturation. Green line represents polynomial regression corresponding to equation shown.

D201800121.03 San Diego Bay Eelgrass Blue Carbon Study

Figure C-4
Dissolved oxygen inside a seagrass meadow (Oct 2022-Jan 2023)

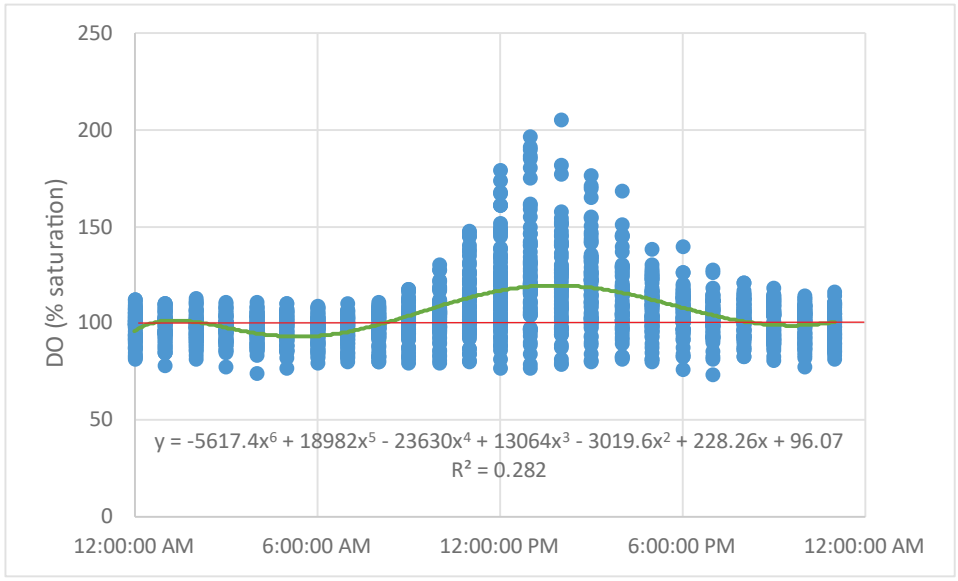

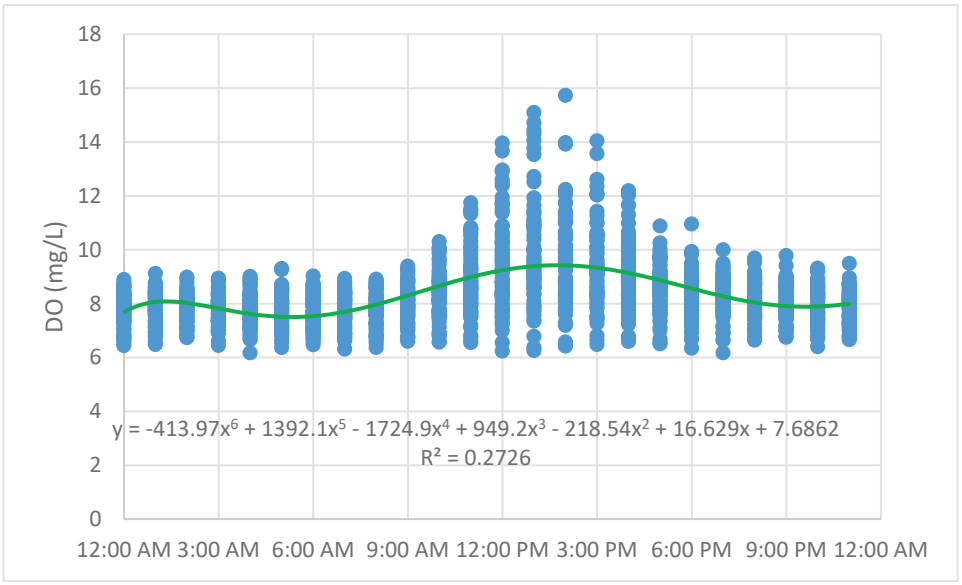

NOTES: Red line represents 100% saturation. Green line represents polynomial regression corresponding to equation shown.

D201800121.03 San Diego Bay Eelgrass Blue Carbon Study

Figure C-5
Dissolved oxygen outside a seagrass meadow (Oct 2022-Jan 2023)

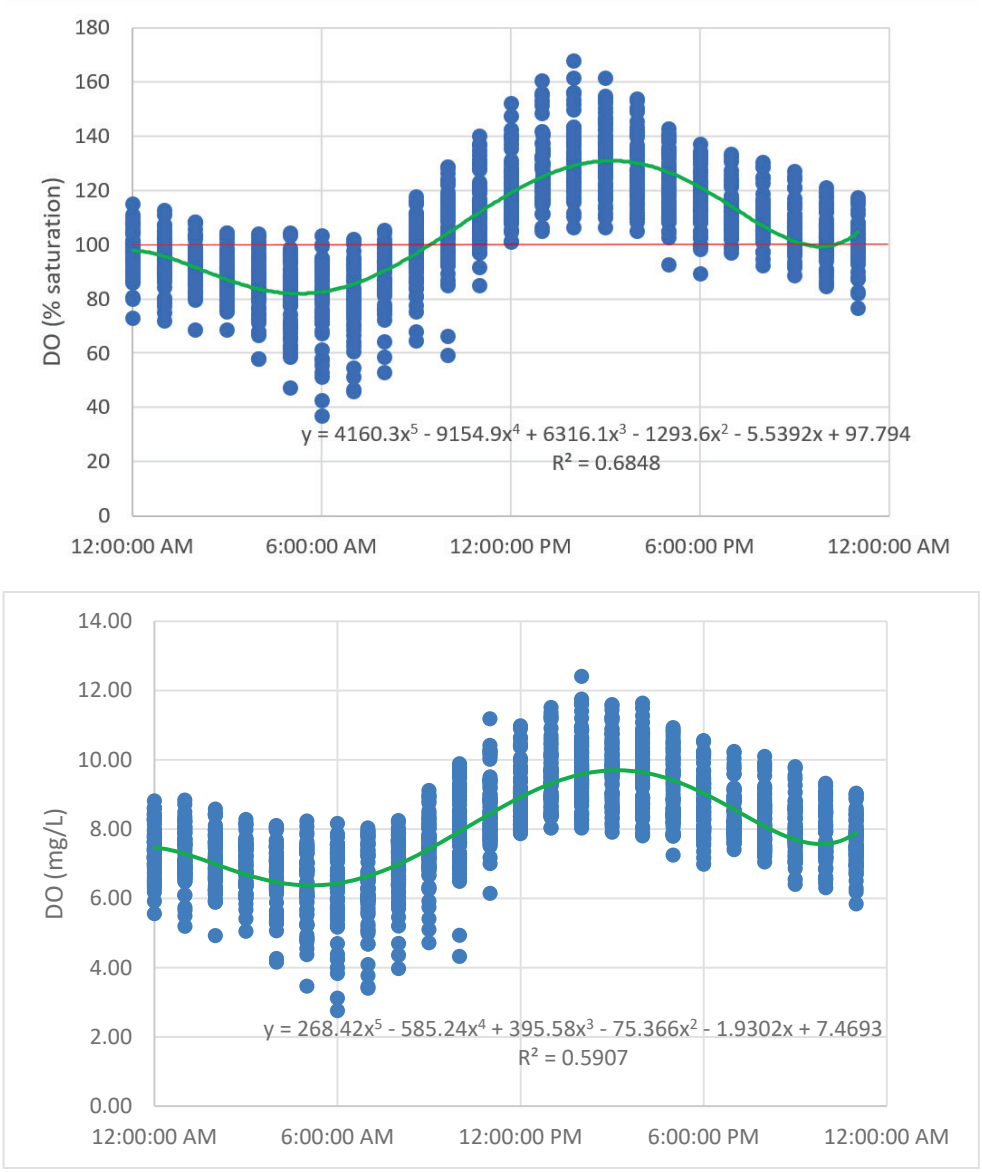

NOTES: Red line represents 100% saturation. Green line represents polynomial regression corresponding to equation shown.

D201800121.03 San Diego Bay Eelgrass Blue Carbon Study

Figure C-6
Dissolved oxygen inside a seagrass meadow (Mar - May 2023)

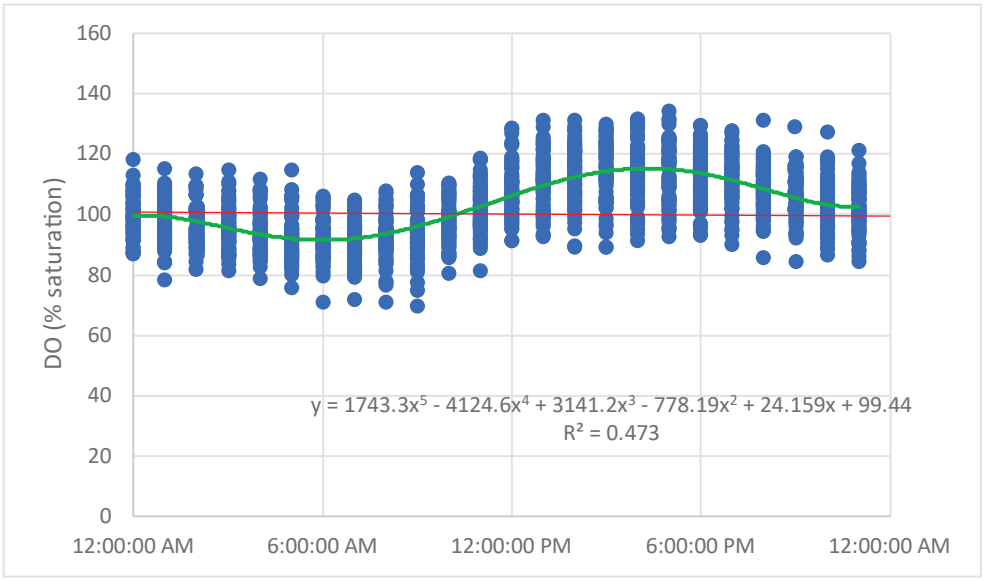

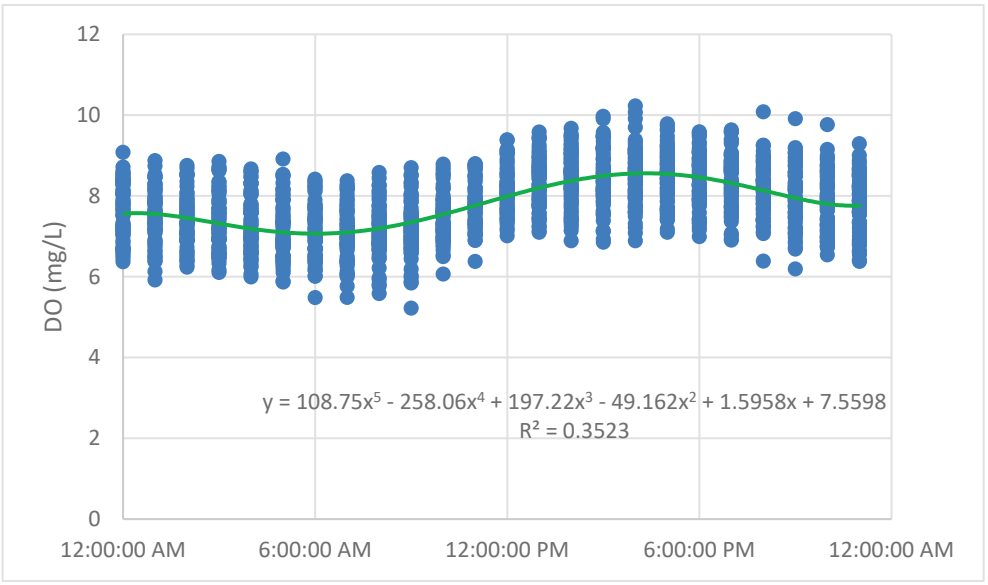

NOTES: Red line represents 100% saturation. Green line represents polynomial regression corresponding to equation shown.

D201800121.03 San Diego Bay Eelgrass Blue Carbon Study

Figure C-7
Dissolved oxygen outside a seagrass meadow (Mar - May 2023)

Appendix D. Radioisotope Analysis Interpretation (Flett Research Ltd.)

Core C

Interpretation of Pb-210, Ra-226 and Cs-137 Results

Flett Research Ltd.
440 DeSalaberry Ave. Winnipeg, MB R2L 0Y7
Fax/Phone: (204) 667-2505
Email: flett@flettresearch.ca Webpage: http://www.flettresearch.ca

Client: Juang, Alicia

Address:	180 Grand Ave, Suite 1050, Oakland, CA 94610, USA
Transaction ID:	1033
Project:	San Diego Eelgrass Blue Carbon
Core ID:	Core C
Matrix:	Sediment
PO/Contract No.:	TOE Oct 20-22
Sampling Date:	25-Oct-22
Date Received:	8-Nov-22
Analysis Dates:	November 23 - April 13, 2023
Analysts:	L. Hesketh-Jost; X. Hu
Date Issued:	25-May-23

Results authorized by Dr. Robert J. Flett, Chief Scientist

INTERPRETATION

Observations:

Among the 14 sections which were chosen for radioisotope analyses, large quantity of shell fragments (23% - 62% of total dry weight) were observed in the core interval of 24 - 80 cm. Shell presence (~5 - 18% of total dry weight) was also observed in the rest of sections which were analyzed. The shells and sediments in each sample were separated by wet sieving using a 2-mm mesh stainless steel sieve. Deionized water was used to wash off the sediments attached to the surface of the shells. Fine sediments from each section were passed through the sieve and then oven dried and analyzed for radioisotopes. The reported activities are in the unit of DPM/g (dry weight of sediment). Based upon previous experiences, the shells do not have detectable Pb-210. By removing the shells, dilution of Pb-210 can be minimized and the accuracy of analysis can be largely enhanced.

The dry bulk densities were not directly measured due to the presence of shell fragments, i.e. it was difficult to determine the exact wet volume of each section. However, it is possible to estimate the wet volume of each section by adding up the volume of water, the volume of dry sediment and the volume of dry shell fragments.

Volume of wet sample (cm^3) = Volume of water + Volume of dry sediment + Volume of shells
= [Weight of water (g) / 1.00 (g/cm^3)] + [Weight of sediment (g) / 2.65 (g/cm^3)]
+ [Weight of shells (g) / 2.20 (g/cm^3)]
where 1) density of water is 1.00 g/cm^3, 2) density of sediment is 2.65 g/cm^3, and 3) density of shells is 2.20 g/cm^3.

The dry bulk density of the shell-free sediment can be calculated as: Dry weight of sediment (g) / Volume of wet sample (cm^3) . The results are reported in column P on worksheet 'Dry Bulk Density' and plotted on page 5 on worksheet 'Modeling'.

The shell-free sediment was weighed for all radioisotope analyses.

A regular Pb-210 profile exhibits an exponential decrease in total Pb-210 activity as a function of depth. This core shows an irregular Pb-210 profile. The Pb-210 activities vary between 0.42 - 0.72 DPM/g in the upper 19 sections (extrapolated depths 0 - 21.5 cm) of the core, with a transient increase to 1.37 DPM/g in section 10 (extrapolated depth 8 - 10.5 cm). Below 21.5 cm (extrapolated depth), the Pb-210 activities increase from 0.25 DPM/g in section 23 (extrapolated depth 21.5 - 29 cm) to 0.41 DPM/g in section 32 (extrapolated depth 39.5 - 55 cm), then decrease to 0.21 DPM/g in section 38 (extrapolated depth 70 - 87.5 cm) (column Q on worksheet 'Modeling').

Ra-226 was measured at 0.11 DPM/g, 0.26 DPM/g, 0.25 DPM/g, 0.21 DPM/g and 0.29 DPM/g in section 10, section 23, section 32, section 38 and section 42, respectively (column S and page 3 on worksheet 'Modeling'). Duplicate analyses were performed on section 23 (24 - 26 cm), but the results are 0.13 DPM/g and 0.42 DPM/g, respectively. Both sample bottles were re-counted and the recounting results were close to the initial counting results. It is likely that the significant difference between the duplicate analyses was due to the inhomogeneity of the sample, which consists of fine sand and coarse sand. The average of four measurements (duplicate analyses and recounting) was reported (Page 8).

Unsupported Pb-210 is the amount of the Pb-210 isotope that is in excess to the background Pb-210 produced in the sediments by Ra-226. The unsupported Pb-210 is assumed to be from direct atmospheric deposition of Pb-210 plus the import of Pb-210 from the watershed and adjacent sediments. Net unsupported Pb-210 (column W, and page 4 on worksheet 'Modeling') was calculated by subtracting the nearest neighbouring Ra-226 measurement from each total Pb-210 value, unless noted otherwise. Detectable atmospheric sourced Pb-210 is present in the upper 21.5 cm (extrapolated depth) and possibly in section 45 - 50 cm as well.

Cs-137 measurements were performed in five sections in the core interval of 9 - 50 cm. No detectable Cs-137 was found (Pages 17 & 18).

Linear regression model of Unsupported Pb-210 activity vs. Cumulative Dry Weight (g/cm^2):

When applying the linear regression model, it is assumed that the input of Pb-210 and the sediment accumulation rate are constant. The irregular Pb-210 profile in the upper 32 sections (extrapolated depth 0 - 55 cm) indicates non-constant sediment accumulation, and therefore the regression model cannot be applied to the core.

CRS model of Age at bottom of Extrapolated section in years vs. Depth of bottom edge of current section in cm:

The CRS model assumes constant input of Pb-210 and a core that is long enough to include all of the measurable atmospheric source Pb-210, i.e. it contains a complete Pb-210 inventory. Although it appears that the Pb-210 background level may have been achieved in section 38 (extrapolated depth 70 - 87.5 cm), we have little confidence that a true Pb-210 inventory can be calculated because of the irregular Pb-210 profile, and therefore the model cannot be applied to the core.

Conclusion:

It is unclear that whether or not dredging and/or disposal events occurred at this coring site. The low unsupported Pb-210 activity and Cs-137 activity may be due to hydrodynamic activity which strips the sediment of organic matter for which Pb-210 and Cs-137 have an affinity. Detectable atmospheric sourced Pb-210 was found in the upper 21.5 cm (extrapolated depth) of this core, indicate that these sediments are likely modern. It is impossible to confidently determine the date of deposition of any sediments in this core interval, other than to say they appear to be less than 44.6 years old (2 half-lives of Pb-210), the maximum age that can be estimated in this core. Below 21.5 cm of the core, the sediments are likely to be older than 44.6 years.

Overall, the analytical quality of radioisotope data (based upon the recovery of spike, the results of repeat analyses, CRM and blanks) is considered good.

Calculation of Sediment Accumulation Rates and Ages

Flett Research Ltd.
440 DeSalaberry Ave. Winnipeg, MB R2L 0Y7
Fax/Phone (204) 667-2505
E-mail: flett@flettresearch.ca Webpage: http://www.flettresearch.ca

Client: Juang, Alicia

Address: 180 Grand Ave, Suite 1050, Oakland, CA 94610, USA
Core ID: Core C
Date Received: 8-Nov-22
Sampling Date: 25-Oct-22
Date Issued: 25-May-23

Matrix: Sediment
Transaction ID: 1033
PO/Contract No.: TOE Oct 20-22

Pb-210, Ra-226 and dry bulk density results as reported on other sheets within this workbook are summarized in the table below and are used to estimate accumulation rates and ages for the core. Two models are available for these calculations: the Constant Rate of Supply (CRS) model and the Linear Regression Model.

In order to date a sediment core, we need to determine the atmospheric sourced Pb-210 (= unsupported Pb-210) that is in 10+ sediment core sections. We analyze the sediment for TOTAL Pb-210 which includes both unsupported Pb-210 AND Pb-210 also being produced by decay of natural Ra-226 in the sediment. Due to secular equilibrium of Ra-226/Pb-210, sediment derived Pb-210 is expected to have the same activity as the Ra-226 and therefore we estimate the sediment sourced Pb-210 (=supported Pb-210) by using radon emanation to determine the Ra-226 in 3+ sections of the core. This allows the required calculation: unsupported Pb-210 = Total Pb-210 – supported Pb-210.

Results Authorized by Dr. Robert J. Flett, Chief Scientist

Section Number	Sample ID	Upper Depth (cm) Provided by client	Lower Depth (cm) Provided by client	Extrapolated Upper Section Depth (cm)	Extrapolated Lower Section Depth (cm)	Dry Bulk Density (Dry wt./Wet vol.) (g/cm3)	Midpoint Depth of Current Section (cm) Not Used	Mass in Extrapolated Section (g/cm2)	Cumulative Mass to Bottom of Current Section (g/cm2)	Plot-point of Cumulative Mass in Current Section (g/cm2)	Pb-210 Total Activity (DPM/g Dry Wt.)	Pb-210 COUNTING Error ± 1 S.D. (DPM/g Dry Wt.)	Pb-210 Background Activity from measured Ra-226 (DPM/g Dry Wt.)	Ra-226 Combined Error ± 1 S.D. (DPM/g Dry Wt.)	Estimated Pb-210 Background Activity from nearest neighbouring Ra-226 (DPM/g Dry Wt.)	Pb-210 Unsupported Activity (DPM/g Dry Wt.)	Pb-210 Unsupported Activity (DPM/cm^2) in each section	Age at Bottom of Extrapolated Section in Years (CRS Model Estimate)	CRS Sediment Accumulation Rate ($g/cm^2/yr$)	Age at Bottom of Extrapolated Section in Years (Linear Regression Model Estimate)
1	C0-1	0.0	1.0	0.00	1.50	1.731		2.597	2.597	0.866	0.73	0.07			0.11	0.61	1.593			
3	C2-3	2.0	3.0	1.50	3.50	1.777		3.555	6.151	4.374	0.49	0.06			0.11	0.37	1.320			
5	C4-5	4.0	5.0	3.50	5.50	1.660		3.320	9.471	7.811	0.57	0.06			0.11	0.46	1.512			
7	C6-7	6.0	7.0	5.50	8.00	1.505		3.762	13.234	10.976	0.72	0.06			0.11	0.61	2.281			
10	C9-10	9.0	10.0	8.00	10.50	1.589		3.972	17.206	15.617	1.37	0.10	0.11	0.01		1.26	4.998			
12	C11-12	11.0	12.0	10.50	13.00	1.575		3.937	21.143	18.781	0.42	0.05			0.11	0.31	1.215			
15	C14-15	14.0	15.0	13.00	16.50	1.437		5.031	26.174	23.299	0.56	0.05			0.11	0.45	2.260			
19	C18-19	18.0	19.0	16.50	21.50	1.455		7.276	33.450	29.084	0.46	0.05			0.11	0.34	2.487			
23	C24-26	24.0	26.0	21.50	29.00	0.803		6.022	39.473	36.261	0.25	0.04	0.26	0.01		-0.01				
27	C32-34	32.0	34.0	29.00	39.50	0.685		7.189	46.661	42.211	0.33	0.05			0.25	0.09	0.634			
32&32Dup	C45-50	45.0	50.0	39.50	55.00	0.907		14.065	60.727	53.921	0.41	0.05	0.25	0.01		0.16	2.231			
35	C60-65	60.0	65.0	55.00	70.00	1.255		18.823	79.550	70.138	0.30	0.05			0.25	0.05	0.968			
38	C75-80	75.0	80.0	70.00	87.50	1.260		22.046	101.595	88.998	0.21	0.04	0.21	0.01		0.00				
42	C95-100	95.0	100.0	87.50	100.00	1.455		18.189	119.784	116.147	0.23	0.03	0.29	0.01		-0.07				

Q:\Clients A-L\Juang, Alicia - ESA\2022(1033)\Radioisotopes\C\Pb-210, Ra-226 and Cs-137 Juang Core C May 25-23 Final.xlsm

Dup (Duplicate): Two subsamples of the same sample were carried through the analytical procedure in an identical manner.

 Sample depths are provided by the client. Errors in that data may affect the validity of sediment accumulation rates, Pb-210 inventory and age calculations.
Note: Results relate only to the items tested and as received.

Total Pb-210 Activity vs. Accumulated Mass

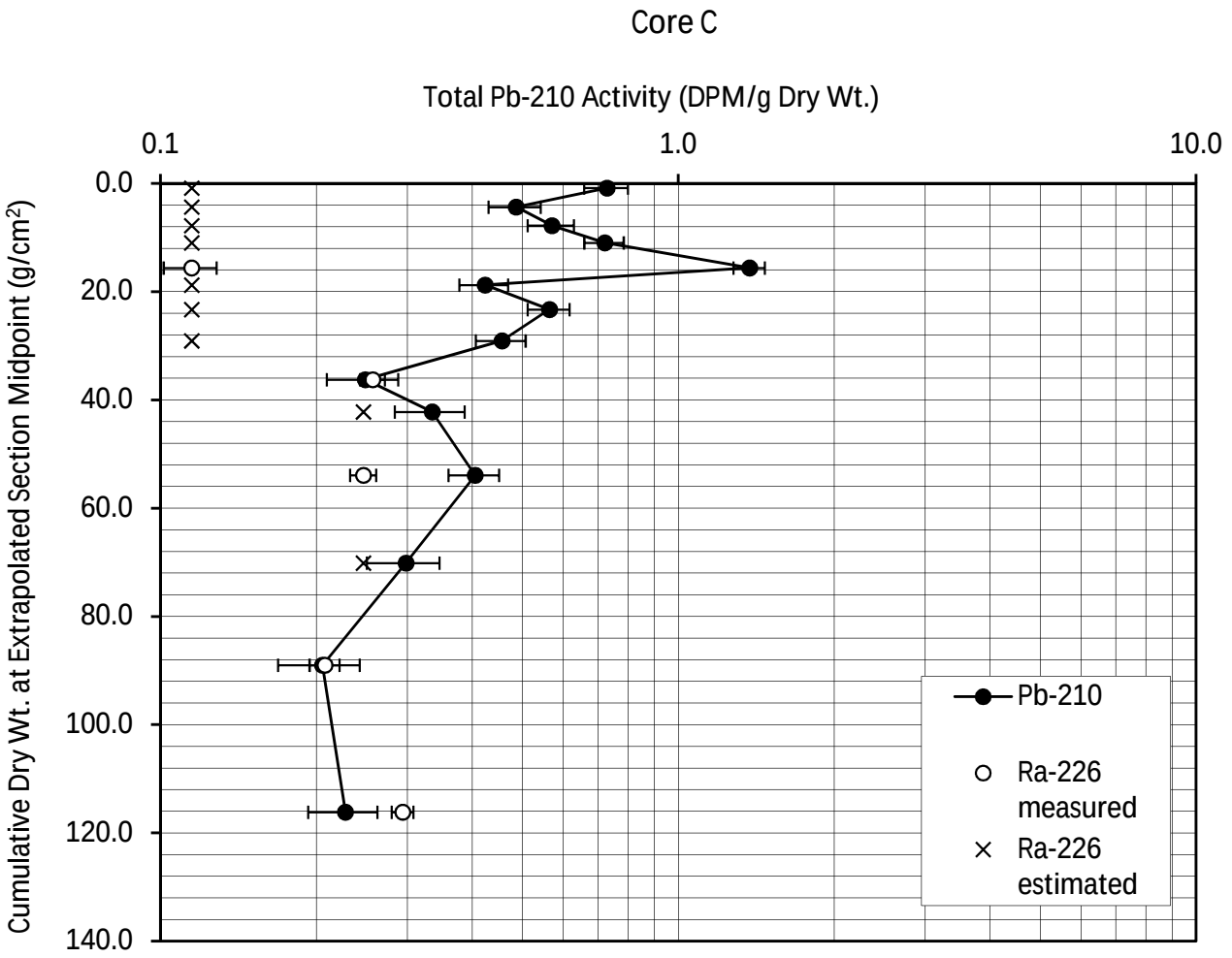

Unsupported Pb-210 Activity vs. Accumulated Mass

Core C

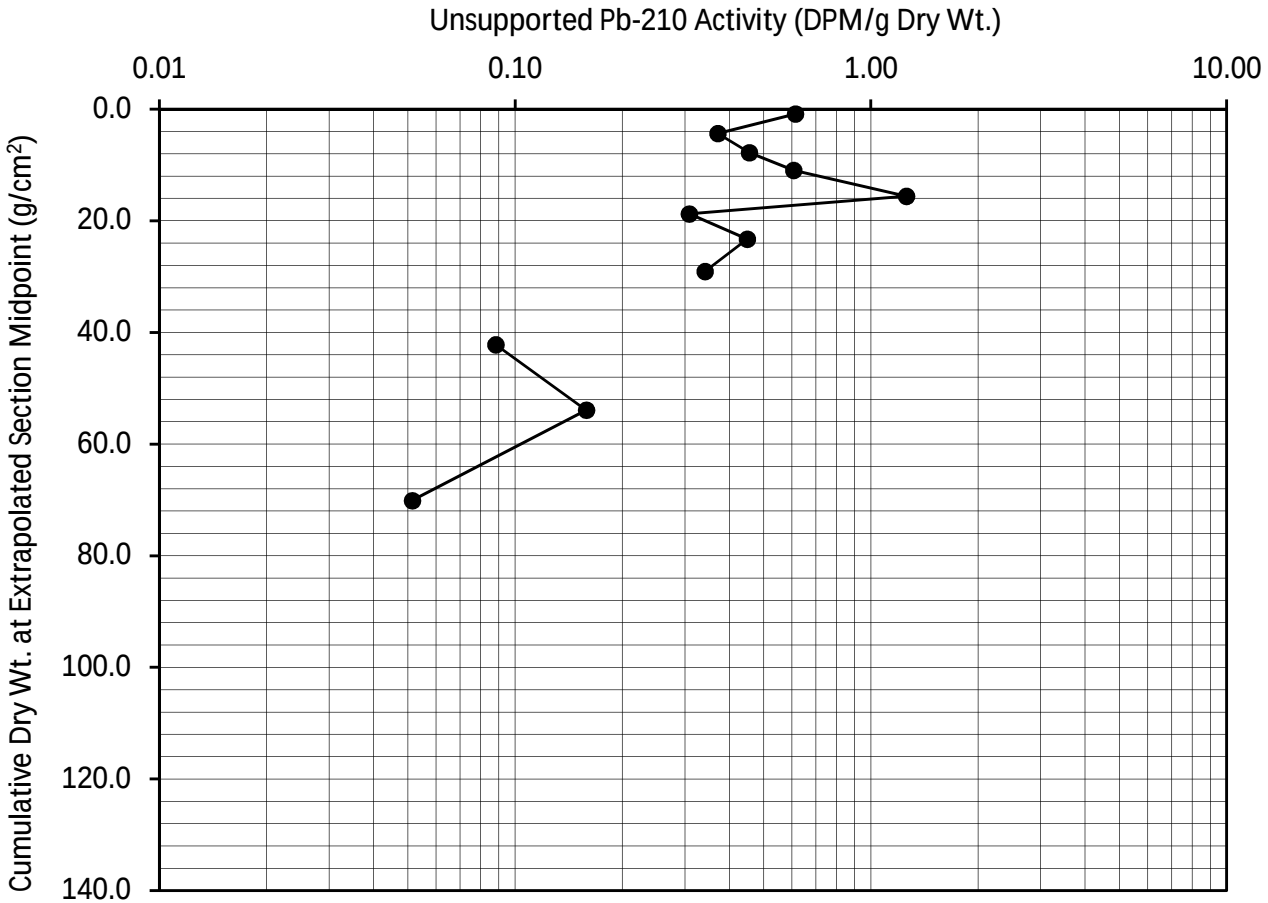

Dry Bulk Density vs. Accumulated Mass [Shell Free]

Core C

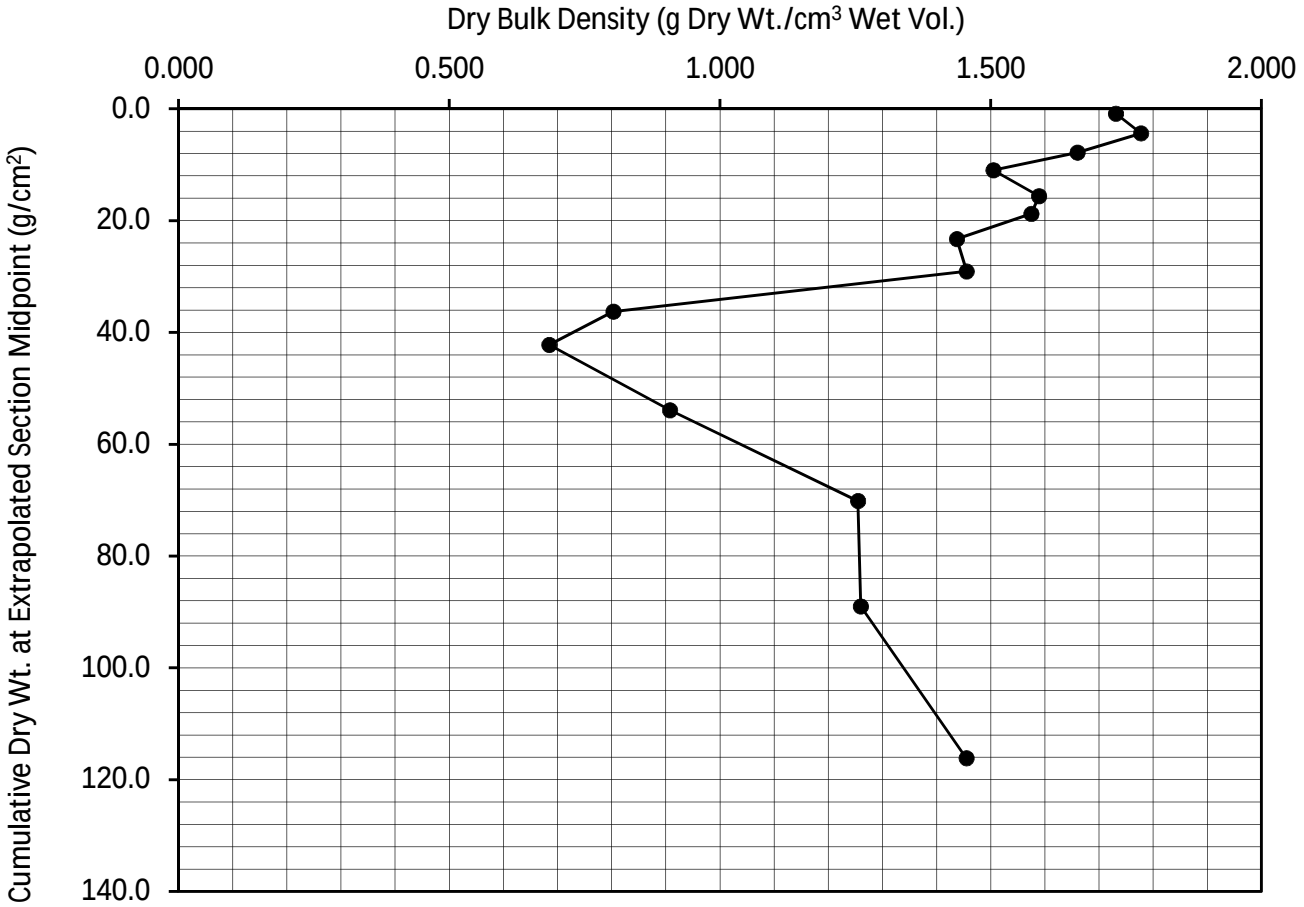

Q:\Clients A-L\Juang, Alicia - ESA\2022(1033)\Radioisotopes\C\Pb-210, Ra-226 and Cs-137 Juang Core C May 25-23 Final.xlsm

Dry Bulk Density, Percent Loss on Drying and Porosity

Flett Research Ltd.

440 DeSalaberry Ave. Winnipeg, MB R2L 0Y7

Fax/Phone: (204) 667-2505

E-mail: flett@flettresearch.ca Webpage: http://www.flettresearch.ca

Client: Juang, Alicia

Address: 180 Grand Ave, Suite 1050, Oakland, CA 94610, USA
Core ID: Core C
Date Received: November 8, 2022
Sampling Date: October 25, 2022
Date Issued: 25-May-23

Matrix: Sediment
Transaction ID: 1033
PO/Contract No.: TOE Oct 20-22
Analysis Dates: November 23, 2022 to March 14, 2023
Analyst: L. Hesketh-Jost

Analytical Method: N10020 Measurement of Dry Bulk Density and Other Sediment Characteristics (version 1)

Comments: The dry bulk densities were not directly measured due to the presence of shell fragments in most of the sections. Each entire wet sample was oven dried at 50C. Gross wet weight, gross dry weight and the weight of empty jar were recorded to calculate %loss on drying. After the sample was re-wetted with deionized water, the sediment and the shells were separated using a 2-mm mesh sieve. Dry weight of sediments and dry weight shells were recorded.

The dry bulk density of the shell-free sediment in each section was calculated by dividing the dry weight of the sediment (g) by the total wet volume (ml). The total wet volume (ml) of each section was estimated by summing up the volume of water, the volume of dry sediment and the volume of dry shell fragments. See details on worksheet 'Interpretation' (Page 1).

The shell-free sediment was weighed for radioisotope analyses.

Estimated Uncertainty:

Results authorized by Dr. Robert J. Flett, Chief Scientist

Section Number	LAB ID	Sample ID	Upper Depth (cm) Provided by client	Lower Depth (cm) Provided by client		Volume of wet sample (ml)	Weight of wet sample (g)	Weight of dry sample (g)	Weight of Dry Sediment (g)	Dry Bulk Density (Dry wt./Wet vol.) (g/cm^3) (Shell Free)	% Loss on Drying	% Porosity
1	112618	C0-1	0.0	1.0		34.144	75.376	67.211	59.104	1.731	10.83%	23.91%
3	112620	C2-3	2.0	3.0		32.857	70.814	61.310	58.398	1.777	13.42%	28.93%
5	112622	C4-5	4.0	5.0		39.242	82.450	69.981	65.145	1.660	15.12%	31.77%
7	112624	C6-7	6.0	7.0		42.669	89.522	76.795	64.211	1.505	14.22%	29.83%
10	112627	C9-10	9.0	10.0		37.040	76.356	63.737	58.856	1.589	16.53%	34.07%
12	112629	C11-12	11.0	12.0		31.634	67.353	58.416	49.817	1.575	13.27%	28.25%
15	112632	C14-15	14.0	15.0		33.938	70.364	59.865	48.783	1.437	14.92%	30.94%
19	112636	C18-19	18.0	19.0		44.143	91.991	78.602	64.241	1.455	14.55%	30.33%
23	112640	C24-26	24.0	26.0		64.343	129.721	112.535	51.667	0.803	13.25%	26.71%
27	112644	C32-34	32.0	34.0		88.133	178.574	157.258	60.338	0.685	11.94%	24.19%
32	112649	C45-50	45.0	50.0		273.899	524.560	424.330	248.547	0.907	19.11%	36.59%
35	112652	C60-65	60.0	65.0		275.853	554.610	461.940	346.162	1.255	16.71%	33.59%
38	112655	C75-80	75.0	80.0		230.270	459.443	379.023	290.081	1.260	17.50%	34.92%
42	112659	C95-100	95.0	100.0		242.127	475.554	378.054	352.327	1.455	20.50%	40.27%

Loss of water or sediment during collecting the core, sectioning of core, sub-sampling for analyses or storage and transportation, will bias the result of the dry bulk density. Sample depthsare provided by the client. Errors in that data may affect the validity of sediment quality data.

Note: Results relate only to the samples tested and as received.

Results of Pb-210 by Po-210 analysis

Flett Research Ltd.
440 DeSalaberry Ave. Winnipeg, MB R2L 0Y7
Fax/Phone: (204) 667-2505
E-mail: flett@flettresearch.ca Webpage: http://www.flettresearch.ca

Client: Juang, Alicia

Address: 180 Grand Ave, Suite 1050, Oakland, CA 94610, USA
Core ID: Core C
Date Received: 8-Nov-22
Sampling Date: 25-Oct-22
Date Issued: 25-Apr-23

Matrix: Sediment
Transaction ID: 1033
PO/Contract No.: TOE Oct 20-22
Analysis Dates: 19-Dec-22 to 19-Mar-23
Analyst: L. Hesketh-Jost

Analytical Method: N20110 Determination of Lead-210 by Measurement of Po-210 in Sediment, Soil and Peat by Alpha Spectrometry (Version 7)
Comments:

Detection Limit: The method detection limit (MDL) for 0.25 - 0.5 g (dry wt.) sample is between 0.05 - 0.1 DPM Po-210/g dry sample at a 95% confidence level for 60,000 second counting time and is based on greater than 20 method blanks. This can vary slightly and depends upon the amount of sample, detector and recovery efficiency of each sample.

Estimated Uncertainty: As Po-210 (Pb-210) activity drops, error increases due to increasing counting error. When gross counts are less than 100 the dominant error becomes counting error which is equal to √gross counts/gross counts. When Po-210 (Pb-210) activity exceeds 5 DPM/g the method uncertainty is ± 11% . When activities are between 1 and 5 DPM/g, the method uncertainty is ± 17%. When activities are between 0.2 and 1 DPM/g, the method uncertainty is ± 25%. Uncertainties are expressed at 95% confidence level (k=2).

Results authorized by Dr. Robert J. Flett, Chief Scientist

Section Number	LAB ID	Sample ID	Upper Depth (cm) Provided by client	Lower Depth (cm) Provided by client	Po-209 Counts Less Detector Back-ground	Net Po-210 Counts [Gross counts Less Detector and Po-209 Spiking Solution Backgrounds]	Weight of Sample Counted (g)	Count Time (sec)	Po-210 Total Activity (DPM/g Dry Wt.)	Po-210 COUNTING Error ± 1 S.D. (DPM/g Dry Wt.)	Comments Code
1	112618	C0-1	0.0	1.0	2632	108	0.551	60000	0.73	0.07	
3	112620	C2-3	2.0	3.0	2715	76	0.558	60000	0.49	0.06	
5	112622	C4-5	4.0	5.0	2902	96	0.567	60000	0.57	0.06	
7	112624	C6-7	6.0	7.0	2954	132	0.600	60000	0.72	0.06	
10	112627	C9-10	9.0	10.0	2606	206	0.563	60000	1.37	0.10	
12	112629	C11-12	11.0	12.0	2757	87	0.722	60000	0.42	0.05	
15	112632	C14-15	14.0	15.0	3252	121	0.644	60000	0.56	0.05	
19	112636	C18-19	18.0	19.0	2859	86	0.638	60000	0.46	0.05	
23	112640	C24-26	24.0	26.0	2498	41	0.647	60000	0.25	0.04	
27	112644	C32-34	32.0	34.0	2356	43	0.530	60000	0.33	0.05	
32&32Dup	112649	C45-50	45.0	50.0					0.41	0.05	
35	112652	C60-65	60.0	65.0	2732	42	0.500	60000	0.30	0.05	
38	112655	C75-80	75.0	80.0	2868	33	0.542	60000	0.21	0.04	
42	112659	C95-100	95.0	100.0	2804	44	0.674	60000	0.23	0.03	

Quality Control Samples

Section Number	LAB ID	Sample ID			Po-209 Counts Less Detector Back-ground	Net Po-210 Counts	Weight of Sample Counted (g)	Count Time (sec)	Po-210 Total Activity (DPM/g)	Po-210 COUNTING Error +/- 1 S.D. (DPM/g)	CRM Recovery on Counting Date
RegBlk1		Reagent Blank w/o Po-209 spike			-2	3					
BLKwSpike1		Reagent Blank with Po-209 spike			2882	-1					
RegBlk2		Reagent Blank w/o Po-209 spike			-9	2					
BLKwSpike2		Reagent Blank with Po-209 spike			3036	7					
32	112649	C45-50					0.672	60000	0.40	0.05	
32Dup	112649	C45-50 Duplicate					0.687	60000	0.41	0.05	
CRM1		IAEA447 (17.64 DPM/g)					0.359	60000	17.07	0.40	96.8%Rec
CRM2		IAEA447 (17.51 DPM/g)					0.367	60000	16.27	0.41	92.9%Rec

Q:\Clients A-L\Juang, Alicia - ESA\2022(1033)\Radioisotopes\C\Pb-210, Ra-226 and Cs-137 Juang Core C May 25-23 Final.xlsm

Dup (duplicate): Two subsamples of the same sample were carried through the analytical procedure in an identical manner.

Note: Results relate only to the samples tested and as received. Sample depths are provided by the client.
ISO / IEC 17025:2017 Accredited with the Canadian Association for Laboratory Accreditation (CALA Accreditation No. A3306)

Results of Ra-226 Analysis by Rn-222 Emanation

Flett Research Ltd.
440 DeSalaberry Ave., Winnipeg, MB R2L 0Y7
Fax/Phone: (204) 667-2505
Email: flett@flettresearch.ca Webpage: http://www.flettresearch.ca

Client: Juang, Alicia

Address: 180 Grand Ave, Suite 1050, Oakland, CA 94610, USA
Core ID: Core C
Date Received: 8-Nov-22
Sampling Date: 25-Oct-22
Date Issued: 25-Apr-23

Matrix: Sediment
Transaction ID: 1033
PO/Contract No.: TOE Oct 20-22
Analysis Dates: 22-Dec-22 to 29-Mar-23
Analyst: L. Hesketh-Jost & X. Hu

Analytical Method: N40110 Determination of Radium-226 in Sediment, Soil and Peat by Radon-222 Emanation (Version 4)

Comments:

Detection Limit: The method detection limit (MDL) is dependent on the amount of sample analyzed. For a 60,000 second counting time the MDL at 95% confidence for 2 g of dry sample is 0.1 DPM/g and for 0.5 g of dry sample is 0.5 DPM/g.

Estimated Uncertainty: The estimate of uncertainty of measurement for this method in this laboratory is approximately ±12% at 95% confidence level (approximately 40,000 counts in 60,000 seconds).

Results authorized by Dr. Robert J. Flett, Chief Scientist

Section Number	Lab ID	Sample ID	Upper Depth (cm) Provided by client	Lower Depth (cm) Provided by client	Weight of Sample Counted (g)	Count Time (sec)	Ra-226 Activity (DPM/g Dry Wt.)	Combined Error: 1 SD (DPM/g Dry Wt.)	Comments Code for Ra-226 Analysis
10	112627	C9-10	9	10	2.541	60000	0.11	0.01	
23&23Dup	112640	C24-26	24	26			0.26	0.01	
32	112649	C45-50	45	50	2.529	60000	0.25	0.01	
38	112655	C75-80	75	80	2.577	60000	0.21	0.01	
42	112659	C95-100	95	100	2.600	60000	0.29	0.01	
Quality Control Samples									
23	112640	C24-26	24	26	2.566	60000	0.13	0.01	
23Dup	112640	C24-26 Duplicate	24	26	2.555	60000	0.42	0.02	
23ReC	112640	C24-26 ReCount	24	26	2.566	60000	0.11	0.01	
23DupReC	112640	Ra-226 24 - 26 cm Dup recount	24	26	2.555	60000	0.37	0.01	

Q:\Clients A-L\Juang, Alicia - ESA\2022(1033)\Radioisotopes\C\Pb-210, Ra-226 and Cs-137 Juang Core C May 25-23 Final.xlsm
Duplicate: Two subsamples of the same sample were carried through the analytical procedure in an identical manner.
Re-count: The sample bottle was re-sealed after the initial analysis, and was re-counted after 11 or more days of Rn-222 ingrowth.

Note: Results relate only to the samples tested and as received. Sample depths are provided by the client.
ISO / IEC 17025:2017 Accredited with the Canadian Association for Laboratory Accreditation (CALA Accreditation No. A3306)

Radium Analysis by Rn-222 Emanation

Ra Sample Number:	2431
Section Number	10
Sample ID	C9-10
Core ID	Core C
Lucas Cell No.	3
Number of days since Rn board last run	1
Dry weight of sample counted (g)	2.541
Total count in period	1407
Total count in period (carryover corrected)	1389
Cell Blank count (CPM)	0.523
System Blank (DPM)	0.390
System Efficiency	0.804
Count duration (minutes)	1000

Typical carryover is about 1 - 2 % of the net counts (gross counts less system background) of the sample counted on the previous day. The carryover is subtracted from the gross counts of current sample. This correction is not required if the sample is run after a blank.

Carryover correction?	Yes		
Gross counts of previous sample	2463	Mean of last 10 carryover measurements	1.06%
Counts carried over from previous sample	18	Mean of last 6 system background measurements	795

	Year	Month	Day	Hour	Minute	Second	Ingrowth time (Days)	Ingrowth factor	Decay correction
When sample last stripped	2022	12	23	15	41	0	11.94	0.88501	0.92490
When cell filled	2023	1	4	14	8	37			
Beginning time of count	2023	1	4	16	9	0			

Counts per minute	1.39				
Gross CPM less Cell Blank (CPM)	0.87				
CPM (decay during count corrected)	0.94				
DPM Sample +System (efficiency corrected)	1.17				
DPM sample	0.88	Error ± 1 SD	0.1027	DPM	
DPM/g	0.34				
Ra-226 DPM/g	0.11	Error ± 1 SD	0.0135	DPM/g	Error % = 11.7
Ra-226 pCi/g	0.05				

Chemist	XH
PMT High Voltage +ve	770
HV Power supply	Spectrum Technologies
Alpha Counter	Spectrum Technologies
Region of Interest Ch.#s	28-1022
PMT	6655A - #1
Preamp	Canberra 2007P tube base
Amp Gain	1

Radium Analysis by Rn-222 Emanation

Ra Sample Number:	2432
Section Number	23
Sample ID	C24-26
Core ID	Core C
Lucas Cell No.	3
Number of days since Rn board last run	1
Dry weight of sample counted (g)	2.566
Total count in period	1467
Total count in period (carryover corrected)	n/a
Cell Blank count (CPM)	0.523
System Blank (DPM)	0.390
System Efficiency	0.804
Count duration (minutes)	1000

Typical carryover is about 1 - 2 % of the net counts (gross counts less system background) of the sample counted on the previous day. The carryover is subtracted from the gross counts of current sample. This correction is not required if the sample is run after a blank.

Carryover correction? No

	Year	Month	Day	Hour	Minute	Second	Ingrowth time (Days)	Ingrowth factor	Decay correction
When sample last stripped	2022	12	23	15	41	0	13.00	0.90525	0.92490
When cell filled	2023	1	5	15	47	1			
Beginning time of count	2023	1	5	17	47	24			

Counts per minute	1.47			
Gross CPM less Cell Blank (CPM)	0.94			
CPM (decay during count corrected)	1.02			
DPM Sample +System (efficiency corrected)	1.27			
DPM sample	0.97	Error ± 1 SD	0.1032	DPM
DPM/g	0.38			
Ra-226 DPM/g	0.13	Error ± 1 SD	0.0134	DPM/g
Ra-226 pCi/g	0.06			

Error % = 10.6

Chemist	XH
PMT High Voltage +ve	770
HV Power supply	Spectrum Technologies
Alpha Counter	Spectrum Technologies
Region of Interest Ch.#s	28-1022
PMT	6655A - #1
Preamp	Canberra 2007P tube base
Amp Gain	1

Radium Analysis by Rn-222 Emanation

Ra Sample Number:	2433
Section Number	42
Sample ID	C95-100
Core ID	Core C
Lucas Cell No.	3
Number of days since Rn board last run	1
Dry weight of sample counted (g)	2.600
Total count in period	2380
Total count in period (carryover corrected)	n/a
Cell Blank count (CPM)	0.523
System Blank (DPM)	0.390
System Efficiency	0.804
Count duration (minutes)	1000

Typical carryover is about 1 - 2 % of the net counts (gross counts less system background) of the sample counted on the previous day. The carryover is subtracted from the gross counts of current sample. This correction is not required if the sample is run after a blank.

Carryover correction? No

	Year	Month	Day	Hour	Minute	Second	Ingrowth time (Days)	Ingrowth factor	Decay correction
When sample last stripped	2022	12	23	15	40	0	13.93	0.91993	0.92490
When cell filled	2023	1	6	14	3	41			
Beginning time of count	2023	1	6	16	4	4			

Counts per minute	2.38				
Gross CPM less Cell Blank (CPM)	1.86				
CPM (decay during count corrected)	2.01				
DPM Sample +System (efficiency corrected)	2.50				
DPM sample	2.29	Error ± 1 SD	0.1105	DPM	
DPM/g	0.88				
Ra-226 DPM/g	0.29	Error ± 1 SD	0.0142	DPM/g	Error % = 4.8
Ra-226 pCi/g	0.13				

Chemist	XH
PMT High Voltage +ve	770
HV Power supply	Spectrum Technologies
Alpha Counter	Spectrum Technologies
Region of Interest Ch.#s	28-1022
PMT	6655A - #1
Preamp	Canberra 2007P tube base
Amp Gain	1

Radium Analysis by Rn-222 Emanation

Ra Sample Number:	2434
Section Number	23Dup
Sample ID	C24-26 Duplicate
Core ID	Core C
Lucas Cell No.	3
Number of days since Rn board last run	1
Dry weight of sample counted (g)	2.555
Total count in period	3055
Total count in period (carryover corrected)	3038
Cell Blank count (CPM)	0.523
System Blank (DPM)	0.390
System Efficiency	0.804
Count duration (minutes)	1000

Typical carryover is about 1 - 2 % of the net counts (gross counts less system background) of the sample counted on the previous day. The carryover is subtracted from the gross counts of current sample. This correction is not required if the sample is run after a blank.

Carryover correction?	Yes		
Gross counts of previous sample	2380	Mean of last 10 carryover measurements	1.06%
Counts carried over from previous sample	17	Mean of last 6 system background measurements	795

	Year	Month	Day	Hour	Minute	Second	Ingrowth time (Days)	Ingrowth factor	Decay correction
When sample last stripped	2022	12	23	15	40	0	15.09	0.93513	0.92490
When cell filled	2023	1	7	17	56	17			
Beginning time of count	2023	1	7	19	56	40			

Counts per minute	3.04				
Gross CPM less Cell Blank (CPM)	2.52				
CPM (decay during count corrected)	2.72				
DPM Sample +System (efficiency corrected)	3.38				
DPM sample	3.20	Error ± 1 SD	0.1155	DPM	
DPM/g	1.25				
Ra-226 DPM/g	0.42	Error ± 1 SD	0.0151	DPM/g	Error % = 3.6
Ra-226 pCi/g	0.19				

Chemist	RF
PMT High Voltage +ve	770
HV Power supply	Spectrum Technologies
Alpha Counter	Spectrum Technologies
Region of Interest Ch.#s	28-1022
PMT	6655A - #1
Preamp	Canberra 2007P tube base
Amp Gain	1

Radium Analysis by Rn-222 Emanation

Ra Sample Number:	2432ReC
Section Number	23ReC
Sample ID	C24-26ReCount
Core ID	Core C
Lucas Cell No.	3
Number of days since Rn board last run	1
Dry weight of sample counted (g)	2.566
Total count in period	1417
Total count in period (carryover corrected)	n/a
Cell Blank count (CPM)	0.523
System Blank (DPM)	0.390
System Efficiency	0.804
Count duration (minutes)	1000

Typical carryover is about 1 - 2 % of the net counts (gross counts less system background) of the sample counted on the previous day. The carryover is subtracted from the gross counts of current sample. This correction is not required if the sample is run after a blank.

Carryover correction? No

	Year	Month	Day	Hour	Minute	Second	Ingrowth time (Days)	Ingrowth factor	Decay correction
When sample last stripped	2023	1	5	14	18	0	14.93	0.93314	0.92490
When cell filled	2023	1	20	12	34	36			
Beginning time of count	2023	1	20	14	34	59			

Counts per minute	1.42			
Gross CPM less Cell Blank (CPM)	0.89			
CPM (decay during count corrected)	0.97			
DPM Sample +System (efficiency corrected)	1.20			
DPM sample	0.87	Error ± 1 SD	0.1026	DPM
DPM/g	0.34			
Ra-226 DPM/g	0.11	Error ± 1 SD	0.0133	DPM/g
Ra-226 pCi/g	0.05			

Error % = 11.8

Chemist	XH
PMT High Voltage +ve	770
HV Power supply	Spectrum Technologies
Alpha Counter	Spectrum Technologies
Region of Interest Ch.#s	28-1022
PMT	6655A - #1
Preamp	Canberra 2007P tube base
Amp Gain	1

Radium Analysis by Rn-222 Emanation

Ra Sample Number:	2434ReC
Section Number	23DupReC
Sample ID	C24-26 DuplicateReCount
Core ID	Core C
Lucas Cell No.	3
Number of days since Rn board last run	1
Dry weight of sample counted (g)	2.555
Total count in period	2764
Total count in period (carryover corrected)	n/a
Cell Blank count (CPM)	0.523
System Blank (DPM)	0.390
System Efficiency	0.804
Count duration (minutes)	1000

Typical carryover is about 1 - 2 % of the net counts (gross counts less system background) of the sample counted on the previous day. The carryover is subtracted from the gross counts of current sample. This correction is not required if the sample is run after a blank.

Carryover correction? No

	Year	Month	Day	Hour	Minute	Second	Ingrowth time (Days)	Ingrowth factor	Decay correction
When sample last stripped	2023	1	7	16	26	0	14.05	0.92159	0.92490
When cell filled	2023	1	21	17	35	48			
Beginning time of count	2023	1	21	19	36	11			

Counts per minute (gross)	2.76			
Gross CPM less Cell Blank (CPM)	2.24			
CPM (decay during count corrected)	2.42			
DPM Sample +System (efficiency corrected)	3.01			
DPM sample	2.85	Error ± 1 SD	0.1137 DPM	
DPM/g	1.11			
Ra-226 DPM/g	0.37	Error ± 1 SD	0.0148 DPM/g	Error % = 4.0
Ra-226 pCi/g	0.17			

Chemist	RF
PMT High Voltage +ve	770
HV Power supply	Spectrum Technologies
Alpha Counter	Spectrum Technologies
Region of Interest Ch.#s	28-1022
PMT	6655A - #1
Preamp	Canberra 2007P tube base
Amp Gain	1

Radium Analysis by Rn-222 Emanation

Ra Sample Number:	2461
Section Number	32
Sample ID	C45-50
Core ID	Core C
Lucas Cell No.	3
Number of days since Rn board last run	1
Dry weight of sample counted (g)	2.529
Total count in period	2226
Total count in period (carryover corrected)	2188
Cell Blank count (CPM)	0.536
System Blank (DPM)	0.405
System Efficiency	0.806
Count duration (minutes)	1000

Typical carryover is about 1 - 2 % of the net counts (gross counts less system background) of the sample counted on the previous day. The carryover is subtracted from the gross counts of current sample. This correction is not required if the sample is run after a blank.

Carryover correction?	Yes		
Gross counts of previous sample	4253	Mean of last 10 carryover measurements	1.12%
Counts carried over from previous sample	38	Mean of last 6 system background measurements	818

	Year	Month	Day	Hour	Minute	Second	Ingrowth time (Days)	Ingrowth factor	Decay correction
When sample last stripped	2023	2	24	14	38	0	18.95	0.96772	0.92490
When cell filled	2023	3	15	13	20	6			
Beginning time of count	2023	3	15	15	20	29			

Counts per minute	2.19				
Gross CPM less Cell Blank (CPM)	1.65				
CPM (decay during count corrected)	1.79				
DPM Sample +System (efficiency corrected)	2.22				
DPM sample	1.87	Error ± 1 SD	0.1076	DPM	
DPM/g	0.74				
Ra-226 DPM/g	0.25	Error ± 1 SD	0.0142	DPM/g	Error % = 5.8
Ra-226 pCi/g	0.11				

Chemist	XH
PMT High Voltage +ve	770
HV Power supply	Spectrum Technologies
Alpha Counter	Spectrum Technologies
Region of Interest Ch.#s	28-1022
PMT	6655A - #1
Preamp	Canberra 2007P tube base
Amp Gain	1

Radium Analysis by Rn-222 Emanation

Ra Sample Number:	2479
Section Number	38
Sample ID	C75-80
Core ID	Core C
Lucas Cell No.	3
Number of days since Rn board last run	1
Dry weight of sample counted (g)	2.577
Total count in period	1910
Total count in period (carryover corrected)	1871
Cell Blank count (CPM)	0.536
System Blank (DPM)	0.405
System Efficiency	0.806
Count duration (minutes)	1000

Typical carryover is about 1 - 2 % of the net counts (gross counts less system background) of the sample counted on the previous day. The carryover is subtracted from the gross counts of current sample. This correction is not required if the sample is run after a blank.

Carryover correction?	Yes		
Gross counts of previous sample	4276	Mean of last 10 carryover measurements	1.12%
Counts carried over from previous sample	39	Mean of last 6 system background measurements	818

	Year	Month	Day	Hour	Minute	Second	Ingrowth time (Days)	Ingrowth factor	Decay correction
When sample last stripped	2023	3	17	15	43	0	10.97	0.86293	0.92490
When cell filled	2023	3	28	14	54	29			
Beginning time of count	2023	3	28	16	54	52			

Counts per minute	1.87			
Gross CPM less Cell Blank (CPM)	1.34			
CPM (decay during count corrected)	1.44			
DPM Sample +System (efficiency corrected)	1.79			
DPM sample	1.61	Error ± 1 SD	0.1065	DPM
DPM/g	0.62			
Ra-226 DPM/g	0.21	Error ± 1 SD	0.0138	DPM/g
Ra-226 pCi/g	0.09			

Error % = 6.6

Chemist	XH
PMT High Voltage +ve	770
HV Power supply	Spectrum Technologies
Alpha Counter	Spectrum Technologies
Region of Interest Ch.#s	28-1022
PMT	6655A - #1
Preamp	Canberra 2007P tube base
Amp Gain	1

Results of Cs-137 Analysis

Flett Research Ltd.

440 DeSalaberry Ave. Winnipeg, MB R2L 0Y7

Fax/Phone: (204) 667-2505

E-mail: flett@flettresearch.ca Webpage: http://www.flettresearch.ca

Client: Juang, Alicia

Address: 180 Grand Ave, Suite 1050, Oakland, CA 94610, USA
Core ID: Core C
Date Received: 8-Nov-22
Sampling Date: 25-Oct-22
Date Issued: 25-Apr-23

Matrix: Sediment
Transaction ID: 1033
PO/Contract No.: TOE Oct 20-22
Analysis Dates: 16-Feb-23 to 13-Apr-23
Analyst: X. Hu

Analytical Method: N30120 Measurement of Gamma-Ray Emitting Radionuclides in Sediment/Soil Samples by Gamma Spectrometry Using HPGe Detectors (Version 4)

Comments: <2SD: The measured Cs-137 activity is less than 2 counting errors (i.e. 2 SD), suggesting no significant presence of Cs-137 in this sample.

Detection Limit: The method detection limit (MDL) of Cs-137 is 0.3 DPM/g for a 9 g of dry sample and 0.1 DPM/g for a 32 g of dry sample for an 80,000 seconds counting

Estimated Uncertainty: The estimated uncertainty of this method for Cs-137 has been determined to be ± 10% at 95% confidence for samples with activities between 0.5 and 20 DPM/g, counting time 80,000 seconds and sample weights ranging from 9 to 32 grams. Method uncertainty can increase to 85% for samples with activities near detection limit (0.1 - 0.3 DPM/g).

Results authorized by Dr. Robert J. Flett, Chief Scientist

Section Number	LAB ID	Sample ID	Upper Depth (cm) Provided by client	Lower Depth (cm) Provided by client	Weight of Sample Counted (g)	Sample Thickness (mm)	Count Time (sec)	Integral NET Cs-137 Peak Area (Counts)	Cs-137 Counting Error 1 SD (Counts)	Efficiency for Gammas Fractional	Cs-137 Activity DPM/g (dry wt.) on Counting Date	Counting Error ± 1 S.D. (DPM/g Dry Wt.)	Detector Used	Comments Code
10	112627	C9-10	9.0	10.0	27.364	6.800	80000	49	53	0.0261	0.06	0.07	GMX	<2SD
15	112632	C14-15	14.0	15.0	20.482	5.425	160000	45	47	0.0239	0.04	0.04	GEM	<2SD
23	112640	C24-26	24.0	26.0	22.135	5.600	80000	-41	50	0.0270	-0.06	0.07	GMX	<2SD
27	112644	C32-34	32.0	34.0	27.232	6.750	80000	-22	35	0.0230	-0.03	0.05	GEM	<2SD
32	112649	C45-50	45.0	50.0	20.021	5.300	80000	8	34	0.0240	0.01	0.06	GEM	<2SD

Efficiency Data

NBS Clay Calibration Standard	Weight (g)	Thickness (mm)	Count Time (sec)	Efficiency for Gammas Fractional Jan 9-23
GMX 32g 10 mm	32.00	10	5000	0.0237
GMX 24g 7.5mm	24.00	7.5	5000	0.0254
GMX 15g 5mm	15.00	5.0	5000	0.0276
GMX 9g 3mm	9.00	3.0	5000	0.0291
GMX 2.85g 0.8mm	2.854	0.8	10000	0.0306
GEM 32g 10 mm	32.00	10	5000	0.0205
GEM 24g 7.5mm	24.00	7.5	5000	0.0222
GEM 15g 5mm	15.00	5	5000	0.0243
GEM 9g 3mm	9.00	3	5000	0.0256
GEM 2.85g 0.8mm	2.854	0.8	10000	0.0269

Q:\Clients A-L\Juang, Alicia - ESA\2022(1033)\Radioisotopes\C\Pb-210, Ra-226 and Cs-137 Juang Core C May 25-23 Final.xlsm

Note: Results relate only to the samples tested and as received. Sample depths are provided by the client.

Cs-137: ISO / IEC 17025:2017 Accredited with the Canadian Association for Laboratory Accreditation (CALA Accreditation No. A3306)

Cs-137 in Sediments

Core C

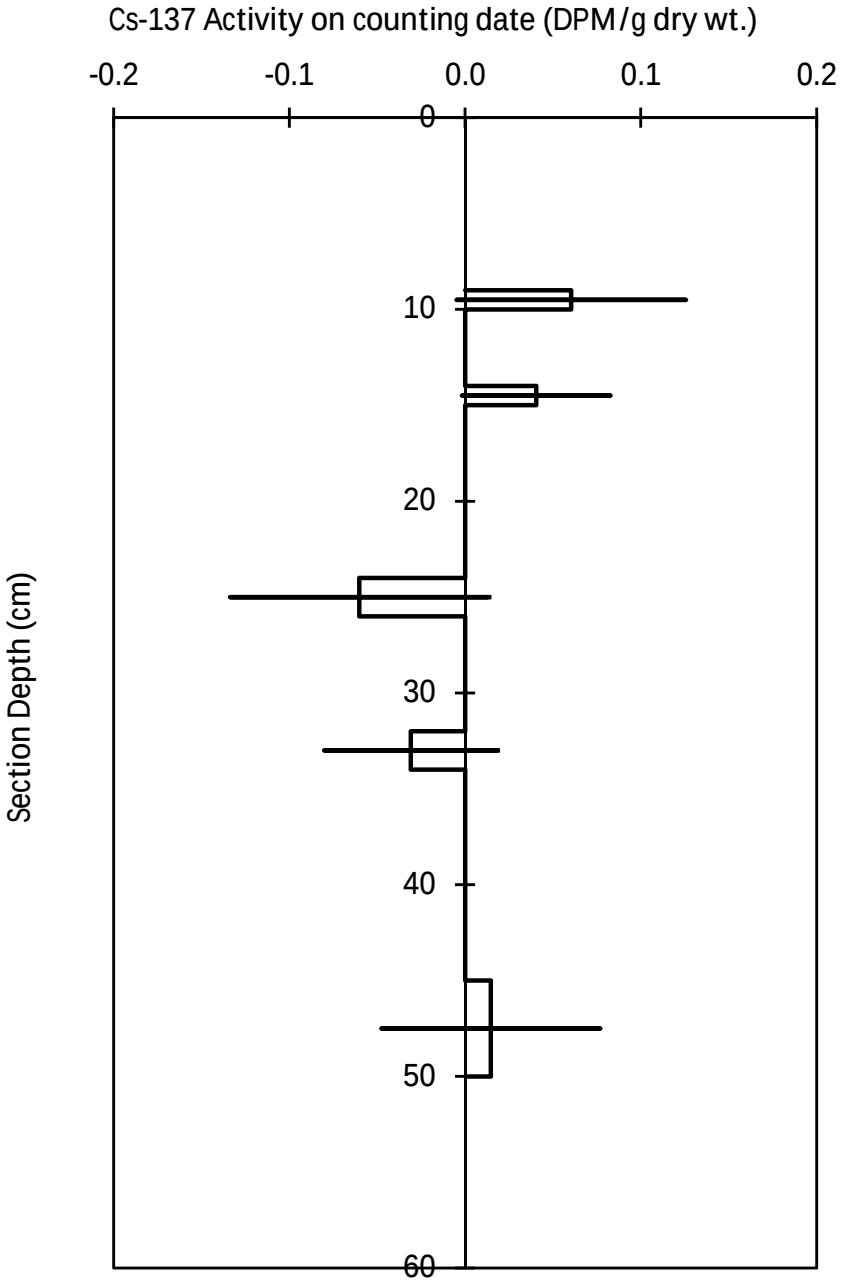

Note: The bar plotted at the midpoint depth of each section represents +/- 1 standard deviation of the Cs-137 counting error.

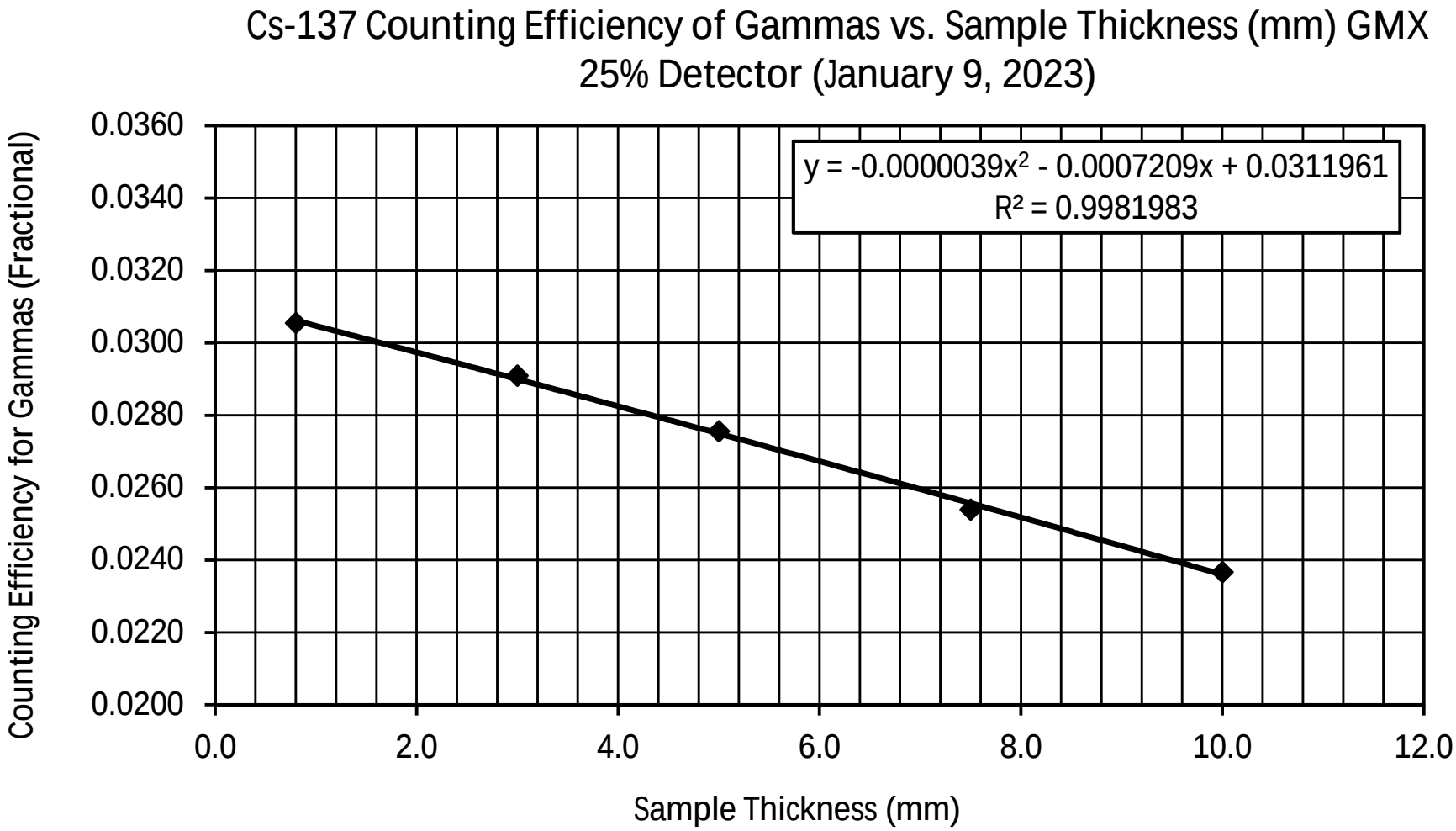
Cs-137 Counting Efficiency of Gammas vs. Sample Thickness (mm) GMX 25% Detector (January 9, 2023)
y = -0.0000039x2 - 0.0007209x + 0.0311961
R2 = 0.9981983
Counting Efficiency for Gammas (Fractional)
0.0360
0.0340
0.0320
0.0300
0.0280
0.0260
0.0240
0.0220
0.0200
0.0
2.0
4.0
6.0
8.0
10.0
12.0
Sample Thickness (mm)

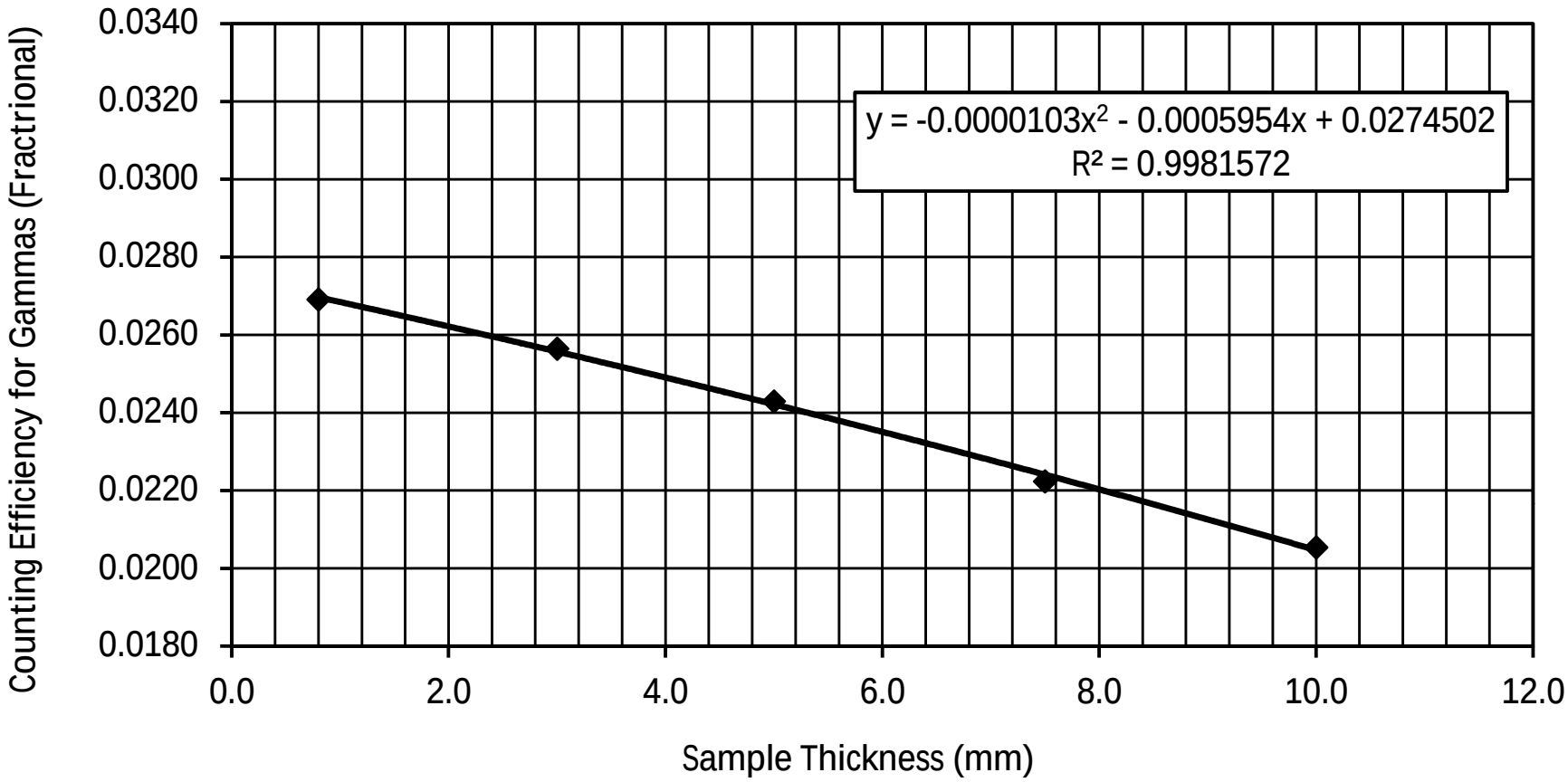
Cs-137 Counting Efficiency of Gammas vs. Sample Thickness (mm) GEM 19% Detector (January 9, 2023)
y = -0.0000103x² - 0.0005954x + 0.0274502
R² = 0.9981572
Counting Efficiency for Gammas (Fractrional)
0.0340
0.0320
0.0300
0.0280
0.0260
0.0240
0.0220
0.0200
0.0180
0.0
2.0
4.0
6.0
8.0
10.0
12.0
Sample Thickness (mm)

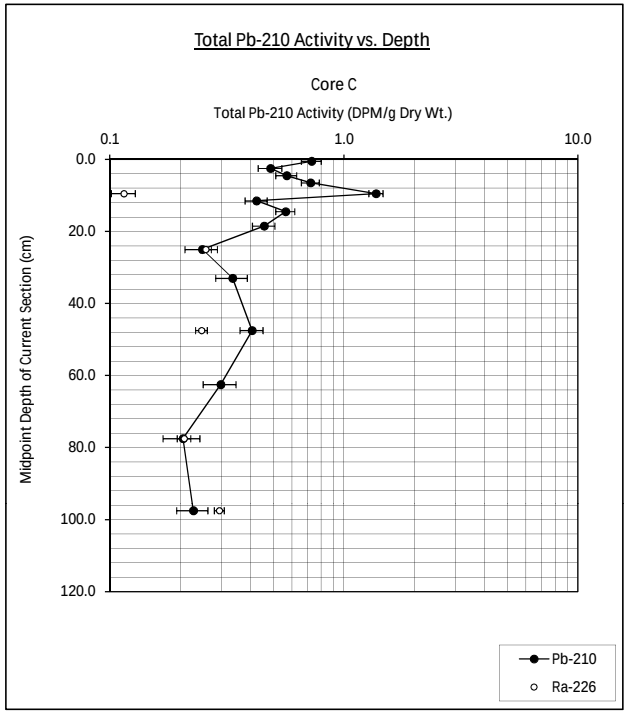
Total Pb-210 Activity vs. Depth
Core C
Total Pb-210 Activity (DPM/g Dry Wt.)
0.1
1.0
10.0
0.0
20.0
40.0
60.0
80.0
100.0
120.0
Midpoint Depth of Current Section (cm)
Pb-210
Ra-226

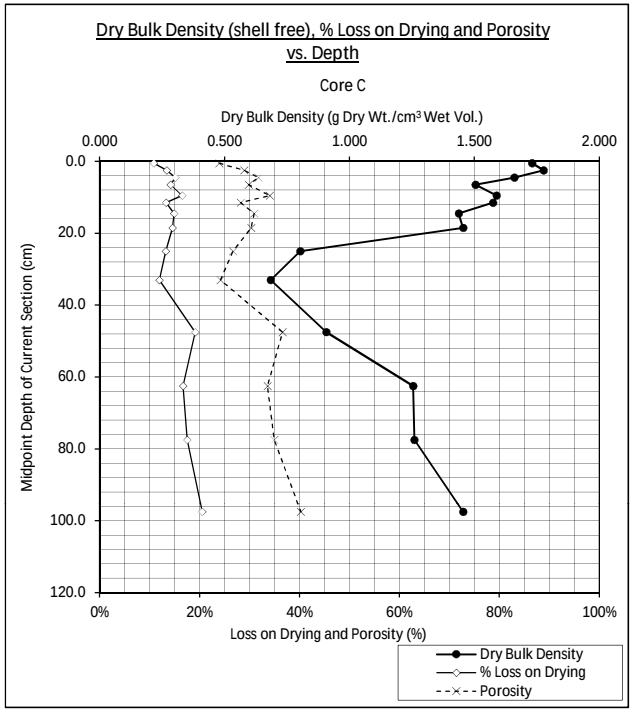
Dry Bulk Density (shell free), % Loss on Drying and Porosity vs. Depth
Core C
Dry Bulk Density (g Dry Wt./cm³ Wet Vol.)
0.000
0.500
1.000
1.500
2.000
0.0
20.0
40.0
60.0
80.0
100.0
120.0
Midpoint Depth of Current Section (cm)
0%
20%
40%
60%
80%
100%
Loss on Drying and Porosity (%)
Dry Bulk Density
% Loss on Drying
Porosity

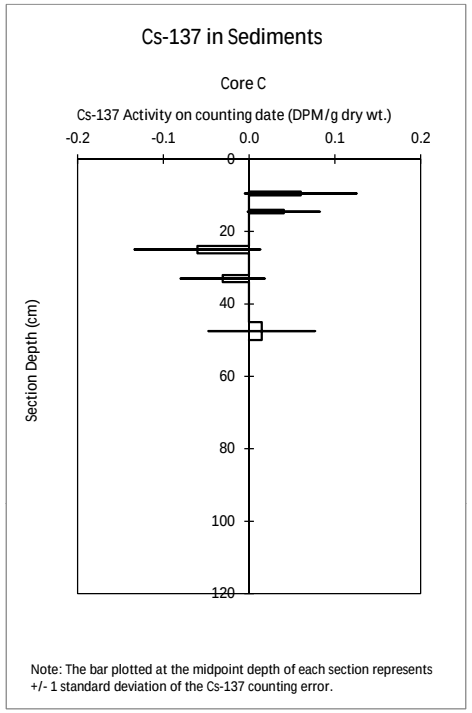
Cs-137 in Sediments
Core C
Cs-137 Activity on counting date (DPM/g dry wt.)
-0.2
-0.1
0.0
0.1
0.2
0
20
40
60
80
100
120
Section Depth (cm)
Note: The bar plotted at the midpoint depth of each section represents +/- 1 standard deviation of the Cs-137 counting error.

Core C Supplementary Calculations

Supplementary Calculations - July 25, 2023

Flett Research Ltd.

440 DeSalaberry Ave. Winnipeg, MB R2L 0Y7

Fax/Phone: (204) 667-2505

Email: flett@flettresearch.ca Webpage: http://www.flettresearch.ca

Client: Juang, Alicia

Address:	180 Grand Ave, Suite 1050, Oakland, CA 94610, USA
Transaction ID:	1033
Project:	San Diego Eelgrass Blue Carbon
Core ID:	**Core C**
Matrix:	Sediment
PO/Contract No.:	TOE Oct 20-22
Sampling Date:	25-Oct-22
Date Received:	8-Nov-22
Analysis Dates:	November 23 - April 13, 2023
Analysts:	L. Hesketh-Jost; X. Hu
Date Issued:	25-Jul-23

Results authorized by Dr. Robert J. Flett, Chief Scientist

INTERPRETATION

CRS model of Age at bottom of Extrapolated section in years vs. Depth of bottom edge of current section in cm:

The CRS model assumes constant input of Pb-210 and a core that is long enough to include all of the measurable atmospheric source Pb-210, i.e. it contains a complete Pb-210 inventory. If one assumes that the Pb-210 activity in section 38 (0.21 DPM/g, C75-80, extrapolated depth 70 - 87.5 cm) is at the background Pb-210 level, the model can be applied. However, in section 23 (C24-26, extrapolated depth 21.5 - 29 cm), the unsupported Pb-210 activity is zero. In order to apply the CRS model, an artificial unsupported Pb-210 activity of 0.05 DPM/g is assigned to this section 23.

The estimated age at the bottom of each section is shown in column AB (Page 2, worksheet 'Modeling'). The average sediment accumulation rate, from core surface to the extrapolated bottom depth of any section, can be calculated by dividing the cumulative dry mass at the bottom of the extrapolated section by the calculated age at that depth. For example, the average sediment accumulation rate, from the core surface to the bottom of section 32 (C45-50, extrapolated depth 55 cm) can be calculated as: 60.727 / 100.2 = 0.6061 g/cm^2/yr. The individual sediment accumulation rate for each section is shown in column AC on Page 2. Plots of age vs. depth, sediment accumulation rate vs. depth and sediment accumulation rate vs. age are seen in Pages s6, s7 and s8, respectively.

Conclusion:

It is unclear that whether or not dredging and/or disposal events occurred at this coring site. The low unsupported Pb-210 activity and Cs-137 activity may be due to hydrodynamic activity which strips the sediment of organic matter for which Pb-210 and Cs-137 have an affinity. Detectable atmospheric sourced Pb-210 was found in the upper 21.5 cm (extrapolated depth) of this core and indicates that these sediments are likely modern (i.e. < 50 yrs old).

It appears that sandy sediments have diluted the atmospheric sourced Pb-210 in core interval of 21.5 - 39.5 cm (extrapolated depth). The CRS model predicts that these sediments were rapidly deposited. This rapid deposit of sandy sediments, which contain little atmospheric sourced Pb-210, would result in the Pb-210 profile observed on Page s3 over the 21.5 - 39.5 cm (extrapolated depth) core interval.

The average sediment accumulation rate (in mm/yr), from core surface to the extrapolated bottom depth of section 32 (C45-50, extrapolated depth 55 cm), can be calculated by dividing the depth at the bottom of the extrapolated section by the calculated age at that depth. For example, it can be calculated as: 55 (cm) / 100.2 (yr) = 0.55 (cm/yr).

It is cautioned that the uncertainty of predicted ages in this core is high and the ages are gross approximations only, due to the relatively low activities and irregular shape of Pb-210 profile.

Calculation of Sediment Accumulation Rates and Ages

Flett Research Ltd.

440 DeSalaberry Ave. Winnipeg, MB R2L 0Y7

Fax/Phone (204) 667-2505

E-mail: flett@flettresearch.ca Webpage: http://www.flettresearch.ca

Client: Juang, Alicia

Address: 180 Grand Ave, Suite 1050, Oakland, CA 94610, USA

Core ID: Core C

Date Received: 8-Nov-22

Sampling Date: 25-Oct-22

Date Issued: 25-Jul-23

Matrix: Sediment

Transaction ID: 1033

PO/Contract No.: TOE Oct 20-22

Pb-210, Ra-226 and dry bulk density results as reported on other sheets within this workbook are summarized in the table below and are used to estimate accumulation rates and ages for the core. Two models are available for these calculations: the Constant Rate of Supply (CRS) model and the Linear Regression Model.

In order to date a sediment core, we need to determine the atmospheric sourced Pb-210 (= unsupported Pb-210) that is in 10+ sediment core sections. We analyze the sediment for TOTAL Pb-210 which includes both unsupported Pb-210 AND Pb-210 also being produced by decay of natural Ra-226 in the sediment. Due to secular equilibrium of Ra-226/Pb-210, sediment derived Pb-210 is expected to have the same activity as the Ra-226 and therefore we estimate the sediment sourced Pb-210 (=supported Pb-210) by using radon emanation to determine the Ra-226 in 3+ sections of the core. This allows the required calculation: unsupported Pb-210 = Total Pb-210 – supported Pb-210.

Results Authorized by Dr. Robert J. Flett, Chief Scientist

Section Number	Sample ID	Upper Depth (cm) Provided by client	Lower Depth (cm) Provided by client	Extrapolated Upper Section Depth (cm)	Extrapolated Lower Section Depth (cm)	Dry Bulk Density (Dry wt./Wet vol.) (g/cm3)	Midpoint Depth of Current Section (cm) Not Used	Mass in Extrapolated Section (g/cm2)	Cumulative Mass to Bottom of Current Section (g/cm2)	Plot-point of Cumulative Mass in Current Section (g/cm2)	Pb-210 Total Activity (DPM/g Dry Wt.)	Pb-210 COUNTING Error ± 1 S.D. (DPM/g Dry Wt.)	Pb-210 Background Activity from measured Ra-226 (DPM/g Dry Wt.)	Ra-226 Combined Error ± 1 S.D. (DPM/g Dry Wt.)	Estimated Pb-210 Background Activity from nearest neighbouring Ra-226 (DPM/g Dry Wt.)	Pb-210 Unsupported Activity (DPM/g Dry Wt.)	Pb-210 Unsupported Activity (DPM/cm^2) in each section	Age at Bottom of Extrapolated Section in Years (CRS Model Estimate)	CRS Sediment Accumulation Rate (g/cm^2/yr)	Age at Bottom of Extrapolated Section in Years (Linear Regression Model Estimate)
1	C0-1	0.0	1.0	0.00	1.50	1.731	0.5	2.597	2.597	0.866	0.73	0.07			0.11	0.61	1.593	2.4	1.0636	
3	C2-3	2.0	3.0	1.50	3.50	1.777	2.5	3.555	6.151	4.374	0.49	0.06			0.11	0.37	1.320	4.6	1.6357	
5	C4-5	4.0	5.0	3.50	5.50	1.660	4.5	3.320	9.471	7.811	0.57	0.06			0.11	0.46	1.512	7.3	1.2372	
7	C6-7	6.0	7.0	5.50	8.00	1.505	6.5	3.762	13.234	10.976	0.72	0.06			0.11	0.61	2.281	11.8	0.8309	
10	C9-10	9.0	10.0	8.00	10.50	1.589	9.5	3.972	17.206	15.617	1.37	0.10	0.11	0.01		1.26	4.998	24.8	0.3070	
12	C11-12	11.0	12.0	10.50	13.00	1.575	11.5	3.937	21.143	18.781	0.42	0.05			0.11	0.31	1.215	28.9	0.9543	
15	C14-15	14.0	15.0	13.00	16.50	1.437	14.5	5.031	26.174	23.299	0.56	0.05			0.11	0.45	2.260	38.3	0.5326	
19	C18-19	18.0	19.0	16.50	21.50	1.455	18.5	7.276	33.450	29.084	0.46	0.05			0.11	0.34	2.487	53.5	0.4803	
23	C24-26	24.0	26.0	21.50	29.00	0.803	25.0	6.022	39.473	36.261	0.25	0.04	0.26	0.01		0.05	0.301	55.9	2.4755	
27	C32-34	32.0	34.0	29.00	39.50	0.685	33.0	7.189	46.661	42.211	0.33	0.05			0.25	0.09	0.634	61.7	1.2353	
32&32Dup	C45-50	45.0	50.0	39.50	55.00	0.907	47.5	14.065	60.727	53.921	0.41	0.05	0.25	0.01		0.16	2.231	100.2	0.3657	
35	C60-65	60.0	65.0	55.00	70.00	1.255	62.5	18.823	79.550	70.138	0.30	0.05			0.25	0.05	0.968			
38	C75-80	75.0	80.0	70.00	87.50	1.260	77.5	22.046	101.595	88.998	0.21	0.04	0.21	0.01		0.00	0.000			
42	C95-100	95.0	100.0	87.50	100.00	1.455	97.5	18.189	119.784	116.147	0.23	0.03	0.29	0.01						

Note: These modeling results are gross approximations only.

Z:\Shared\Projects\2018\D180121.02 - Eelgrass Blue Carbon Study\03 Working Documents\Y2_Task06 - Sampling\Lab data RAW\Flett\Supplementary Calculations_Juang_Core C_Jul 25-23.xlsm

Dup (Duplicate): Two subsamples of the same sample were carried through the analytical procedure in an identical manner.

Sample depths are provided by the client. Errors in that data may affect the validity of sediment accumulation rates, Pb-210 inventory and age calculations.

Note: Results relate only to the items tested and as received.

Total Pb-210 Activity vs. Accumulated Mass

Core C

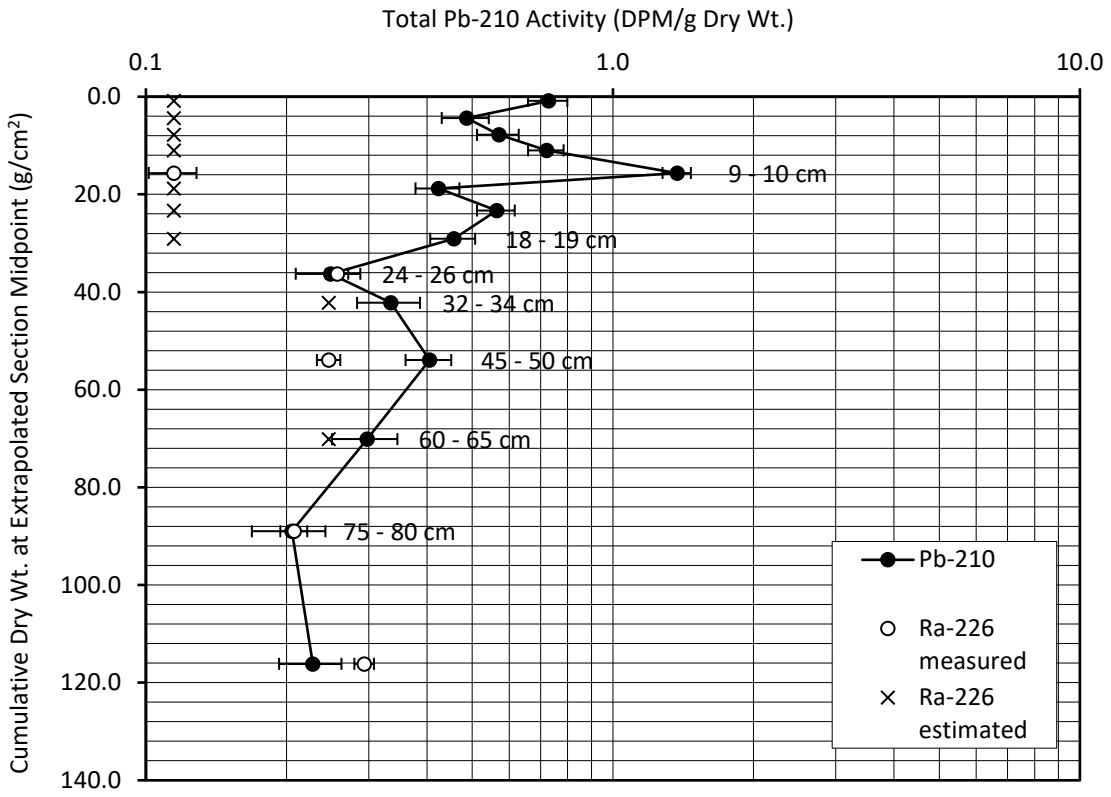

Unsupported Pb-210 Activity vs. Accumulated Mass

Core C

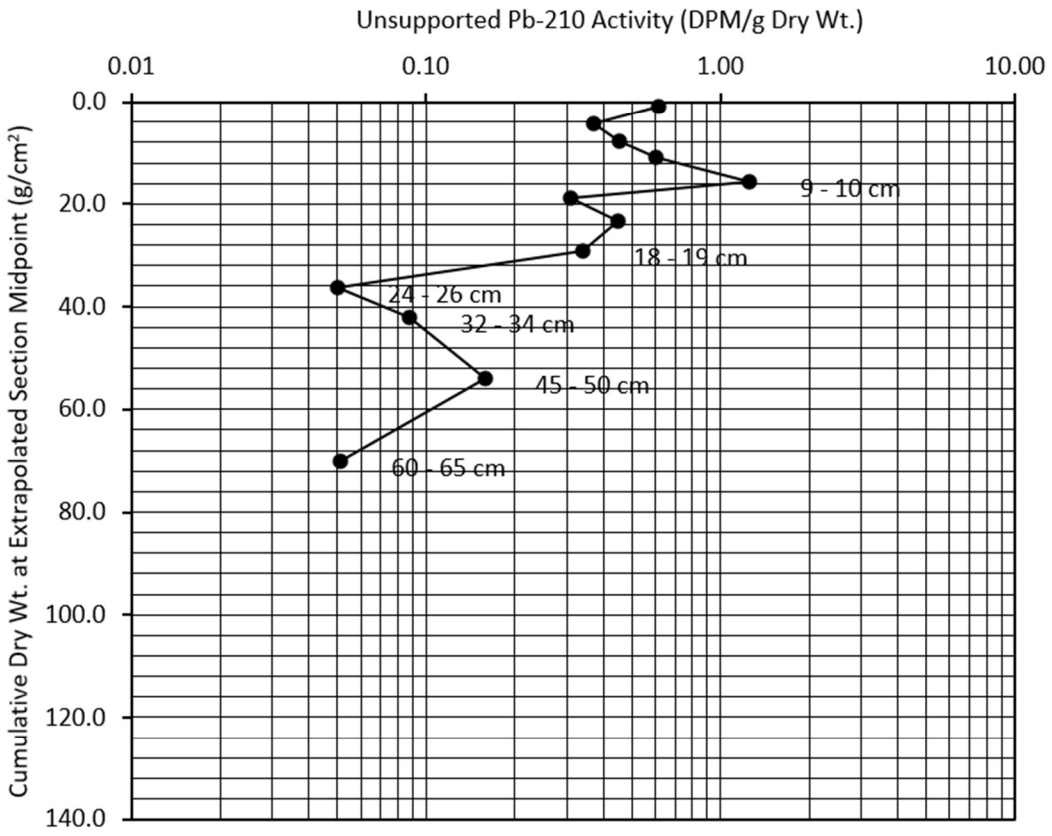

Z:\Shared\Projects\2018\D180121.02 - Eelgrass Blue Carbon Study\03 Working Documents\Y2_Task06 - Sampling\Lab data RAW\Flett\Supplementary Calculations_Juang_Core C_Jul 25-23.xlsm

Dry Bulk Density vs. Accumulated Mass

Core C

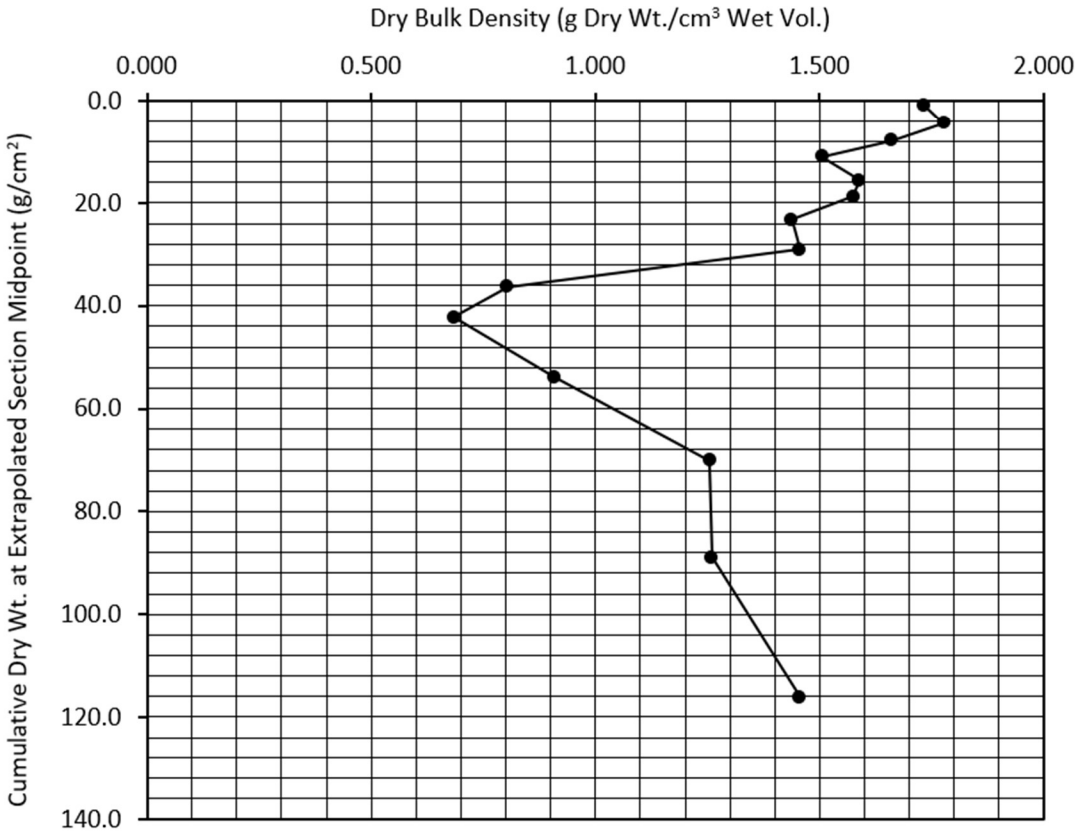

Z:\Shared\Projects\2018\D180121.02 - Eelgrass Blue Carbon Study\03 Working Documents\Y2_Task06 - Sampling\Lab data RAW\Flett\Supplementary Calculations_Juang_Core C_Jul 25-23.xlsm

Age (yr) vs. Depth (cm)
CRS Model

Gross approximations only.

Core C

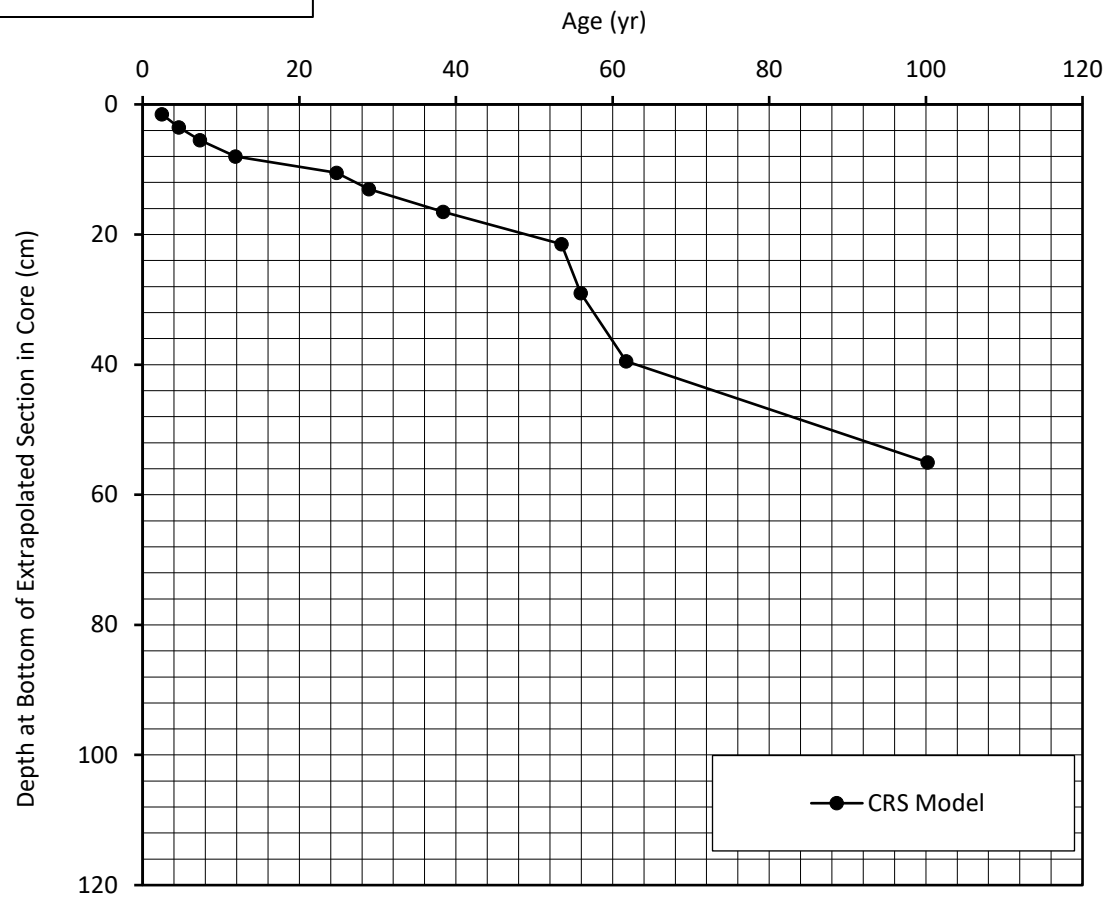

Z:\Shared\Projects\2018\D180121.02 - Eelgrass Blue Carbon Study\03 Working Documents\Y2_Task06 - Sampling\Lab data RAW\Flett\Supplementary Calculations_Juang_Core C_Jul 25-23.xlsm

CRS Sediment Accumulation Rate (g/cm²/year) vs. Depth at the Bottom of Extrapolated Section in Core (cm)

Gross approximations only.

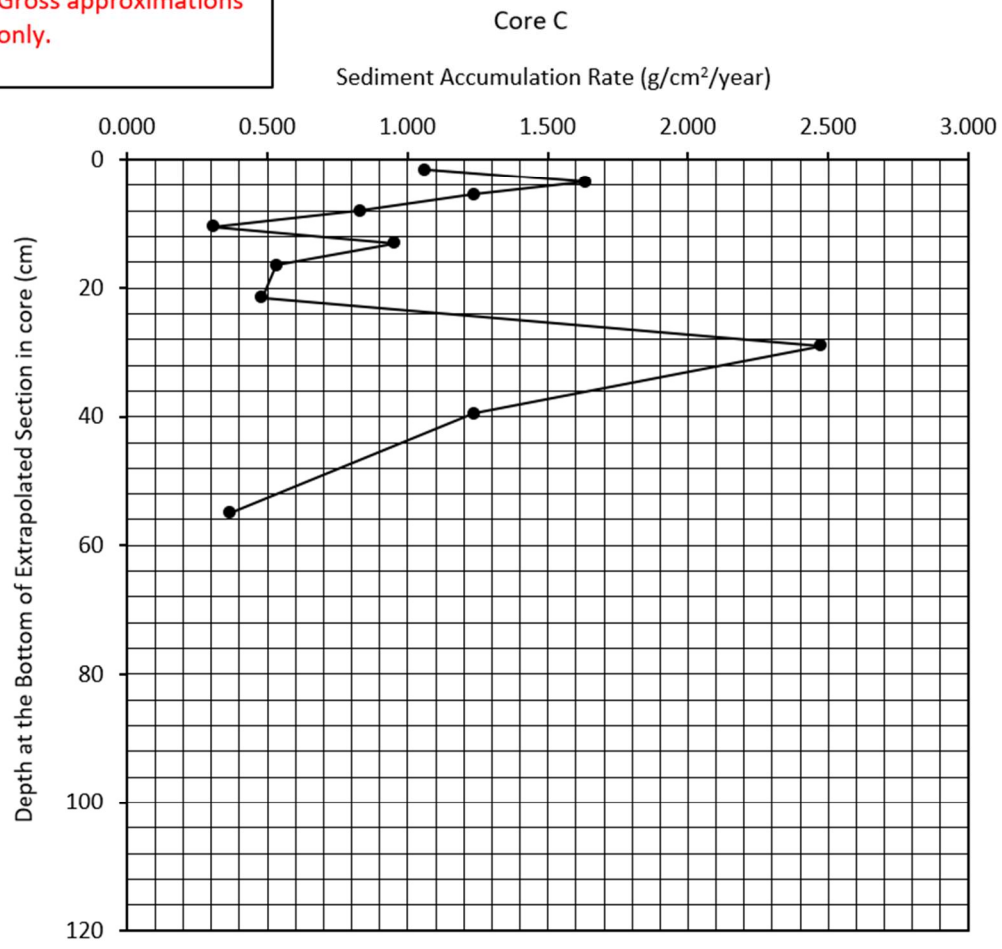

Z:\Shared\Projects\2018\D180121.02 - Eelgrass Blue Carbon Study\03 Working Documents\Y2_Task06 - Sampling\Lab data RAW\Flett\Supplementary Calculations_Juang_Core C_Jul 25-23.xlsm

CRS Sediment Accumulation Rate (g/cm²/year) vs. Age at Bottom of Extrapolated Section (yr)

Gross approximations only.

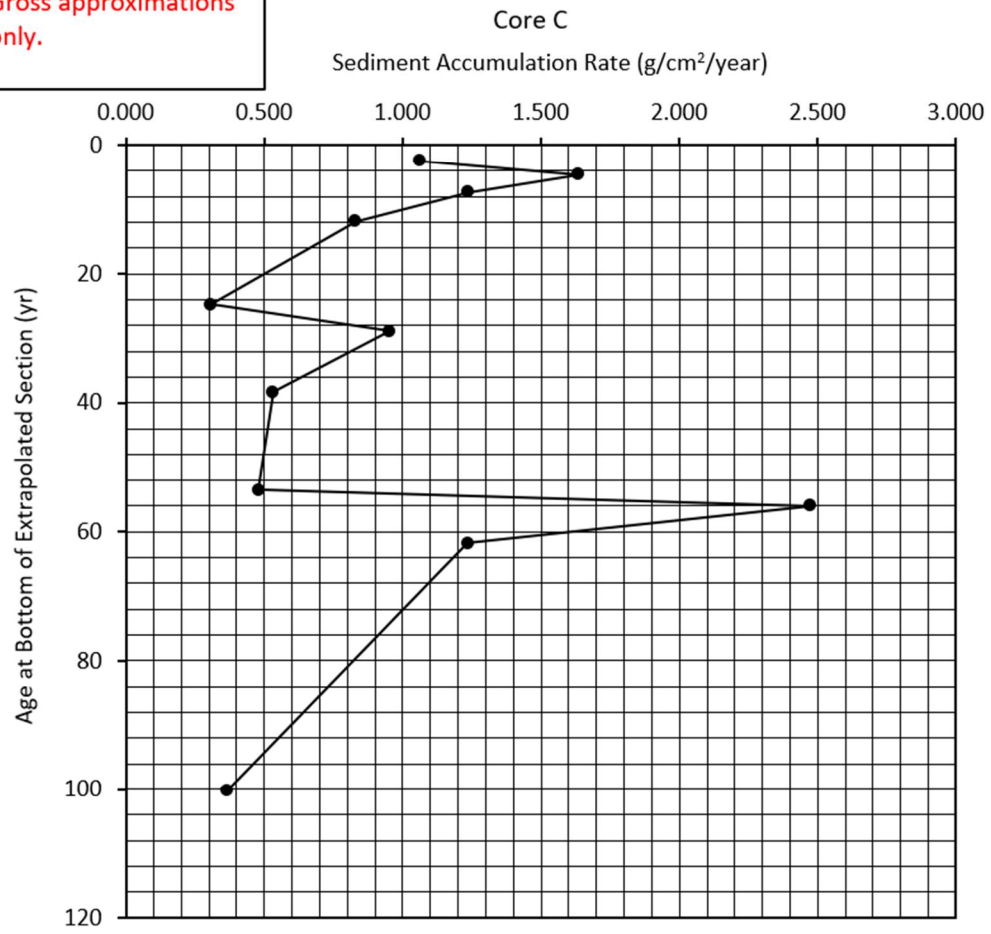

Z:\Shared\Projects\2018\D180121.02 - Eelgrass Blue Carbon Study\03 Working Documents\Y2_Task06 - Sampling\Lab data RAW\Flett\Supplementary Calculations_Juang_Core C_Jul 25-23.xlsm

Core F

Interpretation of Pb-210, Ra-226 and Cs-137 Results

Flett Research Ltd.
440 DeSalaberry Ave. Winnipeg, MB R2L 0Y7
Fax/Phone: (204) 667-2505
Email: flett@flettresearch.ca Webpage: http://www.flettresearch.ca

Client: Juang, Alicia

Address:	180 Grand Ave, Suite 1050, Oakland, CA 94610, USA
Transaction ID:	1033
Project:	San Diego Eelgrass Blue Carbon
Core ID:	Core F
Matrix:	Sediment
PO/Contract No.:	TOE Oct 20-22
Sampling Date:	24-Oct-22
Date Received:	8-Nov-22
Analysis Dates:	November 18, 2022 - March 14, 2023
Analysts:	L. Hesketh-Jost; X. Hu
Date Issued:	13-Apr-23

Results authorized by Dr. Robert J. Flett, Chief Scientist

INTERPRETATION

Observations:

A regular Pb-210 profile exhibits an exponential decrease in total Pb-210 activity as a function of depth. In this core, the total Pb-210 activities are low, varying between 0.71 - 1.11 DPM/g, and the Pb-210 profile is nearly vertical (Pages 2, 3 & 7).

In the upper 21.5 cm (extrapolated depth), the dry bulk densities vary between 0.935 - 1.225 g/cm^3. Below 21.5 cm (extrapolated depth), the dry bulk densities vary between 0.823 - 0.971 g/cm^3 (Pages 2, 5 & 6).

Ra-226 was measured at 0.62, 0.70, 0.72, 0.76 and 1.09 DPM/g in section 10, section 23, section 32, section 36 and section 42, respectively (Pages 2, 8-13). Those results are not significantly different (i.e. the difference is less than 3 standard deviations) than the Pb-210 activities measured in the same sections, indicating that detectable atmospheric sourced Pb-210 was not found in those five sections, and is unlikely to be found in any of the sections of this core.

The significant increase of Ra-226 activity observed in section 42 (depth 95 - 100 cm) suggests that the composition and the source of the sediment may be different than the rest of the core.

Cs-137 was measured in five sections in the core interval of 14 - 50 cm. No detectable Cs-137 was found (Pages 14 & 15).

Linear regression model of Unsupported Pb-210 activity vs. Cumulative Dry Weight (g/cm^2):

When applying the linear regression model, it is assumed that the input of Pb-210 and the sediment accumulation rate are constant. The model cannot be applied to this core, due to the lack of detectable unsupported Pb-210.

CRS model of Age at bottom of Extrapolated section in years vs. Depth of bottom edge of current section in cm:

The CRS model assumes constant input of Pb-210 and a core that is long enough to include all of the measurable atmospheric source Pb-210, i.e. it contains a complete Pb-210 inventory. The model cannot be applied to this core, due to the lack of detectable unsupported Pb-210.

Conclusion:

The low unsupported Pb-210 activity may be due to hydrodynamic activity which strips the sediment of organic matter for which Pb-210 and Cs-137 have an affinity. Thus, sediment accumulation could be occurring but atmospheric Pb-210 (i.e. Pb-210 in excess of that produced by the in-situ Ra-226) is not being incorporated. Due to the extremely low unsupported Pb-210 activities throughout the core, it is not possible to assign a reliable age to the sediment at any depth in the core.

If this sampling site had been dredged regularly before the sediment core was taken, then the average sediment accumulation rate (cm/yr) may be estimated by dividing the depth of sediments which was removed (cm) by the period of time between two adjacent dredging events (years), provided the dredging record is available.

Overall, the analytical quality of radioisotope data (based upon the recovery of spike, the results of repeat analyses, CRM and blanks) is considered good.

Calculation of Sediment Accumulation Rates and Ages

Flett Research Ltd.
440 DeSalaberry Ave. Winnipeg, MB R2L 0Y7
Fax/Phone (204) 667-2505
E-mail: flett@flettresearch.ca Webpage: http://www.flettresearch.ca

Client: Juang, Alicia

Address: 180 Grand Ave, Suite 1050, Oakland, CA 94610, USA
Core ID: Core F
Date Received: 8-Nov-22
Sampling Date: 24-Oct-22
Date Issued: 12-Apr-23

Matrix: Sediment
Transaction ID: 1033
PO/Contract No.: TOE Oct 20-22

Pb-210, Ra-226 and dry bulk density results as reported on other sheets within this workbook are summarized in the table below and are used to estimate accumulation rates and ages for the core. Two models are available for these calculations: the Constant Rate of Supply (CRS) model and the Linear Regression Model.

In order to date a sediment core, we need to determine the atmospheric sourced Pb-210 (= unsupported Pb-210) that is in 10+ sediment core sections. We analyze the sediment for TOTAL Pb-210 which includes both unsupported Pb-210 AND Pb-210 also being produced by decay of natural Ra-226 in the sediment. Due to secular equilibrium of Ra-226/Pb-210, sediment derived Pb-210 is expected to have the same activity as the Ra-226 and therefore we estimate the sediment sourced Pb-210 (=supported Pb-210) by using radon emanation to determine the Ra-226 in 3+ sections of the core. This allows the required calculation: unsupported Pb-210 = Total Pb-210 – supported Pb-210.

Results Authorized by Dr. Robert J. Flett, Chief Scientist

Section Number	Sample ID	Upper Depth (cm) Provided by client	Lower Depth (cm) Provided by client	Extrapolated Upper Section Depth (cm)	Extrapolated Lower Section Depth (cm)	Dry Bulk Density (Dry wt./Wet vol.) (g/cm3)	Midpoint Depth of Current Section (cm) Not Used	Mass in Extrapolated Section (g/cm2)	Cumulative Mass to Bottom of Current Section (g/cm2)	Plot-point of Cumulative Mass in Current Section (g/cm2)	Pb-210 Total Activity (DPM/g Dry Wt.)	Pb-210 COUNTING Error ± 1 S.D. (DPM/g Dry Wt.)	Pb-210 Background Activity from measured Ra-226 (DPM/g Dry Wt.)	Ra-226 Combined Error ± 1 S.D. (DPM/g Dry Wt.)	Estimated Pb-210 Background Activity from nearest neighbouring Ra-226 (DPM/g Dry Wt.)	Pb-210 Unsupported Activity (DPM/g Dry Wt.)	Pb-210 Unsupported Activity (DPM/cm^2) in each section	Age at Bottom of Extrapolated Section in Years (CRS Model Estimate)	CRS Sediment Accumulation Rate ($g/cm^2/yr$)	Age at Bottom of Extrapolated Section in Years (Linear Regression Model Estimate)
1	F0-1	0.0	1.0	0.00	2.50	1.025		2.563	2.563	0.513	0.79	0.08			0.62	0.17	not sig.			
5	F4-5	4.0	5.0	2.50	7.00	1.225		5.512	8.076	5.013	0.81	0.09			0.62	0.19	not sig.			
10	F9-10	9.0	10.0	7.00	12.00	1.010		5.050	13.126	10.601	0.77	0.09	0.62	0.02		0.15	not sig.			
15&15Dup	F14-15	14.0	15.0	12.00	16.50	0.935		4.207	17.332	15.463	0.86	0.10			0.62	0.23	not sig.			
19	F18-19	18.0	19.0	16.50	21.50	1.093		5.464	22.796	19.518	0.82	0.08			0.70	0.12	not sig.			
23	F24-26	24.0	26.0	21.50	27.00	0.841		4.623	27.419	25.738	0.99	0.12	0.70	0.02		0.29	not sig.			
25	F28-30	28.0	30.0	27.00	31.00	0.941		3.764	31.184	29.301	0.77	0.09			0.70	0.07	not sig.			
27	F32-34	32.0	34.0	31.00	35.00	0.868		3.473	34.657	32.920	0.82	0.08			0.70	0.12	not sig.			
29	F36-38	36.0	38.0	35.00	41.50	0.971		6.312	40.969	36.599	0.83	0.08			0.72	0.11	not sig.			
32	F45-50	45.0	50.0	41.50	52.50	0.833		9.162	50.131	45.966	0.71	0.10	0.72	0.02		*0.00*	not sig.			
34	F55-60	55.0	60.0	52.50	62.50	0.823		8.227	58.358	54.244	0.91	0.09			0.72	0.19	not sig.			
36	F65-70	65.0	70.0	62.50	75.00	0.898		11.224	69.582	62.847	0.94	0.09	0.76	0.02		0.18	not sig.			
39	F80-85	80.0	85.0	75.00	90.00	0.884		13.258	82.839	76.210	1.10	0.10			1.09	*0.00*	not sig.			
42	F95-100	95.0	100.0	90.00	100.00	0.842		8.423	91.262	89.156	1.11	0.13	1.09	0.02		0.02	not sig.			

Q:\Clients A-L\Juang, Alicia - ESA\2022(1033)\Radioisotopes\F\Pb-210, Ra-226 and Cs-137 Juang Core F Apr 13-23 Final.xlsm

Dup (Duplicate): Two subsamples of the same sample were carried through the analytical procedure in an identical manner.

 Sample depths are provided by the client. Errors in that data may affect the validity of sediment accumulation rates, Pb-210 inventory and age calculations.
Note: Results relate only to the items tested and as received.

Total Pb-210 Activity vs. Accumulated Mass

Core F

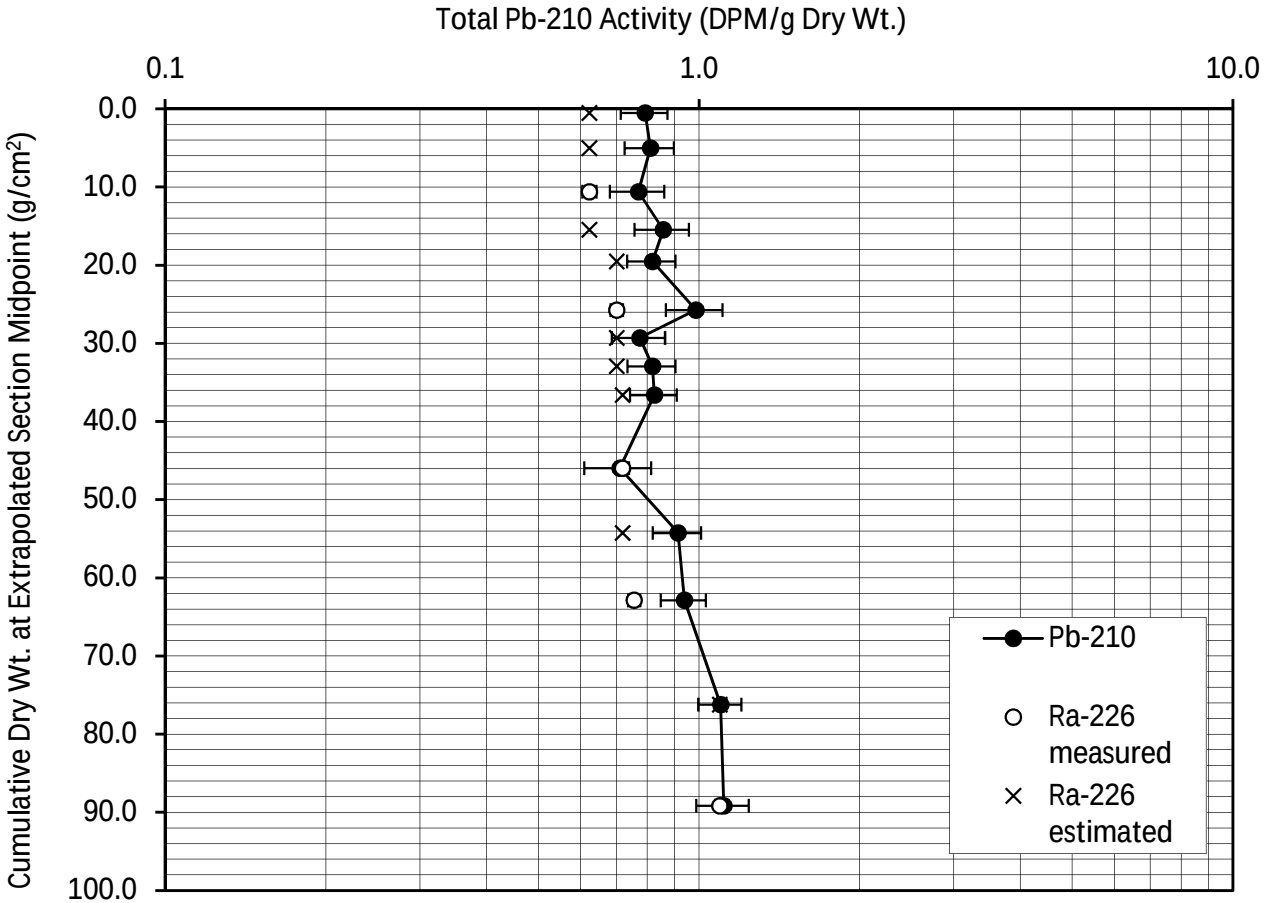

Q:\Clients A-L\Juang, Alicia - ESA\2022(1033)\Radioisotopes\F\Pb-210, Ra-226 and Cs-137 Juang Core F Apr 13-23 Final.xlsm

Unsupported Pb-210 Activity vs. Accumulated Mass

Core F

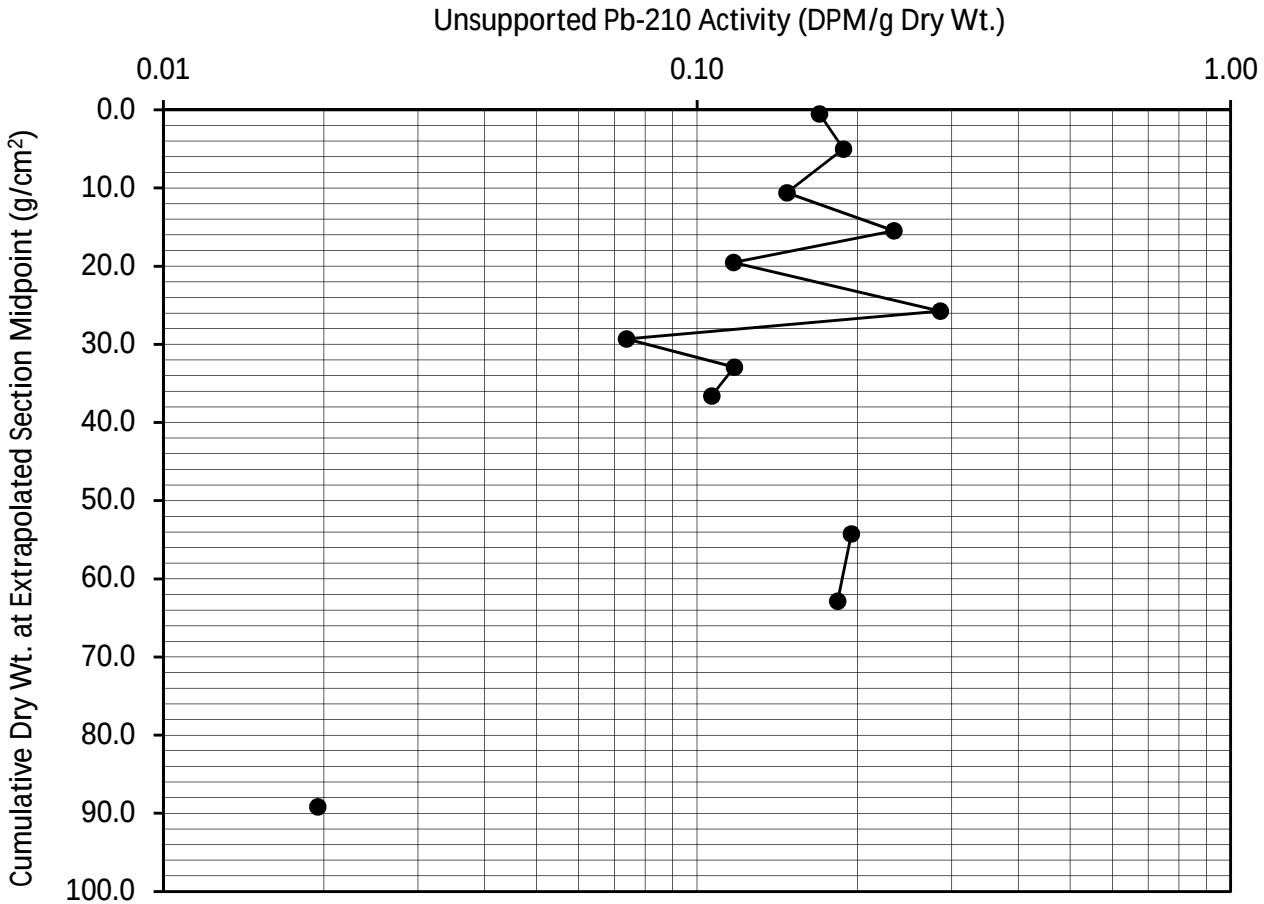

Dry Bulk Density vs. Accumulated Mass

Core F

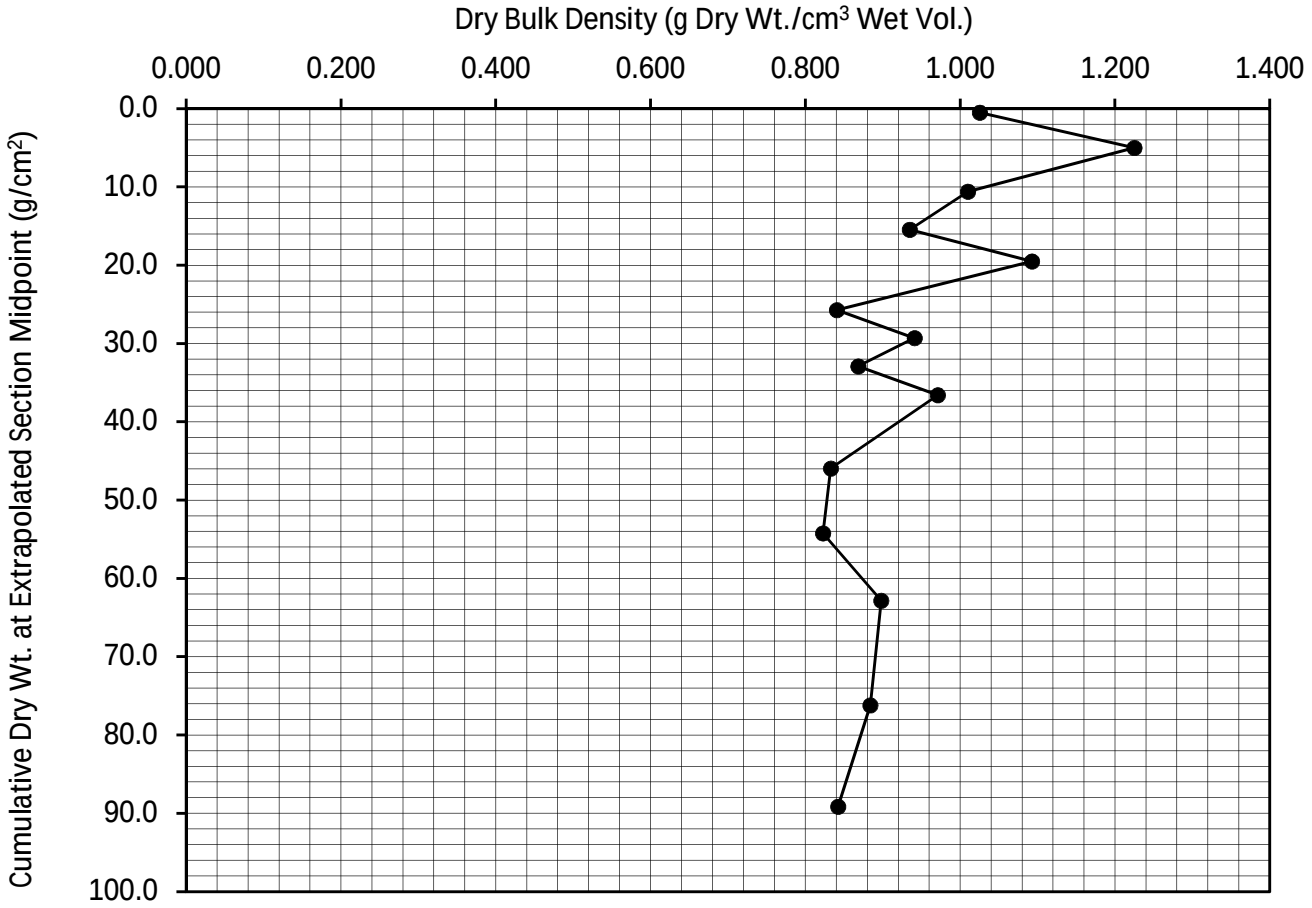

Q:\Clients A-L\Juang, Alicia - ESA\2022(1033)\Radioisotopes\F\Pb-210, Ra-226 and Cs-137 Juang Core F Apr 13-23 Final.xlsm

Dry Bulk Density, Percent Loss on Drying and Porosity

Flett Research Ltd.

440 DeSalaberry Ave. Winnipeg, MB R2L 0Y7

Fax/Phone: (204) 667-2505

E-mail: flett@flettresearch.ca Webpage: http://www.flettresearch.ca

Client: Juang, Alicia

Address: 180 Grand Ave, Suite 1050, Oakland, CA 94610, USA
Core ID: Core F
Date Received: November 8, 2022
Sampling Date: October 24, 2022
Date Issued: 12-Apr-23

Matrix: Sediment
Transaction ID: 1033
PO/Contract No.: TOE Oct 20-22
Analysis Dates: November 18, 2022 to February 27, 2023
Analyst: L. Hesketh-Jost

Analytical Method: N10020 Measurement of Dry Bulk Density and Other Sediment Characteristics (version 1)
Comments:

Estimated Uncertainty: For samples with %LOD less than 90%, the estimated uncertainty in laboratory measurements of dry bulk density has been determined to be less than 3%. When samples have a high water content (>90% LOD) uncertainty may increase to 8%. Method uncertainties are expressed at a 95% confidence level of (k=2).

Results authorized by Dr. Robert J. Flett, Chief Scientist

Section Number	LAB ID	Sample ID	Upper Depth (cm) Provided by client	Lower Depth (cm) Provided by client		Volume of wet sample (ml)	Weight of wet sample (g)	Weight of dry sample (g)		Dry Bulk Density (Dry wt./Wet vol.) (g/cm3)	% Loss on Drying	% Porosity
1	112534	F0-1	0.0	1.0		4.907	8.182	5.031		1.025	38.51%	64.21%
5	112538	F4-5	4.0	5.0		4.907	8.773	6.011		1.225	31.48%	56.29%
10	112543	F9-10	9.0	10.0		4.907	8.086	4.956		1.010	38.71%	63.79%
15&15Dup	112548	F14-15	14.0	15.0						0.935	41.46%	66.20%
19	112552	F18-19	18.0	19.0		4.907	8.358	5.362		1.093	35.85%	61.06%
23	112556	F24-26	24.0	26.0		4.907	7.533	4.125		0.841	45.24%	69.45%
25	112558	F28-30	28.0	30.0		4.907	7.900	4.618		0.941	41.54%	66.88%
27	112560	F32-34	32.0	34.0		4.907	7.628	4.261		0.868	44.14%	68.62%
29	112562	F36-38	36.0	38.0		4.907	7.973	4.765		0.971	40.24%	65.38%
32	112565	F45-50	45.0	50.0		4.907	7.613	4.087		0.833	46.32%	71.86%
34	112567	F55-60	55.0	60.0		4.907	7.477	4.037		0.823	46.01%	70.10%
36	112569	F65-70	65.0	70.0		4.907	7.698	4.406		0.898	42.76%	67.09%
39	112572	F80-85	80.0	85.0		4.907	7.742	4.337		0.884	43.98%	69.39%
42	112575	F95-100	95.0	100.0		4.907	7.552	4.133		0.842	45.27%	69.68%
Quality Control Samples												
15	112548	F14-15	14.0	15.0		4.907	7.859	4.610		0.939	41.34%	66.21%
15Dup	112548	F14-15 Duplicate	14.0	15.0		4.907	7.812	4.564		0.930	41.58%	66.19%

Dup : Duplicate - two subsamples of the same sample carried through the analytical procedure in an identical manner. Duplicate data is reported as a mean in the main data table.

Loss of water or sediment during collecting the core, sectioning of core, sub-sampling for analyses or storage and transportation, will bias the result of the dry bulk density. Sample depths are provided by the client. Errors in that data may affect the validity of sediment quality data.

Note: Results relate only to the samples tested and as received.

Results of Pb-210 by Po-210 analysis

Flett Research Ltd.
440 DeSalaberry Ave. Winnipeg, MB R2L 0Y7
Fax/Phone: (204) 667-2505
E-mail: flett@flettresearch.ca Webpage: http://www.flettresearch.ca

Client: Juang, Alicia

Address: 180 Grand Ave, Suite 1050, Oakland, CA 94610, USA
Core ID: Core F
Date Received: 8-Nov-22
Sampling Date: 24-Oct-22
Date Issued: 12-Apr-23

Matrix: Sediment
Transaction ID: 1033
PO/Contract No.: TOE Oct 20-22
Analysis Dates: 24-Nov-22 to 11-Mar-23
Analyst: L. Hesketh-Jost

Analytical Method: N20110 Determination of Lead-210 by Measurement of Po-210 in Sediment, Soil and Peat by Alpha Spectrometry (Version 6)
Comments:

Detection Limit: The method detection limit (MDL) for 0.25 - 0.5 g (dry wt.) sample is between 0.05 - 0.1 DPM Po-210/g dry sample at a 95% confidence level for 60,000 second counting time and is based on greater than 20 method blanks. This can vary slightly and depends upon the amount of sample, detector and recovery efficiency of each sample.

Estimated Uncertainty: As Po-210 (Pb-210) activity drops, error increases due to increasing counting error. When gross counts are less than 100 the dominant error becomes counting error which is equal to √gross counts/gross counts. When Po-210 (Pb-210) activity exceeds 5 DPM/g the method uncertainty is ± 11% . When activities are between 1 and 5 DPM/g, the method uncertainty is ± 17%. When activities are between 0.2 and 1 DPM/g, the method uncertainty is ± 25%. Uncertainties are expressed at 95% confidence level (k=2).

Results authorized by Dr. Robert J. Flett, Chief Scientist

Section Number	LAB ID	Sample ID	Upper Depth (cm) Provided by client	Lower Depth (cm) Provided by client	Po-209 Counts Less Detector Back-ground	Net Po-210 Counts [Gross counts Less Detector and Po-209 Spiking Solution Backgrounds]	Weight of Sample Counted (g)	Count Time (sec)	Po-210 Total Activity (DPM/g Dry Wt.)	Po-210 Counting Error ± 1 S.D. (DPM/g Dry Wt.)	Comments Code
1	112534	F0-1	0.0	1.0	2409	100	0.513	60000	0.79	0.08	
5	112538	F4-5	4.0	5.0	2101	90	0.518	60000	0.81	0.09	
10	112543	F9-10	9.0	10.0	1910	74	0.494	60000	0.77	0.09	
15&15Dup	112548	F14-15	14.0	15.0					0.86	0.10	
19	112552	F18-19	18.0	19.0	1851	94	0.605	60000	0.82	0.08	
23	112556	F24-26	24.0	26.0	1364	69	0.498	60000	0.99	0.12	
25	112558	F28-30	28.0	30.0	1864	77	0.520	60000	0.77	0.09	
27	112560	F32-34	32.0	34.0	2202	95	0.513	60000	0.82	0.08	
29	112562	F36-38	36.0	38.0	2175	102	0.553	60000	0.83	0.08	
32	112565	F45-50	45.0	50.0	1320	52	0.537	60000	0.71	0.10	
34	112567	F55-60	55.0	60.0	2058	94	0.487	60000	0.91	0.09	
36	112569	F65-70	65.0	70.0	1959	109	0.577	60000	0.94	0.09	
39	112572	F80-85	80.0	85.0	2040	119	0.517	60000	1.10	0.10	
42	112575	F95-100	95.0	100.0	1319	80	0.530	60000	1.11	0.13	

Quality Control Samples

Section Number	LAB ID	Sample ID			Po-209 Counts Less Detector Back-ground	Net Po-210 Counts	Weight of Sample Counted (g)	Count Time (sec)	Po-210 Total Activity (DPM/g)	Po-210 COUNTING Error +/- 1 S.D. (DPM/g)	CRM Recovery on Counting Date
RegBlk1		Reagent Blank w/o Po-209 spike			-3	3					
BLKwSpike1		Reagent Blank with Po-209 spike			2803	5					
RegBlk2		Reagent Blank w/o Po-209 spike			-7	2					
BLKwSpike2		Reagent Blank with Po-209 spike			3173	3					
15	112548	F14-15					0.521	60000	0.87	0.09	
15Dup	112548	F14-15 Duplicate					0.502	60000	0.84	0.11	
CRM1		IAEA447 (17.67 DPM/g)					0.340	60000	16.85	0.45	95.4%Rec
CRM2		IAEA447 (17.52 DPM/g)					0.363	60000	16.80	0.42	95.9%Rec

Q:\Clients A-L\Juang, Alicia - ESA\2022(1033)\Radioisotopes\F\Pb-210, Ra-226 and Cs-137 Juang Core F Apr 13-23 Final.xlsm

Dup (duplicate): Two subsamples of the same sample were carried through the analytical procedure in an identical manner.

Note: Results relate only to the samples tested and as received. Sample depths are provided by the client.
ISO / IEC 17025:2017 Accredited with the Canadian Association for Laboratory Accreditation (CALA Accreditation No. A3306)

Results of Ra-226 Analysis by Rn-222 Emanation

Flett Research Ltd.
440 DeSalaberry Ave., Winnipeg, MB R2L 0Y7
Fax/Phone: (204) 667-2505
Email: flett@flettresearch.ca Webpage: http://www.flettresearch.ca

Client: Juang, Alicia

Address: 180 Grand Ave, Suite 1050, Oakland, CA 94610, USA
Core ID: Core F
Date Received: 8-Nov-22
Sampling Date: 24-Oct-22
Date Issued: 12-Apr-23

Matrix: Sediment
Transaction ID: 1033
PO/Contract No.: TOE Oct 20-22
Analysis Dates: 22-Dec-22 to 14-Mar-23
Analyst: L. Hesketh-Jost & X. Hu

Analytical Method: N40110 Determination of Radium-226 in Sediment, Soil and Peat by Radon-222 Emanation (Version 4)

Comments:

Detection Limit: The method detection limit (MDL) is dependent on the amount of sample analyzed. For a 60,000 second counting time the MDL at 95% confidence for 2 g of dry sample is 0.1 DPM/g and for 0.5 g of dry sample is 0.5 DPM/g.

Estimated Uncertainty: The estimate of uncertainty of measurement for this method in this laboratory is approximately ±12% at 95% confidence level (approximately 40,000 counts in 60,000 seconds).

Results authorized by Dr. Robert J. Flett, Chief Scientist

Section Number	Lab ID	Sample ID	Upper Depth (cm) Provided by client	Lower Depth (cm) Provided by client	Weight of Sample Counted (g)	Count Time (sec)	Ra-226 Activity (DPM/g Dry Wt.)	Combined Error: 1 SD (DPM/g Dry Wt.)	Comments Code for Ra-226 Analysis
10	112543	F9-10	9	10	2.090	60000	0.62	0.02	
23	112556	F24-26	24	26	2.210	60000	0.70	0.02	
32	112565	F45-50	45	50	2.006	60000	0.72	0.02	
36	112569	F65-70	65	70	2.123	60000	0.76	0.02	
42	112575	F95-100	95	100	2.047	60000	1.09	0.02	

Q:\Clients A-L\Juang, Alicia - ESA\2022(1033)\Radioisotopes\F\Pb-210, Ra-226 and Cs-137 Juang Core F Apr 13-23 Final.xlsm

Note: Results relate only to the samples tested and as received. Sample depths are provided by the client.
ISO / IEC 17025:2017 Accredited with the Canadian Association for Laboratory Accreditation (CALA Accreditation No. A3306)

Radium Analysis by Rn-222 Emanation

Ra Sample Number:	2425
Section Number	10
Sample ID	F9-10
Core ID	Core F
Lucas Cell No.	3
Number of days since Rn board last run	1
Dry weight of sample counted (g)	2.090
Total count in period	3537
Total count in period (carryover corrected)	3496
Cell Blank count (CPM)	0.523
System Blank (DPM)	0.390
System Efficiency	0.804
Count duration (minutes)	1000

Typical carryover is about 1 - 2 % of the net counts (gross counts less system background) of the sample counted on the previous day. The carryover is subtracted from the gross counts of current sample. This correction is not required if the sample is run after a blank.

Carryover correction?	Yes		
Gross counts of previous sample	4637	Mean of last 10 carryover measurements	1.06%
Counts carried over from previous sample	41	Mean of last 6 system background measurements	795

	Year	Month	Day	Hour	Minute	Second	Ingrowth time (Days)	Ingrowth factor	Decay correction
When sample last stripped	2022	12	26	11	31	0	14.20	0.92374	0.92490
When cell filled	2023	1	9	16	21	26			
Beginning time of count	2023	1	9	18	21	49			

Counts per minute	3.50				
Gross CPM less Cell Blank (CPM)	2.97				
CPM (decay during count corrected)	3.21				
DPM Sample +System (efficiency corrected)	4.00				
DPM sample	3.91	Error ± 1 SD	0.1196	DPM	
DPM/g	1.87				
Ra-226 DPM/g	0.62	Error ± 1 SD	0.0191	DPM/g	Error % = 3.1
Ra-226 pCi/g	0.28				

Chemist	XH
PMT High Voltage +ve	770
HV Power supply	Spectrum Technologies
Alpha Counter	Spectrum Technologies
Region of Interest Ch.#s	28-1022
PMT	6655A - #1
Preamp	Canberra 2007P tube base
Amp Gain	1

Radium Analysis by Rn-222 Emanation

Ra Sample Number:	2426
Section Number	23
Sample ID	F24-26
Core ID	Core F
Lucas Cell No.	3
Number of days since Rn board last run	1
Dry weight of sample counted (g)	2.210
Total count in period	4075
Total count in period (carryover corrected)	4046
Cell Blank count (CPM)	0.523
System Blank (DPM)	0.390
System Efficiency	0.804
Count duration (minutes)	1000

Typical carryover is about 1 - 2 % of the net counts (gross counts less system background) of the sample counted on the previous day. The carryover is subtracted from the gross counts of current sample. This correction is not required if the sample is run after a blank.

Carryover correction?	Yes		
Gross counts of previous sample	3537	Mean of last 10 carryover measurements	1.06%
Counts carried over from previous sample	29	Mean of last 6 system background measurements	795

	Year	Month	Day	Hour	Minute	Second	Ingrowth time (Days)	Ingrowth factor	Decay correction
When sample last stripped	2022	12	26	11	30	0	15.13	0.93554	0.92490
When cell filled	2023	1	10	14	36	56			
Beginning time of count	2023	1	10	16	37	19			

Counts per minute	4.05				
Gross CPM less Cell Blank (CPM)	3.52				
CPM (decay during count corrected)	3.81				
DPM Sample +System (efficiency corrected)	4.74				
DPM sample	4.65	Error ± 1 SD	0.1237	DPM	
DPM/g	2.10				
Ra-226 DPM/g	0.70	Error ± 1 SD	0.0187	DPM/g	Error % = 2.7
Ra-226 pCi/g	0.32				

Chemist	XH
PMT High Voltage +ve	770
HV Power supply	Spectrum Technologies
Alpha Counter	Spectrum Technologies
Region of Interest Ch.#s	28-1022
PMT	6655A - #1
Preamp	Canberra 2007P tube base
Amp Gain	1

Radium Analysis by Rn-222 Emanation

Ra Sample Number:	2427
Section Number	42
Sample ID	F95-100
Core ID	Core F
Lucas Cell No.	3
Number of days since Rn board last run	1
Dry weight of sample counted (g)	2.047
Total count in period	5568
Total count in period (carryover corrected)	5533
Cell Blank count (CPM)	0.523
System Blank (DPM)	0.390
System Efficiency	0.804
Count duration (minutes)	1000

Typical carryover is about 1 - 2 % of the net counts (gross counts less system background) of the sample counted on the previous day. The carryover is subtracted from the gross counts of current sample. This correction is not required if the sample is run after a blank.

Carryover correction?	Yes		
Gross counts of previous sample	4075	Mean of last 10 carryover measurements	1.06%
Counts carried over from previous sample	35	Mean of last 6 system background measurements	795

	Year	Month	Day	Hour	Minute	Second	Ingrowth time (Days)	Ingrowth factor	Decay correction
When sample last stripped	2022	12	26	11	30	0	16.06	0.94550	0.92490
When cell filled	2023	1	11	12	51	1			
Beginning time of count	2023	1	11	14	51	24			

Counts per minute	5.53				
Gross CPM less Cell Blank (CPM)	5.01				
CPM (decay during count corrected)	5.42				
DPM Sample +System (efficiency corrected)	6.74				
DPM sample	6.71	Error ± 1 SD	0.1345	DPM	
DPM/g	3.28				
Ra-226 DPM/g	1.09	Error ± 1 SD	0.0219	DPM/g	Error % = 2.0
Ra-226 pCi/g	0.49				

Chemist	XH
PMT High Voltage +ve	770
HV Power supply	Spectrum Technologies
Alpha Counter	Spectrum Technologies
Region of Interest Ch.#s	28-1022
PMT	6655A - #1
Preamp	Canberra 2007P tube base
Amp Gain	1

Radium Analysis by Rn-222 Emanation

Ra Sample Number:	2460
Section Number	32
Sample ID	F45-50
Core ID	Core F
Lucas Cell No.	3
Number of days since Rn board last run	1
Dry weight of sample counted (g)	2.006
Total count in period	3926
Total count in period (carryover corrected)	3890
Cell Blank count (CPM)	0.536
System Blank (DPM)	0.405
System Efficiency	0.806
Count duration (minutes)	1000

Typical carryover is about 1 - 2 % of the net counts (gross counts less system background) of the sample counted on the previous day. The carryover is subtracted from the gross counts of current sample. This correction is not required if the sample is run after a blank.

Carryover correction?	Yes		
Gross counts of previous sample	4045	Mean of last 10 carryover measurements	1.12%
Counts carried over from previous sample	36	Mean of last 6 system background measurements	818

	Year	Month	Day	Hour	Minute	Second	Ingrowth time (Days)	Ingrowth factor	Decay correction
When sample last stripped	2023	2	24	14	39	0	16.17	0.94660	0.92490
When cell filled	2023	3	12	18	41	52			
Beginning time of count	2023	3	12	20	42	15			

Counts per minute	3.89				
Gross CPM less Cell Blank (CPM)	3.35				
CPM (decay during count corrected)	3.63				
DPM Sample +System (efficiency corrected)	4.50				
DPM sample	4.32	Error ± 1 SD	0.1215	DPM	
DPM/g	2.16				
Ra-226 DPM/g	0.72	Error ± 1 SD	0.0202	DPM/g	Error % = 2.8
Ra-226 pCi/g	0.32				

Chemist	RF
PMT High Voltage +ve	770
HV Power supply	Spectrum Technologies
Alpha Counter	Spectrum Technologies
Region of Interest Ch.#s	28-1022
PMT	6655A - #1
Preamp	Canberra 2007P tube base
Amp Gain	1

Radium Analysis by Rn-222 Emanation

Ra Sample Number:	2462
Section Number	36
Sample ID	F65-70
Core ID	Core F
Lucas Cell No.	3
Number of days since Rn board last run	1
Dry weight of sample counted (g)	2.123
Total count in period	4071
Total count in period (carryover corrected)	4036
Cell Blank count (CPM)	0.536
System Blank (DPM)	0.405
System Efficiency	0.806
Count duration (minutes)	1000

Typical carryover is about 1 - 2 % of the net counts (gross counts less system background) of the sample counted on the previous day. The carryover is subtracted from the gross counts of current sample. This correction is not required if the sample is run after a blank.

Carryover correction?	Yes		
Gross counts of previous sample	3926	Mean of last 10 carryover measurements	1.12%
Counts carried over from previous sample	35	Mean of last 6 system background measurements	818

	Year	Month	Day	Hour	Minute	Second	Ingrowth time (Days)	Ingrowth factor	Decay correction
When sample last stripped	2023	3	1	10	35	0	12.26	0.89161	0.92490
When cell filled	2023	3	13	16	51	46			
Beginning time of count	2023	3	13	18	52	9			

Counts per minute	4.04			
Gross CPM less Cell Blank (CPM)	3.50			
CPM (decay during count corrected)	3.78			
DPM Sample +System (efficiency corrected)	4.70			
DPM sample	4.81	Error ± 1 SD	0.1252	DPM
DPM/g	2.27			
Ra-226 DPM/g	0.76	Error ± 1 SD	0.0197	DPM/g
Ra-226 pCi/g	0.34			

Error % = 2.6

Chemist	XH
PMT High Voltage +ve	770
HV Power supply	Spectrum Technologies
Alpha Counter	Spectrum Technologies
Region of Interest Ch.#s	28-1022
PMT	6655A - #1
Preamp	Canberra 2007P tube base
Amp Gain	1

Results of Cs-137 Analysis

Flett Research Ltd.
440 DeSalaberry Ave. Winnipeg, MB R2L 0Y7
Fax/Phone: (204) 667-2505
E-mail: flett@flettresearch.ca Webpage: http://www.flettresearch.ca

Client: Juang, Alicia

Address: 180 Grand Ave, Suite 1050, Oakland, CA 94610, USA
Core ID: Core F
Date Received: 8-Nov-22
Sampling Date: 24-Oct-22
Date Issued: 12-Apr-23

Matrix: Sediment
Transaction ID: 1033
PO/Contract No.: TOE Oct 20-22
Analysis Dates: 17-Feb-23 to 11-Mar-23
Analyst: X. Hu

Analytical Method: N30120 Measurement of Gamma-Ray Emitting Radionuclides in Sediment/Soil Samples by Gamma Spectrometry Using HPGe Detectors (Version 4)
Comments: <2SD: The measured Cs-137 activity is less than 2 counting errors (i.e. 2 SD), suggesting no significant presence of Cs-137 in this sample.
Detection Limit: The method detection limit (MDL) of Cs-137 is 0.3 DPM/g for a 9 g of dry sample and 0.1 DPM/g for a 32 g of dry sample for an 80,000 seconds counting
Estimated Uncertainty: The estimated uncertainty of this method for Cs-137 has been determined to be ± 10% at 95% confidence for samples with activities between 0.5 and 20 DPM/g, counting time 80,000 seconds and sample weights ranging from 9 to 32 grams. Method uncertainty can increase to 85% for samples with

Results authorized by Dr. Robert J. Flett, Chief Scientist

Section Number	LAB ID	Sample ID	Upper Depth (cm) Provided by client	Lower Depth (cm) Provided by client	Weight of Sample Counted (g)	Sample Thickness (mm)	Count Time (sec)	Integral NET Cs-137 Peak Area (Counts)	Cs-137 Counting Error 1 SD (Counts)	Efficiency for Gammas Fractional	Cs-137 Activity DPM/g (dry wt.) on Counting Date	Counting Error ± 1 S.D. (DPM/g Dry Wt.)	Detector Used	Comments Code
15	112548	F14-15	14.0	15.0	24.536	5.550	80000	57	33	0.0238	0.09	0.05	GEM	<2SD
19	112552	F18-19	18.0	19.0	15.759	3.725	80000	-30	51	0.0285	-0.06	0.10	GMX	<2SD
23	112556	F24-26	24.0	26.0	15.813	3.625	80000	15	33	0.0252	0.03	0.07	GEM	<2SD
25	112558	F28-30	28.0	30.0	29.100	7.075	80000	2	35	0.0227	0.00	0.05	GEM	<2SD
32	112565	F45-50	45.0	50.0	11.339	2.400	80000	26	50	0.0294	0.07	0.13	GMX	<2SD

Efficiency Data

NBS Clay Calibration Standard	Weight (g)	Thickness (mm)	Count Time (sec)	Efficiency for Gammas Fractional Jan. 9-23
GMX 32g 10 mm	32.00	10	5000	0.0237
GMX 24g 7.5mm	24.00	7.5	5000	0.0254
GMX 15g 5mm	15.00	5.0	5000	0.0276
GMX 9g 3mm	9.00	3.0	5000	0.0291
GMX 2.85g 0.8mm	2.854	0.8	10000	0.0306
GEM 32g 10 mm	32.00	10	5000	0.0205
GEM 24g 7.5mm	24.00	7.5	5000	0.0222
GEM 15g 5mm	15.00	5	5000	0.0243
GEM 9g 3mm	9.00	3	5000	0.0256
GEM 2.85g 0.8mm	2.854	0.8	10000	0.0269

Note: Results relate only to the samples tested and as received. Sample depths are provided by the client.
Cs-137: ISO / IEC 17025:2017 Accredited with the Canadian Association for Laboratory Accreditation (CALA Accreditation No. A3306)

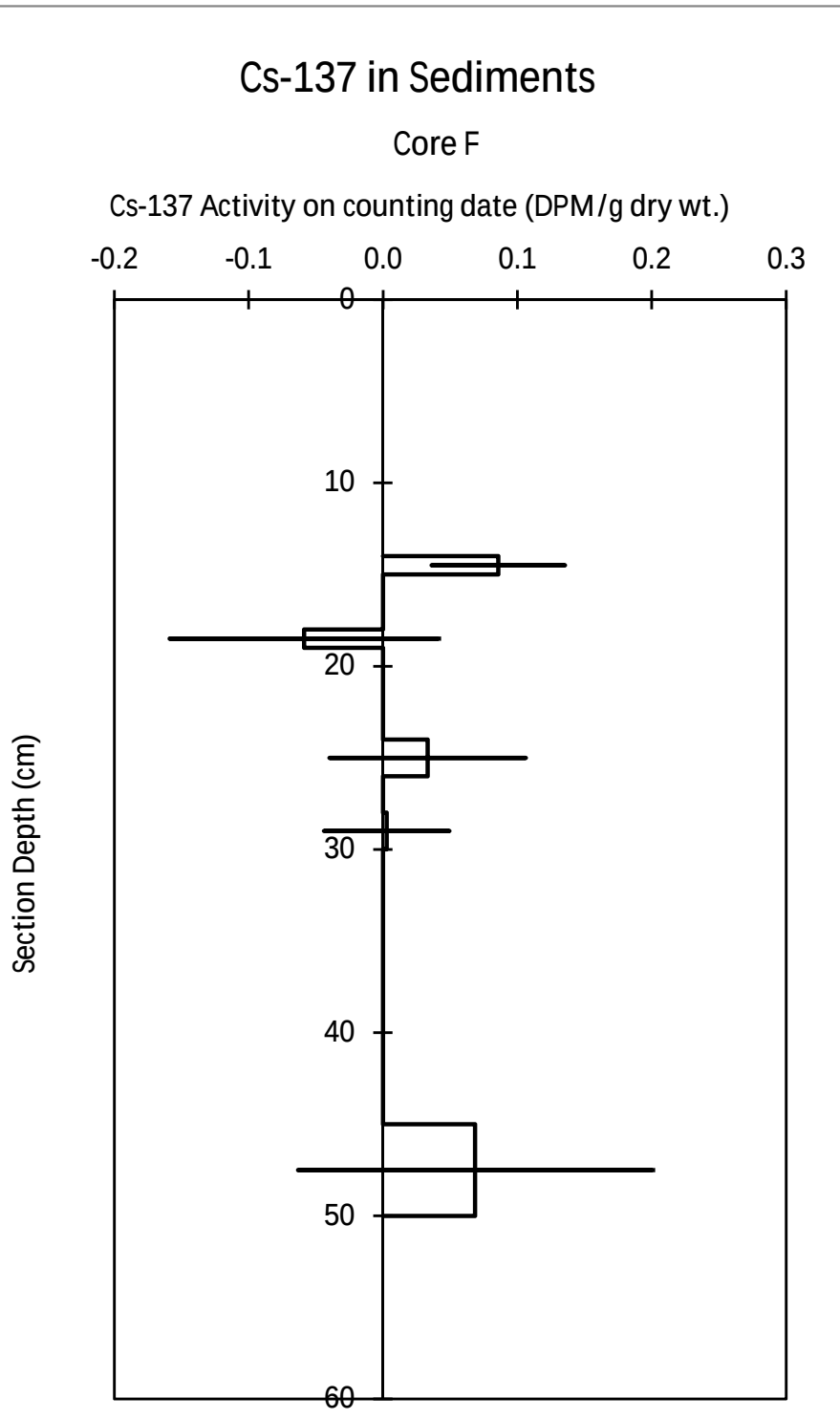

Note: The bar plotted at the midpoint depth of each section represents +/- 1 standard deviation of the Cs-137 counting error.

Q:\Clients A-L\Juang, Alicia - ESA\2022(1033)\Radioisotopes\F\Pb-210, Ra-226 and Cs-137 Juang Core F Apr 13-23 Final.xlsm

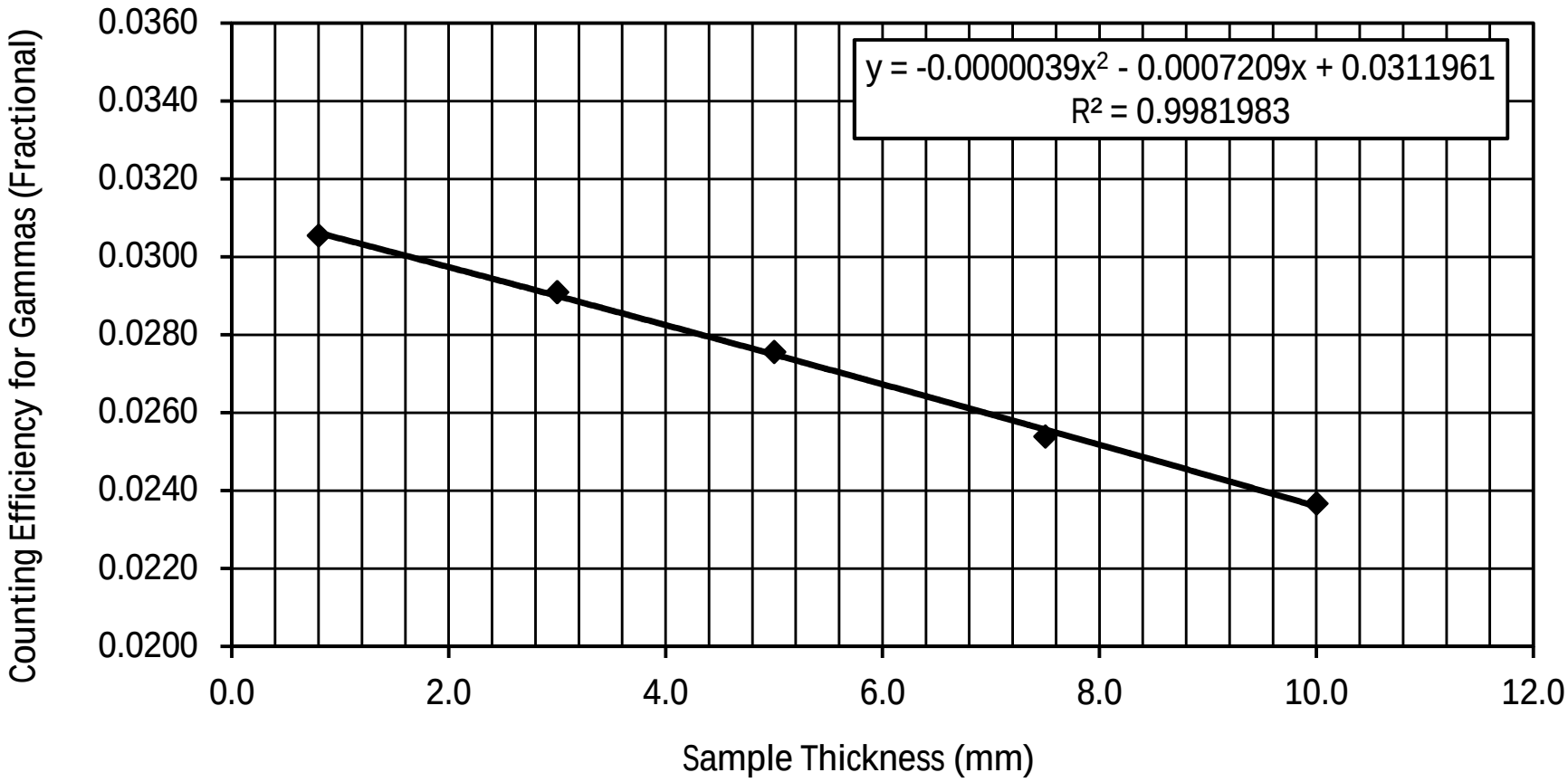
Cs-137 Counting Efficiency of Gammas vs. Sample Thickness (mm) GMX 25% Detector (Jan. 9, 2023)
y = -0.0000039x2 - 0.0007209x + 0.0311961
R2 = 0.9981983
Counting Efficiency for Gammas (Fractional)
0.0360
0.0340
0.0320
0.0300
0.0280
0.0260
0.0240
0.0220
0.0200
0.0
2.0
4.0
6.0
8.0
10.0
12.0
Sample Thickness (mm)

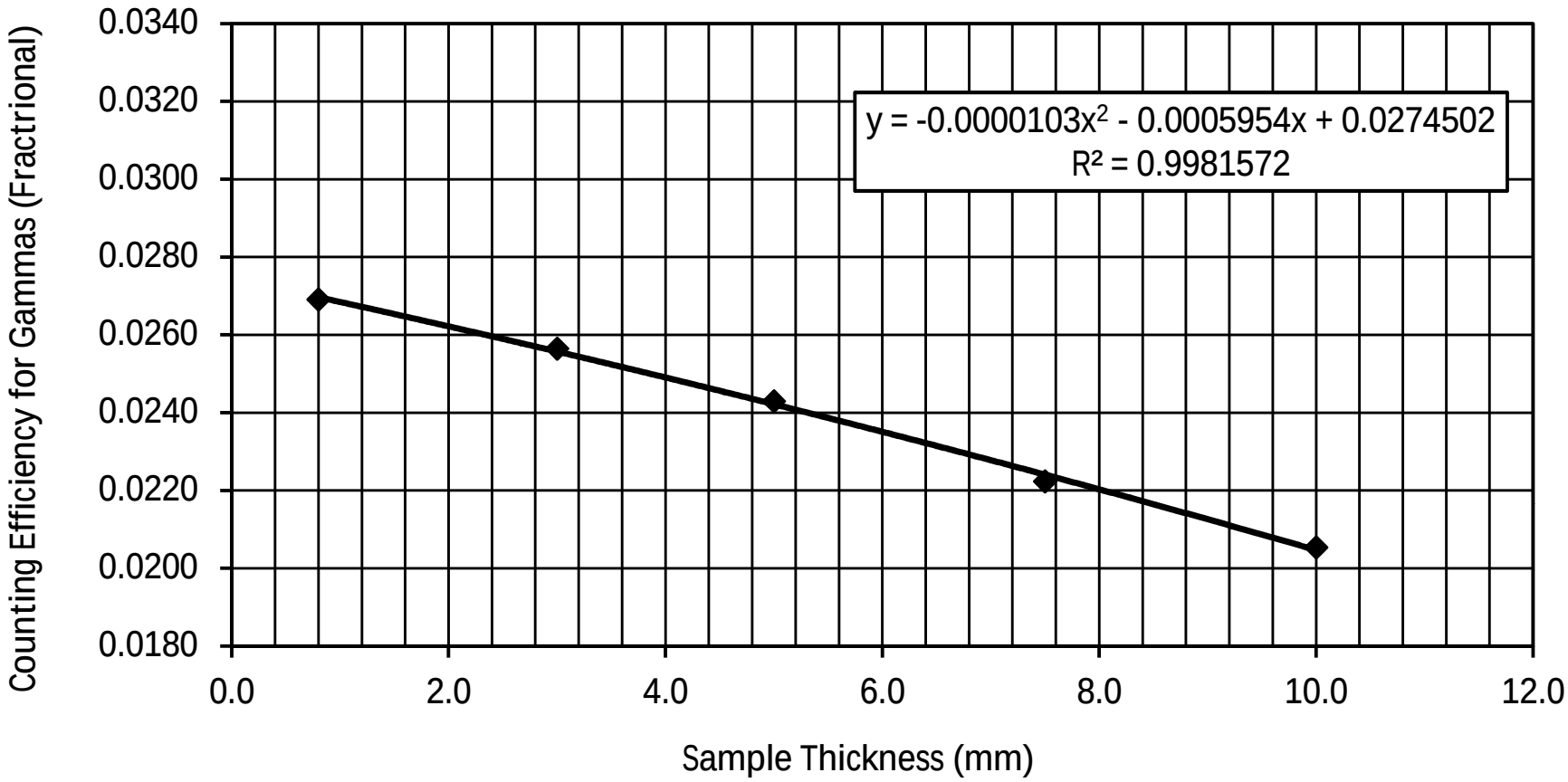
Cs-137 Counting Efficiency of Gammas vs. Sample Thickness (mm) GEM 19% Detector (Jan. 9, 2023)
y = -0.0000103x² - 0.0005954x + 0.0274502
R² = 0.9981572
Counting Efficiency for Gammas (Fractrional)
0.0340
0.0320
0.0300
0.0280
0.0260
0.0240
0.0220
0.0200
0.0180
0.0
2.0
4.0
6.0
8.0
10.0
12.0
Sample Thickness (mm)

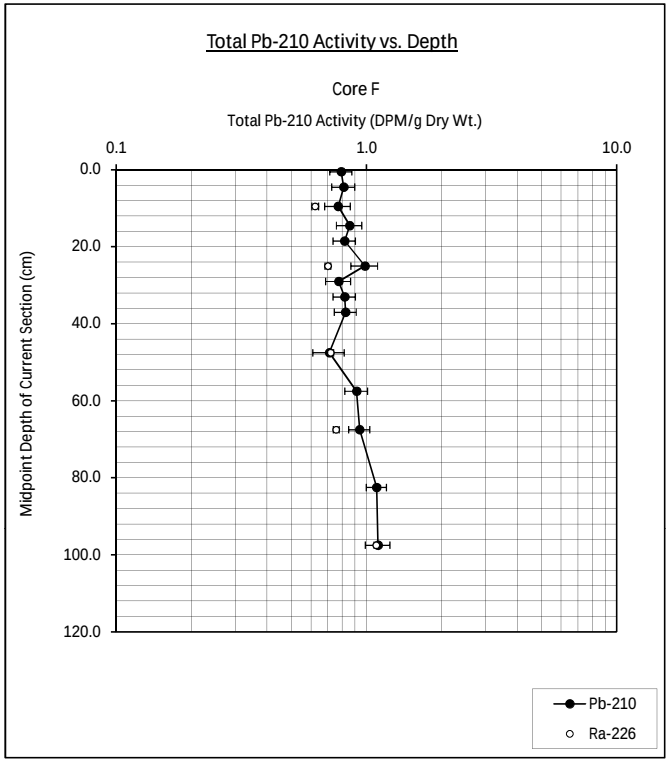

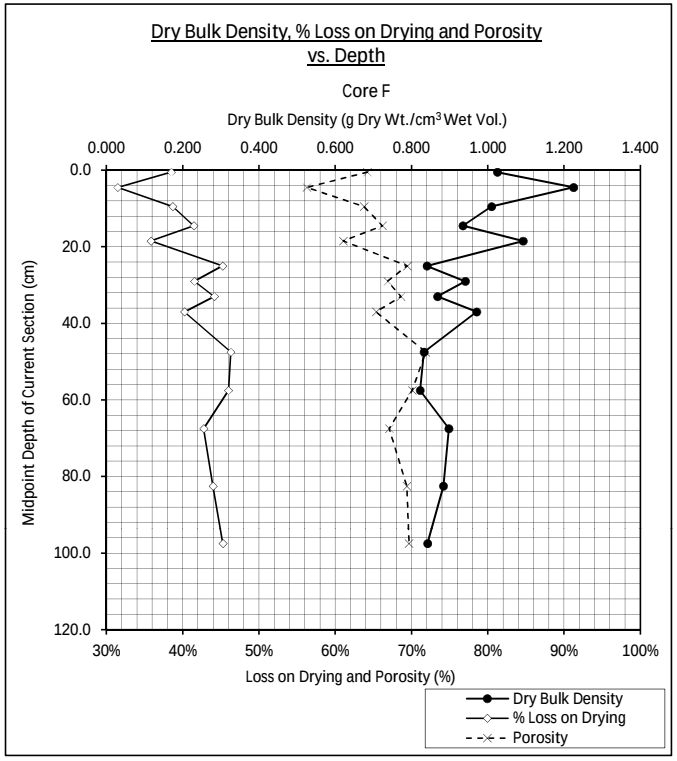

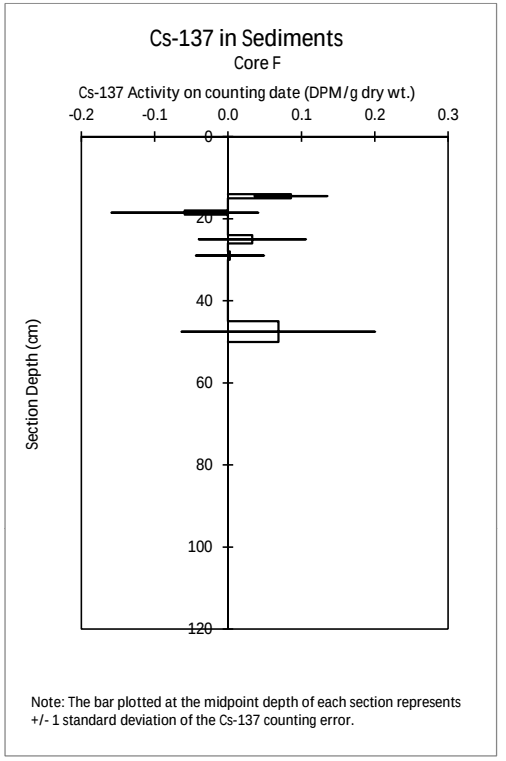

Note: The bar plotted at the midpoint depth of each section represents +/- 1 standard deviation of the Cs-137 counting error.

Core OB

Interpretation of Pb-210, Ra-226 and Cs-137 Results

Flett Research Ltd.
440 DeSalaberry Ave. Winnipeg, MB R2L 0Y7
Fax/Phone: (204) 667-2505
Email: flett@flettresearch.ca Webpage: http://www.flettresearch.ca

Client: Juang, Alicia

Address:	180 Grand Ave, Suite 1050, Oakland, CA 94610, USA
Transaction ID:	1033
Project:	San Diego Eelgrass Blue Carbon
Core ID:	Core OB
Matrix:	Sediment
PO/Contract No.:	TOE Oct 20-22
Sampling Date:	24-Oct-22
Date Received:	8-Nov-22
Analysis Dates:	November 18, 2022 - April 13, 2023
Analysts:	L. Hesketh-Jost; X. Hu
Date Issued:	9-May-23

Results authorized by Dr. Robert J. Flett, Chief Scientist

INTERPRETATION

Observations:

A regular Pb-210 profile exhibits an exponential decrease in total Pb-210 activity as a function of depth. In this core, the total Pb-210 activities are low (column Q on worksheet 'Modeling'), varying between 0.91 - 1.46 DPM/g, and the total Pb-210 activity profile is nearly vertical (Page 3 on worksheet 'Modeling').

The sediments in this core are clayey. The dry bulk densities increase from 0.720 g/cm^3 in section 1 (extrapolated depth 0 - 1.5 cm) to 0.826 g/cm^3 in section 3 (extrapolated depth 1.5 - 3.5 cm), decrease to 0.753 g/cm^3 in section 5 (extrapolated depth 3.5 - 7 cm) and then vary between 0.672 g/cm^3 - 0.693 g/cm^3 in sections 10 - 19 (extrapolated depth 7 - 21.5 cm). The dry bulk densities then gradually increase with depth to 0.846 g/cm^3 in section 29 (extrapolated depth 34 - 38 cm) and vary between 0.759 g/cm^3 - 0.814 g/cm^3 in sections 30 - 42 (extrapolated depth 38 - 100 cm) (column K and page 5 on worksheet 'Modeling').

Ra-226 was measured at 0.71 DPM/g, 0.81 DPM/g, 0.75 DPM/g, 0.80 DPM/g and 1.02 DPM/g in section 10, section 23, section 32, section 36 and section 42, respectively (column S and page 3 on worksheet 'Modeling'). Net unsupported Pb-210 (column W, and page 4 on worksheet 'Modeling') was calculated by subtracting the nearest neighbouring Ra-226 measurement from each total Pb-210 value, unless noted otherwise. The Pb-210 activity (0.91 DPM/g) in section 36 (depth 65 - 70 cm) barely exceeds the Ra-226 activity measured in the same section, suggesting that background Pb-210 activity has been achieved in this core.

Cs-137 was measured in 8 sections in the core interval of 14 - 50 cm. No detectable Cs-137 was observed in core interval of 14 - 19 cm or core interval of 45 - 50 cm. In core interval of 24 - 45 cm the Cs-137 activities are low but significantly above background, varying between 0.11 - 0.20 DPM/g (Pages 14 & 17).

Linear regression model of Unsupported Pb-210 activity vs. Cumulative Dry Weight (g/cm^2):

When applying the linear regression model, it is assumed that the input of Pb-210 and the sediment accumulation rate are constant. If this coring site has not been disturbed by dredging and disposal activities, then the model can be applied to sections 5 - 23 (extrapolated depth 3.5 - 28 cm). Although some variation in the sediment accumulation rate is apparent, it appears that the average sediment accumulation rate in this core interval will be reasonably estimated. This estimate of sediment accumulation rate is used to verify the CRS model for the same core interval.

The regression results are seen on Page a1 (worksheet 'Modeling). The model predicts (R^2 = 0.8703) an average sediment accumulation rate of 0.5115 g/cm^2/yr when the unsupported Pb-210 activity was calculated by subtracting the nearest Ra-226 measurement from each total Pb-210 value. The age at the bottom of any core section in the 3.5 - 28 cm core interval can be estimated by dividing the cumulative dry weight/cm^2 by the accumulation rate. However, it must be added to the age of 2.0 years previously calculated for the bottom of section 3 (extrapolated depth 3.5 cm) by the CRS model. For example, the age at the bottom of section 15 (extrapolated depth 16.5 cm) is calculated as 2.0 + (11.943 - 2.732) / 0.5115 = 20.0 yr. The age estimate at the bottom of each section is shown on Pages 2 (column AD) & a2.

CRS model of Age at bottom of Extrapolated section in years vs. Depth of bottom edge of current section in cm:

The CRS model assumes constant input of Pb-210 and a core that is long enough to include all of the measurable atmospheric source Pb-210, i.e. it contains a complete Pb-210 inventory. If this coring site has not been disturbed by dredging and disposal activities, i.e. the Pb-210 inventory is unaltered, and one assumes that the activity in section 36 (0.91 DPM/g) is at the background Pb-210 level, the model can be applied.

The estimated age at the bottom of each section is shown in column AB (Page 2, worksheet 'Modeling'). The average sediment accumulation rate, from core surface to the extrapolated bottom depth of any section, can be calculated by dividing the cumulative dry mass at the bottom of the extrapolated section by the calculated age at that depth. For example, the average sediment accumulation rate, from the core surface to the bottom of section 15 (extrapolated depth 16.5 cm) can be calculated as: 11.943 / 13.4 = 0.8913 g/cm^2/yr. The individual sediment accumulation rate for each section is shown in column AC on Page 2. Plots of age vs. depth, sediment accumulation rate vs. depth and sediment accumulation rate vs. age are seen in Pages a2, a3 and a4, respectively.

Conclusion:

It is unclear that whether or not dredging and/or disposal events occurred at this coring site. The low but detectable unsupported Pb-210 activities in the upper 62.5 cm (extrapolated depth) of this core, indicate that these sediments are likely modern. The lack of detectable unsupported Pb-210 activities below 62.5 cm depth indicate that the sediments below 62.5 cm could possibly be older than 67 years (~3 half-lives of Pb-210), the maximum age that can be estimated in this core.

In core interval of 24 - 45 cm, the low but detectable Cs-137 activity suggests that the sediments in this portion of the core probably are modern, i.e. sediments were deposited less than 2022 - 1963 = 59 years ago.

Overall, the analytical quality of radioisotope data (based upon the recovery of spike, the recovery of CRM, the results of repeat analyses and blanks) is considered good. It is not possible to assign a reliable age to the sediment at any depth in the core.

Comments on the modeling results

Both the linear regression model and the CRS model were applied to the data set, assuming that the sediments at this sampling site were not disturbed in the past ~100 years, i.e. the sediments were not dredged and no dredged sediments were deposited.

The sediment accumulation rates are relatively high and highly variable, ranging between 0.2267 g/cm^2/yr and 1.9248 g/cm^2/yr in core interval of 0 - 52.5 cm (extrapolated depth)(by the CRS model) (Pages 2, a3 & a4).

Over the interval of sections 5 - 23 (extrapolated depth 3.5 - 28 cm), the only portion of the core where the models could be compared, the CRS model predicts an average sediment accumulation rate of 0.8575 g/cm^2/yr, while the regression model predicts an average rate of 0.5115 g/cm^2/yr. These results are significantly different and suggest that the assumptions of the models may not be completely satisfied. However, the ages estimated by both models are not incompatible with the conclusions above.

It is cautioned that the uncertainty of predicted ages in this core is high and the ages are gross approximations only, due to the irregular shape of Pb-210 profile.

Calculation of Sediment Accumulation Rates and Ages

Flett Research Ltd.
440 DeSalaberry Ave. Winnipeg, MB R2L 0Y7
Fax/Phone (204) 667-2505
E-mail: flett@flettresearch.ca Webpage: http://www.flettresearch.ca

Client: Juang, Alicia

Address: 180 Grand Ave, Suite 1050, Oakland, CA 94610, USA
Core ID: Core OB
Date Received: 8-Nov-22
Sampling Date: 24-Oct-22
Date Issued: 09-May-23

Matrix: Sediment
Transaction ID: 1033
PO/Contract No.: TOE Oct 20-22

Pb-210, Ra-226 and dry bulk density results as reported on other sheets within this workbook are summarized in the table below and are used to estimate accumulation rates and ages for the core. Two models are available for these calculations: the Constant Rate of Supply (CRS) model and the Linear Regression Model.

In order to date a sediment core, we need to determine the atmospheric sourced Pb-210 (= unsupported Pb-210) that is in 10+ sediment core sections. We analyze the sediment for TOTAL Pb-210 which includes both unsupported Pb-210 AND Pb-210 also being produced by decay of natural Ra-226 in the sediment. Due to secular equilibrium of Ra-226/Pb-210, sediment derived Pb-210 is expected to have the same activity as the Ra-226 and therefore we estimate the sediment sourced Pb-210 (=supported Pb-210) by using radon emanation to determine the Ra-226 in 3+ sections of the core. This allows the required calculation: unsupported Pb-210 = Total Pb-210 – supported Pb-210.

Results Authorized by Dr. Robert J. Flett, Chief Scientist

Section Number	Sample ID	Upper Depth (cm) Provided by client	Lower Depth (cm) Provided by client	Extrapolated Upper Section Depth (cm)	Extrapolated Lower Section Depth (cm)	Dry Bulk Density (Dry wt./Wet vol.) (g/cm3)	Midpoint Depth of Current Section (cm) Not Used	Mass in Extrapolated Section (g/cm2)	Cumulative Mass to Bottom of Current Section (g/cm2)	Plot-point of Cumulative Mass in Current Section (g/cm2)	Pb-210 Total Activity (DPM/g Dry Wt.)	Pb-210 COUNTING Error ± 1 S.D. (DPM/g Dry Wt.)	Pb-210 Background Activity from measured Ra-226 (DPM/g Dry Wt.)	Ra-226 Combined Error ± 1 S.D. (DPM/g Dry Wt.)	Estimated Pb-210 Background Activity from nearest neighbouring Ra-226 (DPM/g Dry Wt.)	Pb-210 Unsupported Activity (DPM/g Dry Wt.)	Pb-210 Unsupported Activity (DPM/cm^2) in each section	Age at Bottom of Extrapolated Section in Years (CRS Model Estimate)	CRS Sediment Accumulation Rate ($g/cm^2/yr$)	Age at Bottom of Extrapolated Section in Years (Linear Regression Model Estimate)
1	OB0-1	0.0	1.0	0.00	1.50	0.720		1.079	1.079	0.360	1.22	0.15			0.71	0.51	0.552	1.0	1.0981	
3	OB2-3	2.0	3.0	1.50	3.50	0.826		1.652	2.732	1.906	1.03	0.10			0.71	0.32	0.532	2.0	1.6924	
5	OB4-5	4.0	5.0	3.50	7.00	0.753		2.636	5.368	3.485	1.46	0.15			0.71	0.75	1.985	5.9	0.6711	7.1
10	OB9-10	9.0	10.0	7.00	12.00	0.693		3.464	8.832	7.100	1.18	0.15	0.71	0.02		0.46	1.611	9.5	0.9671	13.9
15&15Dup	OB14-15	14.0	15.0	12.00	16.50	0.691		3.111	11.943	10.561	1.21	0.13			0.71	0.50	1.560	13.4	0.7982	20.0
19	OB18-19	18.0	19.0	16.50	21.50	0.672		3.361	15.304	13.288	1.23	0.12			0.81	0.42	1.397	17.3	0.8523	26.5
23	OB24-26	24.0	26.0	21.50	28.00	0.755		4.906	20.210	17.946	1.13	0.13	0.81	0.02		0.32	1.552	22.3	0.9750	36.1
26	OB30-32	30.0	32.0	28.00	34.00	0.802		4.811	25.022	22.616	0.99	0.11			0.81	0.17	0.833	25.4	1.5703	
29	OB36-38	36.0	38.0	34.00	38.00	0.846		3.385	28.407	27.561	0.95	0.10			0.81	0.13	0.443	27.2	1.9248	
30	OB38-40	38.0	40.0	38.00	40.00	0.806		1.612	30.020	29.213	1.13	0.11			0.75	0.38	0.617	29.8	0.6151	
31	OB40-45	40.0	45.0	40.00	45.00	0.770		3.848	33.868	31.944	1.01	0.12			0.75	0.26	1.012	34.6	0.7984	
32	OB45-50	45.0	50.0	45.00	52.50	0.779		5.846	39.714	35.816	1.34	0.15	0.75	0.02		0.59	3.452	60.4	0.2267	
34	OB55-60	55.0	60.0	52.50	62.50	0.801		8.011	47.725	43.719	1.10	0.12			0.75	0.35	2.809			
36	OB65-70	65.0	70.0	62.50	75.00	0.797		9.960	57.685	51.709	0.91	0.11	0.80	0.02		0.00	0.000			
39	OB80-85	80.0	85.0	75.00	90.00	0.759		11.384	69.069	63.377	1.24	0.13			1.02	0.00				
42	OB95-100	95.0	100.0	90.00	100.00	0.814		8.143	77.212	75.177	1.13	0.15	1.02	0.02		0.00				

Note: These modeling results are gross approximations only.

Q:\Clients A-L\Juang, Alicia - ESA\2022(1033)\Radioisotopes\OB\Pb-210, Ra-226 and Cs-137 Juang Core OB May 9-23 Final.xlsm

Dup (Duplicate): Two subsamples of the same sample were carried through the analytical procedure in an identical manner.

 Sample depths are provided by the client. Errors in that data may affect the validity of sediment accumulation rates, Pb-210 inventory and age calculations.
Note: Results relate only to the items tested and as received.

Total Pb-210 Activity vs. Accumulated Mass

Core OB

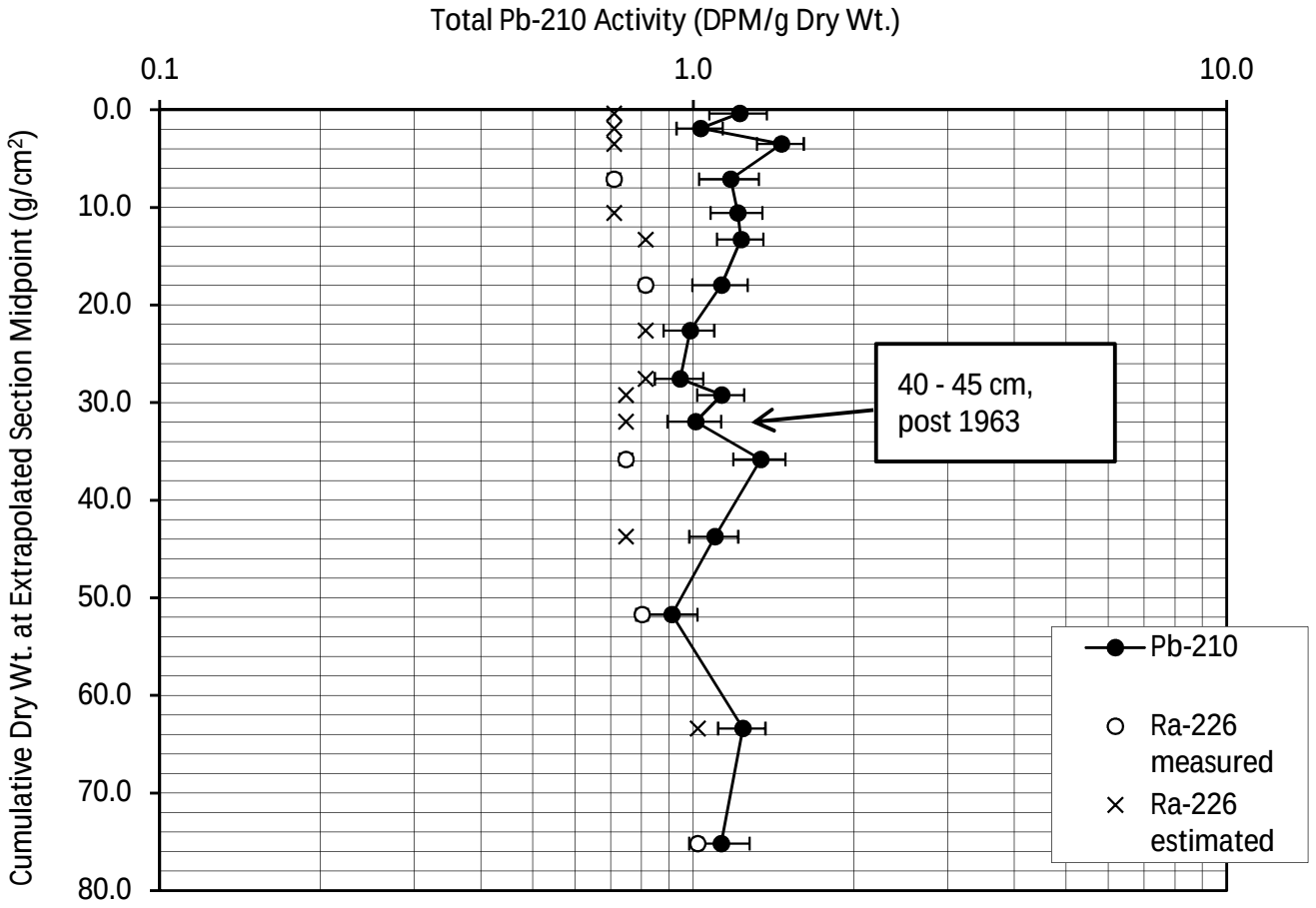

Q:\Clients A-L\Juang, Alicia - ESA\2022(1033)\Radioisotopes\OB\Pb-210, Ra-226 and Cs-137 Juang Core OB May 9-23 Final.xlsm

Unsupported Pb-210 Activity vs. Accumulated Mass

Core OB

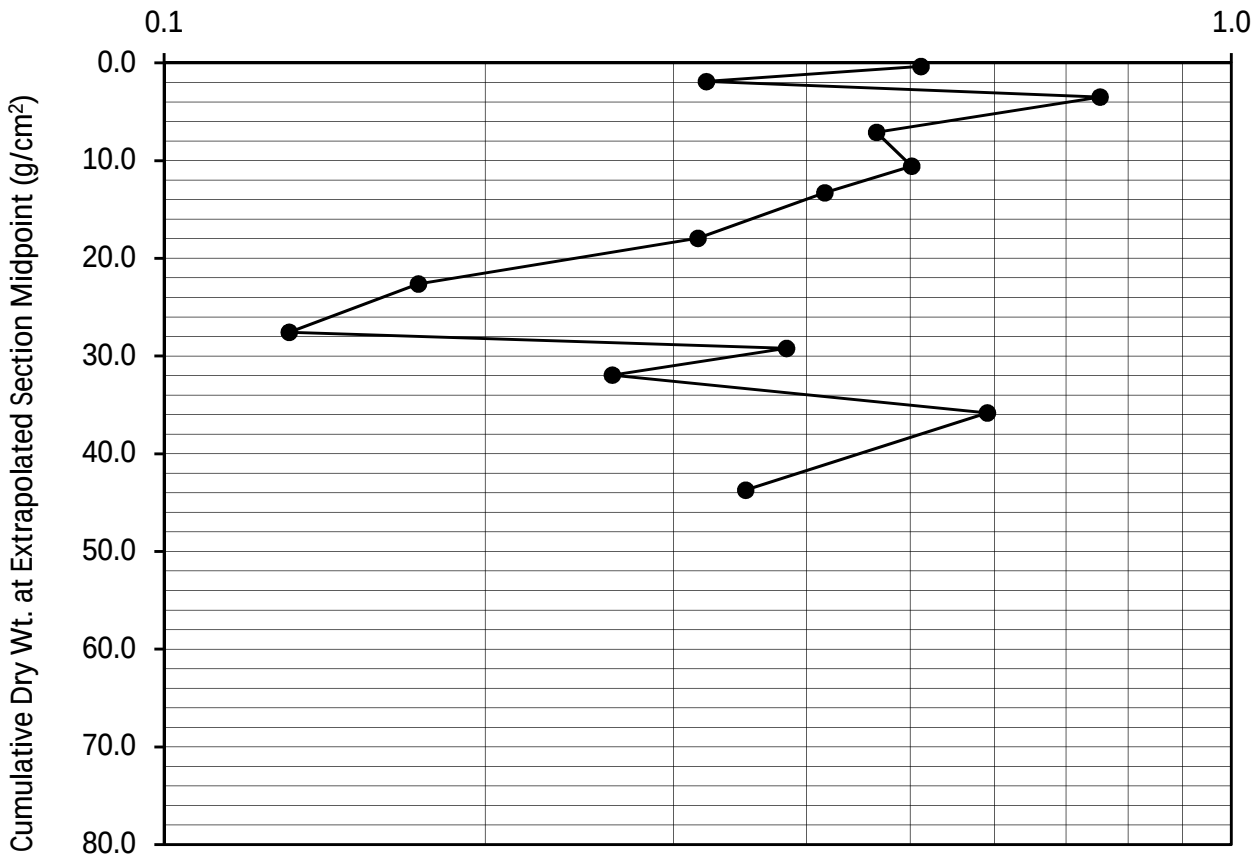

Dry Bulk Density vs. Accumulated Mass

Core OB

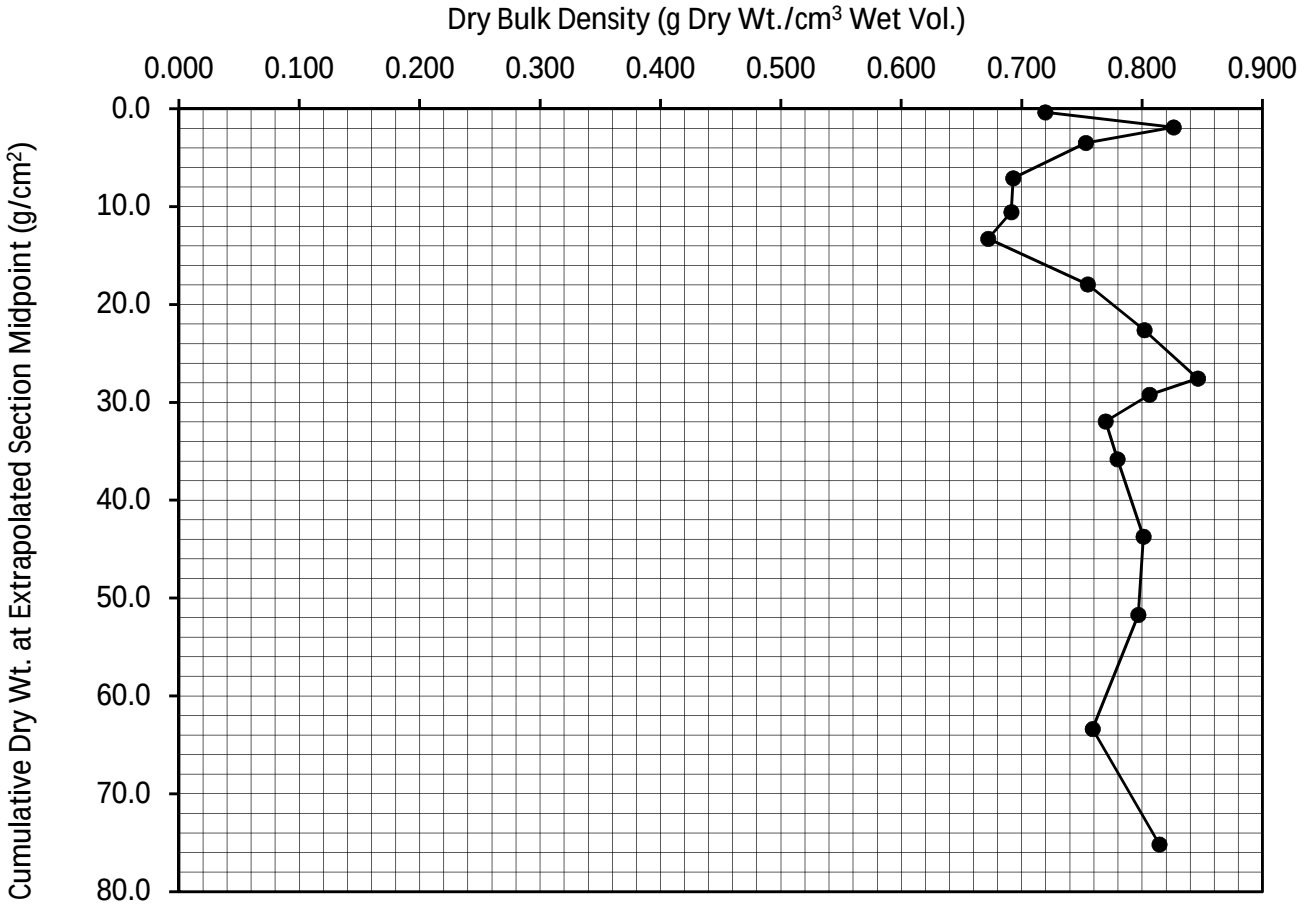

Q:\Clients A-L\Juang, Alicia - ESA\2022(1033)\Radioisotopes\OB\Pb-210, Ra-226 and Cs-137 Juang Core OB May 9-23 Final.xlsm

Dry Bulk Density, Percent Loss on Drying and Porosity

Flett Research Ltd.

440 DeSalaberry Ave. Winnipeg, MB R2L 0Y7

Fax/Phone: (204) 667-2505

E-mail: flett@flettresearch.ca Webpage: http://www.flettresearch.ca

Client: Juang, Alicia

Address: 180 Grand Ave, Suite 1050, Oakland, CA 94610, USA
Core ID: Core OB
Date Received: November 8, 2022
Sampling Date: October 24, 2022
Date Issued: 25-Apr-23

Matrix: Sediment
Transaction ID: 1033
PO/Contract No.: TOE Oct 20-22
Analysis Dates: November 18, 2022 to April 6, 2023
Analyst: L. Hesketh-Jost

Analytical Method: N10020 Measurement of Dry Bulk Density and Other Sediment Characteristics (version 1)
Comments:

Estimated Uncertainty: For samples with %LOD less than 90%, the estimated uncertainty in laboratory measurements of dry bulk density has been determined to be less than 3%. When samples have a high water content (>90% LOD) uncertainty may increase to 8%. Method uncertainties are expressed at a 95% confidence level of (k=2).

Results authorized by Dr. Robert J. Flett, Chief Scientist

Section Number	LAB ID	Sample ID	Upper Depth (cm) Provided by client	Lower Depth (cm) Provided by client		Volume of wet sample (ml)	Weight of wet sample (g)	Weight of dry sample (g)		Dry Bulk Density (Dry wt./Wet vol.) (g/cm3)	% Loss on Drying	% Porosity
1	112576	OB0-1	0.0	1.0		4.907	7.167	3.531		0.720	50.73%	74.10%
3	112578	OB2-3	2.0	3.0		4.907	7.479	4.054		0.826	45.79%	69.80%
5	112580	OB4-5	4.0	5.0		4.907	7.260	3.696		0.753	49.09%	72.63%
10	112585	OB9-10	9.0	10.0		4.907	7.058	3.400		0.693	51.83%	74.55%
15&15Dup	112590	OB14-15	14.0	15.0						0.691	51.78%	74.25%
19	112594	OB18-19	18.0	19.0		4.907	6.975	3.298		0.672	52.72%	74.93%
23	112598	OB24-26	24.0	26.0		4.907	7.251	3.704		0.755	48.92%	72.28%
26	112601	OB30-32	30.0	32.0		4.907	7.387	3.935		0.802	46.73%	70.35%
29	112604	OB36-38	36.0	38.0		4.907	7.534	4.153		0.846	44.88%	68.90%
30	112605	OB38-40	38.0	40.0		4.905	7.413	3.954		0.806	46.66%	70.52%
31	112606	OB40-45	40.0	45.0		4.905	7.298	3.775		0.770	48.27%	71.82%
32	112607	OB45-50	45.0	50.0		4.907	7.322	3.825		0.779	47.76%	71.27%
34	112609	OB55-60	55.0	60.0		4.907	7.399	3.931		0.801	46.87%	70.67%
36	112611	OB65-70	65.0	70.0		4.907	7.378	3.910		0.797	47.00%	70.67%
39	112614	OB80-85	80.0	85.0		4.907	7.216	3.724		0.759	48.39%	71.16%
42	112617	OB95-100	95.0	100.0		4.907	7.417	3.996		0.814	46.12%	69.72%
Quality Control Samples												
15	112590	OB14-15	14.0	15.0		4.907	7.030	3.391		0.691	51.76%	74.16%
15Dup	112590	OB14-15 Duplicate	14.0	15.0		4.907	7.042	3.394		0.692	51.80%	74.34%

Dup : Duplicate - two subsamples of the same sample carried through the analytical procedure in an identical manner. Duplicate data is reported as a mean in the main data table.

Loss of water or sediment during collecting the core, sectioning of core, sub-sampling for analyses or storage and transportation, will bias the result of the dry bulk density. Sample depths are provided by the client. Errors in that data may affect the validity of sediment quality data.

Note: Results relate only to the samples tested and as received.

Results of Pb-210 by Po-210 analysis

Flett Research Ltd.
440 DeSalaberry Ave. Winnipeg, MB R2L 0Y7
Fax/Phone: (204) 667-2505
E-mail: flett@flettresearch.ca Webpage: http://www.flettresearch.ca

Client: Juang, Alicia

Address: 180 Grand Ave, Suite 1050, Oakland, CA 94610, USA
Core ID: Core OB
Date Received: 8-Nov-22
Sampling Date: 24-Oct-22
Date Issued: 25-Apr-23

Matrix: Sediment
Transaction ID: 1033
PO/Contract No.: TOE Oct 20-22
Analysis Dates: 24-Nov-22 to 13-Apr-23
Analyst: L. Hesketh-Jost

Analytical Method: N20110 Determination of Lead-210 by Measurement of Po-210 in Sediment, Soil and Peat by Alpha Spectrometry (Version 7)
Comments:

Detection Limit: The method detection limit (MDL) for 0.25 - 0.5 g (dry wt.) sample is between 0.05 - 0.1 DPM Po-210/g dry sample at a 95% confidence level for 60,000 second counting time and is based on greater than 20 method blanks. This can vary slightly and depends upon the amount of sample, detector and recovery efficiency of each sample.

Estimated Uncertainty: As Po-210 (Pb-210) activity drops, error increases due to increasing counting error. When gross counts are less than 100 the dominant error becomes counting error which is equal to √gross counts/gross counts. When Po-210 (Pb-210) activity exceeds 5 DPM/g the method uncertainty is ± 11% . When activities are between 1 and 5 DPM/g, the method uncertainty is ± 17%. When activities are between 0.2 and 1 DPM/g, the method uncertainty is ± 25%. Uncertainties are expressed at 95% confidence level (k=2).

Results authorized by Dr. Robert J. Flett, Chief Scientist

Section Number	LAB ID	Sample ID	Upper Depth (cm) Provided by client	Lower Depth (cm) Provided by client	Po-209 Counts Less Detector Back-ground	Net Po-210 Counts [Gross counts Less Detector and Po-209 Spiking Solution Backgrounds]	Weight of Sample Counted (g)	Count Time (sec)	Po-210 Total Activity (DPM/g Dry Wt.)	Po-210 COUNTING Error ± 1 S.D. (DPM/g Dry Wt.)	Comments Code
1	112576	OB0-1	0.0	1.0	1291	75	0.462	60000	1.22	0.15	
3	112578	OB2-3	2.0	3.0	1766	105	0.561	60000	1.03	0.10	
5	112580	OB4-5	4.0	5.0	1173	101	0.573	60000	1.46	0.15	
10	112585	OB9-10	9.0	10.0	1032	64	0.513	60000	1.18	0.15	
15&15Dup	112590	OB14-15	14.0	15.0					1.21	0.13	
19	112594	OB18-19	18.0	19.0	1677	109	0.515	60000	1.23	0.12	
23	112598	OB24-26	24.0	26.0	1206	75	0.535	60000	1.13	0.13	
26	112601	OB30-32	30.0	32.0	1592	86	0.534	60000	0.99	0.11	
29	112604	OB36-38	36.0	38.0	1831	95	0.535	60000	0.95	0.10	
30	112605	OB38-40	38.0	40.0	1498	98	0.570	60000	1.13	0.11	
31	112606	OB40-45	40.0	45.0	1526	76	0.486	60000	1.01	0.12	
32	112607	OB45-50	45.0	50.0	1160	82	0.514	60000	1.34	0.15	
34	112609	OB55-60	55.0	60.0	1463	98	0.595	60000	1.10	0.12	
36	112611	OB65-70	65.0	70.0	1494	78	0.559	60000	0.91	0.11	
39	112614	OB80-85	80.0	85.0	1597	98	0.483	60000	1.24	0.13	
42	112617	OB95-100	95.0	100.0	1055	61	0.498	60000	1.13	0.15	

Quality Control Samples

Section Number	LAB ID	Sample ID			Po-209 Counts Less Detector Back-ground	Net Po-210 Counts	Weight of Sample Counted (g)	Count Time (sec)	Po-210 Total Activity (DPM/g)	Po-210 COUNTING Error +/- 1 S.D. (DPM/g)	CRM Recovery on Counting Date
RegBlk1		Reagent Blank w/o Po-209 spike			-3	3					
BLKwSpike1		Reagent Blank with Po-209 spike			2803	5					
RegBlk2		Reagent Blank w/o Po-209 spike			-7	2					
BLKwSpike2		Reagent Blank with Po-209 spike			3173	3					
15	112590	OB14-15					0.488	60000	1.00	0.12	
15Dup	112590	OB14-15 Duplicate					0.495	60000	1.43	0.15	
CRM1		IAEA447 (17.67 DPM/g)					0.340	60000	16.85	0.45	95.4%Rec
CRM2		IAEA447 (17.52 DPM/g)					0.363	60000	16.80	0.42	95.9%Rec

Q:\Clients A-L\Juang, Alicia - ESA\2022(1033)\Radioisotopes\OB\Pb-210, Ra-226 and Cs-137 Juang Core OB May 9-23 Final.xlsm

Dup (duplicate): Two subsamples of the same sample were carried through the analytical procedure in an identical manner.

Note: Results relate only to the samples tested and as received. Sample depths are provided by the client.
ISO / IEC 17025:2017 Accredited with the Canadian Association for Laboratory Accreditation (CALA Accreditation No. A3306)

Results of Ra-226 Analysis by Rn-222 Emanation

Flett Research Ltd.
440 DeSalaberry Ave., Winnipeg, MB R2L 0Y7
Fax/Phone: (204) 667-2505
Email: flett@flettresearch.ca Webpage: http://www.flettresearch.ca

Client: Juang, Alicia

Address: 180 Grand Ave, Suite 1050, Oakland, CA 94610, USA
Core ID: Core OB
Date Received: 8-Nov-22
Sampling Date: 24-Oct-22
Date Issued: 25-Apr-23

Matrix: Sediment
Transaction ID: 1033
PO/Contract No.: TOE Oct 20-22
Analysis Dates: 22-Dec-22 to 15-Mar-23
Analyst: L. Hesketh-Jost & X. Hu

Analytical Method: N40110 Determination of Radium-226 in Sediment, Soil and Peat by Radon-222 Emanation (Version 4)

Comments:

Detection Limit: The method detection limit (MDL) is dependent on the amount of sample analyzed. For a 60,000 second counting time the MDL at 95% confidence for 2 g of dry sample is 0.1 DPM/g and for 0.5 g of dry sample is 0.5 DPM/g.

Estimated Uncertainty: The estimate of uncertainty of measurement for this method in this laboratory is approximately ±12% at 95% confidence level (approximately 40,000 counts in 60,000 seconds).

Results authorized by Dr. Robert J. Flett, Chief Scientist

Section Number	Lab ID	Sample ID	Upper Depth (cm) Provided by client	Lower Depth (cm) Provided by client	Weight of Sample Counted (g)	Count Time (sec)	Ra-226 Activity (DPM/g Dry Wt.)	Combined Error: 1 SD (DPM/g Dry Wt.)	Comments Code for Ra-226 Analysis
10	112585	OB9-10	9	10	2.078	60000	0.71	0.02	
23	112598	OB24-26	24	26	2.146	60000	0.81	0.02	
32	112607	OB45-50	45	50	2.050	60000	0.75	0.02	
36	112611	OB65-70	65	70	2.074	60000	0.80	0.02	
42	112617	OB95-100	95	100	2.070	60000	1.02	0.02	

Q:\Clients A-L\Juang, Alicia - ESA\2022(1033)\Radioisotopes\OB\Pb-210, Ra-226 and Cs-137 Juang Core OB May 9-23 Final.xlsm

Note: Results relate only to the samples tested and as received. Sample depths are provided by the client.
ISO / IEC 17025:2017 Accredited with the Canadian Association for Laboratory Accreditation (CALA Accreditation No. A3306)

Radium Analysis by Rn-222 Emanation

Ra Sample Number:	2428
Section Number	10
Sample ID	OB9-10
Core ID	Core OB
Lucas Cell No.	3
Number of days since Rn board last run	1
Dry weight of sample counted (g)	2.078
Total count in period	3991
Total count in period (carryover corrected)	3940
Cell Blank count (CPM)	0.523
System Blank (DPM)	0.390
System Efficiency	0.804
Count duration (minutes)	1000

Typical carryover is about 1 - 2 % of the net counts (gross counts less system background) of the sample counted on the previous day. The carryover is subtracted from the gross counts of current sample. This correction is not required if the sample is run after a blank.

Carryover correction?	Yes		
Gross counts of previous sample	5568	Mean of last 10 carryover measurements	1.06%
Counts carried over from previous sample	51	Mean of last 6 system background measurements	795

	Year	Month	Day	Hour	Minute	Second	Ingrowth time (Days)	Ingrowth factor	Decay correction
When sample last stripped	2022	12	26	12	38	0	17.10	0.95493	0.92000
When cell filled	2023	1	12	15	8	0			
Beginning time of count	2023	1	12	17	50	36			

Counts per minute	3.94				
Gross CPM less Cell Blank (CPM)	3.42				
CPM (decay during count corrected)	3.71				
DPM Sample +System (efficiency corrected)	4.62				
DPM sample	4.43	Error ± 1 SD	0.1221	DPM	
DPM/g	2.13				
Ra-226 DPM/g	0.71	Error ± 1 SD	0.0196	DPM/g	Error % = 2.8
Ra-226 pCi/g	0.32				

Chemist	XH
PMT High Voltage +ve	770
HV Power supply	Spectrum Technologies
Alpha Counter	Spectrum Technologies
Region of Interest Ch.#s	28-1022
PMT	6655A - #1
Preamp	Canberra 2007P tube base
Amp Gain	1

Radium Analysis by Rn-222 Emanation

Ra Sample Number:	2429
Section Number	23
Sample ID	OB24-26
Core ID	Core OB
Lucas Cell No.	3
Number of days since Rn board last run	1
Dry weight of sample counted (g)	2.146
Total count in period	4599
Total count in period (carryover corrected)	4565
Cell Blank count (CPM)	0.523
System Blank (DPM)	0.390
System Efficiency	0.804
Count duration (minutes)	1000

Typical carryover is about 1 - 2 % of the net counts (gross counts less system background) of the sample counted on the previous day. The carryover is subtracted from the gross counts of current sample. This correction is not required if the sample is run after a blank.

Carryover correction?	Yes		
Gross counts of previous sample	3991	Mean of last 10 carryover measurements	1.06%
Counts carried over from previous sample	34	Mean of last 6 system background measurements	795

	Year	Month	Day	Hour	Minute	Second	Ingrowth time (Days)	Ingrowth factor	Decay correction
When sample last stripped	2022	12	26	12	37	0	18.15	0.96273	0.92490
When cell filled	2023	1	13	16	16	51			
Beginning time of count	2023	1	13	18	17	15			

Counts per minute	4.57				
Gross CPM less Cell Blank (CPM)	4.04				
CPM (decay during count corrected)	4.37				
DPM Sample +System (efficiency corrected)	5.44				
DPM sample	5.24	Error ± 1 SD	0.1264	DPM	
DPM/g	2.44				
Ra-226 DPM/g	0.81	Error ± 1 SD	0.0196	DPM/g	Error % = 2.4
Ra-226 pCi/g	0.37				

Chemist	XH
PMT High Voltage +ve	770
HV Power supply	Spectrum Technologies
Alpha Counter	Spectrum Technologies
Region of Interest Ch.#s	28-1022
PMT	6655A - #1
Preamp	Canberra 2007P tube base
Amp Gain	1

Radium Analysis by Rn-222 Emanation

Ra Sample Number:	2430
Section Number	42
Sample ID	OB95-100
Core ID	Core OB
Lucas Cell No.	3
Number of days since Rn board last run	1
Dry weight of sample counted (g)	2.070
Total count in period	5416
Total count in period (carryover corrected)	5376
Cell Blank count (CPM)	0.523
System Blank (DPM)	0.390
System Efficiency	0.804
Count duration (minutes)	1000

Typical carryover is about 1 - 2 % of the net counts (gross counts less system background) of the sample counted on the previous day. The carryover is subtracted from the gross counts of current sample. This correction is not required if the sample is run after a blank.

Carryover correction?	Yes		
Gross counts of previous sample	4599	Mean of last 10 carryover measurements	1.06%
Counts carried over from previous sample	40	Mean of last 6 system background measurements	795

	Year	Month	Day	Hour	Minute	Second	Ingrowth time (Days)	Ingrowth factor	Decay correction
When sample last stripped	2022	12	26	12	37	0	19.22	0.96928	0.92490
When cell filled	2023	1	14	17	52	0			
Beginning time of count	2023	1	14	19	52	23			

Counts per minute	5.38				
Gross CPM less Cell Blank (CPM)	4.85				
CPM (decay during count corrected)	5.25				
DPM Sample +System (efficiency corrected)	6.53				
DPM sample	6.33	Error ± 1 SD	0.1319	DPM	
DPM/g	3.06				
Ra-226 DPM/g	1.02	Error ± 1 SD	0.0212	DPM/g	Error % = 2.1
Ra-226 pCi/g	0.46				

Chemist	RF
PMT High Voltage +ve	770
HV Power supply	Spectrum Technologies
Alpha Counter	Spectrum Technologies
Region of Interest Ch.#s	28-1022
PMT	6655A - #1
Preamp	Canberra 2007P tube base
Amp Gain	1

Radium Analysis by Rn-222 Emanation

Ra Sample Number:	2459
Section Number	32
Sample ID	OB45-50
Core ID	Core OB
Lucas Cell No.	3
Number of days since Rn board last run	1
Dry weight of sample counted (g)	2.050
Total count in period	4045
Total count in period (carryover corrected)	n/a
Cell Blank count (CPM)	0.536
System Blank (DPM)	0.405
System Efficiency	0.806
Count duration (minutes)	1000

Typical carryover is about 1 - 2 % of the net counts (gross counts less system background) of the sample counted on the previous day. The carryover is subtracted from the gross counts of current sample. This correction is not required if the sample is run after a blank.

Carryover correction? No

	Year	Month	Day	Hour	Minute	Second	Ingrowth time (Days)	Ingrowth factor	Decay correction
When sample last stripped	2023	2	24	14	39	0	15.12	0.93540	0.92490
When cell filled	2023	3	11	17	28	59			
Beginning time of count	2023	3	11	19	29	22			

Counts per minute	4.05			
Gross CPM less Cell Blank (CPM)	3.51			
CPM (decay during count corrected)	3.79			
DPM Sample +System (efficiency corrected)	4.71			
DPM sample	4.60	Error ± 1 SD	0.1234	DPM
DPM/g	2.24			
Ra-226 DPM/g	0.75	Error ± 1 SD	0.0201	DPM/g
Ra-226 pCi/g	0.34			

Error % = 2.7

Chemist	RF
PMT High Voltage +ve	770
HV Power supply	Spectrum Technologies
Alpha Counter	Spectrum Technologies
Region of Interest Ch.#s	28-1022
PMT	6655A - #1
Preamp	Canberra 2007P tube base
Amp Gain	1

Radium Analysis by Rn-222 Emanation

Ra Sample Number:	2463
Section Number	36
Sample ID	OB65-70
Core ID	Core OB
Lucas Cell No.	3
Number of days since Rn board last run	1
Dry weight of sample counted (g)	2.074
Total count in period	4253
Total count in period (carryover corrected)	4217
Cell Blank count (CPM)	0.536
System Blank (DPM)	0.405
System Efficiency	0.806
Count duration (minutes)	1000

Typical carryover is about 1 - 2 % of the net counts (gross counts less system background) of the sample counted on the previous day. The carryover is subtracted from the gross counts of current sample. This correction is not required if the sample is run after a blank.

Carryover correction?	Yes		
Gross counts of previous sample	4071	Mean of last 10 carryover measurements	1.12%
Counts carried over from previous sample	36	Mean of last 6 system background measurements	818

	Year	Month	Day	Hour	Minute	Second	Ingrowth time (Days)	Ingrowth factor	Decay correction
When sample last stripped	2023	3	1	10	34	0	13.19	0.90838	0.92490
When cell filled	2023	3	14	15	6	38			
Beginning time of count	2023	3	14	17	7	1			

Counts per minute	4.22			
Gross CPM less Cell Blank (CPM)	3.68			
CPM (decay during count corrected)	3.98			
DPM Sample +System (efficiency corrected)	4.94			
DPM sample	4.99	Error ± 1 SD	0.1259	DPM
DPM/g	2.41			
Ra-226 DPM/g	0.80	Error ± 1 SD	0.0202	DPM/g
Ra-226 pCi/g	0.36			

Error % = 2.5

Chemist	XH
PMT High Voltage +ve	770
HV Power supply	Spectrum Technologies
Alpha Counter	Spectrum Technologies
Region of Interest Ch.#s	28-1022
PMT	6655A - #1
Preamp	Canberra 2007P tube base
Amp Gain	1

Results of Cs-137 Analysis

Flett Research Ltd.

440 DeSalaberry Ave. Winnipeg, MB R2L 0Y7

Fax/Phone: (204) 667-2505

E-mail: flett@flettresearch.ca Webpage: http://www.flettresearch.ca

Client: Juang, Alicia

Address: 180 Grand Ave, Suite 1050, Oakland, CA 94610, USA

Core ID: Core OB

Date Received: 8-Nov-22

Sampling Date: 24-Oct-22

Date Issued: 25-Apr-23

Matrix: Sediment

Transaction ID: 1033

PO/Contract No.: TOE Oct 20-22

Analysis Dates: 15-Feb-23 to 11-Apr-23

Analyst: X. Hu

Analytical Method: N30120 Measurement of Gamma-Ray Emitting Radionuclides in Sediment/Soil Samples by Gamma Spectrometry Using HPGe Detectors (Version 4)

Comments: <2SD: The measured Cs-137 activity is less than 2 counting errors (i.e. 2 SD), suggesting no significant presence of Cs-137 in this sample.

Detection Limit: The method detection limit (MDL) of Cs-137 is 0.3 DPM/g for a 9 g of dry sample and 0.1 DPM/g for a 32 g of dry sample for an 80,000 seconds counting

Estimated Uncertainty: The estimated uncertainty of this method for Cs-137 has been determined to be ± 10% at 95% confidence for samples with activities between 0.5 and 20 DPM/g, counting time 80,000 seconds and sample weights ranging from 9 to 32 grams. Method uncertainty can increase to 85% for samples with activities near detection limit (0.1 - 0.3 DPM/g).

Results authorized by Dr. Robert J. Flett, Chief Scientist

Section Number	LAB ID	Sample ID	Upper Depth (cm) Provided by client	Lower Depth (cm) Provided by client	Weight of Sample Counted (g)	Sample Thickness (mm)	Count Time (sec)	Integral NET Cs-137 Peak Area (Counts)	Cs-137 Counting Error 1 SD (Counts)	Efficiency for Gammas Fractional	Cs-137 Activity DPM/g (dry wt.) on Counting Date	Counting Error ± 1 S.D. (DPM/g Dry Wt.)	Detector Used	Comments Code
15	112590	OB14-15	14.0	15.0	10.476	3.250	160000	138	71	0.0288	0.20	0.10	GMX	<2SD
19	112594	OB18-19	18.0	19.0	12.332	2.800	80000	59	50	0.0291	0.14	0.12	GMX	<2SD
23	112598	OB24-26	24.0	26.0	28.018	6.400	80000	122	39	0.0232	0.17	0.05	GEM	
26	112601	OB30-32	30.0	32.0	21.435	4.800	160000	231	50	0.0244	0.19	0.04	GEM	
29	112604	OB36-38	36.0	38.0	29.314	6.600	80000	177	54	0.0263	0.20	0.06	GMX	
30	112605	OB38-40	38.0	40.0	26.067	5.950	160000	159	47	0.0235	0.11	0.03	GEM	
31	112606	OB40-45	40.0	45.0	30.131	6.175	160000	228	76	0.0266	0.13	0.04	GMX	
32	112607	OB45-50	45.0	50.0	19.255	4.425	80000	33	52	0.0279	0.05	0.09	GMX	<2SD

Efficiency Data

NBS Clay Calibration Standard	Weight (g)	Thickness (mm)	Count Time (sec)		Efficiency for Gammas Fractional Jan 9-23	#REF!
GMX 32g 10 mm	32.00	10	5000		0.0237	#REF!
GMX 24g 7.5mm	24.00	7.5	5000		0.0254	#REF!
GMX 15g 5mm	15.00	5.0	5000		0.0276	#REF!
GMX 9g 3mm	9.00	3.0	5000		0.0291	#REF!
GMX 2.85g 0.8mm	2.854	0.8	10000		0.0306	#REF!
GEM 32g 10 mm	32.00	10	5000		0.0205	#REF!
GEM 24g 7.5mm	24.00	7.5	5000		0.0222	#REF!
GEM 15g 5mm	15.00	5	5000		0.0243	#REF!
GEM 9g 3mm	9.00	3	5000		0.0256	#REF!
GEM 2.85g 0.8mm	2.854	0.8	10000		0.0269	#REF!

Q:\Clients A-L\Juang, Alicia - ESA\2022(1033)\Radioisotopes\OB\Pb-210, Ra-226 and Cs-137 Juang Core OB May 9-23 Final.xlsm

Note: Results relate only to the samples tested and as received. Sample depths are provided by the client.

Cs-137: ISO / IEC 17025:2017 Accredited with the Canadian Association for Laboratory Accreditation (CALA Accreditation No. A3306)

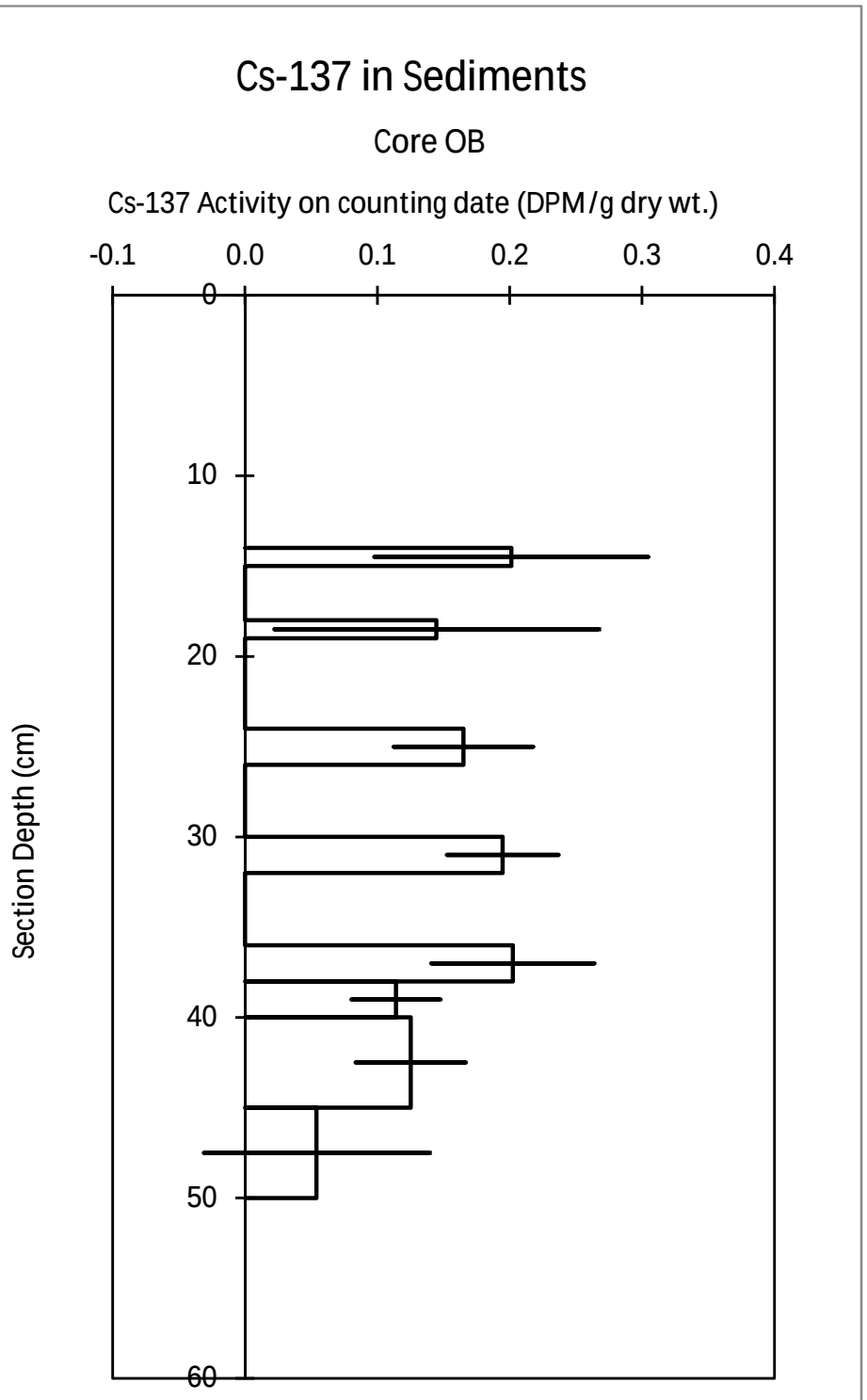

Note: The bar plotted at the midpoint depth of each section represents +/- 1 standard deviation of the Cs-137 counting error.

Q:\Clients A-L\Juang, Alicia - ESA\2022(1033)\Radioisotopes\OB\Pb-210, Ra-226 and Cs-137 Juang Core OB May 9-23 Final.xlsm

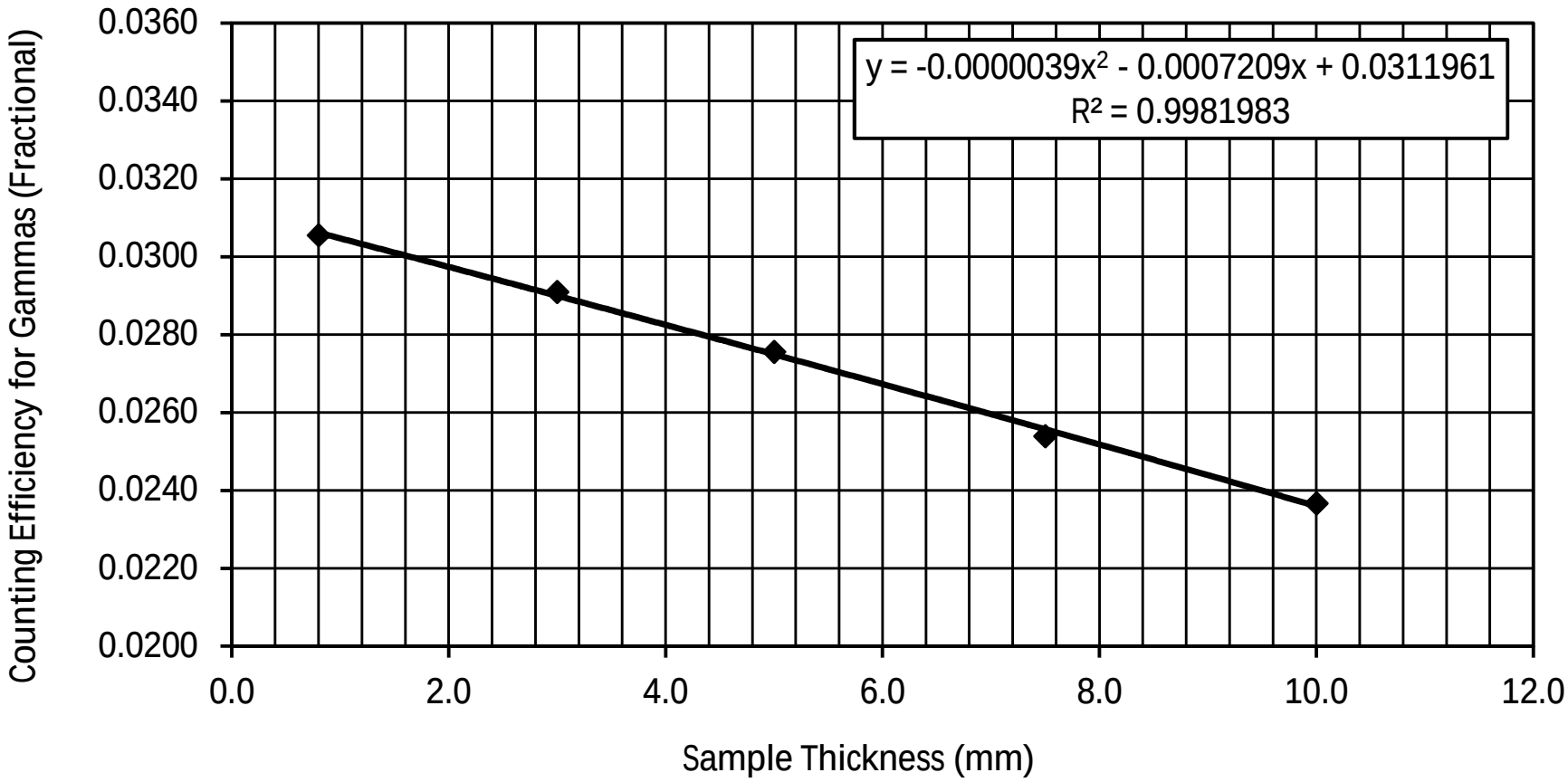
Cs-137 Counting Efficiency of Gammas vs. Sample Thickness (mm) GMX 25% Detector (January 9, 2023)
y = -0.0000039x2 - 0.0007209x + 0.0311961
R2 = 0.9981983
Counting Efficiency for Gammas (Fractional)
0.0360
0.0340
0.0320
0.0300
0.0280
0.0260
0.0240
0.0220
0.0200
0.0
2.0
4.0
6.0
8.0
10.0
12.0
Sample Thickness (mm)

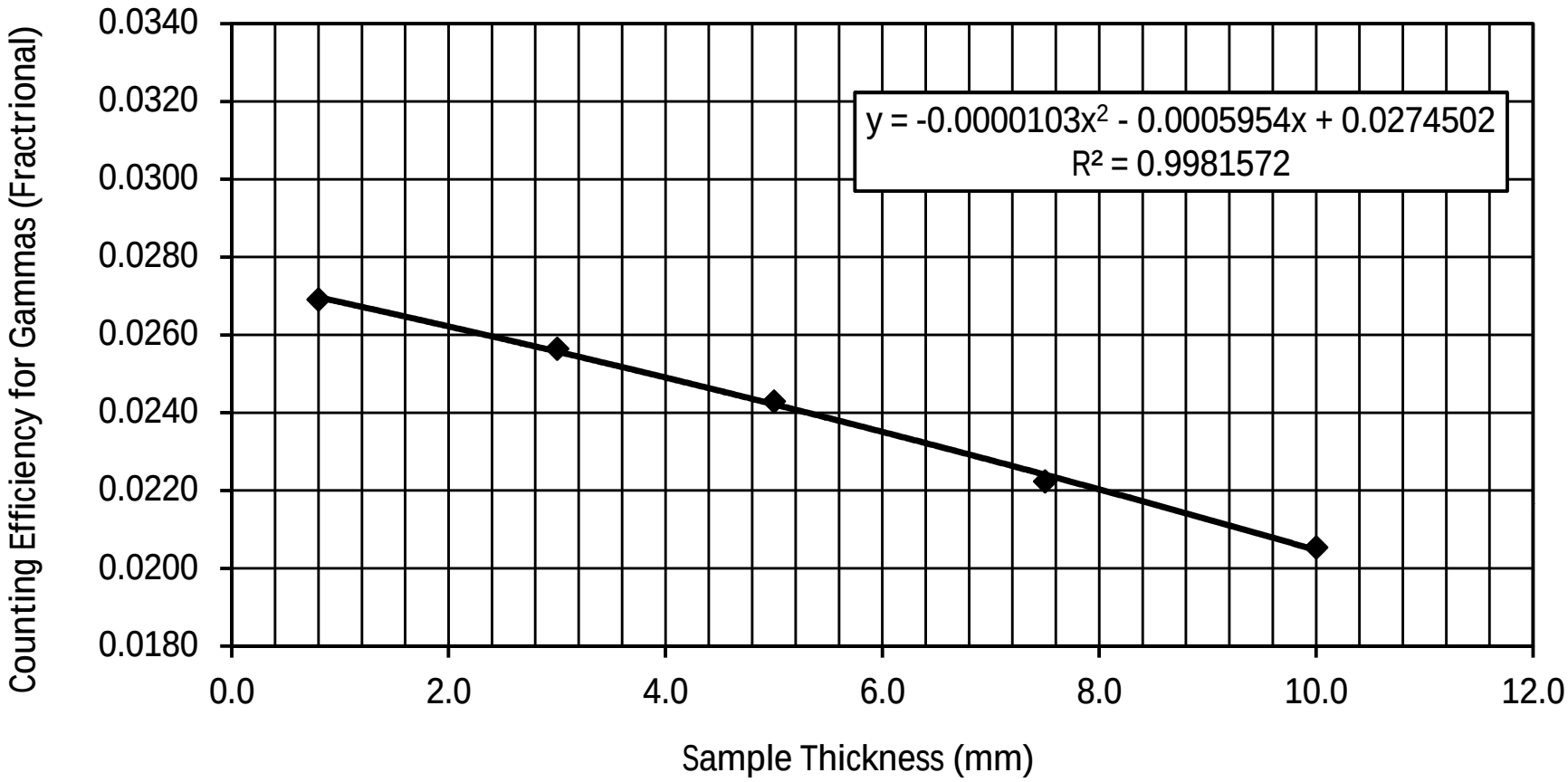
Cs-137 Counting Efficiency of Gammas vs. Sample Thickness (mm) GEM 19% Detector (January 9, 2023)
y = -0.0000103x² - 0.0005954x + 0.0274502
R² = 0.9981572
Counting Efficiency for Gammas (Fractrional)
0.0340
0.0320
0.0300
0.0280
0.0260
0.0240
0.0220
0.0200
0.0180
0.0
2.0
4.0
6.0
8.0
10.0
12.0
Sample Thickness (mm)

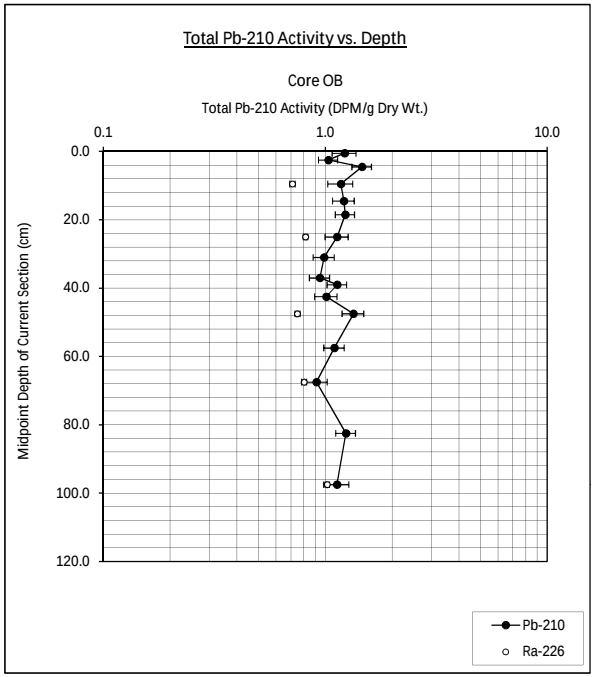

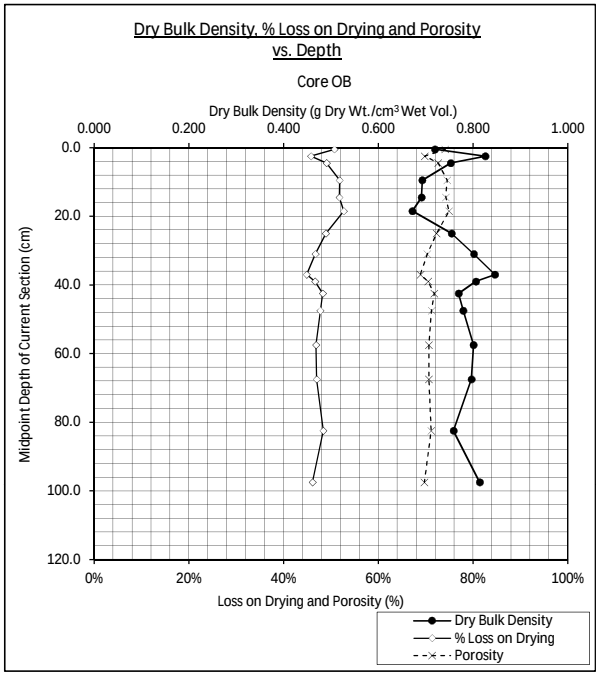

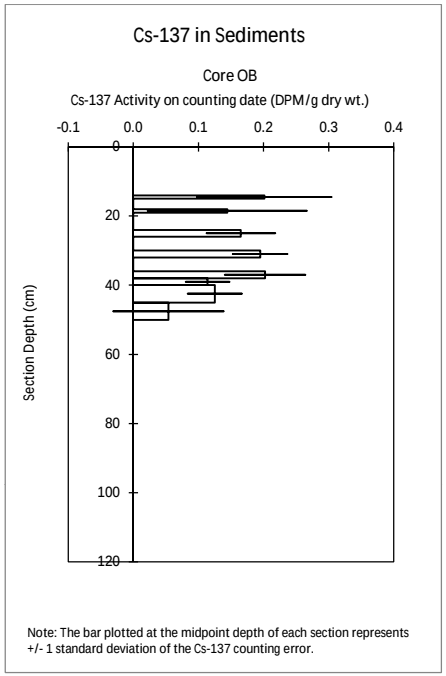

Note: The bar plotted at the midpoint depth of each section represents +/- 1 standard deviation of the Cs-137 counting error.

Linear Regression of Unsupported Pb-210 Activity vs. Accumulated Mass

(Unsupported activity calculated by subtracting the nearest neighbouring Ra-226 measurement from each total Pb-210 value)

Core OB

Gross approximations only.

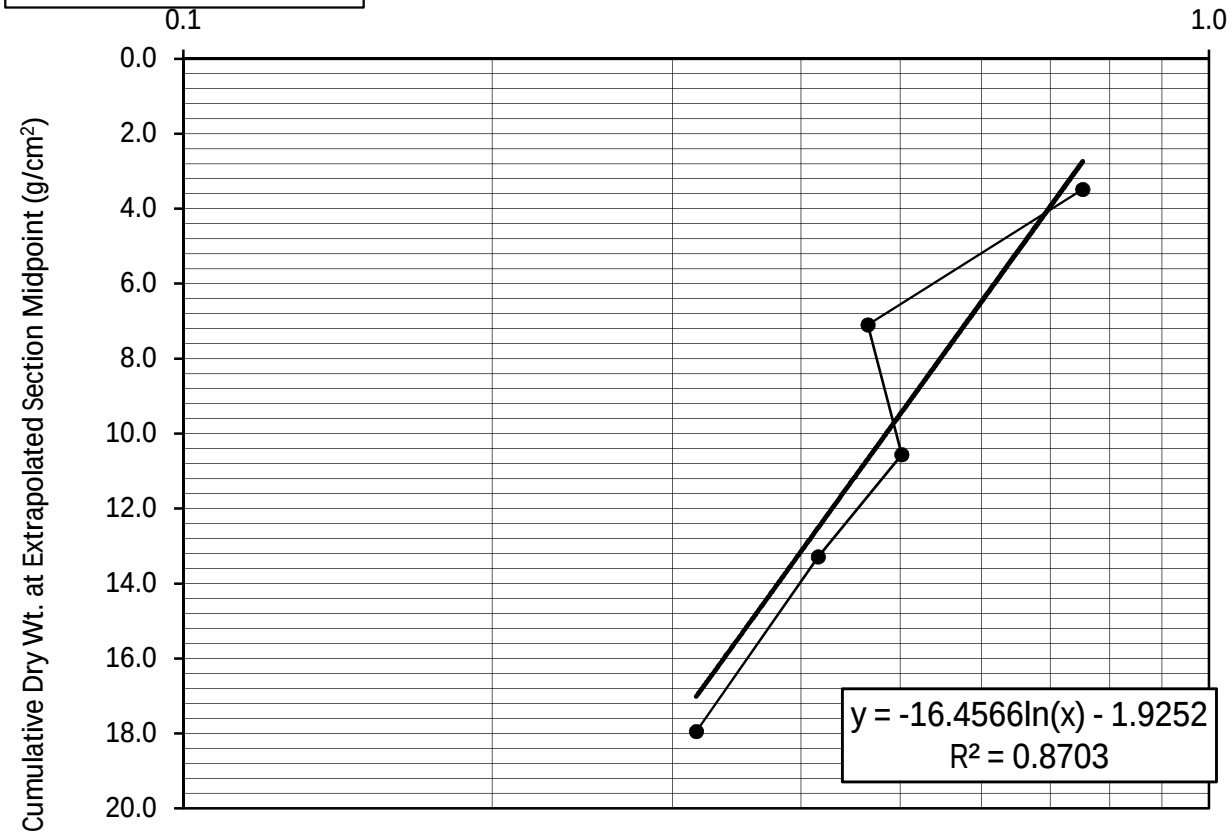

Sediment Accumulation Rate in sections 5 - 23 (extrapolated depth 3.5 - 28 cm):
= (-16.4566) x 0.6931 / (-22.3) = 0.5115 (g/cm²/yr)

Gross approximations only.

Age (yr) vs. Depth (cm)
CRS Model vs. Linear Regression Model

Core OB

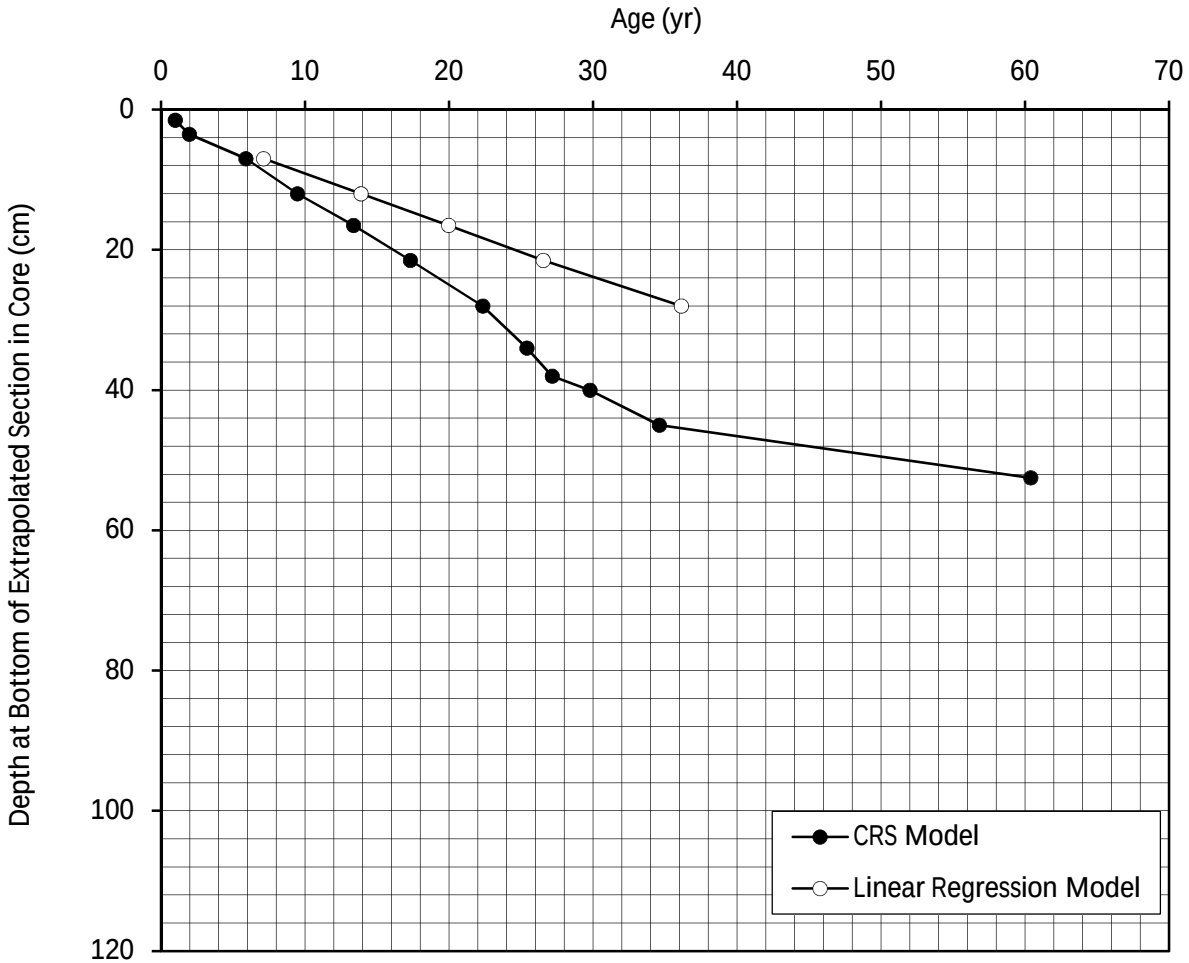

Q:\Clients A-L\Juang, Alicia - ESA\2022(1033)\Radioisotopes\OB\Pb-210, Ra-226 and Cs-137 Juang Core OB May 9-23 Final.xlsm

CRS Sediment Accumulation Rate (g/cm^2/year) vs. Depth at the Bottom of Extrapolated Section in Core (cm)

Gross approximations only.

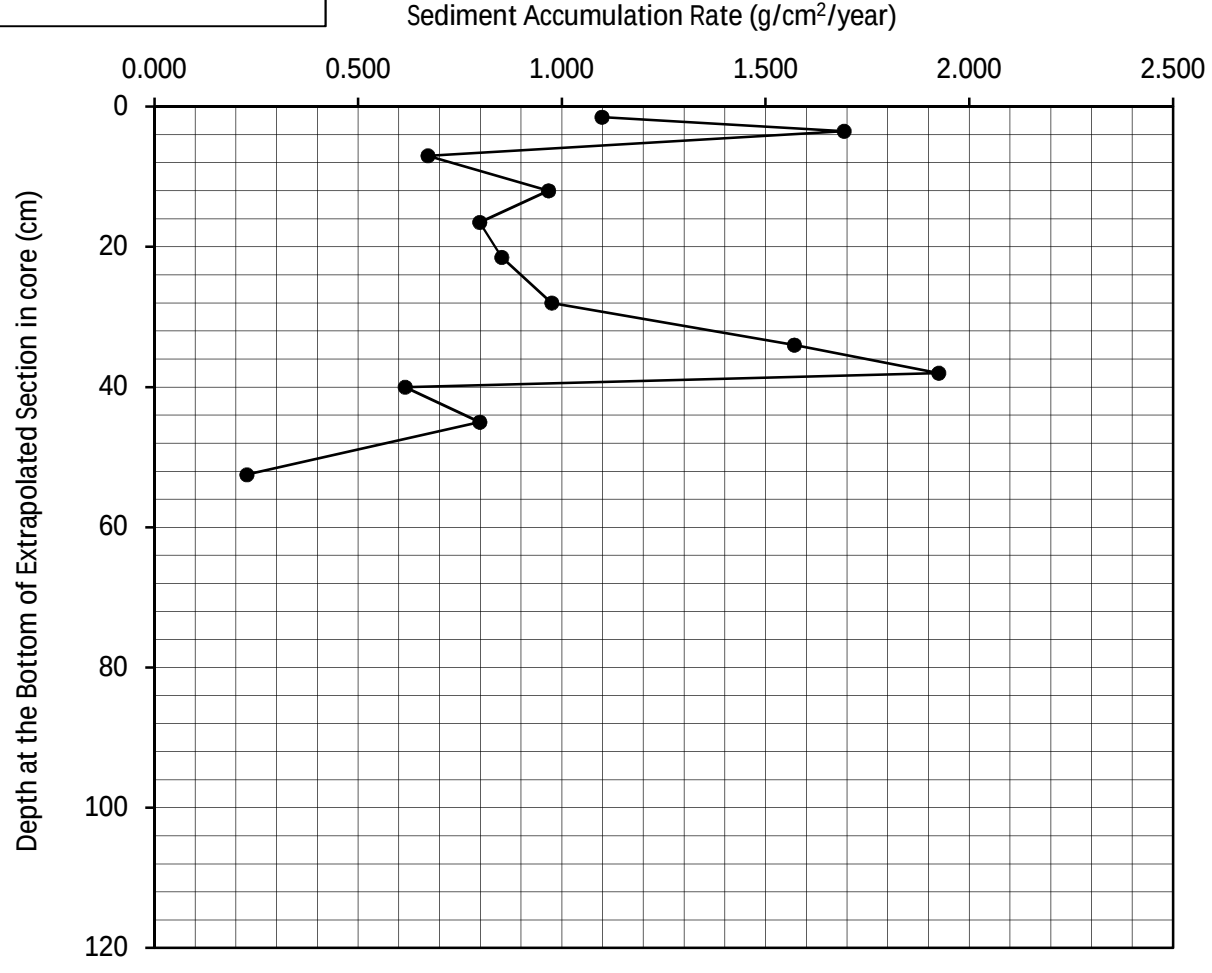

CRS Sediment Accumulation Rate (g/cm^2/year) vs. Age at Bottom of Extrapolated Section (yr)

Gross approximations only.